

# Functional Core-Shell Nanoparticles for Enzyme Immobilization

Zur Erlangung des akademischen Grades eines

DOKTORS DER NATURWISSENSCHAFTEN

(Dr. rer. nat.)

Karlsruher Institut für Technologie (KIT)

Fakultät für Chemie und Biowissenschaften

genehmigte

DISSERTATION

von

**Dominic Charles André Keller, M.Sc.**

aus

Oberursel (Taunus), Deutschland

Dekan: Prof. Dr. Willem M. Klopper

Referent: Dr. Guillaume Delaittre

Koreferent: Prof. Dr. Manfred Wilhelm

Koreferent: Prof. Dr. Frank Breitling

Tag der mündlichen Prüfung: 24.07.2017



Die vorliegende Arbeit wurde im Zeitraum von März 2014 bis April 2017 unter Anleitung von Dr. Guillaume Delaittre und Prof. Dr. Christopher Barner-Kowollik am Karlsruher Institut für Technologie - Universitätbereich angefertigt.

Meiner Familie gewidmet.

*And all that is now*  
*And all that is gone*  
*And all that's to come*  
*And everything under the sun is in tune*



# Abstract

In the present thesis, the synthesis of end-group functionalized amphiphilic block copolymer nanoparticles (NPs) for protein immobilization is reported. In the first part, two routes towards monofunctionalized nanoparticles are investigated. A novel initiator for nitroxide mediated polymerization (NMP) bearing a protected nitrilotriacetic acid (NTA) moiety is synthesized and characterized by nuclear magnetic resonance (NMR) spectroscopy and electrospray-ionization mass spectrometry (ESI-MS). The initiator was then employed in the controlled polymerization of oligo(ethylene glycol) methacrylate-based macroinitiators. Nanoparticles are prepared by either bulk polymerization of styrene and subsequent nanoprecipitation or by aqueous emulsion polymerization of *n*-butyl methacrylate *via* polymerization-induced self-assembly (PISA). The final polymers are characterized by NMR spectroscopy, size exclusion chromatography (SEC), and dynamic light scattering (DLS), which demonstrate the formation of amphiphilic polymer nanoparticles for both synthetic routes. After deprotection of NTA, complexation of nickel ions on PISA-based nanoparticles is assessed by DLS and inductively coupled plasma optical emission spectroscopy/mass spectrometry (ICP-OES/MS). Finally, immobilization of His-tagged horseradish peroxidase (HRP) and ester hydrolase (Mes1 esterase) are carried out, resulting in catalytically active nanobiocatalysts, as shown by UV-Vis measurements.

In the second part, multifunctional nano-objects are prepared by reversible addition-fragmentation transfer (RAFT) polymerization. Three new chain transfer agents, able to specifically immobilize His-, SNAP-, and Halo-tagged proteins, are synthesized and analyzed by NMR and ESI-MS. RAFT polymerizations of OEGMA and fluorophores is performed with each chain transfer agent, resulting in well-defined hydrophilic polymers. Employing mixtures of functionalized macro RAFT agents in either chain extension with styrene and nanoprecipitation or aqueous RAFT PISA with benzyl methacrylate (BzMA) results in the formation of multifunctional fluorescent nanoparticles. Variations in the degree of polymerization of PBzMA and molar mass of macro RAFT agents during the PISA process affect particle morphologies, resulting in

mono- and multifunctional spheres, worms, and vesicles as SEC, DLS, and transmission electron microscopy (TEM) confirmed.

Finally, end-group functionalized macro RAFT agents are used for the coating of magnetic iron oxide nanoparticles (IONPs) to afford multifunctional nanocomposites. Functionalization of the IONPs with a methacrylate-based silane provides surface-bound groups for direct attachment of the polymers. Aminolysis and subsequent Michael addition of macro RAFT agents with methacrylate-containing particles did not result in the formation of covalent linkages as analysis *via* attenuated total reflection Fourier-transform infrared (ATR-FTIR) spectroscopy and energy-dispersive X-ray (EDX) spectroscopy proved. In a second approach, "grafting through" by RAFT polymerization in alcoholic media did lead to partially polymer-coated IONPs as indicated by ATR-FTIR spectroscopy, time-of-flight secondary ion mass spectrometry (ToF-SIMS), and X-ray photoelectron spectroscopy (XPS). However, even though a range of experimental parameters such as initiator and additional monomer concentration were varied, fully coated IONPs were not obtained due strong magnetic aggregation and incomplete silanization of particles.

# Zusammenfassung

Im Rahmen der vorliegenden Arbeit wird die Synthese endgruppenfunktionalisierter amphiphiler Blockcopolymer-Nanopartikel zur Immobilisierung von Proteinen beschrieben. Im ersten Teil werden zwei, zu monofunktionalisierten Nanopartikeln führende, Routen untersucht. Dafür wird ein neuartiger Initiator, welcher eine geschützte Nitrilotriessigsäure (NTA) -gruppe aufweist, zur Nitroxid-vermittelten Polymerisation (NMP) synthetisiert und mittels Kernresonanzspektroskopie (NMR) und Elektrosprayionisations-Massenspektrometrie (ESI-MS) charakterisiert. Anschließend wird dieser in der kontrollierten Polymerisation von Oligo(ethylen glycol) methacrylat-basierten Makroinitiatoren verwendet. Nanopartikel werden entweder durch Massepolymerisation von Styrol und anschließender Nanofällung oder mittels wässriger Emulsionspolymerisation von *n*-Butylacrylat *via* polymerisationinduzierter Selbstassemblierung (PISA) hergestellt. Die Charakterisierung der finalen Polymere erfolgt mittels NMR Spektroskopie, Größenausschlusschromatographie (SEC) und dynamischer Lichtstreuung (DLS), welche die Bildung amphiphiler Polymernanopartikel für beide synthetische Routen beweisen. Nach Entschützung der NTA-Gruppe erfolgt eine Komplexierung von Nickelionen der PISA-basierten Nanopartikel, die über DLS und optischer Emissionsspektrometrie mittels induktiv gekoppelten Plasma-/Massenspektroskopie (ICP-OES/MS) analysiert werden. Letztlich wird die Immobilisierung von His-markierten Meerrettichperoxidase (HRP) und Esterhydrolase (Mes 1 Esterase) durchgeführt. Anschließende UV-Vis Messungen beweisen die enzymatische Aktivität der Nanokatalysatoren.

Im zweiten Teil werden multifunktionale Nanoobjekte durch reversible Addition-Fragmentierung Kettentransfer (RAFT) Polymerisation hergestellt. Drei neuartige Kettenübertragungsmittel, welche spezifisch His-, SNAP- und Halo-markierte Proteine immobilisieren können, wurden synthetisiert und mittels NMR und ESI-MS analysiert. Die RAFT Polymerisationen mit OEGMA, einem Fluorophor und je einem der drei Kettenübertragungsmittel ergeben wohldefinierte hydrophile Polymere. Die Bildung multifunktionaler, fluoreszierender Nanopartikel erfolgt durch Zugabe unterschiedlicher Mischverhältnisse der Makro-RAFT-Reagenzien in der

Kettenverlängerung von Styrol und Nanofällung oder mittels wässriger RAFT PISA mit Benzylmethacrylat (BzMA). Des Weiteren wird durch Variation des Polymerisationsgrades von PBzMA und des Molekulargewichts der Makro-RAFT-Reagenzien die Teilchenmorphologie während des PISA Prozesses beeinflusst, die zu mono- und multifunktionalen Sphären, Wurm-Strukturen und Vesikeln führen, wie SEC, DLS und Transmissionselektronenmikroskopie (TEM) bestätigt.

Abschließend werden die endgruppenfunktionalisierten Makro-RAFT-Reagenzien zur Beschichtung von magnetischen Eisenoxid-Nanopartikeln (IONPs) verwendet, um multifunktionale Nanokomposite zu erhalten. Die Funktionalisierung der IONPs durch ein methacrylat-basiertes Silan stellt oberflächengebundene Gruppen zur direkten Befestigung der Polymere zur Verfügung. Aminolyse und anschließende Michael Addition der Makro-RAFT-Reagenzien mit den methacrylat-tragenden Partikeln führte nicht zur Ausbildung kovalenter Bindungen, was durch abgeschwächte Totalreflexions-Fourier-Transformations Infrarotspektroskopie (ATR-FTIR) und energiedispersive Röntgenspektroskopie (EDX) bewiesen wird. In einem zweiten Ansatz werden teilbeschichtete IONPs mittels Durchpfropfen *via* RAFT Polymerisation in alkoholischen Medien erhalten und mittels ATR-FTIR, Sekundärionen-Massenspektrometrie (ToF-SIMS) und Röntgenphotoelektronenspektroskopie (XPS) analysiert. Trotz der Anpassung einer Reihe von experimenteller Parameter, wie Initiatoren- und Monomerkonzentration, konnten komplettbeschichtete IONPs nicht erhalten werden, da die Partikel durch ihren ausgeprägten Magnetismus aggregierten und nicht vollständig silanisiert waren.



# Contents

Abstract .....	I
Zusammenfassung.....	III
Contents .....	VI
1. Introduction.....	1
2. Theory and Background .....	6
2.1. Radical Polymerization .....	6
2.1.1. Free Radical Polymerization (FRP).....	6
2.1.2. Reversible-Deactivation Radical Polymerization (RDRP).....	9
2.1.3. Nitroxide-Mediated Polymerization (NMP) .....	9
2.1.4. Atom-Transfer Radical Polymerization (ATRP).....	16
2.1.5. Reversible Addition-Fragmentation Chain Transfer (RAFT) Polymerization .....	18
2.2. Polymerization-Induced Self-Assembly (PISA) .....	24
2.2.1. Surface-Functionalized PISA Objects.....	28
2.3. Enzyme Immobilization .....	45
2.3.1. Polyhistidine tag (His-tag).....	49
2.3.2. SNAP-tag.....	50
2.3.3. HaloTag.....	51
2.4. Grafting Process .....	53
3. Amphiphilic Block Copolymer Nanoparticles by Nitroxide-Mediated Polymerization .....	56
3.1. Synthesis of pNTA-Functionalized NMP Initiator .....	58
3.2. Initiation Evaluation of pNTA-functionalized NMP Initiator .....	61
3.3. Synthesis of Hydrophilic Macroinitiators .....	62
3.4. Nanoparticle Formation <i>via</i> Chain Extension and Nanoprecipitation.....	67
3.5. Nanoparticle Formation by Polymerization-Induced Self-Assembly.....	70
3.6. Enzyme Immobilization and Biocatalytic Assay on Functionalized PISA Nanoparticles.....	75
3.7. Conclusion and Outlook .....	79
4. Amphiphilic Block Copolymer Nanoparticles by RAFT-Mediated Polymerization .....	82
4.1. Synthesis of Functionalized RAFT CTAs .....	83
4.2. Synthesis of Fluorescent Hydrophilic Block Segments for PISA .....	90
4.3. Multifunctional Nanoparticles <i>via</i> Chain Extension and Nanoprecipitation.....	96

4.4.	Multifunctional Nano-Objects by RAFT PISA.....	101
4.5.	Conclusion and Outlook .....	116
5.	Polymer-Coated Iron Oxide Nanoparticles for Enzyme Immobilization .....	120
5.1.	Synthesis of Functionalized Low Molar Mass RAFT CTAs.....	122
5.2.	Functionalization of Iron Oxide Nanoparticles.....	123
5.3.	TESPMA-IONP Surface Functionalization by Aminolysis and Michael Addition.....	128
5.4.	TESPMA-IONP Surface Functionalization by "Grafting Through".....	130
5.5.	Conclusion and Outlook .....	136
6.	Conclusion .....	140
7.	Experimental Section.....	144
7.1.	Characterization Methods.....	144
7.2.	Amphiphilic Block Copolymer Nanoparticles by NMP-Mediated Polymerization .....	148
7.2.1.	Materials.....	148
7.2.2.	Synthetic Procedures.....	148
7.3.	Amphiphilic Block Copolymer Nanoparticles by RAFT-Mediated Polymerization .....	154
7.3.1.	Materials.....	154
7.3.2.	Synthetic Procedures.....	155
7.4.	Polymer-Coated Iron Oxide Nanoparticles for Enzyme Immobilization .....	163
7.4.1.	Materials.....	163
7.4.2.	Synthetic Procedures.....	164
	Bibliography.....	166
	Appendix.....	178
	Abbreviations .....	184
	Declaration .....	187
	Curriculum Vitae.....	188
	List of Publications.....	189
	Acknowledgements .....	190



# 1

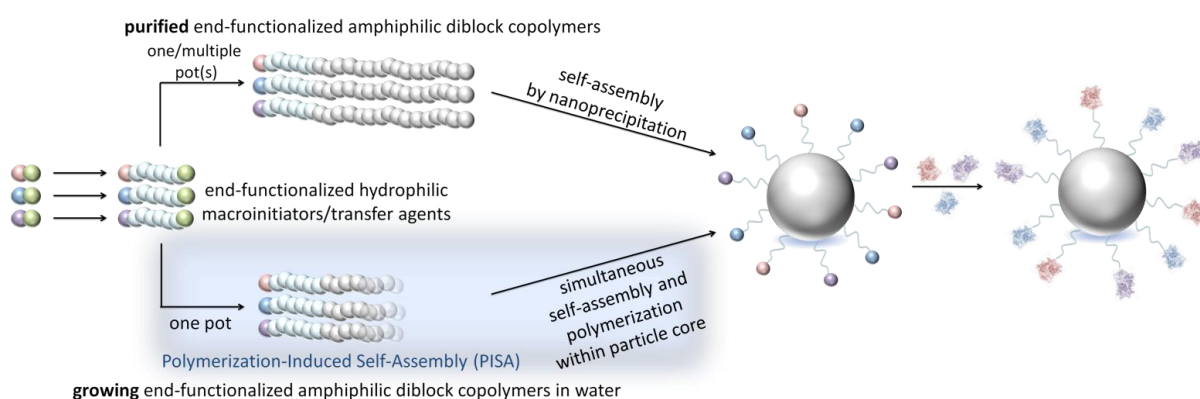
## Introduction

Enzymes are proteins (except for some being RNA) that catalyze many biochemical reactions within living systems and have been used for food processing since ancient times. Since the beginning of the 20th century, constant developments in biotechnology have paved the way for the use of enzymes on an industrial scale as catalysts in pharmaceutical and chemical processes, for production of fine chemicals,<sup>1-2</sup> in biofuel cells,<sup>3</sup> and in diagnostics.<sup>4-5</sup> Compared to classical chemical synthesis, the use of enzymes can be advantageous for several reasons: enzymes catalyze reactions under very mild conditions with regard to temperature and pH in aqueous media, while organic synthesis often requires the use of organic solvents due to the specific solubility of the reagents. Furthermore, enzymes lower the activation energy of a reaction drastically increasing the reaction rates and are highly substrate-specific, reducing the formation of undesirable byproducts which would have to be separated from the product. However, due to the lack of long-term stability and inefficient recovery of enzymes in solution, many potential applications cannot be realized. Protein immobilization is an essential tool to circumvent these disadvantages as it provides numerous benefits such as enhanced stability towards denaturation conditions (e.g., pH, temperature, non-aqueous solvents, ...) and facile recovery of the enzymes after reaction, which led to the use of enzymes as biosensors and in enzymatic cascades. Among the physical and chemical immobilization techniques, site-specific binding of functional groups to recombinant fusion proteins is a promising route, which has limited influence on the proteins tertiary structure thereby leaving the activity mostly unchanged. However, while many inorganic materials are utilized as solid supports to immobilize

proteins,<sup>6-9</sup> the use of amphiphilic block copolymers as solid supports is still poorly explored. Early examples of the preparation of amphiphilic block copolymer 2D structures such as thin films led to successful surface immobilization of enzymes.<sup>10-11</sup> Still, especially three dimensional structures such as spheres and vesicles offer a significantly higher surface-area-to-volume ratios than two dimensional structures. Furthermore, dispersed nanoparticle systems bear the advantage of being readily physically transferable, making them ideal candidates for applications in microfluidic reactors. A straightforward way into introduce functionality to polymers is to synthesize the initiators or chain transfer agents accordingly. This way one functional group per chain can be incorporated, thereby offering a good control of functionality. Combining multiple initiators or chain transfer agents can lead to multifunctional nanostructures. Particularly, the use of multifunctionalized nanoparticles, with its aforementioned benefits, is an auspicious method to colocalize multiple enzymes for the implementation of cascade reactions. In general, the formation of amphiphilic block copolymer nanoparticles can be realized by methods such as oil-in-water (O/W) emulsions, solvent evaporation, solvent diffusion, and nanoprecipitation with the latter being particularly suitable for amphiphilic polymers.<sup>12</sup> While nanoprecipitation is a facile process to create nanoparticles, it suffers from practical limitations which can result in flocculation and aggregation of particles. During the last decade a new approach, namely polymerization-induced self-assembly (PISA), was introduced and has gained increasing interest ever since. PISA is based on the compatibility of reversible-deactivation radical polymerization (RDRP) techniques with aqueous media. In a one-step process, hydrophilic molecular precursors are extended with a hydrophobic second block in an emulsion or dispersion polymerization process. As a result, the process leads to amphiphilic block copolymers and their *in situ* self-assembly into nano-objects, concurrent to the growth step.<sup>13</sup> Depending on the nature and structure of the constituting block copolymers and on the molar mass of the hydrophobic component, a control over the particle size and the morphology, varying from spheres to worms/fibers and vesicles, can be achieved. Therefore, the use of functional RDRP precursors in PISA processes is a promising strategy to yield tunable polymeric supports for protein immobilization, which has yet to be explored intensely.

In the present work, novel initiators and chain transfer agents were developed for NMP and RAFT polymerizations. End-group functionalized macromolecules were utilized in

bulk and aqueous emulsion polymerizations for the synthesis of amphiphilic block copolymers and their corresponding nano-objects for protein immobilization. The synthetic pathway starting from functionalized initiators or chain transfer agents towards end-functionalized nanoparticles is depicted in Scheme 1. Finally, partially polymer-coated iron oxide nanoparticles (IONPs) as solid supports for site-specific enzyme immobilization were synthesized *via* "grafting to" and "grafting through" approaches using the aforementioned functionalized macro RAFT agents.



**Scheme 1.** Complete synthetic pathway from end-functionalized initiators/chain transfer agents (left) to enzyme immobilization onto nanoparticles (right).





# Theory and Background

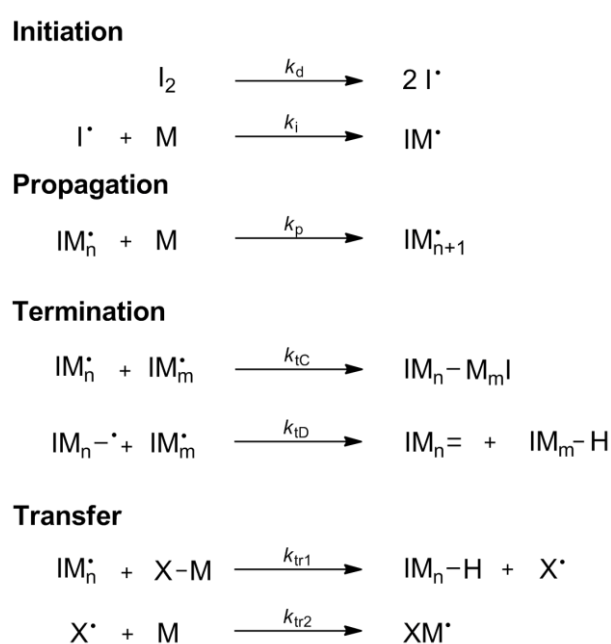
## 2.1. Radical Polymerization

Over the past decades radical polymerization has proved to be one of the most widely used methods on an industrial scale and in the field of scientific research for polymer synthesis. Starting in the 1980s, radical polymerization became the most widely employed process to produce high molar mass polymers for commercial production.<sup>14</sup> At first, free radical polymerization was the simplest and most employed polymerization technique, while controlled radical processes (see 2.1.2) became increasingly popular - mostly in the academic field - starting in the late 1980s to early 1990s. The growth of interest can be largely attributed to the discovery and introduction of techniques like nitroxide-mediated polymerization (NMP), atom transfer radical polymerization (ATRP), and reversible addition-fragmentation chain transfer (RAFT) polymerization, which provide a pseudo-living character to the polymerization process.<sup>15</sup> Nowadays, the controlled polymerization techniques are omnipresent in scientific research and cover more than two thirds of all papers on radical polymerization,<sup>14</sup> while free radical polymerization still plays an essential role in today's industrial polymer production.

### 2.1.1. Free Radical Polymerization (FRP)

One of the simplest and fastest ways of obtaining polymers is through the use of free radical polymerization (FRP). As of today it is still the most widely utilized

polymerization technique for industrially relevant polymers and approximately 50 wt% of all synthetic polymers worldwide are produced using FRP.<sup>16</sup> The advantage of FRP is the ability to polymerize a vast array of different monomers. Its tolerance towards many functionalities (e.g., hydroxyl, carbonyl, amino groups), its compatibility with various reaction conditions, the relative simplicity of implementation and the potential to perform reactions in polar solvents, make the versatility of this technique apparent. The general mechanism of a free radical polymerization includes four reaction steps depicted in Scheme 2.



**Scheme 2.** The four steps of free radical polymerization.

The first reaction step of a free radical polymerization is the initiation. For this process, a suitable initiator, usually a highly energetic compound such as diazo and peroxide molecules like 2,2'-azobis(2-methylpropionitrile) (AIBN) or dibenzoyl peroxide (DBPO), respectively, decomposes homolytically into two highly reactive radicals under stimulation by an external trigger (e.g., electrochemical processes, temperature, or irradiation).<sup>17</sup> The initiator rate constant of decomposition  $k_d$  varies with the reaction conditions and can range from  $10^{-1}$  to  $10^{-6} \text{ s}^{-1}$ . The generated radicals can then add onto the reactive double bond of a monomer molecule, which leads to a monomer species with a radical chain end functionality. The following propagation reaction (chain growth) represents the consecutive addition of monomer units to the radical chain ends.

Depending on the stability of the formed radicals, the propagation rate coefficient  $k_p$  may range from  $10^2 \text{ L mol}^{-1} \text{ s}^{-1}$  for stable radicals, such as with methacrylates or styrene, to  $10^4 \text{ L mol}^{-1} \text{ s}^{-1}$  for unstable radical species based on acrylates.<sup>18-19</sup> Therefore, the chemical structure of the radical species as well as the reaction temperature are essential for an appropriate propagation. While the propagation step is crucial for macromolecular growth, the termination steps cease the process by removing radical species from the polymerization. Disproportionation is one of two possibilities to terminate chain growth. A hydrogen transfer from one radical chain to another results in an unsaturated double bond on one molecule, which may undergo further radical reactions, and one saturated chain on the second molecule rendering it "dead". Combination on the other hand generates one "dead" higher molecular weight chain since two radical chains reacted with each other terminating both radicals. Depending on the steric hindrance of the monomer, one of the termination models is more likely to occur than the other. For high steric hindrance, the disproportionation reaction has a higher impact on radical chains, while for less sterically hindered monomers like styrene combination reactions may occur more often.<sup>20</sup> Since termination reactions are a product of movement of polymer chains within the reaction mixture and therefore its viscosity, the termination rate coefficient  $k_t$  is diffusion-controlled. Hence, high conversions and macromolecular chain length largely influence the termination rate coefficient.<sup>21</sup> Besides the termination reaction another event during the polymerization process may occur and also result in inactive chains. In the chain transfer reaction, an active polymer chain transfers its radical, deactivating it in the process, to an adjacent molecule (e.g., polymer chain, monomer, solvent, transfer agent) which is able to initiate a new chain. While the overall concentration of radicals remains the same, the appearance of smaller polymer chains generated by chain transfer reaction to monomers, solvent and transfer agents negatively affects the molecular weight distribution of the final polymer.

Still, free radical polymerization suffers from a distinct disadvantage: the overall lack of control during the polymerization as opposed to other polymerization techniques such as living anionic polymerization. Without the appropriate control over (i) the end-group functionality of a polymer, (ii) the molar mass, (iii) possible block copolymer composition, and (iv) overall macromolecular architecture, no novel applications for polymers could be attained. Therefore, new polymerization techniques inspired by

living radical anionic polymerization have been developed during the last two decades to address these problems. As a result, reversible-deactivation radical polymerization (RDRP) techniques were introduced. RDRP combines the simplicity of radical polymerization with the benefits of living polymerization processes, resulting in well-defined polymers.

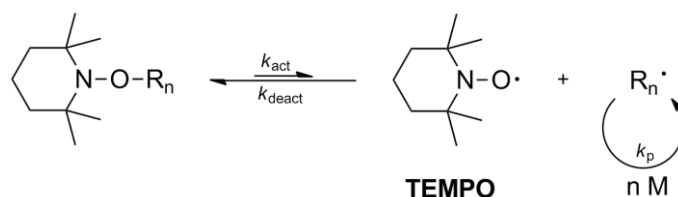
### **2.1.2. Reversible-Deactivation Radical Polymerization (RDRP)**

The inherent disadvantages of FRP led the development of RDRP methods while retaining its main advantages, i.e., the vast variety of monomers that can be polymerized and the compatibility with a range of reaction conditions. RDRP methods generally feature a dynamic equilibrium between a favored dormant species and propagating radical species, thereby limiting the concentration of radicals and ensuring a continuous and uniform addition of monomer units. Hence, RDRPs exhibit a linear increase in molar mass with increasing conversion and narrow dispersities ( $M_w/M_n < 1.3$ ). Thanks to a pseudo-living character and the precisely controlled molar mass, RDRPs allow the synthesis of complex macromolecular architectures in terms of topology (stars, brushes, combs), composition (block and graft copolymers), and distinct end-group functionalities of the polymers. The most commonly applied RDRP techniques are nitroxide-mediated polymerization (NMP), atom transfer radical polymerization (ATRP), and reversible addition-fragmentation chain transfer (RAFT) polymerization, which are all described in the following.

### **2.1.3. Nitroxide-Mediated Polymerization (NMP)**

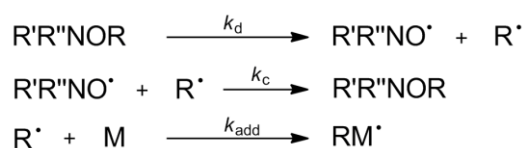
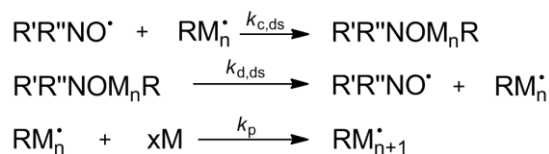
Nitroxide-mediated polymerization was first reported in 1985 by Solomon *et al.* who describing an improved process to control the growth of polymers and reported novel alkoxyamine initiators.<sup>22</sup> Through the work of Hawker,<sup>23</sup> Fukuda,<sup>24</sup> and others<sup>25-26</sup> during 1993-1996, NMP became widely known to the polymer community and many papers on the kinetics and mechanism of the reaction were published ever since. NMP can be initiated in two ways: through the use of alkoxyamines or directly by a classic radical initiator in the presence of a nitroxide. The mechanism of NMP was proposed by

Johnson and follows a two-stage process (Scheme 3).<sup>27</sup> While the initiation step follows a similar fashion to FRP, the subsequent propagation is fundamentally different.

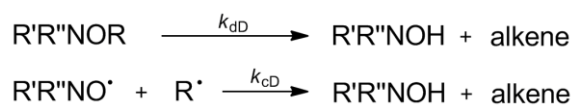


**Scheme 3.** Reversible equilibrium between dormant and active species in NMP, using TEMPO as the nitroxide species.

In NMP, the aforementioned nitroxide reversibly binds to the propagating polymer chain, thereby creating an equilibrium between a "sleeping" or dormant macromolecular species and propagating chains, which is defined by the equilibrium constant  $K = k_{act}/k_{deact}$ . Since  $k_{act}$  is significantly smaller than  $k_{deact}$  most of the polymeric chains are in the dormant state. This reduction of the concentration in propagating radicals leads to a decreased polymerization rate, which in turn increases the polymerization times in NMP. However, the low concentration of propagating radical species ensures the controlled addition of monomer units, resulting in a solid control over the polymerization process.

**Initiation****Propagation****Termination**

Disproportionation



Self-termination



**Scheme 4.** Proposed mechanistic steps during a nitroxide-mediated polymerization (NMP).

The so-called persistent radical effect (PRE) is the key feature of nitroxide-mediated polymerization. When two radicals are generated at the same time and at the same rate, and one is more persistent than the other, an unusually high selectivity for the cross-coupling reaction can be observed. This effect drastically lowers the self-termination reactions which would result in dead polymer chains typically found in free radical polymerizations. In NMP, in the case of a monocomponent system, the PRE occurs through the decomposition of the alkoxyamine initiator into two different radical species affording the transient propagating alkyl radical and the persistent nitroxide radical. During the early stage of the polymerization, self-terminations between transient carbon-centered radicals occur. As a result, an excess of persistent nitroxides is build up, which allows for a good control of the polymerization. This persistence can be attributed to the highly energetic open-shell electronic configuration of nitroxide radicals. This is due to the strongly delocalized three-electron bond between the nitrogen and the oxygen atoms giving considerable thermodynamic stability at the radical center.<sup>28</sup> Hence, dimerization between two nitroxide radicals is highly unlikely.

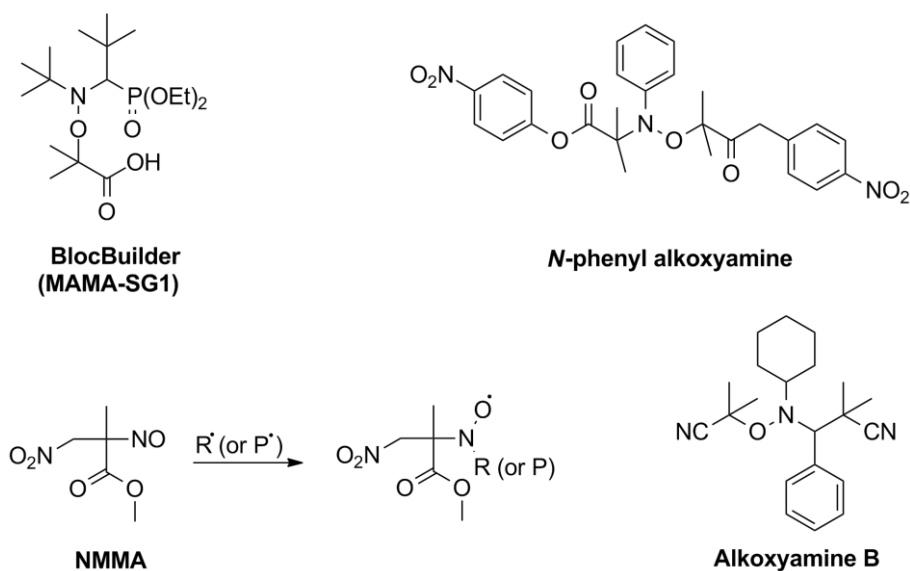
Also, sterically hindered and polar substituents at the  $\alpha$ -carbon of the nitroxide moiety can significantly stabilize the radical center. The most stable nitroxides occur as hindered cyclic compounds while a large number of acyclic nitroxide structures also exist. Their stability is largely attributed to the bulky substituents adjacent to the nitroxide moiety kinetically stabilizing the radical center and preventing possible  $\beta$ -hydrogen abstraction, which would lead to unreactive hydroxylamines. Nitroxides generally display a decreased polarity around the radical center. Having an electron withdrawing group such as ester groups at the  $\alpha$ -carbon increases the electron density of the oxygen atom which results in a reduction of the nitroxide group.<sup>29</sup>

Precursors for the synthesis of the early types of nitroxides (e.g., TEMPO and TEMPO-based derivatives) are commonly, hindered secondary or tertiary amines. Oxidation of these amines is the simplest approach to generate nitroxides. As the main oxidizing reagent, hydrogen peroxide is used in conjunction with sodium tungstate and a weak inorganic base such as sodium bicarbonate. Reaction conditions are usually in protic solvents like methanol or even water, at ambient temperature. Especially for tertiary amines, the reaction with hydrogen peroxide may take from hours to days to reach completion. It must also be noted that for heterocyclic *N*-benzyl type precursors *m*-chloroperbenzoic acid (*m*CPBA) instead of hydrogen peroxide is the reagent of choice. *m*CPBA was successfully employed in the oxidation of several demanding tertiary amines, e.g., azaphenalene- and tetraphenylisoindoline derivatives, to generate the corresponding nitroxides.<sup>30-31</sup> Applying *m*CPBA to  $\alpha$ -aminophosphonates results in the formation of the now widely utilized SG1-type nitroxide derivatives that can be further transformed to alkoxyamine by employing either Grignard reagents or other metal-mediated reactions like atom transfer radical addition (ATRA).<sup>32</sup>

Amongst the earliest examples of nitroxides used in polymerizations is TEMPO. TEMPO and a suitable radical initiator are still attractive initiating systems until today and were first used for the NMP of styrene in bulk to obtain polystyrene with low dispersity and a high degree of control over the polymerization.<sup>24, 33-34</sup> The reaction is controlled due to the aforementioned equilibrium between dormant and active chains and the relatively low equilibrium constant *K* of styrene at 125 °C ( $2.1 \times 10^{-11} \text{ L mol}^{-1} \text{ K}^{-1}$ ), which impedes irreversible termination reactions.<sup>24</sup> However, for other non-styrenic monomers, TEMPO-based homopolymerizations showed a lack of control resulting in broad molar

mass distributions and low conversions. Furthermore, the high temperature needed, restricted adaption of NMP to dispersed systems (e.g., aqueous emulsion polymerization) and the high concentration of dormant radical species during a reaction resulted in extremely long polymerization times.<sup>23</sup> To overcome these limitations the aforementioned alkoxyamines became subject to intensive research by the late 1990s. The two most promising alkoxyamine initiator types were based on 2,2,2-trimethyl-4-phenyl-3-azahexane-3-oyl (TIPNO) and *N*-*tert*-butyl-*N*-[1-diethylphosphono-(2,2-dimethylpropyl)] nitroxide (SG1 or DEPN). Their introduction to NMP progressively allowed the polymerization of acrylates and even acrylamides to high degrees of polymerization and low  $\bar{D}$ .<sup>35</sup> For SG1-based alkoxyamines the most widely used, and commercially available, initiator is BlocBuilder (MAMA-SG1) (Scheme 5). It benefits from good water solubility thanks to its carboxylic end-group and relatively high  $k_a$  ( $0.3 \text{ s}^{-1}$  for styrene at  $120 \text{ }^\circ\text{C}$ ).<sup>36</sup> Controlled methacrylate polymerizations were first accomplished by Charleux and co-workers by adding small amounts of either styrene (4.4 - 8.8 mol%) or acrylonitrile (2.5 mol%) as a co-monomer.<sup>37-38</sup> Strictly speaking, the resulting MMA-polymers were copolymers by definition but displayed physical properties similar to poly(MMA). Without addition of a controlling co-monomer, the reaction would lead to uncontrolled homopolymerization of MMA even if the BlocBuilder was utilized. Since homopolymerization of methacrylates *via* NMP has always been a unfulfilled desire by polymer scientists further structural investigations to alkoxyamines lead to the development of *N*-phenylalkoxyamines. Grubbs and co-workers convincingly demonstrated the effective homopolymerization of MMA and its subsequent chain extension using these alkoxyamines.<sup>39-40</sup> More recently Gigmes and co-workers reported an *in situ* formation of nitroxides decreasing the temperature range for MMA homopolymerization to  $40\text{-}50 \text{ }^\circ\text{C}$ .<sup>41</sup> In this case, a low temperature azo initiator together with a hindered nitroso compound produced a hindered methyl 2-methyl-3-nitro-2-nitrosopropionate (NMMA) within the polymerization mixture which acted as an efficient controlling agent (Scheme 5). After 6.5 h the reaction exceeded 50% conversion with  $\bar{D} < 1.35$  resulting in well-defined poly(MMA). The same conditions were applied to benzyl methacrylate (BzMA) and trifluoroethyl methacrylate (TFEMA) and subsequent chain extension experiments confirmed growth in molar mass with only moderate increase in  $\bar{D}$  (1.22-1.38). Recently, Asua and co-workers reported the synthesis of a new alkoxyamine initiator (Alkoxamine B) for the controlled chain extension of various methacrylates (Scheme 5).<sup>42-43</sup> Homopolymerization of methyl methacrylate with the

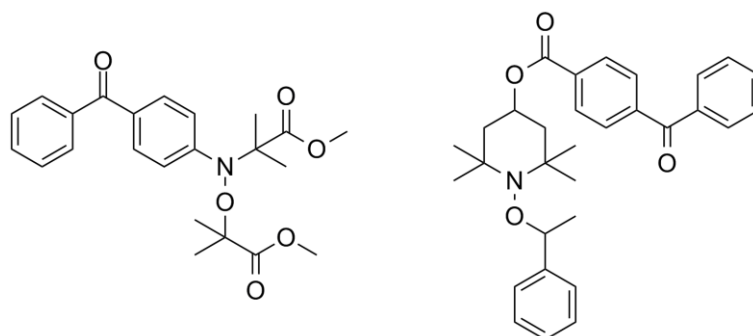
novel alkoxyamine resulted in well-defined polymers ( $D < 1.2$ ) at high conversions (> 80%) within 4-5 h. Subsequently, the macroinitiator was utilized in the chain extension with styrene at 126 °C, yielding PMMA-*b*-PS block copolymers with reasonable dispersities ( $D = 1.85$ ) at 93% conversion.



**Scheme 5.** Chemical structure of BlocBuilder (MAMA-SG1), *N*-phenylalkoxyamine, *in situ* formation of NMMA under moderate temperatures, and novel alkoxyamine initiator, Alkoxyamine B.

With the increasing interest in photopolymers and their impact in material science, recent advances towards nitroxide-mediated photopolymerization have been made (Scheme 6). For this a light-sensitive alkoxyamine is employed, bearing a chromophore group located on the nitroxide moiety. The photolysis of the alkoxyamine leads to the reversible equilibrium which allows a controlled radical photopolymerization. A general problem during the photolysis step arises from the selectivity of the cleavage process. Since both the N-O and the C-O bonds are relatively labile to homolysis the selectivity of the cleavage must be controlled. The dissociation of the N-O bond would not lead to persistent radicals which in turn would result in a loss of control and the formation of dead polymer chains. Hence, the required C-O dissociation quantum yield must be 1.0 ensuring that each absorbed photon generates nitroxide radicals.<sup>44</sup> The distance between the chromophore and the C-O bond plays a significant role in the cleavage process.<sup>45</sup> Employing nitroxide-mediated photopolymerization for surface modification

as an alternative for the widely used dithiocarbamates has been proposed recently giving access to spatially controlled reactions, e.g., for surface patterning<sup>46-47</sup> or self-healing networks.<sup>48</sup>



**Scheme 6.** Light-sensitive alkoxyamines for nitroxide-mediated photopolymerization.

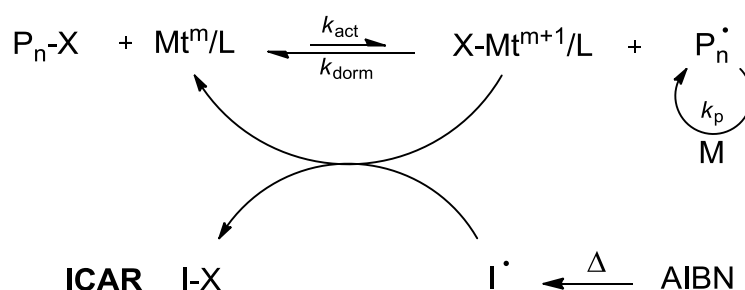
Among the aforementioned fields of application, NMP is also successfully applied in the preparation of polymer-based biomaterials under various conditions. NMP shows clear advantages in the preparation of biomaterials compared to other RDRP techniques such as RAFT and ATRP due to its simplicity, the absence of transition metal catalysts, radical initiators, and sulfur-based transfer agents. A particularly investigated research field is the combination of synthetic polymers with peptides to obtain new materials with the advantageous properties of their intrinsic biofunctionalities. The most common example is the combination of peptides with poly(ethylene glycol) (PEG) and its derivatives to poly(peptide)-based therapeutics.<sup>49-50</sup> A simple route towards the combination of preformed polymer and free peptides or proteins relies on the brush-like poly(oligo ethylene glycol methyl ether methacrylate) (POEGMA) initiated by *N*-hydroxysuccinimidyl (NHS) ester modified SG1 alkoxyamine. Chenal *et al.* demonstrated the efficient conjugation between a neuroprotective tripeptide and lysozyme through the activated ester end-group of a POEGMA-based hydrophilic polymer.<sup>51</sup> On the other hand, a "grafting from" approach was reported by Studer and co-workers.<sup>52</sup> In a preliminary step, a TEMPO-based alkoxyamine was linked to a L-serine side chain. Using standard solution phase peptide chemistry the L-Ser-alkoxyamine initiator was attached to various peptides. Subsequently, the TEMPO-terminated peptide initiators demonstrated good control for the polymerization of styrene, and depending on the

exact structure of the TEMPO derivatives, *n*-butyl acrylate and *N*-isopropylacrylamide, leading to well-defined polymer bioconjugates.

Overall, NMP was successfully applied in a wide variety of application giving access to new and complex macromolecular materials displaying its versatility, simplicity, and robustness which gained drastically in maturity over recent years, even though NMP suffered from a lack of popularity in favor of other RDRP techniques such as RAFT and ATRP.

#### 2.1.4. Atom-Transfer Radical Polymerization (ATRP)

Since atom-transfer radical polymerization (ATRP) was not employed in the current work this chapter will only give a brief introduction. ATRP was first reported in 1995 independently by Sawamoto and Matyjaszewski. Similarly to NMP, the mechanism of ATRP involves a reversible equilibrium between dormant and activate radical species, as depicted in Scheme 7.



**Scheme 7.** Simplified reaction scheme of an (ICAR) ATRP.

In contrast to NMP, the initiation is based on a redox system with a transition metal complex ( $\text{Mt}^m/\text{L}$ ) activating an alkyl halide ( $\text{P}_n\text{-X}$ ). This activation generates a propagating radical species ( $\text{P}_n^\bullet$ ) and a transition metal complex in a higher oxidation state with the coordinated ligand ( $\text{X-Mt}^{m+1}/\text{L}$ ). Polymers obtained by ATRP retain a halide end-group, which can be employed further for post-polymerization modifications. As in free radical polymerization, termination of a propagating radical species occurs once two propagating chains couple, resulting in "dead" chains. Many redox-active transition metal complexes can catalyze the reaction, yet Cu-based complexes such as

CuBr<sub>2</sub>/L are the most prominent ones. Still, ATRP was also employed utilizing other transition metals, such as iron,<sup>53-54</sup> ruthenium,<sup>55-56</sup> and cobalt.<sup>57</sup> Depending on the monomers reactivity the ligands have to be chosen thoughtfully in order to achieve high activation rates. The three most common ligands are 2,2'-bipyridine (bpy), tris[2-(dimethylamino)ethyl]amine (Me<sub>6</sub>TREN), and *N,N,N,N,N*-pentamethyldiethylenetriamine (PMDETA), which all bind to the transition metal through their nitrogen atoms.

In the early development stages of ATRP, the main disadvantage was the presence of residual transition metal in the polymer even after purification. Cu is known to be cytotoxic, thus limiting ATRP for potential biological applications. Furthermore, the transition metal catalyst was sensitive to oxygen or could face solubility issues with the reaction medium.<sup>16</sup> This led to the development of activator regenerated by electron transfer (ARGET) ATRP in which only catalytic amounts of metal complex were needed. Mild reducing agents such as ascorbic acid, glucose, or Sn(II)-octoate are added to the reaction in order to regenerate activating Cu<sup>I</sup> species from oxidative stable, deactivating Cu<sup>II</sup> species *in situ*. Apart from its oxidative stability, ARGET ATRP has been shown to diminish catalyst-induced side reactions and thus made high molar mass copolymer synthesis with high chain end functionality possible.<sup>58</sup> In initiator for continuous activator regeneration (ICAR) ATRP, a thermal radical initiator, e.g., AIBN is utilized to regenerate the activating Cu<sup>I</sup> species continuously. ICAR ARGET was very recently utilized in a polymerization-induced self-assembly process (PISA) in ethanol.<sup>59</sup> Indeed, regular ARGET was employed in PISA before but suffered from the remaining amounts of copper in the final particle emulsion. Crosslinker were added to the formulation to extract the copper during dialysis, which clearly impacted the obtained morphologies. Since polymerization at later stages during PISA is located within the hydrophobic core the Cu<sup>I/II</sup>/L complexes have to be present within the loci of polymerization, which strongly affects PISA. Utilizing ICAR ATRP allowed to circumvent these disadvantages and polymerization at ambient temperature or 65 °C for 48 h resulted in controlled polymerizations of benzyl methacrylate. The emulsions were then analyzed by TEM confirming the fabrication of nanostructures *via* ICAR ATRP/PISA.

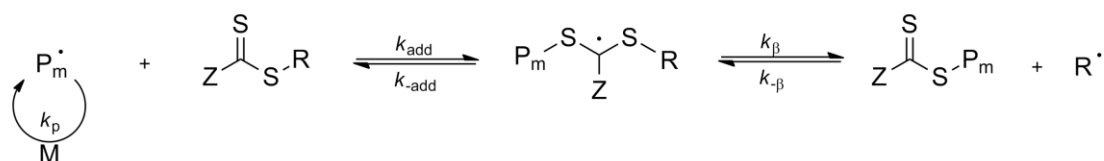
### 2.1.5. Reversible Addition-Fragmentation Chain Transfer (RAFT) Polymerization

Reversible addition-fragmentation chain transfer (RAFT) polymerization is another major RDRP technique which was introduced in 1998 by Moad, Rizzardo, and Thang at CSIRO.<sup>60</sup> The mechanism of RAFT polymerization differs greatly from NMP and ATRP, where for the latter the control is achieved by the persistent radical effect. This leads to dormant polymer chains, a reduced radical concentration, and a reduced polymerization rate as compared to free radical polymerization. However, in RAFT polymerization the control over the reaction is achieved by a chain transfer process. The generally accepted mechanism is depicted in Scheme 8.

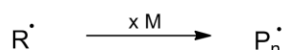
#### Initiation



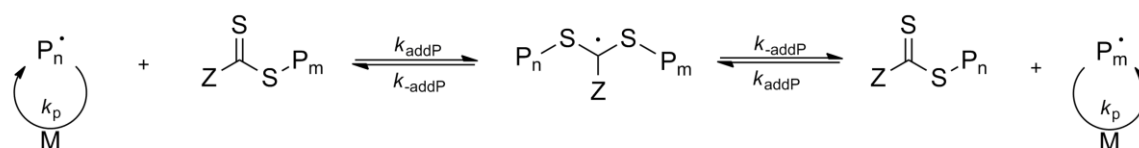
#### Reversible chain transfer (pre-equilibrium)



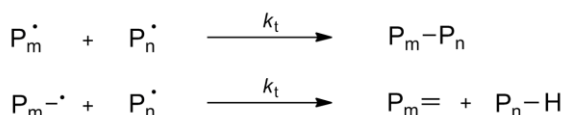
#### Reinitiation



#### Chain equilibrium



#### Termination

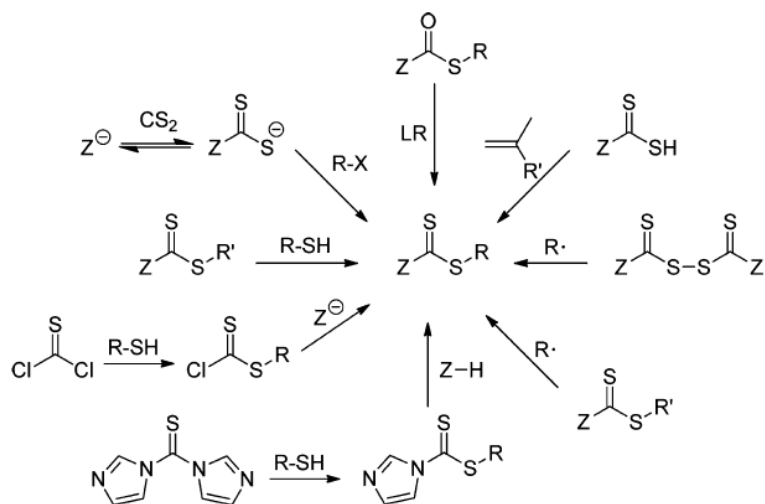


**Scheme 8.** Reaction scheme of the RAFT polymerization mechanism.

The first step of the RAFT process is the generation of radicals either by decomposition of a suitable initiator or by photochemical stimulation of the chain transfer agent (CTA).<sup>61</sup> The radicals propagate with monomer units and react with the C=S double

bond of the thiocarbonylthio compound in an equilibrium reaction forming an intermediate radical species. This intermediate may fragment back to the original RAFT agent or split into an oligomeric RAFT agent and a reinitiating radical R *via*  $\beta$ -scission. During reinitiation the radical R initiates propagation and the resulting macroradical  $P_n$  can subsequently add to the macro RAFT agent in the chain equilibrium. The rapid interchange ( $k_{addP} = 10^6$ - $10^8$  M<sup>-1</sup> s<sup>-1</sup>) in this step ensures that the concentration of propagating radical chains is kept lower than that of the stabilized radical intermediates limiting termination reactions.<sup>62</sup> Still, termination of propagating chains can occur through combination or disproportionation similarly to free radical polymerization. Even though the RAFT mechanism is generally accepted, there is an ongoing debate on the detailed kinetics of the process, i.e., the rapidity with which the various equilibria are established, and what side reactions might occur. A possible side reaction, which results in the retardation of the process, is fragmentation of the intermediate radical species. If fragmentation is slow, the intermediate radical species may be consumed during the reaction either by a propagating radical or by self reaction with another intermediate radical, forming star polymers.<sup>63</sup>

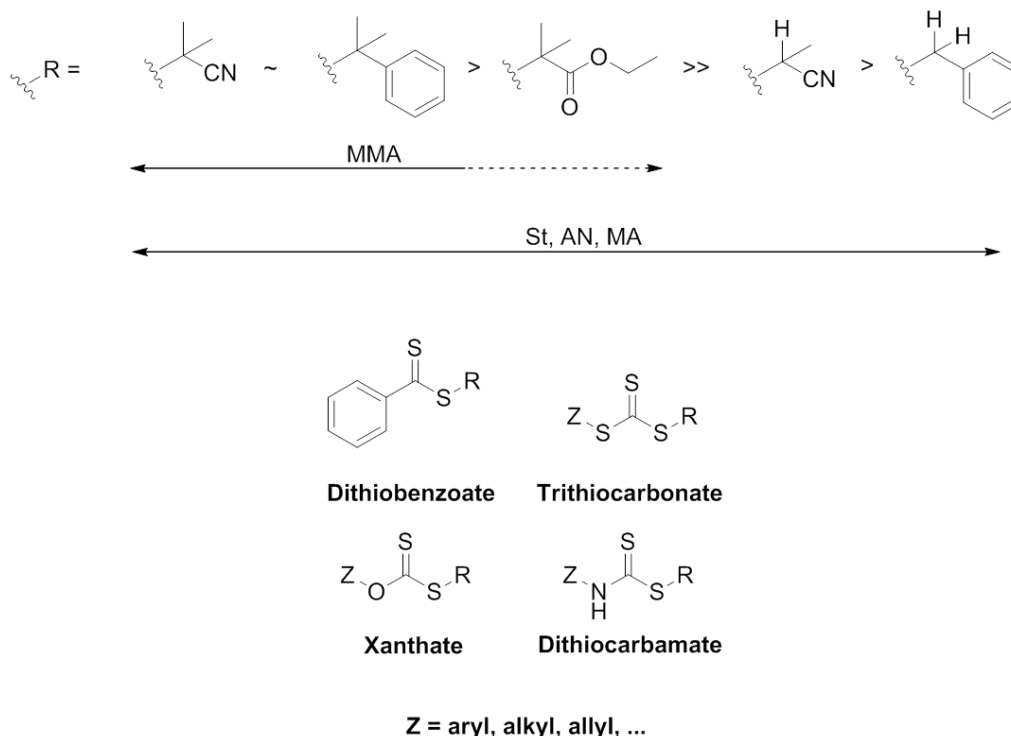
Chain transfer agents can be synthesized by various methods, as depicted in Scheme 9. The most widely applied method is the reaction between a thiocarbodithioate salt and an alkylating agent (R-X) since all forms of RAFT agents can be obtained this way. Alkyl and aryl carbodithioates as dithioester precursors are typically prepared by Grignard reagents (e.g., PhMgBr) with carbon disulfides. On the other hand, trithiocarbonates require the reaction of a precursor Z-H with often a 2–3-fold excess of carbon disulfide in presence of a base, yet stoichiometric carbon disulfide has been shown to result in near-quantitative yields.<sup>64</sup> The preparation of xanthates and dithiocarbamates generally involves strong inorganic bases (e.g., sodium hydroxide, sodium hydride) to form the carbodithioate salts due to low pK<sub>a</sub> values for alcohols and amines. In general, the yield of RAFT agent synthesis is strongly dependent on the structure and reactivity of Z<sup>-</sup>. Poor nucleophilicity of Z<sup>-</sup> can drastically lower yields since additions to carbon disulfides are obstructed.



**Scheme 9.** Schematic depiction of main methods utilized for chain transfer agent synthesis (R-X = Alkylating agent, LR = Lawesson's reagent or equivalent). Adapted with permission from ref<sup>65</sup>. Copyright 2012 American Chemical Society.

Based on the mechanism of the RAFT process, the R and Z group have a significant influence on the success of the polymerization. The R group must be able to stabilize a radical sufficiently to be released from the intermediate radical and must efficiently reinitiate the polymerization ( $k_i > k_p$ ). Therefore, the ability of certain RAFT agents to polymerize specific monomers is highly dependent on the R group with respect to its steric/radical stability and polar effects. While reactive monomers such as styrene or acrylates are more resilient to the choice of radical, other monomers like MMA require either cumyl or cyanoisopropyl based R groups for efficient reinitiation, as reported by Chong *et al.*<sup>66</sup> As a result, RAFT agents are designed to feature structural motifs and electronic properties in their R group similarly to the employed monomer in order to increase the reinitiation capability of expelled radicals. On the other hand, the Z group should ideally activate the C=S double bond towards radical addition but offer only minimal stability to the formed radical intermediate. If the stabilizing effect is too dominant, fragmentation to propagating radical species is impeded, which results in a retardation of the polymerization. Hence, the Z group has to be chosen according to the reactivity of the monomer. Exemplary, RAFT polymerizations of highly reactive monomers such as vinyl acetates are only efficiently mediated by xanthates and dithiocarbamates due to destabilization of the radical intermediate. Still, the two most employed structural motifs of chain transfer agents are dithiobenzoates and

trithiocarbonates which are commercially available with various R and Z groups (Scheme 10).



**Scheme 10.** Chemical structure of various RAFT agents and a selection of R groups for the polymerization of industrial relevant monomers. Fragmentation rates increase and addition rates decrease from left to right. Dashed lines indicate only partial control over the polymerization. MMA = methyl methacrylate, St = styrene, AN = acrylonitrile, MA = methacrylate.

While specific functionalities and properties can be introduced to a RAFT polymer by the choice of monomers, the design of the R and Z groups of the RAFT agent or postpolymerization modifications offer an additional route towards tailored polymer functionalities. Therefore, intense research has been conducted to synthesize novel RAFT agents. Among the most important functional end-groups for conjugation are carboxylic acid and hydroxyl groups. While Lai *et al.* reported the synthesis of various carboxyl functionalized trithiocarbonates, which demonstrated good control over the polymerization of monomers such as styrene, acrylate and acrylamide,<sup>67</sup> Moad and co-workers developed dithioester RAFT agents with the carboxylic functionalities for the polymerization of MMA.<sup>68</sup> A common approach to couple peptides or proteins *via* their

respective amine or hydroxy groups to carboxylic acids is to modify the carboxyl functionality with *N*-hydroxysuccinimide (NHS) resulting in NHS activated ester species. Aqil *et al.* demonstrated the coupling between carboxylic acid functionalized poly(*N*-isopropylacrylamide) (poly(NIPAAm)) using NHS as an activator of the carboxylic acid group which was subsequently coupled with an amine-capped biotin resulting in biotin functionalized poly(NIPAAm), able to conjugate with avidin and streptavidin.<sup>69</sup> Utilizing NHS in the presence of DCC and DMAP led to the formation of activated ester dithiobenzoates.<sup>70</sup> RAFT polymerization of 4-vinylbenzoic acid (VBC) with the NHS activated chain transfer agent yielded narrow molar mass distributions ( $M_w/M_n = 1.03-1.07$ ). However, the experimental molecular weights were higher than targeted, which was explained with the low efficiency of the modified RAFT agent. Unfortunately, the authors did not exploit the NHS-activated end-group further.

More recently new RAFT agents bearing pyridyl disulfide (PDS) and azide functionalities at either the R or Z group have been synthesized, which allow the direct conjugation to (bio)compounds. PDS functionalized RAFT agents that bind to glutathione or a rhodamine B derivative with a terminal thiol was reported by Davis and co-workers.<sup>71</sup> The RAFT agent was synthesized by nucleophilic substitution of a bifunctional trithiocarbonate with a hydroxy-capped PDS. Homopolymerization of oligo ethylene glycol acrylate (OEGA) and subsequent chain extension with styrene showed good control over the polymerization ( $M_w/M_n < 1.3$ ), indicating that the presence of disulfide bonds did not affect the RAFT mechanism. Successful conjugation between PDS-functionalized polymer and glutathione was confirmed by UV-Vis spectroscopy as a strong absorption band of glutathione at 345 nm appeared. Further investigations by Liu *et al.* demonstrated that PDS-functionalized RAFT polymers can be used to conjugate with thiol functionalities present in biomolecules, such as the free, surface-exposed thiol Cys34 in bovine serum albumin (BSA).<sup>72</sup> Moreover, the conjugation occurs *via* a disulfide bond that can be readily reduced *in vivo* to permit the release of the biomolecule from the synthetic polymer. Utilizing azide-functionalized trithiocarbonates, Sumerlin and co-workers described grafted polymers onto alkyne modified BSA.<sup>73</sup> Homopolymerization of PNIPAAm with the functional chain transfer agent showed pseudo-first order kinetics, a linear relationship between molar mass and conversion and low dispersities. The conjugation of PNIPAAm-N<sub>3</sub> and alkyne modified BSA was performed in phosphate buffer with CuSO<sub>4</sub>/ascorbic acid and resulted in a quantitative immobilization of the

protein as depicted by the molar mass increase in SEC and polyacrylamide gel electrophoresis (PAGE).

The same group reported a different approach towards polymer-protein conjugates in which BSA was coupled to a chain transfer agent prior to polymerization.<sup>74</sup> Grafting to a maleimide-functionalized trithiocarbonate to the free thiol of BSA at room temperature *via* Michael addition gave access to a biohybrid RAFT agent. Subsequent polymerization of NIPAAm in water resulted in thermoresponsive polymer-protein conjugates which were easily separated from unconjugated protein by thermal precipitation. After treatment of polymer-protein conjugates with tris(2-carboxyethyl)phosphine hydrochloride (TCEP), SEC analysis revealed reasonable molar mass control during the reaction ( $M_w/M_n = 1.38$ ). Furthermore, circular dichroism and activity assays of BSA-CTA and BSA-PNIPAAm showed no notable effect on the secondary structure of the enzyme. More than 90% of the enzymes activity was maintained as compared to native BSA.

In conclusion, RAFT is one of the most versatile processes as it tolerates a wide variety of reaction conditions, functional groups, numerous monomers and offers multiple ways to synthesize functional polymers for biological applications.

## 2.2. Polymerization-Induced Self-Assembly (PISA)

With the ongoing developments of controlled/living radical polymerization (CRP) techniques over the past two decades well-defined polymer architectures, such as diblock copolymers, became readily available. Amphiphilic block copolymers are of particular interest due to their self-assembly behavior in water and other polar solvents, which has been extensively studied over the past 30 years. In the early 1990's, Eisenberg and co-workers reported the first self-assembly of well-defined amphiphilic block copolymers of poly(4-vinylpyridine)-polystyrene (P4VP-PS) diblock copolymers made by anionic polymerization by dissolving them in DMF and continuously adding water.<sup>75</sup> This self-assembly process is known as nanoprecipitation (or co-solvent method, or solvent displacing method) and is a straightforward approach towards amphiphilic nanoparticles (NPs). In general, an amphiphilic block copolymer is dissolved in a polar organic solvent, such as alcohols, THF, or DMF and the resulting solution is then gradually added into a large amount of water in which the organic solvent is readily miscible. During the addition, the hydrophobic block segments of the polymer will collapse inducing the formation of particles. Afterwards the organic solvent can be removed by evaporation or dialysis. The reverse process can also be applied, i.e., adding water to the solution of block copolymers. The obtained nanoparticle dispersions display unimodal size distributions in the range of 50-300 nm.<sup>76</sup> These particle sizes are crucial for potential pharmaceutical and biomedical applications. For example, biodegradable nanocarriers smaller than 100 nm demonstrated fewer uptake by macrophages of the reticuloendothelial system (RES) while being large enough to pass through vasculature of some tumors and accumulating in the target tissue based on the enhanced permeation and retention effect (EPR).<sup>77-78</sup> Nanoprecipitation can also be utilized for the encapsulation of hydrophobic drugs or proteins through coprecipitation with amphiphilic polymers such as poly(lactide-co-glycolide) (PLGA) in water leading to drug/protein-loaded nanocarriers.<sup>79-80</sup>

While nanoprecipitation offers a facile route towards amphiphilic nanoparticle dispersions, it suffers from practical limitation which can result in flocculation of particles and formation of coagulated aggregates. Furthermore, spherical nanoparticles are the favored morphologies during the phase separation making higher order morphologies such as worms/fibers or vesicles inaccessible. Furthermore,

nanoprecipitation only leads to rather low concentrations of polymeric nanoparticles (typically, 1-2 wt%)

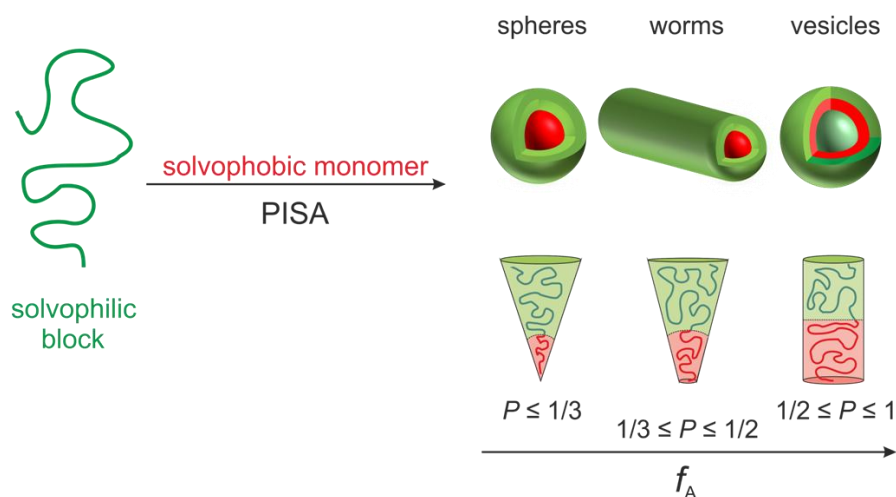


**Figure 1.** Various morphologies achieved by PISA with increasing packing parameter  $P$ .

A more elegant approach towards the synthesis of nanoparticles that has gained significant interest during the last 10 years is polymerization-induced self-assembly (PISA).<sup>81</sup> As the name suggests, the PISA process involves the formation of nanoparticles simultaneously to the polymerization: a macromolecular hydrophilic block segment is chain extended with a hydrophobic monomer in a polar solvent. The growth of the solvophobic block leads to a gradual insolubility of the polymer which drives the *in situ* self-assembly into AB diblock copolymer nano-objects (Figure 1). PISA operates through an emulsion or dispersion polymerization mechanism. In emulsion polymerization, water is the continuous medium and a hydrophobic monomer (which still exhibits a small solubility in water) with a water-soluble macroinitiator or macro chain transfer agent are employed. Once block copolymers start to nucleate into sterically stabilized nano-objects, polymerization continues within the particles as monomers diffuse into the core. In dispersion polymerization, all initial components, including the monomer, are soluble in the continuous medium. However, with increasing chain length the polymer becomes insoluble and forms particles through nucleation of the amphiphilic block copolymers. While any CRP technique is suitable for PISA, the vast majority of examples found in recent literature is based on RAFT-mediated polymerizations.<sup>82-85</sup> Even though NMP and ATRP-mediated PISA formulations are employed and show little

to no difference in terms of nanoparticle morphologies compared to RAFT PISA, both CRPs have distinct disadvantages based on their higher polymerization temperatures and incomplete conversions or the contamination by transition metals.<sup>86-89</sup>

In contrast to nanoprecipitation, PISA offers access to a greater variety of possible nanoparticle morphologies in fewer steps and at significantly higher concentrations. The *in situ* self-assembly of diblock copolymers in dispersed media *via* PISA allows the synthesis of not just spherical nanoparticles exclusively but also high order morphologies such as worms/fibers,<sup>90</sup> vesicles,<sup>91</sup> as well as lamellae<sup>92</sup>, and other unusual nanostructures.<sup>93-94</sup> Yet, the actual mechanism of PISA is complex as various parameters can have a significant influence on the accessible structures and even sometimes contradict expected behavior.<sup>95</sup> One of the most important parameters for the assembly of amphiphiles is the packing parameter  $P$ :

$$P = \frac{V_0}{a * l_c} \quad (1)$$

$V_0$  = volume of hydrophobic segment,  $a$  = interfacial area of block junction,  $l_c$  = length of hydrophobic segment.

In an equilibrium state the formation of morphologies is mainly determined by the interfacial energy between the two block segments and chain stretching of the volume fractions  $f_A$  of the copolymer. In order to minimize the total interfacial energy, the block segments stretch away from a favored coiled chain conformation to reduce the interfacial area. Therefore, if the hydrophobic block is smaller than the hydrophilic, the block copolymer assembles into a spherical core-shell structure ( $P \leq 1/3$ ) (Figure 1). This state is energetically favored as compared to other morphologies since the interfacial area of the system, and hence its interfacial energy, is at a minimum. The gain in enthalpy of the lowered interfacial energy surpasses the loss in entropy when polymer chains are forced to stretch. As the volume fraction of the hydrophobic segment during the polymerization grows, the curvature of the spheres decreases, forcing the polymer chains to rearrange to minimize the entropically unfavorable stretching, which in turn leads to morphological changes from worms/fibers ( $1/3 \leq P \leq 1/2$ ) to vesicles ( $1/2 \leq P \leq 1$ ). While this represents the mechanism for a thermodynamically preferred equilibrium state, kinetically-trapped spherical

nanoparticles have been observed in many aqueous PISA formulations, which is not yet fully understood.

The monomer concentration, hence the final polymer/nanoparticle concentration, during PISA is another crucial factor, especially in dispersion polymerizations. RAFT PISA with the water-miscible 2-hydroxypropyl methacrylate (HPMA) at solid contents lower than 10 wt% resulted in the expected spherical structures, while increasing the degree of polymerization ( $DP_n$ ) lead to no morphological changes. However, increasing the monomer concentration to 20-25 wt% resulted in pure worm and vesicle phases at the same  $DP_n$ s.<sup>96</sup> This drastic change can be explained with the high concentration of polymer particles within the reaction medium. Since the first step towards worm and subsequent vesicle formation is the fusion between multiple particles due to inelastic collisions, a higher concentration leads to higher order morphologies. Finally, the molar mass of the hydrophilic block segment plays an important role during structural formation. Armes and co-workers have demonstrated the influence of  $DP_n$  for a solphophilic poly(glycerol monomethacrylate)-based macroCTA.<sup>97</sup> With a macro chain transfer agent possessing a sufficiently low  $DP_n$  phase-pure transitions were achieved independent of the monomer concentration. This effect is explained with an increasing efficiency of the steric barrier with growing molar mass of the particle-stabilizing macroCTA. At lower masses, i.e., with a lower steric barrier, the formed nanoparticles fuse together more readily to form other morphologies.

Among the disadvantages and limitations of PISA is the lack of morphological reproducibility if no well-documented phase diagram of the polymer system is available. Therefore, it is crucial that a large single batch of macroCTA or macroinitiator is available to establish a phase diagram since different molar masses of the stabilizing segment would likely result in inaccurate phase spaces. While the packing parameter  $P$  offers a simple concept to understand phase transitions during PISA, it is not possible to anticipate the morphologies of final copolymers using the packing parameter as a result of the different relative degrees of solvation of hydrophilic and hydrophobic block segment. In the same regard, it still remains unknown why many aqueous PISA formulations only lead to spherical morphologies even when performed at high solid concentrations. In the case of RAFT-mediated PISA, the system may undergo undesired homogenous nucleation because of the required water-soluble radical initiator. If the macro chain transfer agent concentration is too low, the formed radical species of the

water-soluble initiator will add onto the hydrophobic monomer which in turn precipitates as hydrophobic homopolymer.

Still, the aforementioned experimental control over various morphologies and the resulting new applications, e.g., biocompatible hydrogels or drug-carriers make PISA one of the most popular state-of-the-art techniques in current polymer research.<sup>98-99</sup>

### **2.2.1. Surface-Functionalized PISA Objects**

Currently, the main scientific focus regarding PISA is the exploration of morphological phase transition with various monomers. Many research groups such as those of Charleux, Armes, Lowe, Pan, and Zhang have dedicated substantial effort in the investigation of amphiphilic block copolymer systems by PISA. However, while phase transition changes have been demonstrated for multiple diblock copolymer systems, the full scope of PISA has yet to be explored since PISA offers a facile route towards functionalized nano-materials with tunable properties. Such surface-functionalized materials based on diblock and triblock copolymers are of great interest for biomedical and technological applications as they can be applied as nanocarriers,<sup>100</sup> drug-delivery systems,<sup>101-102</sup> and nanoreactors.<sup>103-104</sup> Therefore, well-controlled polymerizations of complex polymers in various polar and non-polar media make PISA an ideal process for functionalized polymer materials. In general, functionality or reactivity of PISA nano-objects can be introduced in the hydrophilic corona or the hydrophobic core through a functional group on the  $\alpha$ -end of the polymer chain or a functional monomer. Since RAFT polymerization is the most commonly employed RDRP in PISA, RAFT agents may be functionalized before or after polymerization for this purpose. Aminolysis of the thiocarbonylthio groups enables the facile transformation to free thiols, which can partake in a multitude of reactions. However, in copolymer nano-objects prepared by RAFT PISA the terminal Z-group is located within the hydrophobic core restricting its accessibility. Hence, modification of the R-group of RAFT agents is a common way of introducing functionality to RAFTPISA nano-objects. Even though the synthetic possibilities of obtaining functional PISA nano-objects are quite large, only a limited amount of examples are reported as of yet.

Some examples of core-functional PISA nano-objects based on ketone-, aldehyde-, diphenylphosphine-functionalized and diethylacrylamide monomers have been reported and will be briefly discussed at the end of this section.<sup>105-108</sup> Since surface-functional nanoparticles were the subject of this thesis, surface-decorated PISA nano-objects will be the focus of this chapter.

The simplest and most direct way of introducing a functionality on the outer domain of PISA nano-objects is through the implementation of functional monomers in the solvophilic segment. Among those monomers is methacrylic acid (MAA) which was utilized by Boyer and co-workers.<sup>109</sup> They prepared poly((oligo ethylene glycol) methyl ether methacrylate) (POEGMA) homopolymers ( $M_n = 7200 \text{ g mol}^{-1}$ ,  $M_w/M_n = 1.1$ ) by RAFT polymerization and chain extended the macroCTA with varying  $DP_n$  of MAA (Figure 2). After purification of the copolymer, styrene was used in an alcoholic dispersion PISA to form triblock copolymers ([macroCTA]:[styrene] 1:5000). Successful copolymer formation was confirmed by SEC, which depicted a clear shift towards higher molar masses and  $^1\text{H}$  NMR analysis. Conversions after 42 h were generally quite low (5%) and the formed copolymer showed a large increase in dispersity. However, stopping the polymerization at given time points resulted in different nanoparticle morphologies. These were then mixed with  $\text{Fe}^{\text{II}}$  and  $\text{Fe}^{\text{III}}$  salts at a feed ratio of 1:2 ([carboxylic acid]:[Fe]) in water. Via intra- and intermolecular complexation, the iron salts bound to the carboxylic acid groups of the MAA in the shell and subsequent precipitation with ammonia (25% aqueous solution) lead to the formation of ironoxide nanoparticles whose size depended on the concentration of carboxylic acids units but mostly not on the copolymer morphologies in which it was formed (Figure 2). Iron oxide formation had no influence on the polymer morphologies and TEM as well as MRI measurements revealed the placement of iron oxide particles within the polymeric nanostructures. Similarly to MAA, acrylic acid (AA) and 4-vinylpyridine (4VP) have also been employed as functional monomers by Tan *et al.*<sup>110</sup> They reported the synthesis of copolymers of poly((ethylene glycol) methacrylate) with AA and 4VP in a RAFT-mediated copolymerization. The resulting macroCTAs (10-20 wt%) were then used in a photo-initiated PISA process in ethanol/water for 3 h under at 3 W 365 nm LED lamp with MMA as core-forming monomer and *S*-1-dodecyl-*S'*-( $\alpha,\alpha'$ -dimethyl- $\alpha''$ -acetic acid) trithiocarbonate (DDMAT) as a second, hydrophobic RAFT agent (0.25 wt%). Particle growth up to micrometer ranges was explained with a second polymer growth within

nucleated particles mediated by this secondary hydrophobic RAFT agent. The resulting PMMA microspheres displayed very unimodal distributions as indicated by TEM and were subsequently used as precursors to synthesize Ag/PMMA nanocomposite spheres thanks to the carboxylic acid groups of acrylic acid within the hydrophilic block segment. Furthermore, monodisperse pH responsive microspheres were synthesized based on a pure PAA macro RAFT agent. The PAA-stabilized microspheres precipitated at pH 3 due to the weak solubility of protonated PAA chains but showed high colloidal stability at pH 8.

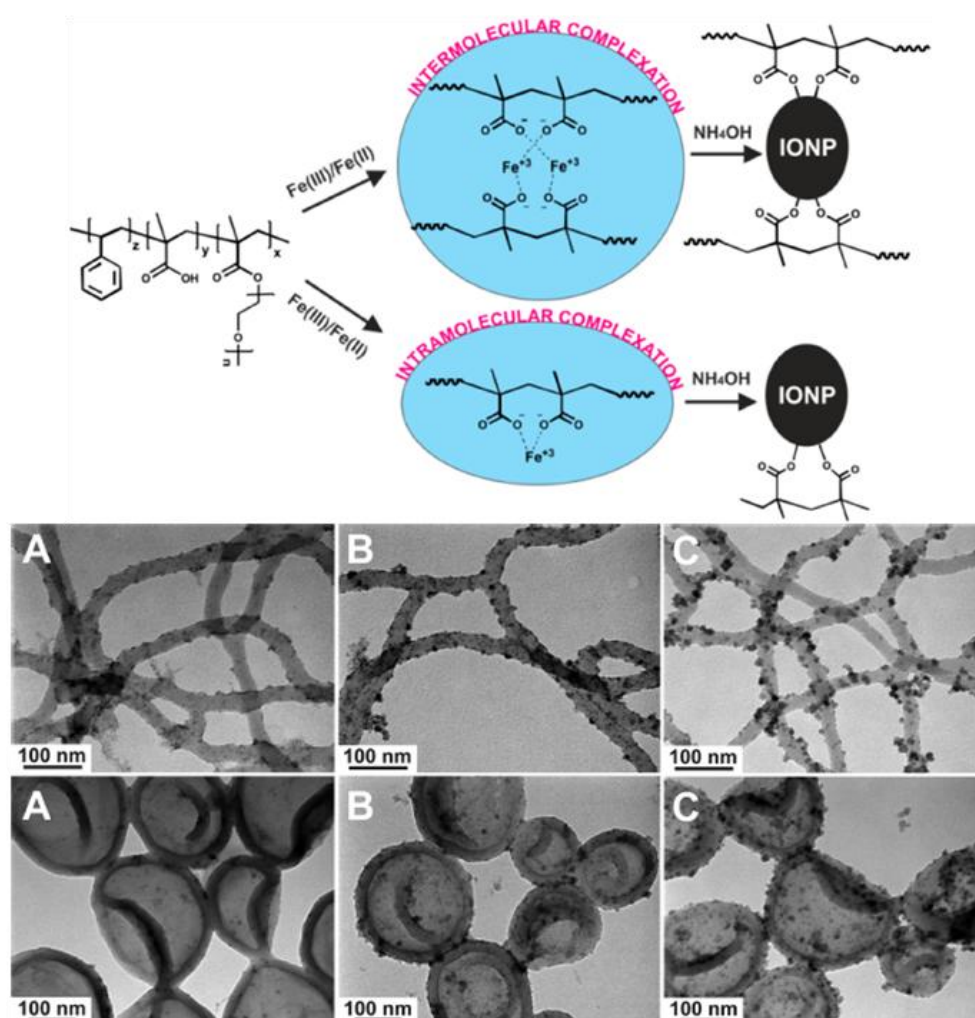


**Figure 2.** (Top) Illustration of iron complexation and iron oxide formation within POEGMA-*b*-PMAA-*b*-PST. (Bottom) TEM images of iron oxide particles/nanocomposite worms and vesicles with varying [MAA]:[Fe] ratio (A) 1:2, (B) 1:4, and (C) 1:6. Adapted with permission from ref <sup>109</sup>. Copyright 2014, American Chemical Society.

Surface-functionalized dialkylphosphonate and phosphonic acid diblock copolymer nano-objects using alcoholic dispersion RAFT PISA were reported by Armes and co-workers,<sup>111</sup> who prepared poly(methacryloyloxymethyl dimethylphosphonate) (PMP) macro RAFT agents with  $DP_n$  24, 32, 42 with good control over the polymerization. Parts of PMP macroCTA were hydrolyzed with trimethylsilyl bromide to obtain poly(methacryloyloxymethylphosphonic acid) (PMPA), which was confirmed by  $^{31}\text{P}$  NMR displaying a phosphor shift from 21.6 ppm to 14.0 ppm. PMP and PMPA macroCTAs (20 wt%) were chain extended in aqueous dispersion PISA with 2-hydroxypropyl methacrylate (HPMA) at pH 5 but only unstable colloidal dispersions with PMA could be obtained. Switching the core-forming block to benzyl methacrylate (BzMA) lead to stable dispersions of PMP-PBzMA in methanol with full conversions and narrow molar mass distributions. TEM analysis confirmed the morphological changes based on the length of macroCTA obtaining micelles, worms, and vesicles for PMP<sub>24-32</sub>. For the PMP<sub>42</sub> macroCTA only spherical nanoparticles were observed due to a higher steric stabilization during BzMA polymerization, which would prevent sphere-sphere fusion. PISA experiments with the hydrolyzed PMPA macroCTA ( $DP_n$  24, 32, 42) under the same conditions resulted mostly in vesicle phases for any macroCTA. Finally, the group demonstrated the effect of  $\text{CaCO}_3$  precipitation in presence of the functional phosphonate suspensions. While non-ionic PMP<sub>24</sub>-PBzMA<sub>300</sub> had little to no effect on the rhombohedra structure of  $\text{CaCO}_3$ , the ionic PMPA<sub>24-42</sub>-PBzMA<sub>45-300</sub> significantly altered the salts morphology resulting in curved edges through occlusion of ionic PMPA in the calcite crystal lattice.

Disulfide-functionalized diblock copolymer worm gels were prepared by RAFT PISA based on PGMA-*b*-PHPMA.<sup>112</sup> One route involved the RAFT polymerization of glycerol monomethacrylate (GMA) with bis(2-(methacryloyloxy)ethyl) disulfide (DSDMA) to obtain PGMA<sub>54</sub>-PDSDMA<sub>0.5</sub> while the second route included a homopolymerization of GMA with a bifunctional disulfide-based dithiobenzoate (DSDB) to afford a disulfide-centered P(G<sub>54</sub>-S)<sub>2</sub> macroCTA (Figure 3). Various molar ratios of either disulfide-based macro RAFT agent ( $M_n$  between 14000 g mol<sup>-1</sup> and 20600 g mol<sup>-1</sup>, respectively) together with pure PGMA<sub>54</sub> macroCTA were used in aqueous dispersion polymerization of HPMA to obtain free-standing gels at room temperature with pure worm phases. To assess the influence of the disulfide bonds on the gel strength, oscillatory rheology studies were conducted with selected gels before and after treatment with a 10-fold excess of

tris(carboxyethyl)phosphine (TCEP) at pH 7 as a disulfide reducing agent. Before TCEP treatment the worm gel moduli  $G'$  and  $G''$  suggested high gel strengths, due to inter-worm linkages within the gels, for both disulfide-functionalized copolymers depending on the mole fraction of disulfide macroCTA. After reduction of the disulfide bonds and hence removal of inter-worm disulfide interactions, the polymer gels became much weaker with comparable gel moduli to non-functionalized PGMA<sub>55</sub>-PHPMA<sub>130</sub> worm gels.

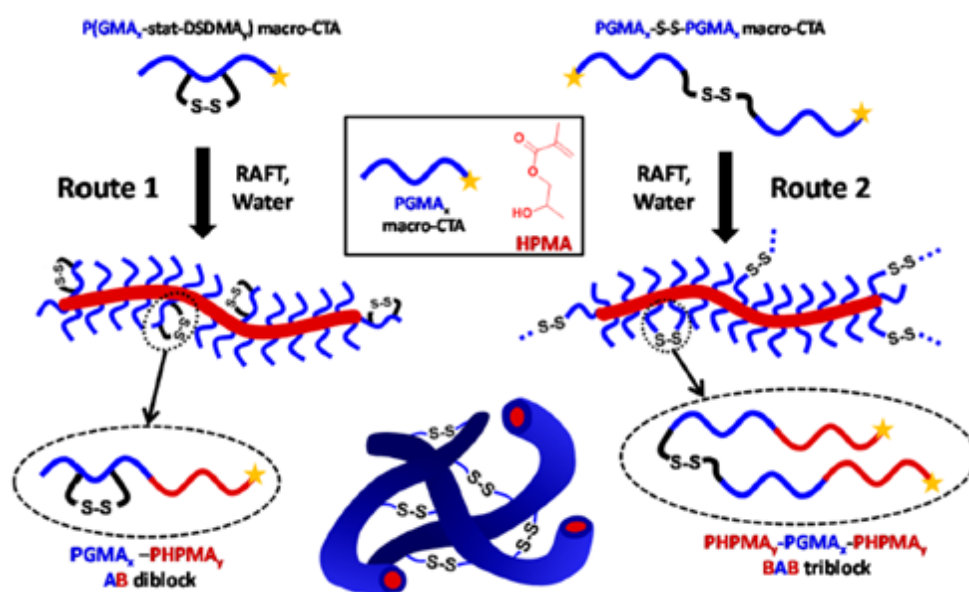


**Figure 3.** (Left) Schematic illustration of disulfide-based diblock copolymer synthesis. Adapted with permission from ref <sup>112</sup>. Copyright 2015, American Chemical Society.

The same group also reported pH responsive PISA objects, yet not based on a functional hydrophilic monomer but on a morpholine end-capped PGMA-PPHMA system.<sup>113</sup> Morpholine-functionalized trithiocarbonate RAFT agents were synthesized and utilized in the homopolymerization of GMA. Subsequent RAFT aqueous dispersion polymerisation of HPMA ( $DP_n$  160) at pH 7 lead to pure worm morphologies. Treatment of the dispersions with HCl triggered a pH-dependent morphology transition from worms (pH 7) to spheres (pH 3) due to the cationic charge of the morpholine which increased the degree of hydration of the PGMA segment and hence reduced the packing parameter  $P$ . This degelation was also confirmed by rheological studies with gel modulus  $G'$  having its maximum at pH 6.8 (342 Pa) and its minimum at pH 3.0 (0.4 Pa). Interestingly, lowering the pH further resulted in a sphere-to-worm regelation which

was weaker than the previous worm gel (48 Pa vs 362 Pa). The authors explained this phase transition with the shielding of cationic charges of the morpholine end-groups by HCl and a decrease in hydration of PGMA. The lower gel modulus was explained with a reduced number of inter-worm contacts due to the electrostatic repulsion of the cationic worms with each other. Yet, lowering the pH back to 7.0 would restore the gel to its original strength (321 Pa vs 342 Pa) making the system almost completely reversible. A stronger focus towards biofunctional nanomaterials for intracellular delivery using galactose-functionalized PISA objects was reported by Ladmiral *et al.*<sup>114</sup> Using a binary mixture of poly(glycol monomethacrylate) (PGMA) and galactose-methacrylate (PGalSMA) (9:1) macro RAFT agents for the aqueous dispersion PISA of HPMA resulted in multiple nano-morphologies depending on the solids wt% and target degree of polymerization of the PHPMA block. Binding assays with galactose-specific lectin RCA<sub>120</sub> and the functional nano-objects were conducted and analyzed by DLS and turbidity measurements. While control experiments with PGMA<sub>51</sub> homopolymer gave no detectable interactions, the PGalSMA functional PISA objects demonstrated very strong interactions with RCA<sub>120</sub>. DLS data proved the formation of large aggregates for PGalSMA functional spheres, worms, and vesicles and that particle morphology influence lectin assay sensitivity since higher order morphologies exhibited a much stronger optical responses than spheres.

In a different approach single electron transfer living radical polymerization (SET-LRP), a technique related to ATRP, was employed to investigate the PISA-mediated synthesis of PMMA-core particles with alginate as the solvophilic segment.<sup>115</sup> Using 30% hydrogen peroxide, commercially available high molar mass alginate ( $M_n = 280000 \text{ g mol}^{-1}$ ) was degraded into lower molar mass alginate ( $M_n = 20000 \text{ g mol}^{-1}$ ), modified with tetrabutylammonium to enhance its solubility in organic solvents, and subsequently reacted with  $\alpha$ -bromoisobutyric acid to afford a hydrophilic alginate-Br initiator. The alginate macroinitiator was then chain extended with MMA using copper wire and Me<sub>6</sub>TREN in a water/methanol solvent system at 25 °C for 4 h ([MMA]:[alginate-Br]:[Me<sub>6</sub>TREN] = 1000:1:20). DLS analysis of alginate-PMMA showed micelle sizes above 300 nm with narrow size distributions ( $PDI < 0.2$ ). TEM investigations confirmed the formation of monodisperse micelles with no other morphologies being present.

Similar to alginate as a natural polymer for particle stabilization, reactive PISA objects were published very recently by Liu *et al.* who reported human serum albumin (HSA)

protein-polymer conjugates *via* aqueous PISA.<sup>116</sup> HSA bearing a single free cysteine group (Cys 34) allowed for a site-specific Michael addition with a maleimide-functionalized hydrophilic ATRP initiator (DBMP) (Figure 4). The HSA-initiator conjugate (HSA-Br) was successfully synthesized as confirmed by electrospray mass ionization spectrometry (ESI-MS) and was subsequently used in HPMA ATRP PISA with various targeted  $DP_n$  in phosphate-buffered saline (PBS) at 4 °C. SEC analysis of hydrolyzed PHPMA of the protein-polymer conjugate indicated reasonably narrow molar mass distributions ( $M_w/M_n < 1.4$ ). Furthermore, DLS and TEM investigations revealed the formation of PISA nano-objects ranging from phase-pure spheres to worms and vesicles, as well as mixed phase systems depending on the  $DP_n$  of PHPMA. Finally, the protein hydrolytic activity towards *p*-nitrophenyl acetate, a well-known substrate for HSA, was demonstrated by monitoring with a UV-Vis spectrophotometer at 400 nm. Comparing the hydrolytic activity of HSA-Br and HSA-PHPMA to free HSA indicated that neither the attachment to the ATRP initiator nor ATRP PISA had a substantial negative influence on the protein activity, as hydrolytic activity deviated only insignificantly. Circular dichroism (CD) scans displayed the intact secondary structure of conjugated HSA after each reaction step. Hence, the authors demonstrated that preformed polymer conjugation with a hydrophilic initiator and subsequent aqueous PISA resulted in surface-reactive protein-polymer nano-objects.

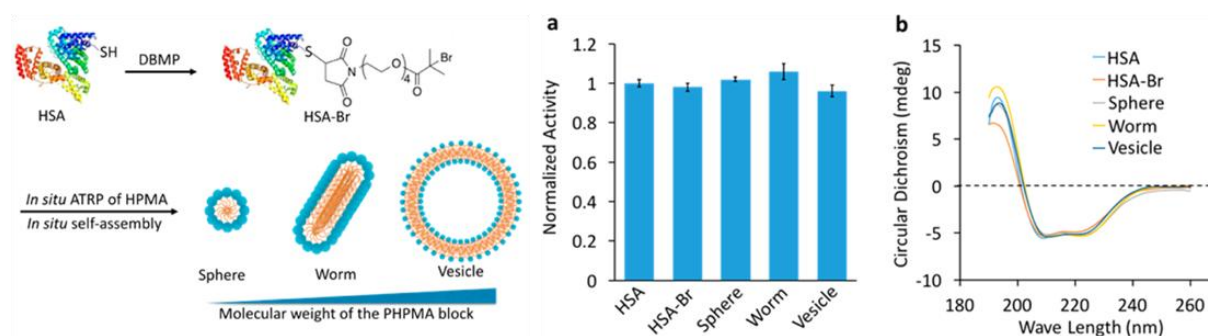


**Figure 4.** (Left) Synthesis of HSA-functionalized ATRP initiator and corresponding formation of nanomorphologies by ATRP PISA. (Right) HSA activity during various states of synthesis/different morphologies and consistency of secondary structure indicated by circular dichroism. Adapted with permission from ref <sup>116</sup>. Copyright 2017, American Chemical Society.

In contrast to simple surface functionality, surface reactivity enables direct synthetic modifications of nanoparticles. Possibly the first report on such surface-reactive PISA objects was by Stucky and co-workers who synthesized azide-functionalized nanospheres by microwave-assisted aqueous dispersion PISA.<sup>117</sup> An azide-functionalized trithiocarbonate RAFT agent was prepared and utilized in homopolymerization of poly(*N,N*-dimethylacrylamide) with good control over chain growth. RAFT PISA of *N*-isopropylacrylamide (NIPAAm) in the presence of *N,N*-dimethylacrylamide afforded PDMA<sub>128</sub>-PNIPAm<sub>200</sub> diblock copolymer crosslinked nanospheres (*Z*-*av.* = 65 nm) with surface-displayed azide-functionality. While the authors also demonstrated core-functionalization with fluorescein *O*-acrylate of the RAFT end-group within the nanoparticles *via* aminolysis/Michael addition, surface reactivity was proven by 1,3-dipolar cycloaddition catalyzed by CuSO<sub>4</sub>/sodium ascorbate between the azide groups and an alkylated dansyl probe. UV-Vis analysis revealed the probe specific absorption bands indicating quantitative conversion on the particles surface.

Surface-functional disulfide-functionalized diblock copolymer worm gels *via* PISA were previously reported by Armes and co-workers (*vide supra*), who also demonstrated surface-reactivity of a similar system by thia-Michael addition.<sup>118</sup> Synthesis of well-defined PGMA<sub>43</sub>-*st*-PDSDMA<sub>1.25</sub> macroCTAs containing small amounts of intramolecular disulfide groups and aqueous RAFT PISA of HPMA led to pure vesicle phases (*Z*-*av.* = 565nm, *PDI* = 0.15) of disulfide-functionalized (PGMA<sub>43</sub>-*st*-PDSDMA<sub>1.25</sub>)-*b*-PHPMA<sub>200</sub> with narrow molar mass distributions ( $M_w/M_n = 1.17$ ), as depicted by TEM and SEC analysis respectively. Reduction of the disulfides to thiols by tributylphosphine led to surface-reactive vesicles which were labeled with a rhodamine B isothiocyanate reagent and visualized by fluorescence microscopy depicting the successful reaction on the vesicles surface. In addition, a thia-Michael addition between the reactive vesicles and 2-[[acryloyloxy]ethyl]trimethylammonium chloride (AETAC) resulted in positively charged vesicles with higher zeta potentials at various pH values as compared to the precursors (Figure 5).

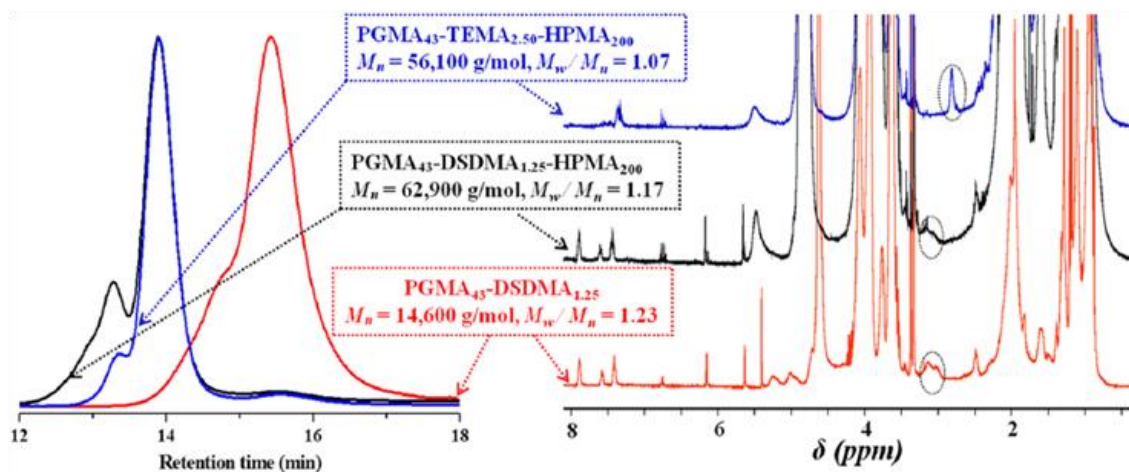


**Figure 5.** (Left) SEC and  $^1\text{H}$  NMR traces of PGMA<sub>43</sub>-*st*-PDSDMA<sub>1.25</sub> macroCTA (red), (PGMA<sub>43</sub>-*st*-PDSDMA<sub>1.25</sub>)-*b*-PHPMA<sub>200</sub> (black) and thiol-functionalized (PGMA<sub>43</sub>-*st*-PTEMA<sub>2.50</sub>)-*b*-PHPMA<sub>200</sub> after reduction (blue). Adapted with permission from ref <sup>118</sup>. Copyright 2012, American Chemical Society.

In a similar approach utilizing BzMA as a hydrophobic core segment, functional poly((methacryloyloxy)ethyl oleate-*b*-benzyl methacrylate) (PMAEO<sub>14</sub>-PBzMA<sub>21-140</sub>) was synthesized *via* RAFT dispersion polymerization in *n*-heptane resulting in pure sphere, worm, and vesicle phases, which could be tuned by  $DP_n$  of PBzMA independently.<sup>119</sup> Post-modification on the reactive surface by thiol-ene reactions with butanethiol, thioglycolic acid, 2-mercaptoethanol, and 2-(Boc-amino)ethanethiol).  $^1\text{H}$  NMR analysis before and after thiol-ene reaction proved the successful coupling by the disappearance of the double bond peaks of PMAEO at 5.3 ppm and the appearance of  $\text{CH}_2\text{-S}$  proton signal at 2.47 ppm. However, for 2-mercaptoethanol, and 2-(Boc-amino)ethanethiol) the conversion were only 60% and 64% respectively, even after 72 h which was explained by the radical quenching of hydroxy groups during the thiol-ene reactions. TEM analysis of the various morphologies after thiol-ene reactions indicated only size increases with no changes to the overall morphologies.

Alkoxysilane-functionalized nano-objects were reported by Thickett and co-workers.<sup>120</sup> 3-(triisopropoxysilyl)propyl methacrylate (IPS) and commercially available 3-(trimethoxysilyl)propyl methacrylate (MPS) were used in a RAFT polymerization to afford the respective homopolymers. Molar mass distributions were especially high for PMPS ( $M_w/M_n > 4.0$ ) due to inter- and intramolecular crosslinking by hydrolysis and condensation of the trimethoxysilane group, which was explained by the time-

consuming purification process prior to analysis leading to the observation of high molar mass peaks. Both macro RAFT agents (10-20 wt%) were further utilized with BzMA ( $DP_n = 100-400$ ) in a RAFT-mediated dispersion polymerization in ethanol at 65 °C up to almost full conversion (> 97%) within 24 h. Vesicles were the most prominent morphology for PMPS<sub>40/65</sub>-PBzMA<sub>100-400</sub> with no pure sphere or worm phases but mixed vesicle + sphere phases for PBzMA  $DP_n < 150$ , while PIPS<sub>40</sub>-PBzMA<sub>400</sub> resulted in kinetically trapped nanospheres with varying sizes (90-280 nm,  $PDI < 0.05$ ) depending on PBzMA  $DP_n$ . To demonstrate the reactivity of alkoxy silane groups within the shell-structure of the nano-objects, a secondary silica shell layer surrounding the polymer nanoparticles was established. Utilizing hydrolysis and condensation of tetraethylorthosilicate (TEOS) lead to an increase in particle size (40-50 nm) and to multi-lobed particles for PIPS<sub>40</sub>-PBzMA<sub>400</sub> as depicted by TEM and SEM analysis. The same reaction parameters however did not seem to have a significant influence on the morphologies and sizes of PMPS<sub>40</sub>-PBzMA<sub>400</sub> possibly due to less efficient hydrolysis of TEOS on the PMPS surface.

Based on a trithiocarbonate RAFT agent holding two TEMPO-alkoxyamine moieties, D'Agosto and co-workers synthesized alkoxyamine-functionalized triblock copolymers to investigate surface-initiated NMP.<sup>121</sup> A trifunctional RAFT agent, with two alkoxyamine end-groups, showed good control ( $M_w/M_n = 1.2-1.3$ ) over the RAFT polymerization of PAA homopolymers in water or dioxane. <sup>1</sup>H NMR revealed a high degree of end-capped alkoxyamine groups on the macro RAFT agent (98%). Subsequent RAFT PISA in water (pH 3.1) with either *n*-butyl acrylate (BMA) or styrene as hydrophobic block segments was carried out with the alkoxyamine macroCTA ( $M_n$  around 8000 g mol<sup>-1</sup>), resulting in turbid latex dispersions of pure nanospheres. Finally, the particles surface reactivity was demonstrated by surface-initiated nitroxide-mediated polymerization of styrene and hydrophilic sodium 4-styrene sulfonate (SSNa). NMP with styrene at 130 °C in water under pressure (3 bar) lead to a large increase in molar mass distribution ( $M_w/M_n = 1.8$ ) and particle size (34 nm to 120 nm) due to the involvement of the trithiocarbonate group during the polymerization. On the other hand, utilizing SSNa in the surface-initiated NMP (20 % conversion) resulted only in a slight increase in particle sizes (50 nm to 72 nm). SEM and EDX analysis depicted the formation of rough spheres after NMP as well as an increase in sulfur content on the surface originally from the SSNa units. At 40% conversion a phase transition of particles

to connected nanofibers and vesicles was observed. The authors explained this morphological transition with a change in balance of hydrophilic/hydrophobic character of the multiblock PSSNa-PAA-PS-PAA-PSSNa copolymer and the high reaction temperature during NMP that softened the PS-core segment. Utilizing the same alkoxyamine-functionalized RAFT agent and the same monomer system, surface-initiated NMP on larger PAA-PS-PAA triblock copolymers was reported.<sup>122</sup> RAFT PISA of styrene in water/methanol (70/30 v/v) at 80 °C using alkoxyamine-PAA<sub>300</sub> macroCTA ( $M_n = 12100 \text{ g mol}^{-1}$ ,  $M_w/M_n = 1.29$ ) led to very large nanospheres with hydrodynamic diameters ranging from 84-238 nm, depending on the  $DP_n$  of PS ( $M_w/M_n = 1.68$ -2.24). Surface-initiated NMP of SSNa from PAA<sub>150</sub>-PS<sub>1800</sub>-PAA<sub>150</sub> nanospheres in water at 130 °C (4 bar) resulted in 255 nm PSSNa-coated particles and an increase in sulfur content in the outer shell as indicated by EDX. This publication demonstrated the surface-reactivity of PISA objects and confirmed the aforementioned results by D'Agosto.

Lowe and co-workers reported the surface reactivity of pentafluorophenyl methacrylate-containing nano-objects *via* RAFT PISA in non-polar solvents.<sup>123</sup> Therein, 12 mol% pentafluorophenyl methacrylate (PFPMA) was copolymerized with stearyl methacrylate (SMA) resulting in well-defined statistical copolymers. RAFT PISA of 3-phenylpropyl methacrylate (PPMA) (20 wt%) in non-polar *n*-octane or *n*-tetradecane with various targeted degrees of polymerization of the core-forming segment resulted in PISA-typical morphological changes from spheres to vesicles. P(SMA<sub>36</sub>-*st*-PFPMA<sub>2</sub>)-*b*-P(PPMA<sub>79</sub>) spherical nanoparticles were reacted with a 80-fold excess of various primary amines (e.g., benzylamine, tetrahydrofurylamine) for 7 days in *n*-octane (50 °C) through the PFPMA residues in the solvophilic block. Successful coupling led to the appearance of small molecule pentafluorophenolate as determined by <sup>19</sup>F NMR and a slight increase in molar mass distributions due to disulfide-coupling of copolymers during the aminolysis of the RAFT end-group within the core for all reactions. Furthermore, FTIR spectroscopy revealed the absence of aromatic C-C stretching bands at 1530 cm<sup>-1</sup> of pentafluorinated aromatics and the appearance of amide C=O bands at 1650 cm<sup>-1</sup> confirming successful surface reactions. Previously, the same group reported a similar approach with Passerini-synthesized PFP-based methacrylic monomers for surface reactions.<sup>124</sup> Copolymerization of these monomers with 2-(dimethylamino)ethyl methacrylate (DMAEMA) resulted in functionalized macro RAFT agents that were

utilized in alcoholic RAFT PISA of PPMA, leading to the full range of nanomorphologies. Surface reactions of the PFP functionality with various thiols (e.g., 1-thio- $\beta$ -D-glucose) was investigated and confirmed by  $^1\text{H}/^{19}\text{F}$  NMR and FTIR through the absence of fluorine in para position and formation of thioether glycopolymer nano-materials. Interestingly, the modification had no effect on the morphology of spheres but modified worms transformed into mixed phases of spheres and worms as depicted by TEM images.

A stronger focus on worm and rod-like nano-objects obtained by RAFT dispersion polymerization with multiple surface functionalities ranging from alkyne, pyridyl disulfide, dopamine,  $\beta$ -thiolactone, to biotin groups has been reported.<sup>125</sup> Trithiocarbonate-based RAFT agents bearing the aforementioned functionalities were utilized in RAFT polymerizations of NIPAm which resulted in functional PNIPAm ( $M_n$  between 5100 and 5510  $\text{g mol}^{-1}$ ) macroCTAs with very narrow molar mass distributions ( $M_w/M_n < 1.12$ ). RAFT PISA of styrene in water with various mixtures of functionalized macro RAFT agents were conducted at 70 °C for 3.5 h. PISA reactions generated narrow monodisperse particle dispersions of PNIPAm<sub>42-46</sub>-PS<sub>31-42</sub> diblock copolymers and exhibited narrow molar mass distributions ( $M_w/M_n < 1.2$ ). After addition of small amounts of toluene (20  $\mu\text{L}/\text{mL}$  latex solution), the dispersions were cooled to 15 °C leading to a temperature-directed morphology transition from spheres to worms. Afterwards, the functionalized worms were cut into 150 nm nanorods by an ultrasound method and analyzed by SEC and TEM (Figure 6). Successful coupling experiments with their respective substrates (e.g., CuAAC click with PNIPAm-N<sub>3</sub>, disulfide exchange with pyridyl disulfide) for single-functionalized and multifunctional worms and rods were performed and confirmed by various characterization methods such as proton NMR, UV-Vis and confocal microscopy.

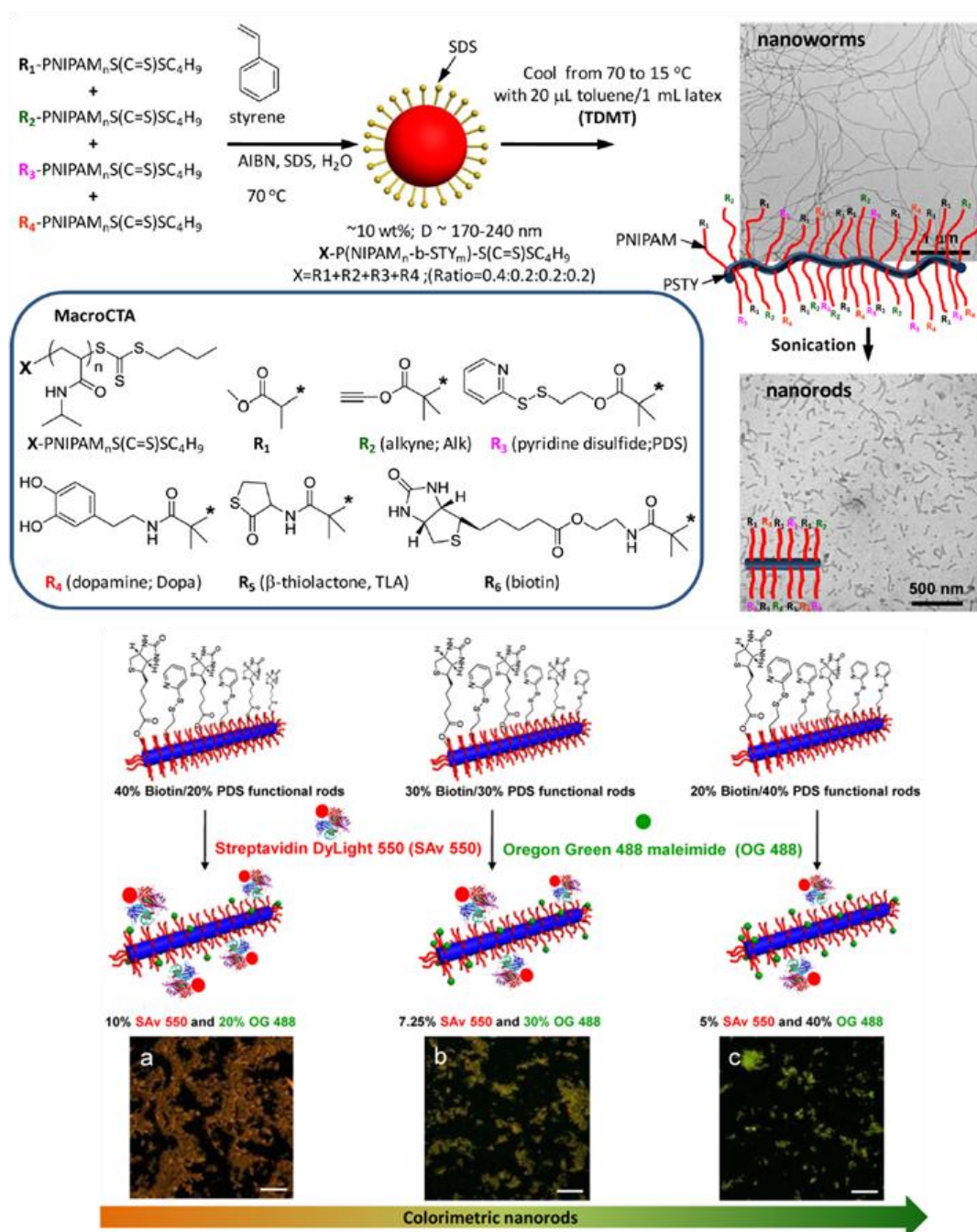


**Figure 6.** (Top) Route towards multifunctional nanoworms and nanorods *via* functionalized RAFT agents. (Bottom) Bioorthogonal conjugation of functional nanorods and fluorescent proteins. Adapted with permission from ref <sup>125</sup>. Copyright 2014, American Chemical Society.

In the area of cross-functionalized PISA nano-objects, core cross-linked micelles (CCM) catalysts based on 4-diphenylphosphinostyrene (DPPS) core-segments were synthesized by RAFT-mediated emulsion polymerization.<sup>107</sup> P(MAA-*co*-OEMA)

macroCTAs were employed to copolymerize styrene, DPPS, and DEGDMA, the latter operating as a cross-linker. DLS and TEM measurements pointed at spherical nanoparticles with diameters ranging between 70-80 nm, while  $^{31}\text{P}$  NMR spectroscopy of the CCM confirmed the incorporation of DPPS in the block copolymer. Subsequently, mass transport to the CCM was investigated by swelling of the micelles at 90 °C with 1-octene and toluene, which resulted in a particle diameter increase and additional proton signals observed by DLS and  $^1\text{H}$  NMR, respectively. Further  $^{31}\text{P}$  NMR analysis spectroscopy revealed that a  $[\text{Rh}(\text{acac})(\text{CO}_2)]$  precatalyst diffused in the particle core and coordinated successfully with the phosphine groups. To explore the catalyst activity, CCM were used as nanoreactors for rhodium-catalyzed hydroformylation of 1-octene under biphasic conditions, demonstrating very high catalytic efficiency and less catalyst deactivation during the reaction.

Delaittre *et al.* employed poly(sodium acrylate) macroalkoxyamine (PNaA-SG1) for the synthesis of pH-responsive nano-objects in the NMP-mediated emulsion polymerization of 4-vinylpyridine (4VP).<sup>126</sup> Complex morphologies such as nanovesicles, worm-like micelles, and multicompartiment micelles were obtained and could be fully dissolved by protonation of the P4VP block at pH 2. Subsequently, increasing the pH to 12 by addition of 1 M NaOH did not lead to the reformation of the initial morphologies but resulted in pure phases of core-shell nanoparticles. A possible explanation of this behavior was that nano-objects acquired during the PISA process represented out-of-equilibrium structure. The same group reported thermoresponsive nano-objects by using PAA-SG1 macroinitiators for the polymerization of *N,N*-diethylacrylamide (DEAAm).<sup>127</sup> Aqueous dispersion polymerization was conducted at 120 °C resulting in nanoparticles with a thermoresponsive core. Due to the thermoresponsiveness of the PDEAAm-core (LCST = 32-34 °C), cooling the system to room temperature turned the particle dispersion into a homogeneous solution of water-soluble block copolymers. Increasing the temperature to 50 °C resulted in the reformation of nanoparticles exhibiting increased particle sizes (Figure 7). When a cross-linker, namely *N,N'*-methylenebis-(acrylamide) (MBAAm), was added to the PISA reaction, the nanoparticles retained their shape in the final dispersion and could not disassemble anymore. Furthermore, the resulting self-stabilized nanogels showed reversible swelling or shrinking properties when temperature changes were applied.

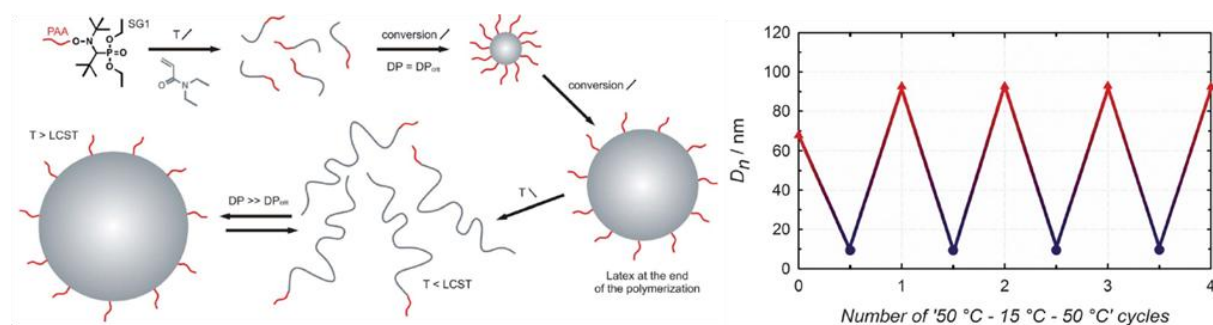


**Figure 7.** Proposed mechanism for PAA-SG1-initiated aqueous dispersion polymerization and evolution of number-average hydrodynamic diameter during cooling and heating cycles of PAA-*b*-PDEAAm. Reproduced from ref. <sup>127</sup> with permission of the Royal Society of Chemistry.

Utilizing 2-(acetoacetoxy)ethyl methacrylate (AEMA) as the core-forming segment in RAFT-mediated dispersion polymerizations, Zhou *et al.* produced keto-functionalized nanospheres and vesicles.<sup>105</sup> Oxime formation through nucleophilic addition of bisoxylamines and the keto-functionalities led to cross-linked nano-objects that retained their morphologies after treatment with  $\text{CHCl}_3$  and DMF. Furthermore,  $\text{Ag}^+$  ions could be complexed by the ketoester groups in the polymer nano-objects and an *in situ* silver nanoparticle formation could be performed by reduction of the complexed  $\text{Ag}^+$  ions with  $\text{NaBH}_4$ . While the morphologies of the polymer nano-objects had no significant influence on the diameter of silver nanoparticles, the silver loading could be further raised by increase of the AEMA/metal ion ratio.

In the same regard, cross-linked and fluorescent nano-objects were reported by Lu and co-workers who used a PHPMA macro RAFT agent for the polymerization of 3-formyl-4-hydroxybenzyl methacrylate (FHMA).<sup>106</sup> Alcoholic dispersion polymerization led to nano-objects with a salicylaldehyde functionality within the core of the particles (Figure 8). Since salicylaldehyde reacts rapidly with hydrazine to salicylaldazine, diluted nanoparticle dispersions were treated with hydrazine hydrate. Cross-linked particles showed only small size increases and demonstrated strong luminescence which was confirmed by fluorescence measurements.

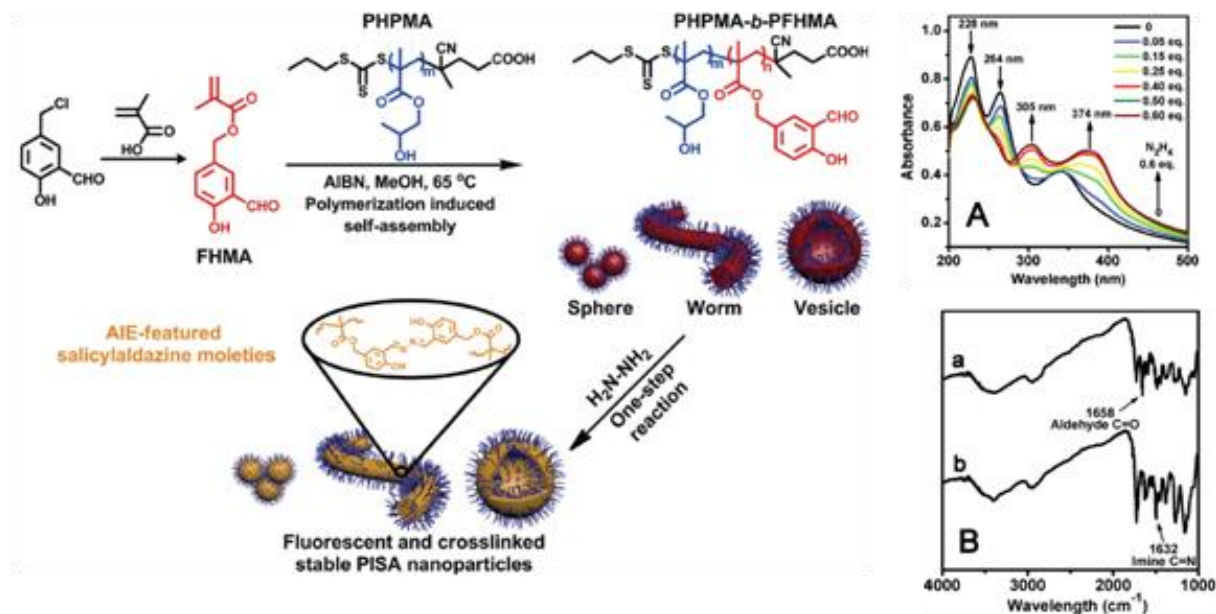


**Figure 8.** Synthetic route of cross-linked stable PHPMA-PFHMA block copolymer nano-objects and UV-Vis spectra (A) of PHPMA-PFHMA copolymer nano-objects upon gradual addition of hydrazine hydrate (0–0.6 eqv. to salicylaldehyde moieties) and FT-IR spectra (B) of the PHPMA-PFHMA copolymer nano-objects before (a) and after cross-linking (b). Reproduced from ref. <sup>106</sup> with permission of The Royal Society of Chemistry.

The solvent influence on the morphology of PISA nano-objects with nucleobase containing core-segments was investigated by O'Reilly and co-workers.<sup>128</sup> In RAFT-mediated dispersion polymerization, a PMMA macroCTA was used to copolymerize adenine- and thymine-containing methacrylate derivatives in either chloroform or 1,4-dioxane. The resulting polymers exhibited reasonably narrow molar mass distributions at conversions above 90% in both solvents. However, copolymerizations in chloroform resulted in spherical micelles exclusively, independent of the degree of polymerization of the nucleobase core-segment while the same reactions in 1,4-dioxane led to spherical micelles and cylindrical worms. This behavior was attributed to the low nucleobase solubility in chloroform in which nucleobase-nucleobase interactions such as H-bonding and  $\pi$ - $\pi$  stacking are the main interactions between monomers and polymers resulting in a lower critical micelle degree of polymerization which negatively affected the chain propagation.

In conclusion, due to the facile synthesis, good control over the final copolymer compositions and decent reproducibility of various nano-morphologies, PISA has become a powerful tool for synthetic polymer scientists. While the field of research is currently focused on utilizing various monomers and investigating the phase transition behavior of these new copolymer compositions, a shift towards more application-based research is observable. Therefore, the current chapter offered a summary of what has been achieved, regarding surface functional/reactive nano-object by PISA.

### 2.3. Enzyme Immobilization

Enzymes, ubiquitously present in living organisms, are protein-based biocatalysts with high efficiencies and selectivities and are therefore utilized in the production of food, pharmacology, and textile industry. Their ability to catalyze very complex chemical transformations, which are otherwise not achievable by ordinary methods of organic chemistry, makes them ideal candidates in the ongoing advances and developments in green and sustainable chemistry. Thanks to recent biotechnological developments, biocatalysts find many applications in chemical industries such as paper, beverage, and biodiesel production.<sup>129-131</sup> Recombinant protein engineering (site-directed mutagenesis, gene shuffling) enables the production of cost-efficient enzymes for commercial uses and offers a tool to specifically tune enzyme properties with regard to substrate specificity, activity, and stability. However, due to the lack of long-term stability and inefficient recovery/reusability of enzymes in solution, many potential applications cannot be realized on an industrial scale. Immobilization of enzymes onto solid support materials is therefore the method of choice to circumvent the aforementioned drawbacks and develop stable and robust biocatalysts. Among the many advantages of enzyme immobilization is the ease of purification, simple handling, and convenient recovery of costly enzymes, as well as improved stability and reduced denaturation towards heat, organic solvents, and changes in pH. Furthermore, enzyme immobilization enables the preparation of multienzyme cascade processes which could otherwise not be realized on an industrial level. With the partition and binding of multiple enzymes onto surfaces unfavorable interactions between catalysts resulting in inhibition or partial deactivation can be prevented. However, compared to free enzymes the activity of immobilized enzymes is generally lower due to conformational changes, depending on the immobilization method. The most prominent immobilization techniques are non-covalent adsorption, immobilization *via* ionic interactions (affinity binding), covalent linkage including cross-linking, and finally entrapment of the enzyme in a polymer gel or porous inorganic materials.

The weakest interactions of immobilized enzyme to their respective substrate are physical adsorptions mainly relying on van der Waals forces and entropy changes. For example, proteins with a high lipophilic surface area, such as lipase, will bind to hydrophobic carriers through hydrogen bonds readily. Pretreatment or chemical

modification of the enzymes is therefore not necessary. Indeed, physical binding is generally weak and the whole process is reversible. As a result, enzymes can leach out of the carrier if the system is applied in aqueous media.<sup>132</sup> Since deposition and absorption of enzymes are not site-specific, the immobilization can negatively affect the overall orientation and structure of the enzymes. These conformational changes can even lead to denaturation of the enzymes, which causes a loss in the catalytic activity.<sup>133</sup> Furthermore, adsorption is not a controlled process and can generate high packing densities on the carrier, which reduces enzyme activity through crowding. The driving force behind enzyme immobilization on hydrophobic surfaces are entropy gains during the adsorption. Hydrogen bonds between water molecules get disrupted when hydrophobic segments of the enzyme and carrier are in the same system since no hydrogen bonds between water and hydrophobic area can be established leading to loss in translational and rotational entropy (solvation shell of water) and an overall unfavorable free energy of the system. By immobilization, the non-polar sites on the surface area exposed to water are reduced to minimize the disruptive effect. Still, enzymes mostly hold hydrophilic amino acid groups on their surface and can form hydrogen bonds with hydrophilic carriers such as Celite, silica gels, porous glass, and cellulose.<sup>134</sup> Another form of physical immobilization is by ionic interactions between charged enzymes and ion exchangers. As a result, the immobilization is simple and reversible but it can be complicated to find suitable settings in which the enzyme is bound strongly to the carrier while retaining its full activity. Further difficulties arise if the substrate or the product themselves are charged resulting in distorted kinetics.

Covalent binding of enzymes to carrier is amongst the most widely methods to immobilize enzymes. The formation of covalent bonds between carrier and enzyme rely on the functional side-chains of amino acids exposed on the enzymes surface. Since most proteins possess naturally present external functional groups, this method is applicable for non-modified proteins similarly to non-covalent adsorption. Indeed, the chemical bond formation between enzyme and carrier hinders leaching of the enzymes in solution and no protein impurities in the product occur. Furthermore, the formation of multiple covalent bonds prevent protein unfolding and denaturation by reducing the conformational flexibility of the enzymes. As a result, covalently immobilized enzymes can be utilized in both aqueous and organic media. Exposed amino acids such as lysine, cysteine, aspartic acid and, glutamic acid can be readily employed.<sup>135</sup> A common way to

establish covalent bonds is to utilize carrier-bound activated NHS ester, epoxy, or maleimide groups that can be attacked by amine or thio functionalities, respectively. Covalent binding offers many benefits but exhibits some distinct disadvantages. Amino acids essential for biocatalytic activity must not be involved in the immobilization process, which may be a difficult requirement in some cases. To circumvent this problem, the coupling reaction can be carried out in the presence of substrate analogs in order to occupy the respective amino groups.<sup>136</sup> Furthermore, chemical modification is known to potentially alter the overall morphology and therefore the catalytic activity of enzymes, yet a guided modification on the proteins surface is possible but still remains a challenge. Hence, controlled site-specific immobilization offering exceptional control over the enzymes orientation on a carrier has been heavily investigated during the last 20 years (*vide infra*) resolving most of the aforementioned hurdles.<sup>137</sup>

Entrapment is based on the non-covalent occlusion of enzymes within sol-gel matrices allowing substrates and products to diffuse through the network. Sol-gels are highly porous silica materials that can exhibit very high thermal and mechanical stability if prepared accordingly but is brittle in its standard form. Because of their simple and benign synthesis, sol-gels are commonly utilized to entrap enzymes.<sup>133</sup> In general, the process involves hydrolytic polymerization of tetraethoxysilane in the presence of the enzymes and a subsequent drying step which heavily influences the morphologies of the silica sol-gel. Drying by evaporation of the water-loaded aquagel results in xerogels, which smaller pores and cages due to capillary stress during process. Alternatively, employing supercritical carbon dioxide to dry the sol-gel maintains the original brittle pore structure.<sup>132</sup> These methods provide facile synthesis to generate sol-gel materials with various properties. Furthermore, additives such as polyethylene glycol (PEG), polyvinyl alcohol, and albumin, can have a stabilizing effect on sol-gel entrapped enzymes resulting in higher biocatalytic activities.

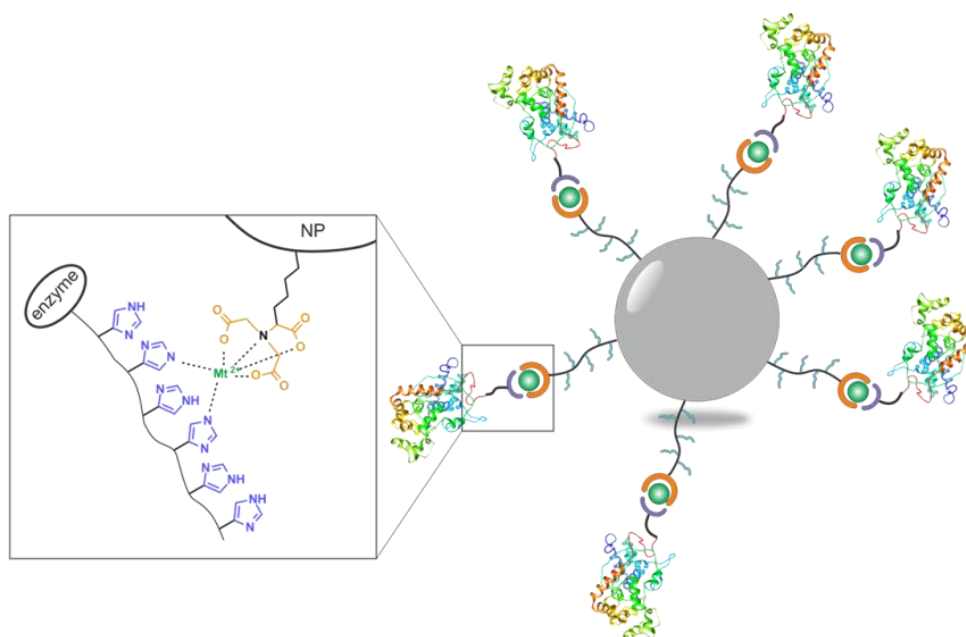
Instead of fixing enzymes to support, the enzymes can also act as their own carrier *via* cross-linking. This method was first described by Richards and co-workers who used di-functional glutaraldehyde to cross-link crystalline enzymes through NH<sub>2</sub> groups.<sup>138</sup> Cross-linked enzyme crystals (CLECs) offer controlled particle sizes (1-100 μm), are easy to recover and exhibit high catalyst productivities. Furthermore, the cross-linking process enhanced the enzyme resistance towards denaturation by heat, proteolysis, and organic solvents, which can be applied to a broad range of enzymes.<sup>139</sup> However,

crystallization of highly pure enzymes is an arduous process and the main disadvantage of this method. Therefore, recent advances in cross-linked enzymes led to the development of cross-linked enzyme aggregates (CLEAs). By addition of salts, water-miscible organic solvents, or non-ionic polymers such as polyethylene glycol to an aqueous solution of enzymes, the precipitation of the latter as physical aggregates can be triggered. These aggregates are held together by physical bonding not affecting the tertiary structure of the enzymes and hence maintaining the catalytic activity. Subsequent cross-linking led to insoluble aggregates that preserved their superstructure. The simplicity of this process and the possibility to tune particle sizes depending on the concentration of glutaraldehyde led to the use of CLEAs in large scale applications since the whole operation can be automatized using 96 well-plates for instance.<sup>140</sup> Still, cross-linking can cause loss of activity if amino acid groups which are essential for the catalytic activity react with the cross-linker either on the surface or the interior of the enzyme through diffusion.

In recent years, several site-specific immobilization techniques able to proceed under mild physiological conditions have received increasing attention. The most promising technique is the use of recombinant fusion proteins, i.e., modified proteins with peptide sequences of genetic material from different sources. This allows the production of proteins with additional amino acid sequences resulting in post-translational modifications. For instance, affinity and fusion tags are incorporated into proteins of interest to increase its over expression in microbial hosts and enhance the native folding. Affinity tags, which generally consist of short peptide sequences, offer the facile purification of proteins and a minimal influence on the tertiary structure. Fusion tags incorporate polypeptide chains, are generally larger than affinity tags, and can increase the protein solubility but need to be removed *via* proteases for crystallization or antibody production.<sup>141</sup> Both methods can also be employed for site-specific enzyme immobilization if a suitable carrier holds their respective binding partners. In the following, a description of the protein tags, which are useful in this context and have been tackled in the present work, is given.

### 2.3.1. Polyhistidine tag (His-tag)

The most widely applied affinity tag for recombinant protein purification is the His-tag.<sup>137</sup> 3-10, but commonly 6, histidine amino acids are sequentially organized and can be positioned at either the *N*- or *C*-terminus of the protein. Due to its small size (0.84 kDa), the His-tag has very little influence on the tertiary structure of the protein and as a result, the bioactivity is rarely affected.<sup>142</sup> Since histidine is the amino acid that demonstrates the highest affinity to transition metal ions, based on the electron donor groups of the imidazole, it is frequently used in immobilized affinity metal chromatography. Developed by Hochuli *et al.* in 1987, Ni(II)-nitrilotriacetic acid (Ni<sup>2+</sup>-NTA) proved high affinity to neighboring histidine groups and was therefore utilized as column material (Scheme 11).<sup>143</sup> Chelate complexes between the polyhistidine sequence and the metal matrices establish weak ionic interactions (single His<sub>6</sub> to Ni<sup>2+</sup>-NTA;  $K_d = 10 \mu\text{M}$ ) that can be broken by competitive binding of soluble imidazole to the solid support, thereby eluting the purified recombinant protein.<sup>144</sup> However, in 1999 Co<sup>2+</sup>-carboxymethylaspartate resins (Co<sup>2+</sup>-CMA) were introduced to bind to His-tagged proteins. Co<sup>2+</sup>-CMA allows the elution under milder conditions and demonstrated less non-specific protein binding than the Ni<sup>2+</sup>-NTA resin. Apart from protein purification His-metal complexes are also used for advanced applications such as biosensors and bioreactors.<sup>145-147</sup> Despite the recent developments in the field of protein immobilization, the facile introduction of the polypeptide and its wide scope of applications make the His-tag the most commonly used affinity tag.<sup>141</sup>

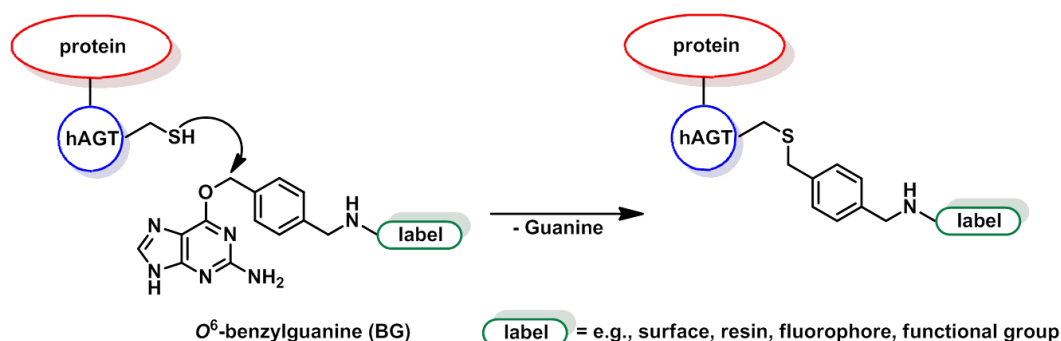


**Scheme 11.** Schematic depiction of His-tagged (violet) protein binding to a NTA containing (orange) solid carrier mediated by metal(II) ions (green).

### 2.3.2. SNAP-tag

In 2003 a new covalent binding protein tag, namely SNAP-tag, was introduced by the group of Johnsson.<sup>148</sup> In contrast to the aforementioned His-tag, covalent labeling with a small molecule is achieved *via* a mutant of the human DNA repair protein *O*<sup>6</sup>-alkylguanine-DNA alkyltransferase (<sup>w160</sup>hAGT). Modified hAGT has been shown to irreversibly transfer alkyl groups from its substrate, *O*<sup>6</sup>-alkylguanine-DNA, to one of its cysteine residues.<sup>149</sup> Since the substrate specificity of hAGT is relatively low, it also reacts readily with the nucleobase *O*<sup>6</sup>-benzylguanine (BG), which can be chemically modified on the benzyl ring, e.g., with fluorophores.<sup>150</sup> This reaction can also be exploited for the specific *in vivo* labeling of hAGT fusion proteins with BG derivatives substituted at the 4-position of the benzyl ring (Scheme 12). Importantly, the rate of the reaction of AGT fusion proteins with BG derivatives is independent of the nature of the label attached to BG, opening up the possibility to label a single SNAP fusion protein with a variety of different probes.<sup>151</sup> Furthermore, SNAP-tag is not restricted to a cellular localization and expression within a specific host and BG substrates are chemically inert towards other proteins. As a result, nonspecific labeling in cellular applications can almost be entirely avoided. Lastly, many SNAP-tag substrates are cell permeable,

permitting labeling of intracellular proteins in live cells as demonstrated by numerous reports with various BG-fluorescein derivatives.<sup>152-153</sup>



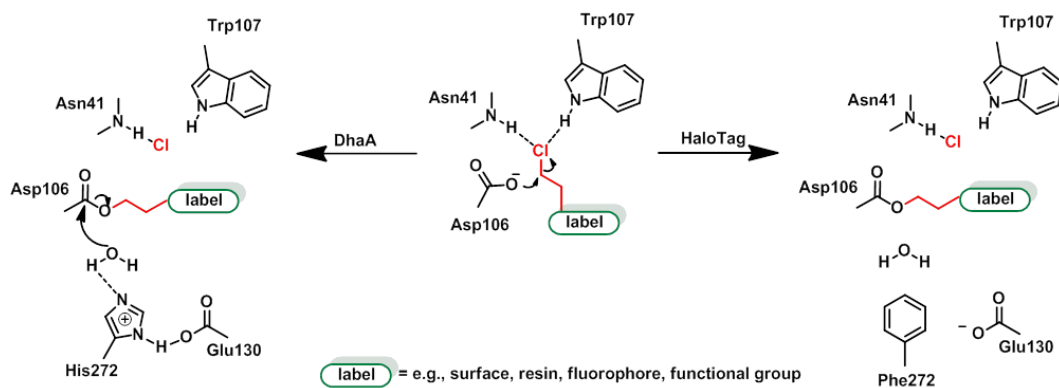
**Scheme 12.** Covalent labeling of an hAGT fusion protein using  $O^6$ -benzylguanine (BG) derivatives.

The SNAP-tag methodology has been applied to the functionalization of nanoparticles. Kampmeier *et al.* demonstrated the immobilization of single chain antibodies on rhodamine labeled silica beads (90 nm),<sup>154</sup> while the immobilization onto BG-bound CdSe-ZnS quantum dots (QDs) allowed for fluorescent imaging for protein interactions *in vitro* and *in vivo*.<sup>155</sup>

### 2.3.3. HaloTag

An additional covalent binding method is the HaloTag, which requires only the conjugation of a simple haloalkane moiety to the desired label. *Via* a nucleophilic displacement mechanism the original haloalkane dehalogenase (DhaA), a bacterial enzyme, removes halides from aliphatic hydrocarbons and forms a covalent ester bond between the haloalkane and Asp106 in the enzyme (Scheme 13).<sup>156</sup> In the wild-type DhaA, His272 catalyzes the hydrolysis of the intermediate, resulting in product release and regeneration of enzyme. HaloTag, on the other hand, carries a substituted Phe272 which cannot act as a base rendering the covalent ester bond stable towards hydrolysis and trapping the reaction intermediate as a stable covalent adduct. HaloTag is a small (34 kDa) and monomeric polypeptide and no eukaryotic cells or most bacteria possess the dehalogenase or its ligands. Therefore, no endogenous equivalent in any of the commonly used experimental biological systems is present that would bind to HaloTag

substrates and interfere with its specificity and efficiency.<sup>157</sup> After fusion at either the *N*- or *C*-terminus of a recombinant protein, HaloTag and its chemically modifiable ligands have been shown to be a valuable tool for protein imaging and purification offering an alternative to the aforementioned protein tags.<sup>157</sup>



**Scheme 13.** Reaction mechanism of wild-type (DhaA) and mutant dehalogenase (HaloTag) with a labeled haloalkane.

## 2.4. Grafting Process

Well-defined polymer coatings are known to effectively tune the physical and chemical properties of the surfaces and therefore offer new possibilities for biomedical applications or as protective layers. Thus, the attachment of tethered polymers onto surfaces has been an ongoing field of interest since the 1980s when first investigations about brush-conformations of coil polymers were reported.<sup>158</sup> In general, formation of polymeric layers can be achieved by either physical deposition or chemisorption (i.e., covalent binding) of the polymer to surfaces. Although deposition of polymer is a facile and straightforward method, weak binding forces between coating material and surface make this approach unfavorable under adverse conditions. Hence, covalent binding of polymers to surfaces through RDRP-mediated chemical grafting processes such as "grafting to", "grafting from", and "grafting through" is applied more frequently (Figure 9).

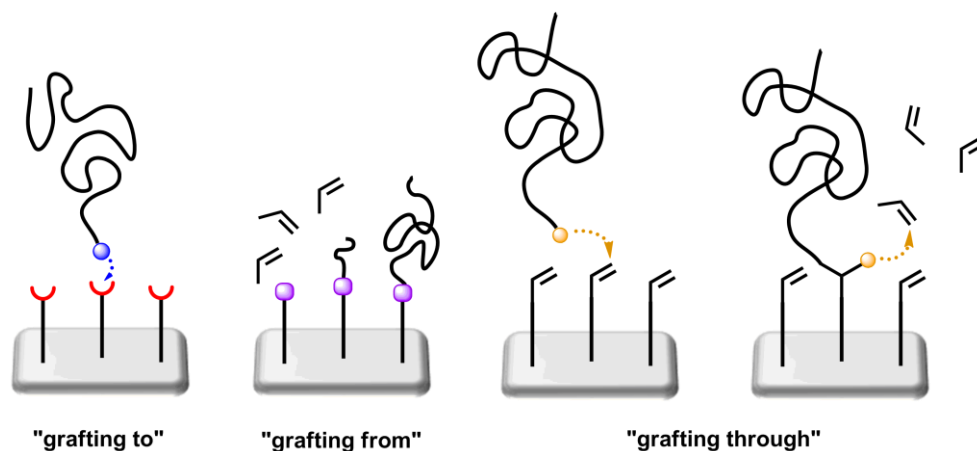


**Figure 9.** Schematic illustration of chemical grafting processes of polymer strands to surfaces.

The "grafting to" approach commonly involves a preformed macromolecule with a functional side or end-group, which allows reactions with groups present on the surface to be coated. Yet this reaction is not known to generate dense polymer layers and the final thickness of the layer is generally smaller than 5 nm due to kinetic hindrance.<sup>159</sup> Once polymer chains cover large parts of the surface the overall concentration of polymers at the interface area becomes larger than in solution. Therefore, further chain

attachment is hindered by the high local concentration at the reactive sites and diffusion of polymer in solution to the surface becomes increasingly limited, resulting in no further reactions and thin polymer films. Even if kinetic aspects were not present the thermodynamic barrier would have to be overcome. The conformational change from coiled polymer chains to stretched would result in a significant loss in entropy, which would only be balanced by an enthalpy gain due to the formation of a covalent bond.

To overcome these intrinsic limitations the widely used "grafting from" approach (also known as surface-initiated polymerization) can be employed. This reaction allows the simultaneous growth of polymer chains on the surface by RDRP. Initiating groups are incorporated at the surface and can react with monomers whose diffusion through growing chains is generally high. Thus, surfaces with a very high grafting densities ( $\sim 1$  chain  $\text{nm}^{-2}$ ) can be achieved. Furthermore, the conformation of homopolymer brushes is simply controlled by the grafting density and the thickness of the layer, which can be adjusted by the degree of polymerization of the growing polymer strands.

In contrast to "grafting from", with surfaces bearing a monomer unit instead of an initiator, the "grafting through" process may be applied. A preformed macroinitiator or macro RAFT agent can incorporate the surface-bound monomer unit into the growing chain during propagation. The continuous growth with further monomers results in surface-attached polymer layers. This process may result in a less controlled amount of incorporated chains for the same reason as for the "grafting to" method.



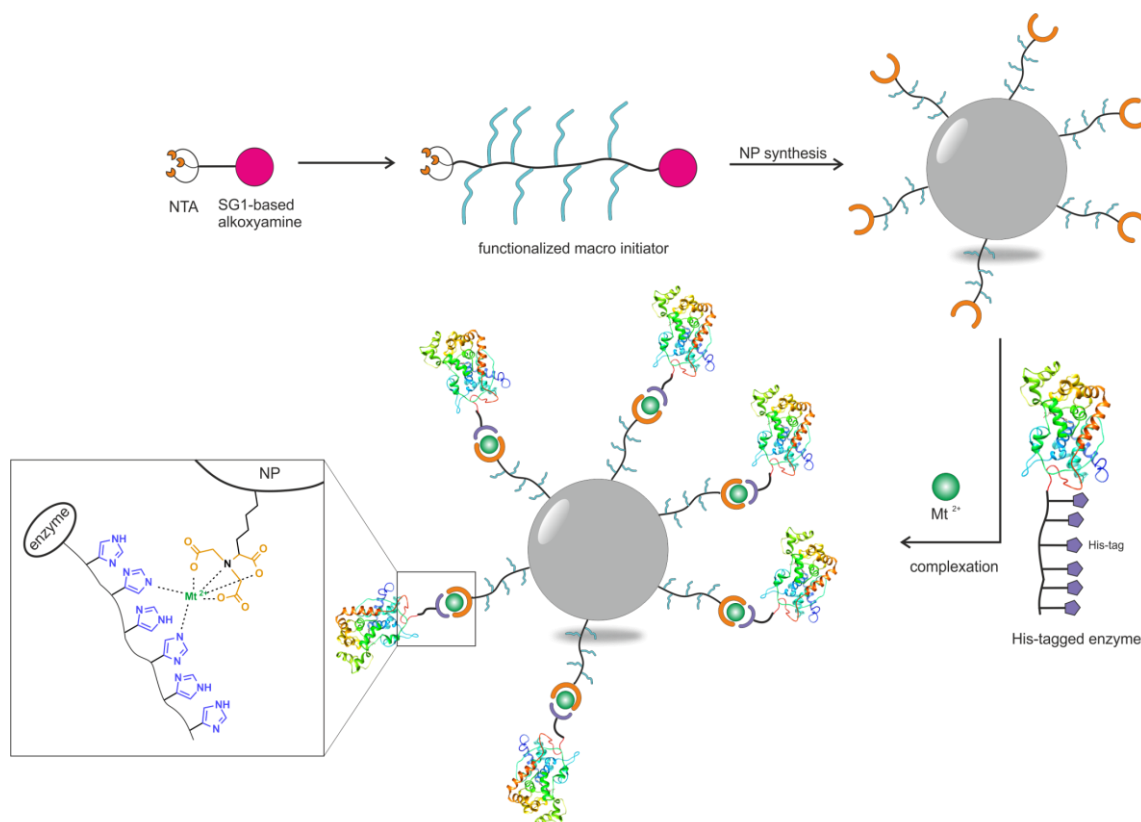
# Amphiphilic Block Copolymer Nanoparticles by Nitroxide-Mediated Polymerization

As described in Chapter 2.3, the use of enzymes catalysis, biosensors, and immunodiagnostics has been a growing topic throughout the last decade. The benefits of immobilizing enzymes onto solid supports are numerous but a recurring issue with immobilization is the coupling through surface-exposed amino acid groups, which is often non-site specific. This in turn may lead to imprecise orientation, altering the conformation of the active site of the biomolecule, which results in lower efficiency and activity. To control the site of attachment on the protein surface, protein tags are employed, with the polyhistidine tag (His-tag) being the most well-known example. Nitrilotriacetic acid (NTA) is a common chelator which complexes  $\text{Ni}^{2+}$  ions and forms a sandwich complex with His-tagged proteins. For biotechnological purposes it would be compelling to immobilize these His-tagged biomolecules onto nano-objects, e.g., nanoparticles, which provide a large specific surface area as well as access to applications where nanotechnology may be beneficial.

The aim of this chapter was the synthesis of polymeric nanoparticles with the ability to specifically immobilize His-tagged enzymes and yield biocatalytic nanoparticles. A suitable system for this purpose is amphiphilic block copolymers as they provide an accessible route to nano-objects. For the formation of amphiphilic block copolymer nanoparticles, either a co-solvent method (nanoprecipitation) or a one-step polymerization-induced self-assembly (PISA) process can be employed. Nitroxide-

### 3. Amphiphilic Block Copolymer Nanoparticles by Nitroxide-Mediated Polymerization

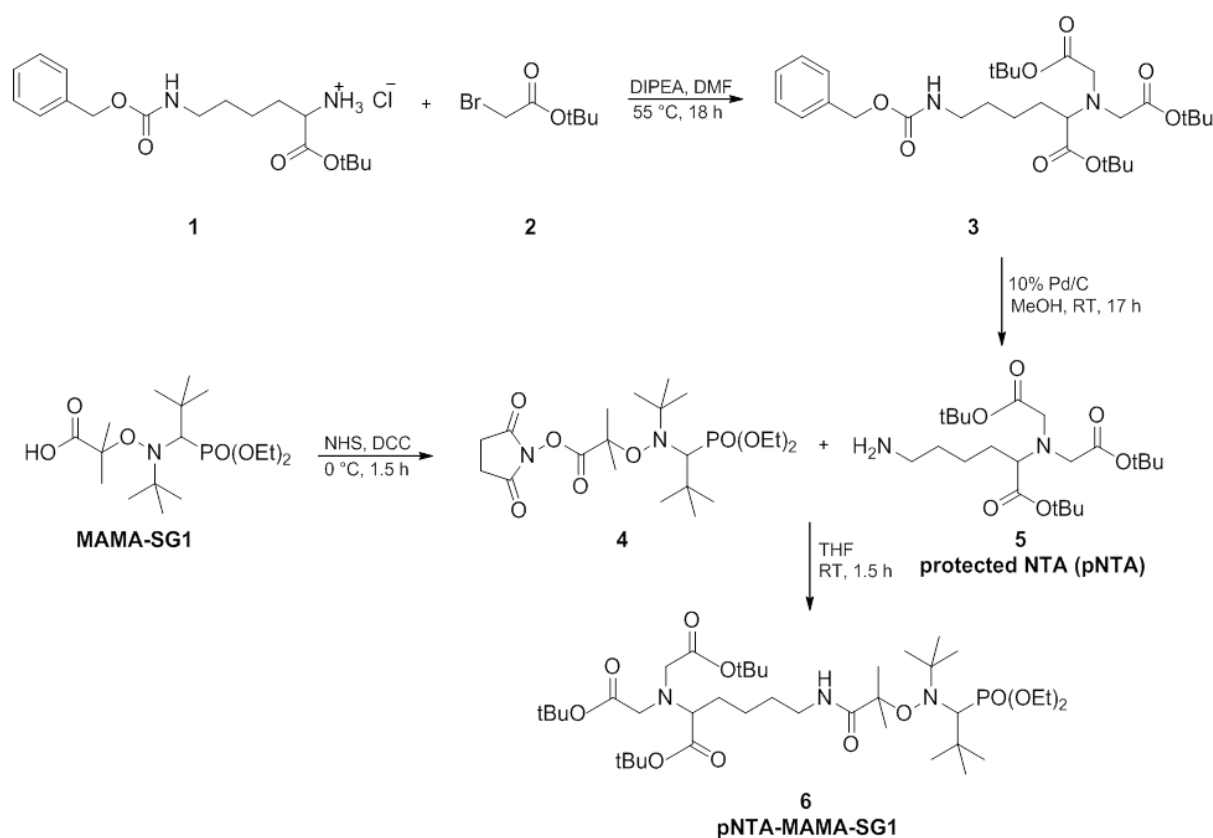
mediated polymerization (NMP) grants an efficient way to obtain well-defined copolymers while also giving access to the control of polymer chain ends. Therefore, the first step towards catalytically active nanoparticle dispersions was the synthesis of a new NMP initiator bearing the His-tag binding NTA motif, which would provide His-tagged binding particles after successful polymerization and self-assembly steps (Scheme 14).



**Scheme 14.** Schematic pathway for obtaining functionalized nanoparticles from a modified SG1-based NMP initiator and His-tagged enzyme immobilization on the particles surface.

### 3.1. Synthesis of pNTA-Functionalized NMP Initiator

The most direct way to obtain a NTA-functionalized NMP initiator is a simple coupling reaction between a commercially available NTA amine derivative and the activated NHS ester of the widely used MAMA-SG1 (BlocBuilder). MAMA-SG1 was chosen because of the relatively low temperatures needed to initiate polymerizations (70-90 °C), as compared to other NMP initiators based on the TEMPO or TIPNO nitroxides.



**Scheme 15.** Complete synthetic pathway for the functionalized NMP initiator pNTA-MAMA-SG1.

Because of the three carboxylic acid groups present on NTA and its related very high polarity, NTA could only be solubilized in water. NHS-activated MAMA-SG1 on the other hand would only dissolve in organic solvents. Therefore, an alternative route was chosen in which the free carboxylic acid groups were replaced with their *tert*-butyl esters and then coupled directly with NHS-MAMA-SG1. The synthetic route to obtain *tert*-butyl protected NTA amine (5) consists of two steps (Scheme

### 3. Amphiphilic Block Copolymer Nanoparticles by Nitroxide-Mediated Polymerization

15), which are literature known.<sup>160</sup> In the first step, (**1**) was deprotonated with DIPEA and underwent a nucleophilic substitution with (**2**) which was added in a two-fold excess. The second step was a hydrogenation with Pd/C in which the benzyl carbamate group was cleaved and the primary amine (**5**) was obtained. In a subsequent step, (**5**) was coupled *via* an nucleophilic amidation to NHS-MAMA-SG1 (**4**). After purification the pNTA-functionalized NMP initiator (**6**) was obtained as a colorless oil. Figure 10 shows the <sup>1</sup>H NMR spectrum and the ESI-MS spectrum of the pure NMP initiator.

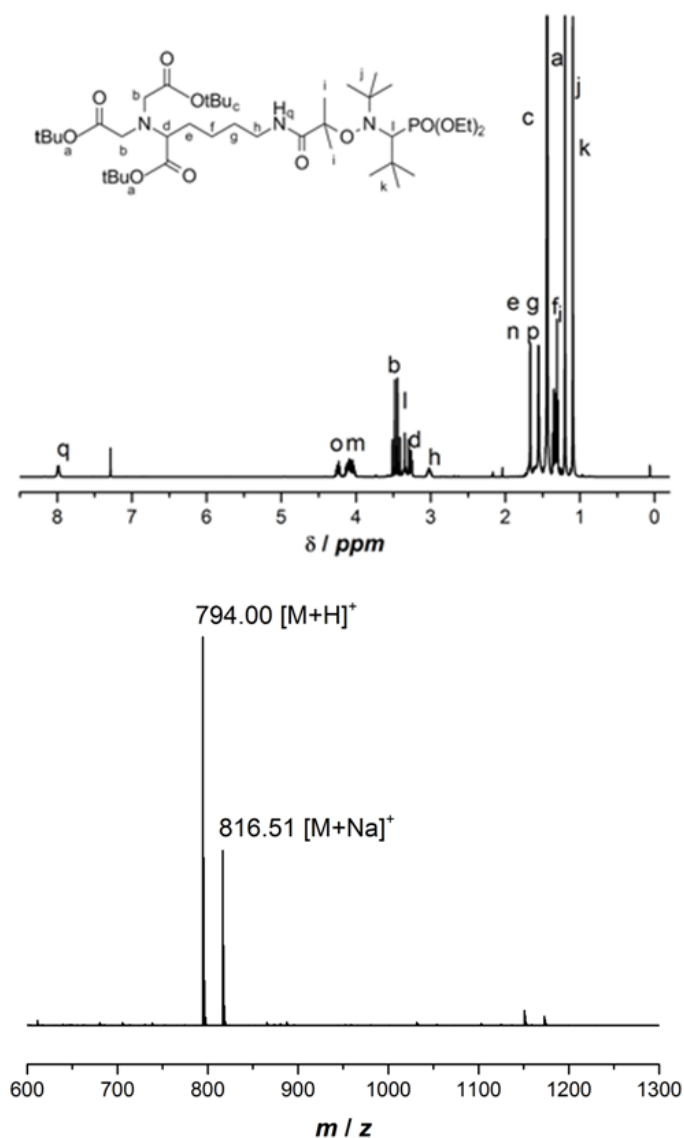
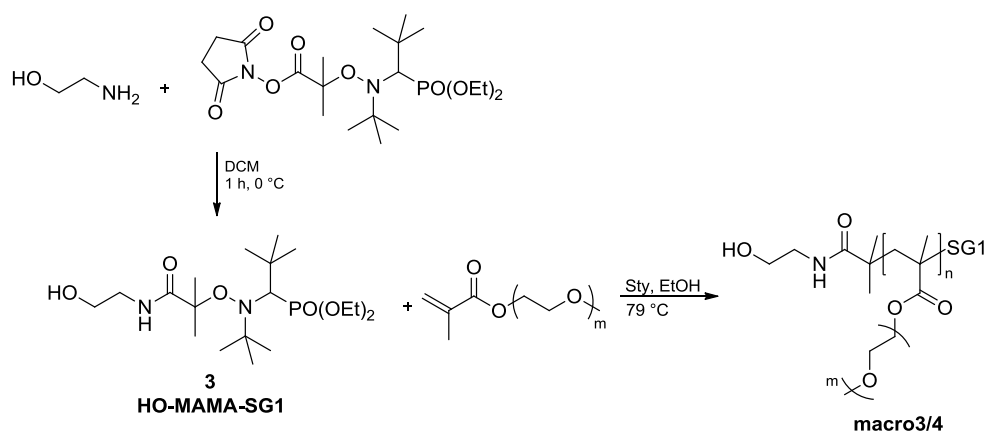


**Figure 10.** <sup>1</sup>H NMR spectrum (top) and ESI-MS spectrum (bottom) of purified pNTA-functionalized NMP initiator.

Since the free carboxylic acid groups of NTA are needed to establish a chelation with  $\text{Ni}^{2+}$  ions, a subsequent deprotection step of the tBu-esters was necessary. This hydrolysis step could either be performed after the synthesis of the pNTA-functionalized macroinitiator or after nanoparticle formation. For a more facile handling of the NMP initiator, the deprotection of the pNTA was performed after particle formation.

In general, a nanoparticle bearing a 100% surface functionalization is the ideal system for efficient His-tagged enzyme immobilization. However, enzymes occupy a certain amount of space themselves, being too close to one another, many NTA groups may be unoccupied as they could not immobilize further enzymes because of steric hindrance. Hence, part of the hydrophilic chains constituting final nanoparticles were thought to be non-functionalized, preferably with an  $\alpha$  end-group, which does not induce immobilization/adsorption in a non-specific way. Therefore, a second, non-protein interacting NMP initiator based on NHS-MAMA-SG1 was synthesized (Scheme 16). Also unwanted and non-specific interactions like adsorption could drastically change the enzymes structure and the conformation of the active site, which may in turn result in decreased activity. The hydroxy group of this second NMP initiator should in theory not interact with the enzymes and was therefore chosen as a suitable candidate.



**Scheme 16.** Synthetic steps for the HO-MAMA-SG1 initiator and the resulting macroinitiator.

### 3.2. Initiation Evaluation of pNTA-functionalized NMP Initiator

Altering the chemical structure of an initiator might greatly influence its performance during a polymerization.<sup>161</sup> Therefore the newly synthesized initiator (**6**) was used in a bulk polymerization with *tert*-butyl acrylate (*t*BA) to evaluate its initiating abilities during NMP. Two experiments were carried out to obtain a low molar mass polymer for electrospray ionization mass spectrometry (ESI-MS) analysis and a high molecular weight polymer for clear size exclusion chromatography (SEC) analysis.

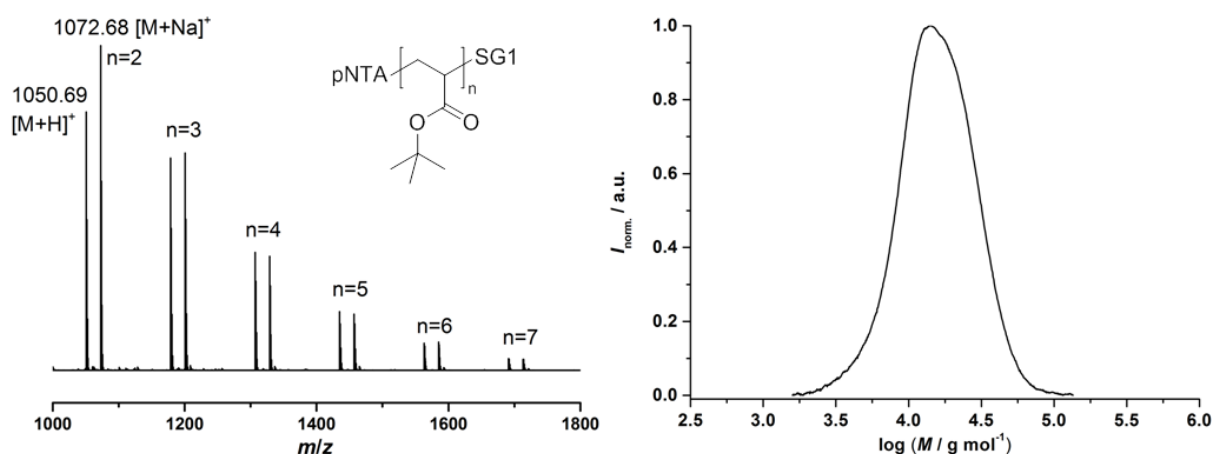


**Figure 11.** (Left) Selected region of the ESI mass spectrum (left) obtained for the short pNTA-PtBA-SG1 and (right) SEC trace of pNTA-poly(*t*BA)-SG1 *via* NMP.  $M_n = 13000 \text{ g mol}^{-1}$  and  $\mathcal{D} = 1.41$ .

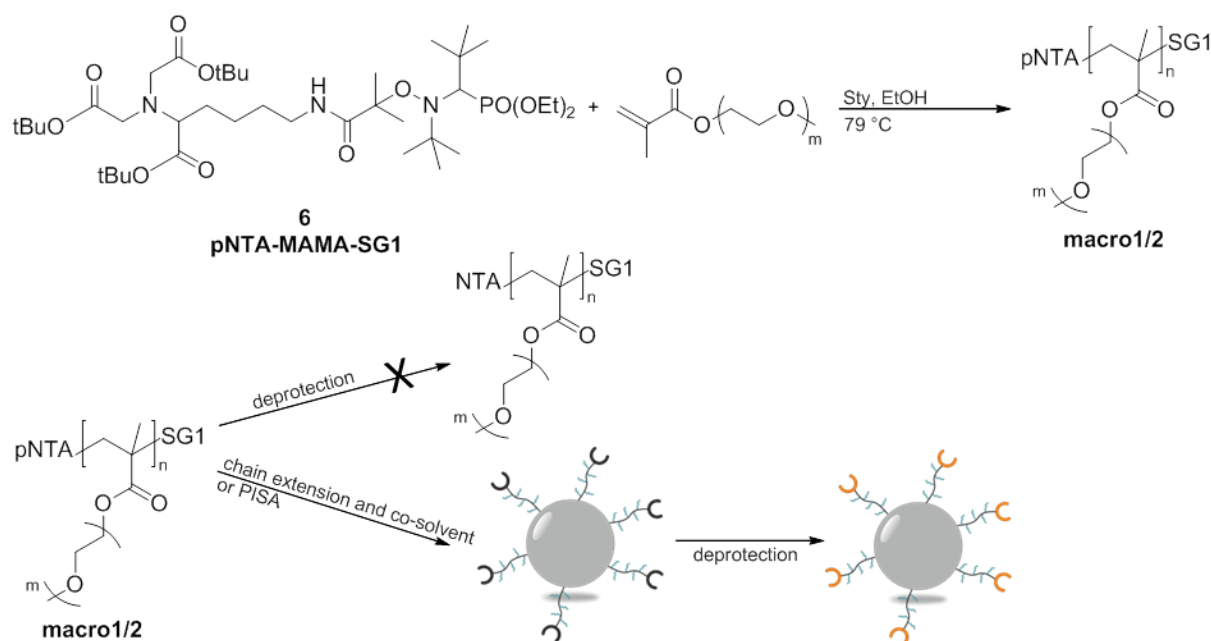
Figure 11 shows the recorded ESI mass spectrum on the left. The distribution nicely correlates with the expected oligomeric structures, ranging from a dimer up to a heptamer with end-groups originating from pNTA-MAMA-SG1 ( $MW 793.52 \text{ g mol}^{-1}$ ), with proton and sodium ionization, respectively. The SEC trace on the right displays the previously mentioned higher molar mass polymer. While the polydispersity of the final polymer is relatively high ( $\mathcal{D} = 1.41$ ) for a reversible-deactivation radical polymerization, adding small amounts (1 mol%) free SG1 would slow down the reaction, creating more dormant species and therefore decrease the polydispersity if an optimized polymerization of *tert*-butyl acrylate with the new NMP initiator was required. The displayed data clearly indicates that pNTA-MAMA-SG1 can successfully

initiate a nitroxide-mediated polymerization and introduce a protected NTA moiety at the alpha extremity of a polymer chain.

### 3.3. Synthesis of Hydrophilic Macroinitiators

For the hydrophilic segment of the amphiphilic block copolymer a variety of monomers can be chosen. PEG-based macromolecules offer antifouling properties<sup>162-163</sup> and biocompatibility<sup>164</sup> and are employed as sterical stabilizers for particles. Furthermore, these macromolecules have been shown to be efficient compatibilizers of nanocomposite colloids in emulsion polymerization.<sup>165-166</sup> Here, a hydrophilic methacrylate was chosen since the resulting polymers are more stable, as compared to acrylates, and lower polymerization temperatures can be used in NMP. As mentioned in Chapter 2.1.3., SG1-mediated polymerizations with methacrylates require a small amount of co-monomer to "control" the reaction. A comonomer with a low propagation rate constant  $k_p$  and a significantly lower NMP equilibrium constant  $K$  are required for the effective control of a methacrylate polymerization<sup>167</sup> (e.g., for MMA,  $k_p = 1.6 \times 10^3 \text{ L mol}^{-1} \text{ s}^{-1}$  and  $K = 1 \times 10^{-7} \text{ L mol}^{-1} \text{ K}^{-1}$  at 90 °C).<sup>168</sup> Styrene fulfils these requirements ( $k_p = 0.9 \times 10^3 \text{ L mol}^{-1} \text{ s}^{-1}$  und  $K = 4 \times 10^{-10} \text{ L mol}^{-1} \text{ K}^{-1}$  at 90 °C)<sup>168</sup> and was therefore chosen as a co-monomer. Since the resulting nanoparticles should not have non-specific interactions between their outer shell and the enzymes, oligo(ethylene glycol) methacrylates were chosen as methacrylate-based hydrophilic segments. Oligo(ethylene glycol) methyl ether methacrylate (OEGMA) are known to be protein repellent, are able to sterically stabilize nanoparticles through their brush-like segments, and show similar beneficial properties to poly(ethylene glycol) (PEG).<sup>169</sup> OEGMA<sub>300</sub> and OEGMA<sub>950</sub> with their number-average molar mass of 300 and 950 g mol<sup>-1</sup> respectively, were utilized.

### 3. Amphiphilic Block Copolymer Nanoparticles by Nitroxide-Mediated Polymerization



**Scheme 17.** Polymerization of OEGMA monomer with pNTA-MAMA-SG1 and possible routes towards a functionalized nanoparticle.

For nitroxide-mediated polymerization-induced self-assembly (NMPISA), OEGMA<sub>300</sub> was not suitable since typical temperatures for NMP are higher than 75 °C while OEGMA<sub>300</sub> shows a lower critical solution temperature (LCST) in water of ca. 64 °C, which causes the polymer to precipitate if this temperature is exceeded.<sup>170</sup> The ease in polymer purification on the other hand - in comparison to OEGMA<sub>950</sub> - made it an ideal candidate for chain extension experiments with styrene resulting in amphiphilic block copolymers, which were then employed in a nanoprecipitation to produce new particles (see Chapter 3.4.). Hence, OEGMA<sub>950</sub> was polymerized to produce a suitable macroinitiator for aqueous NMPISA. Styrene was employed as a controlling comonomer in the polymerization of the OEGMAs for the reasons mentioned above. Figure 12 illustrates the results obtained from kinetic experiments using the pNTA-functionalized NMP initiator (6).

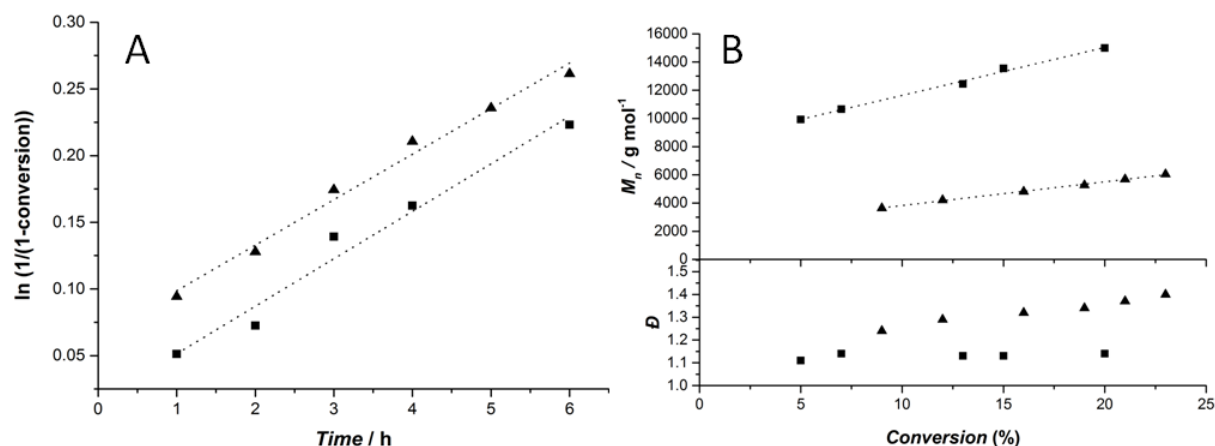


**Figure 12.** (A)  $\ln[1/(1 - \text{conversion})]$  vs time and (B)  $M_n$  or  $\mathcal{D}$  vs conversion plots for the polymerization of OEGMA<sub>300</sub> ( $\blacktriangle$ ) and OEGMA<sub>950</sub> ( $\blacksquare$ ) initiated by pNTA-MAMA-SG1 in the presence of styrene ( $[\text{OEGMA}]/[\text{styrene}] = 10$ ). (A) OEGMA<sub>300</sub> in xylene at 95 °C ( $[\text{OEGMA}]/[\text{pNTA-MAMA-SG1}] = 57$ ,  $[\text{OEGMA}]/[\text{styrene}] = 10$ ,  $[\text{SG1}]/[\text{pNTA-MAMA-SG1}] = 0.1$ ) and (B) OEGMA<sub>950</sub> in ethanol at 79 °C ( $[\text{OEGMA}]/[\text{pNTA-MAMA-SG1}] = 32$ ,  $[\text{OEGMA}]/[\text{styrene}] = 10$ ,  $[\text{SG1}]/[\text{pNTA-MAMA-SG1}] = 0.1$ ).

Evolutions of monomer conversion with time, of the number-average molar mass as well as of the dispersity with conversion is shown in Figure 12. The first-order plot of  $\ln[1/(1 - \text{conversion})]$  vs time (Figure 12 A) indicates a constant concentration of propagating radicals in this conversion range, which is one of the criteria for a controlled polymerization. A similar result is shown in Figure 12 B where the increase in  $M_n$  with conversion also follows a linear trend for both OEGMA polymerizations. Yet, the initiating efficiency of (6) did not seem to be quantitative which might be due to one major reason: Amide-based MAMA-SG1 derivatives possess higher activation energies as compared to unmodified MAMA-SG1 resulting in non-quantitative initiation.<sup>161</sup> The increase in activation energies ( $E_a$ ) (ca. 7-10 kJ mol<sup>-1</sup>) derive from intermolecular hydrogen bonding (IHB) between the alkyl and the nitroxide fragment. Another issue arises from the brush-like structure of POEGMA polymers. The dispersity  $\mathcal{D}$  in this conversion range always stayed below 1.4 indicating a controlled polymerization. Unfortunately, for SEC analysis no adequate calibration was available, which therefore might not lead to values representing actual molar mass of the polymers. Nevertheless, with increased conversion, molar masses did increase as shown in Figure 13. The resulting macroinitiators from these experiments are listed in Table 1.

### 3. Amphiphilic Block Copolymer Nanoparticles by Nitroxide-Mediated Polymerization

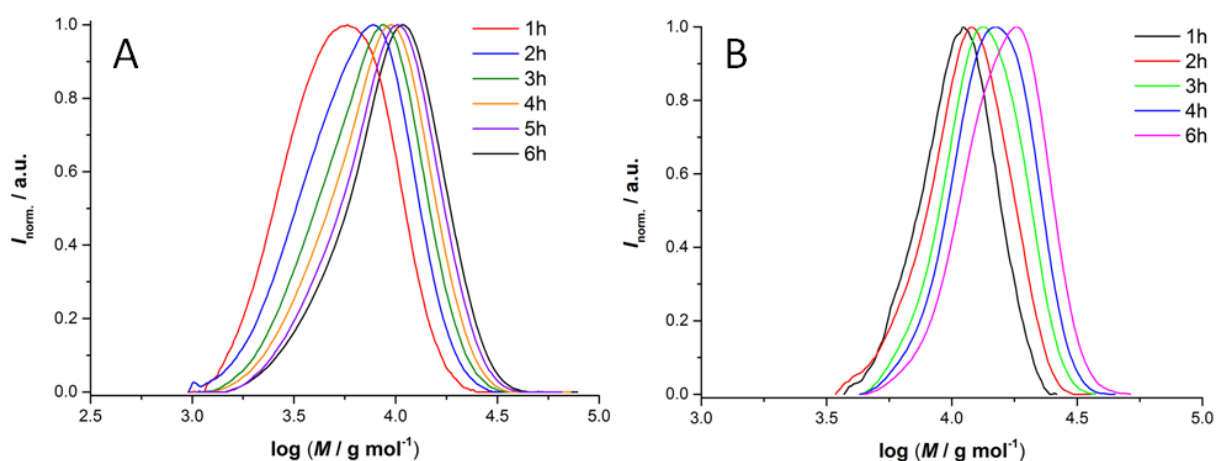


**Figure 13.** Evolution of the size-exclusion chromatograms during the pNTA-MAMA-SG1-initiated polymerization of (A) OEGMA<sub>300</sub> in xylene at 95 °C ([OEGMA]/[pNTA-MAMA-SG1] = 57, [OEGMA]/[styrene] = 10, [SG1]/[pNTA-MAMA-SG1] = 0.1) and (B) OEGMA<sub>950</sub> in ethanol at 79 °C ([OEGMA]/[pNTA-MAMA-SG1] = 32, [OEGMA]/[styrene] = 10, [SG1]/[pNTA-MAMA-SG1] = 0.1) in the presence of a small amount of styrene.

**Table 1.** Main characteristics of the macroalkoxyamines utilized as initiators in bulk or emulsion polymerization.

	structure	target $M_n$ (g mol <sup>-1</sup> ) <sup>a</sup>	$X_{\text{NMR}}$ (%) <sup>b</sup>	$M_{n,\text{SEC}}$ (g mol <sup>-1</sup> ) <sup>c</sup>	$\mathcal{D}^c$
<b>macro1</b>	pNTA-P(OEGMA <sub>300</sub> -CO-S)	17 400	67.3	14 100	1.47
<b>macro2</b>	pNTA-P(OEGMA <sub>950</sub> -CO-S)	30 700	52.5	21 400	1.24
<b>macro3</b>	HO-P(OEGMA <sub>300</sub> -CO-S)	7 500	95.1	6 700	1.54
<b>macro4</b>	HO-P(OEGMA <sub>950</sub> -CO-S)	30 700	13.0	12 500	1.15

<sup>a</sup>at full conversion. <sup>b</sup>OEGMA conversion determined by <sup>1</sup>H NMR spectroscopy. <sup>c</sup>Experimental  $M_n$  obtained by SEC in DMAc using PMMA calibration.

At this stage of the experiments the water soluble macroinitiator still had the protected functional end-group. To transform the species into the nickel-binding free carboxylic acid form, the *t*-butyl esters must be deprotected through hydrolysis. Esters can be hydrolysed under either basic or acid conditions. Since the macroinitiators side-chain featured an ester group itself, harsh reaction conditions must be avoided. For the acidic approach, trifluoroacetic acid (TFA) was employed since it is the most commonly used

acid for this purpose. Looking at the structural motif of SG1 it however appears that a second labile *t*-butyl substituent, attached to the nitrogen of the aminoxy function, is present. In fact, Trimaille *et al.* have shown that TFA treatment of SG1-based polymer-peptide conjugates leads to the cleavage of the *t*-butyl group, which dramatically decreases the thermal lability of the corresponding C-ON alkoxyamine bond and the re-initiation qualities of the alkoxyamine.<sup>171</sup> Replacing the *t*-butyl ester group at the nitrogen with a hydrogen atom increases the bond dissociation energy by 10.7 kcal mol<sup>-1</sup>.<sup>172</sup> Therefore a milder deprotection alternative in form of aqueous phosphoric acid (85 wt% in H<sub>2</sub>O) was employed. Aqueous phosphoric acid is known to be a benign cleaving agent, selectively deprotecting *t*-butyl ester groups with good selectivity towards other functional groups.<sup>173</sup> Simply stirring the functional macroinitiator in aqueous H<sub>3</sub>PO<sub>4</sub> over night at ambient temperature and subsequent dialysis would lead to the desired free carboxylic acid form of NTA.

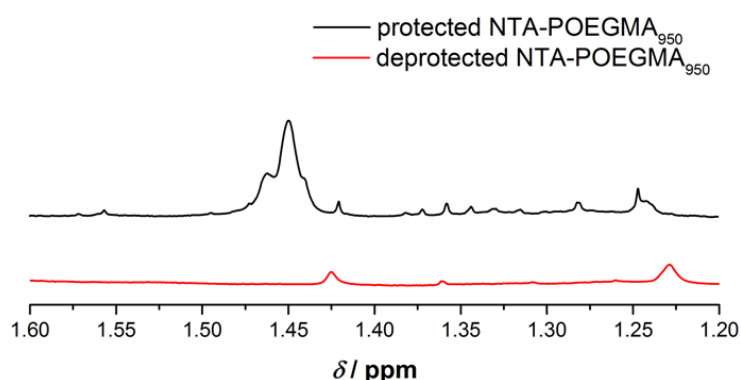


**Figure 14.** Selected region of the <sup>1</sup>H NMR spectra of protected (black) and deprotected (red) macroinitiator.

Figure 14 shows a selected region of the <sup>1</sup>H NMR. It evidences the complete hydrolysis (red) of the *t*-butyl ester groups (black) through the disappearance of its characteristic proton signals at 1.45 ppm.

### 3.4. Nanoparticle Formation *via* Chain Extension and Nanoprecipitation

A convenient method for obtaining nanoparticles based on amphiphilic block copolymers is the so-called co-solvent or nanoprecipitation method. In principle, the polymer is molecularly dissolved in a solvent miscible with water such as THF or DMF and is then added to water in a dropwise manner, leading to nanoprecipitation of the copolymer. Afterwards, the organic solvent is removed from the suspension through evaporation or dialysis. This method can be used for drug encapsulation since loading the nanoparticles with the desired drug simply requires dissolving the drug and polymer together prior to the NP formation. The co-solvent method enables the production of relatively small particles sizes between 100-300 nm, narrow size distributions, and a good colloidal suspension. Amphiphilicity or charged side-chains are not essential for the NP formation since the process is based on the nucleation of small aggregates of macromolecules and the aggregation of those nuclei. Since no external energy input (e.g., sonification, high shearing homogenization) is needed for the nanoparticle formation, the co-solvent method can be considered a mild procedure with modest equipment requirement.<sup>174</sup>

Because of the aforementioned benefits, the first employed route to NTA-functionalized NPs was the co-solvent method. However, PISA experiments carried out in parallel with a deprotected macroinitiator indicated that the deprotection step indeed affected the SG1 moiety negatively, which resulted in loss of control during polymerization (*vide infra*). Therefore, protected pNTA- and HO-functionalized POEGMA<sub>300</sub> macroinitiators (**macro1** and **macro 3**, respectively) were used and separately chain extended with styrene in a bulk polymerization. The resulting SEC traces are shown in Figure 15.

### 3.4. Nanoparticle Formation via Chain Extension and Nanoprecipitation

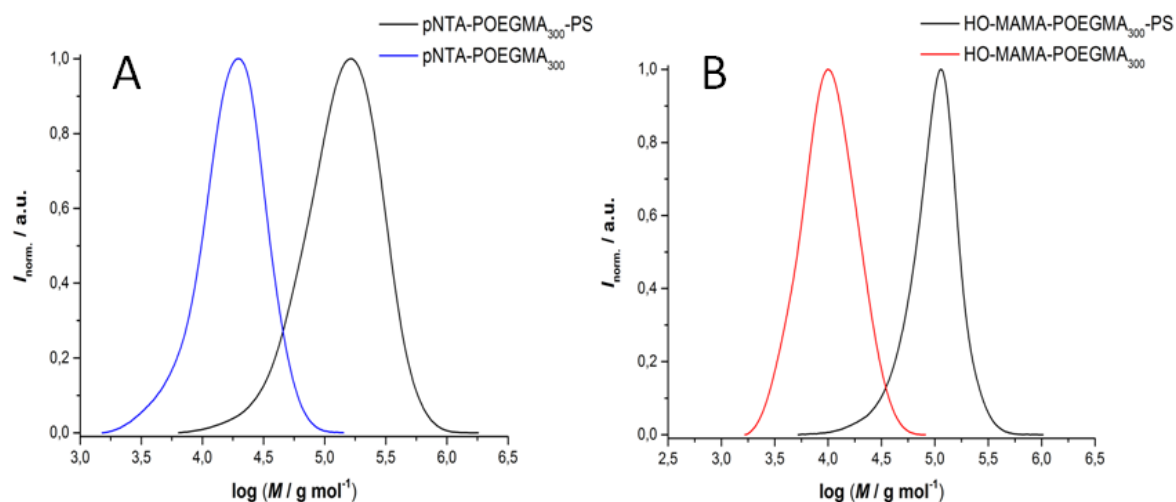


**Figure 15.** SEC traces of the chain extension experiment of (A) pNTA-POEGMA<sub>300</sub>-b-PS (black) and the macroinitiator (blue).  $M_n = 98400 \text{ g mol}^{-1}$  and  $\mathcal{D} = 1.71$  and (B) HO-MAMA-POEGMA<sub>300</sub>-b-PS (black) and the macroinitiator (red).  $M_n = 76700 \text{ g mol}^{-1}$  and  $\mathcal{D} = 1.40$ .

Both chain extensions show a clear shift towards higher molar masses while maintaining a reasonable dispersity. Adding free SG1 to the polymerization would have increased the amount of dormant radical species, resulting in a better control of the process. To obtain nanoparticles with a 10% NTA surface functionalization a mixture of both block copolymers (10 mol% pNTA : 90 mol% HO) was dissolved in THF before water was carefully added through a syringe pump to induce self-assembly and form nanoparticles. After removal of THF the NPs were analyzed by scanning electron microscopy (SEM) and dynamic light scattering (DLS) (Figure 16). The DLS results suggest a narrow, monomodal particle distribution ( $PDI = 0.149$ ) with an average particle size of roughly 400 nm. On the other hand, the SEM image indicated the presence of a variety of morphologies, including the expected spheres, rods, and donut-like nano- and microstructures.

### 3. Amphiphilic Block Copolymer Nanoparticles by Nitroxide-Mediated Polymerization

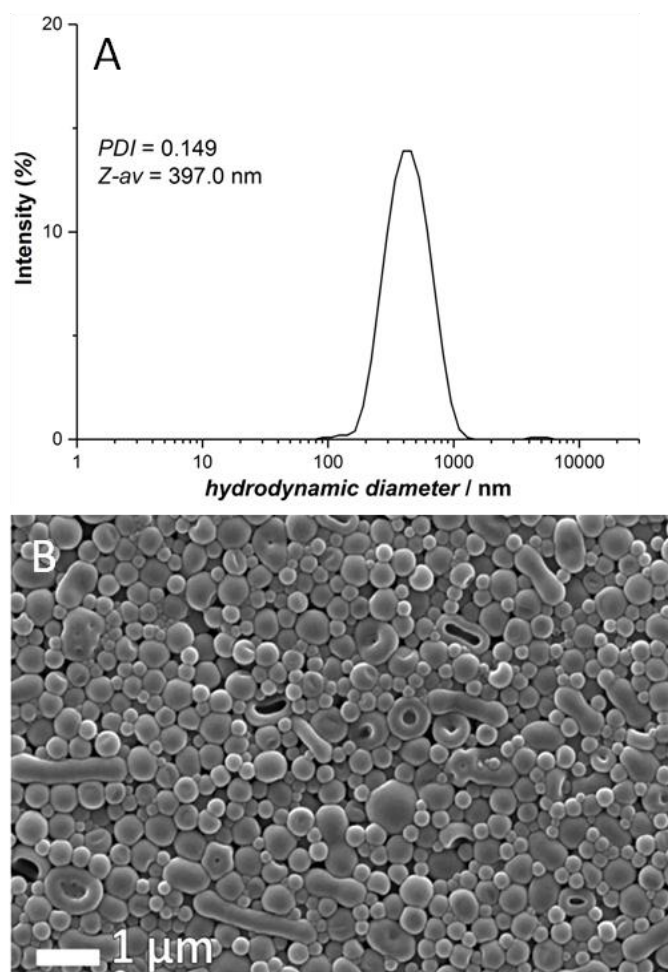


**Figure 16.** (A) Intensity-average hydrodynamic diameter distribution of 10% pNTA-functionalized nanoparticles. (B) Corresponding SEM image.

The nano-/microparticles were then deprotected using aqueous phosphoric acid (85 wt%) and subsequently dialysed against water. Afterwards, nickel complexation and enzyme immobilization experiments with His-tagged horse radish peroxidase (HRP) were performed by Dr. Ana Beloqui. To monitor the enzymatic activity, kinetic assays with ABTS as a substrate were carried out. Figure 17 demonstrates the increase in product formation by the immobilized HRP with progressing time. After washing with imidazole, which removes absorbed enzymes, the enzymatic activity was still present. This proves that the immobilization of the His-tagged enzymes onto the nanoparticles surface was a success. The black data points represent the activity of the HRP on non-deprotected pNTA-functionalized nanoparticles. Here activity is also present due to non-specific interactions between enzymes and polymer. After treatment with imidazole no catalytic activity was observed, confirming that pNTA is unable to bind enzymes. Also a

### 3.5. Nanoparticle Formation by Polymerization-Induced Self-Assembly

higher ABTS oxidation activity for HRP-His<sub>Co(III)</sub>\_NP1 (0.0068 nmol min<sup>-1</sup> μL<sup>-1</sup>) followed by HRP-His<sub>Ni</sub>\_NP1 (0.0037 nmol min<sup>-1</sup> μL<sup>-1</sup>) and HRP-His<sub>Co(II)</sub>\_NP1 (0.0015 nmol min<sup>-1</sup> μL<sup>-1</sup>) was observed. However, cobalt-containing samples resulted in aggregation and flocculation of the particles leading to no reproducible results. Hence, nickel was used as coordination metal for further immobilization experiments (*vide infra*).

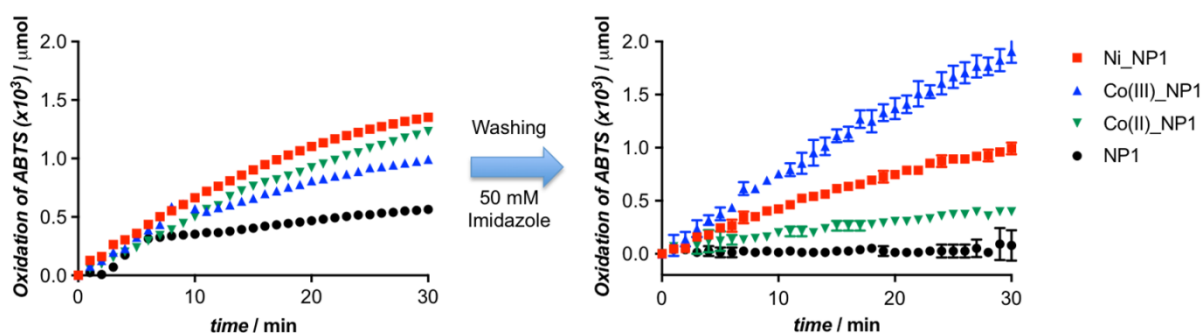


**Figure 17.** ABTS oxidation rates of enzyme NP1 nanoparticles immobilized through Ni(II), Co(III) and Co(II) coordination before and after washing the particles with 50 mM of imidazole. NP1 without metal was assayed as control for non-specific adsorption.

### 3.5. Nanoparticle Formation by Polymerization-Induced Self-Assembly

As described in Chapter 2.2, the polymerization-induced self-assembly process is a recent alternative for nanoparticle formation to the co-solvent method. The main advantages as compared to other self-assembly methods is reduced synthetic effort, the possibility to work at up to 40% solid concentration and the direct access to various nano-object morphologies such as micelles, vesicles, and worms amongst others.<sup>13, 85, 175</sup> To obtain said nanoparticles nitroxide-mediated PISA (NMPISA) in water was conducted in the present study. For the first experiments, methyl methacrylate (MMA) was used as the hydrophobic, core-forming monomer. As with other methacrylates, small amounts of styrene were added to the polymerization as a co-monomer to achieve stable alkoxyamines and to enhance the reversible deactivation process. However, the polymerizations only resulted in low conversions (< 10%) and even after extending the

### 3. Amphiphilic Block Copolymer Nanoparticles by Nitroxide-Mediated Polymerization

reaction times at various temperatures the performance of the polymerization could not be improved.

A methacrylate which has been extensively used in RAFT-PISA experiments, as well as in one report by Qiao *et al.* in NMPISA, was butyl methacrylate (BMA).<sup>176</sup> In the following experiments the OEGMA<sub>950</sub>-based pNTA-functionalized (**macro2**) and non HO-functionalized macroinitiator (**macro4**) were used. The polymerization temperature was set to 85 °C which was also a suitable polymerization temperature for BMA. Because of the high temperature, the OEGMA<sub>300</sub>-based macroinitiators could not be used in these experiments since they would precipitate due to their LCST behaviour in water. Also small amounts of styrene were added to enhance the polymerization process as with other methacrylates. The polymerization time was set to 6 h in which conversions between 30-65% were obtained (depending on the [**macro2**]:[**macro4**] ratio). To obtain even higher conversion the reaction time was increased beyond 6 h, yet this did not lead to higher conversions but to an uncontrolled polymerization process.

In order to obtain nanoparticles with a 100% surface functionalization a polymerization with a fully deprotected NTA-functionalized POEGMA<sub>950</sub> **macro2** was attempted. The SEC trace of the resulting polymer is shown in Figure 18 as well as the SEC traces of the macroinitiator before and after deprotection.

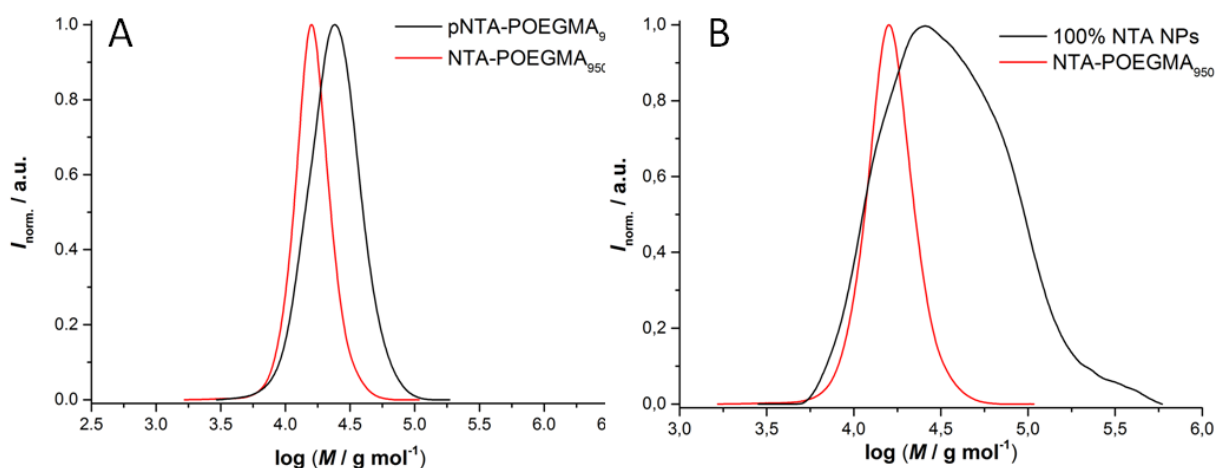


**Figure 18.** (A) SEC traces of the protected (black) and deprotected (red) functionalized macroinitiator **macro2**. (B) SEC trace of the deprotected functionalized macroinitiator (red) and the resulting polymer of the PISA with BMA.

Although the SEC trace shows a clear shift towards higher molar masses, the distribution is neither symmetrical nor narrow ( $D = 1.90$ ). The reaction was clearly not a controlled process. A significant part of the macroinitiator (Figure 18, red) seemed to have not partaken in the polymerization as indicated in the strong tailing. There are two possible explanations for this behavior. Either the dead chains were formed during the synthesis of the macroinitiator (**macro2**) or during the deprotection step of the pNTA. As for the dead chains originating from the macroinitiator synthesis it may be that not all chains were terminated successfully by a styrene-SG1 end-group which is necessary for the stability of the terminal alkoxyamine and hence for the living character of the resulting chains. Indeed, the POEGMA<sub>950</sub> chains were of a rather low  $DP_n$  due to the large mass of the monomer itself, which reduces the effective amount of incorporated styrene. Increasing the fraction of styrene in the POEGMA macroinitiator would likely result in fewer dead chains but would also negatively alter the hydrophilicity of the macroinitiator and its low activation temperature. The other possibility lies in the deprotection step of the macroinitiator mentioned in Chapter 3.3. (Scheme 17). Aqueous phosphoric acid was used as a mild deprotecting agent to cleave the *t*-butyl ester groups at the a chain end and the success of this reaction was confirmed by proton NMR spectroscopy. Due to the low intensity and overlapping of polymer and SG1 signals in the <sup>1</sup>H NMR spectrum, it was difficult to verify if the *t*-butyl groups attached to the nitrogen in SG1 remained intact after the acidic treatment. The two *t*-butyl groups in SG1 were at 1.23 ppm (for the *N*-*t*-butyl group) and at 1.14 ppm (for the *t*-butyl group adjacent to the phosphoester) respectively. Now while the proton signal of the *N*-*t*-butyl group were still visible in Figure 14 after deprotection, the other *t*-butyl group, formally at 1.14 ppm, disappeared. Barreré *et al.* reported that the *t*-butyl group may shift to a lower chemical shift at around 0.5 ppm (in D<sub>2</sub>O) after deprotection with TFA, therefore overlapping with proton signals from the polymer backbone and other aliphatic signals.<sup>172</sup> To circumvent this issue, the following PISA experiments were conducted with the protected functionalized macroinitiator (**macro2**). Once nanoparticles were made *via* PISA the *t*-butyl esters would be cleaved directly on the particles surface with a subsequent dialysis step for purification.

The previous PISA experiment to obtain 100% functionalized nanoparticles was repeated using the protected **macro2**. The SEC characterization and the <sup>1</sup>H NMR spectrum is shown in Figure 19.

### 3. Amphiphilic Block Copolymer Nanoparticles by Nitroxide-Mediated Polymerization

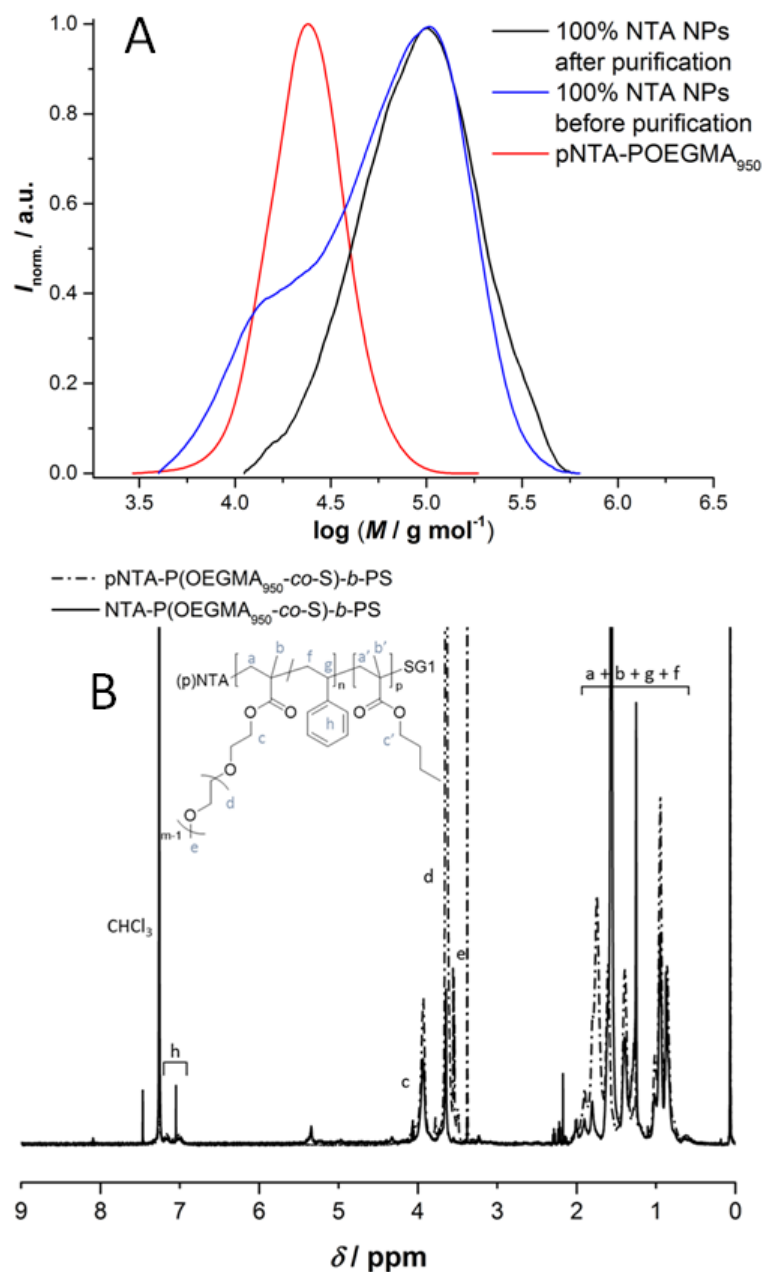


**Figure 19.** (A) SEC traces of the deprotected and purified block copolymer poly(POEGMA<sub>950</sub>-*b*-BMA) from PISA containing a 100% NTA functionalization.  $M_n = 69200 \text{ g mol}^{-1}$  and  $D = 1.60$  (black). (B) Stacked  $^1\text{H}$  NMR spectra before and after deprotection of the purified copolymer.

The SEC trace of the 100% NTA functionalized polymer (Figure 19, blue) indicated the presence of dead macroinitiator. Whether this may be due to a lack of styrene-SG1 end groups in the macroinitiator, a general problem with either the generated alkyl radical or the nitroxide and their  $k_d$  and  $k_c$  values or a negative, unknown influence on the

polymerization qualities resulting from the pNTA functional group, could not be determined. While the polymerization of **macro2** seemed well controlled (Figure 13) it is also known that for increased conversion during the NMP of methacrylates a fraction of dead chains constantly accumulates.<sup>177</sup> Still, an improvement of the reaction compared to the one aforementioned (Figure 18) was noticeable and after removal of unreacted POEGMA chains by centrifugation the purified pNTA-poly(POEGMA<sub>950</sub>-*b*-BMA) amphiphilic block copolymer was obtained. Afterwards, NTA-functionalized nanoparticles were obtained after treatment with aqueous phosphoric acid in water. The purified SEC trace originating from the 100% NTA-functionalized nanoparticles is shown in Figure 19 (black). The resulting stable nanoparticle dispersion obtained from PISA was analyzed by DLS with a narrow distribution and a hydrodynamic number-average diameter of 96 nm.

As mentioned in Chapter 3.4., a complete surface functionalization may not be required. Therefore, a second particle dispersion (**NP3**) with 25% surface functionalization was prepared. **macro2** and **macro4** were used for the initiation of PISA. Similar to Chapter 3.4., a POEGMA<sub>950</sub>-based HO- functionalized macroinitiator as the "diluting" agent was employed. The molar mass of this macroinitiator was chosen to be around 5000 g mol<sup>-1</sup> smaller than the functionalized macroinitiator for the purpose of having the NTA moieties stand out of the corona. The resulting SEC traces are shown in Figure 20. The SEC trace (green) indicated a small amount of unreacted macroinitiator. Whether this came from either functionalized macroinitiator was not possible to determine. However, compared to the SEC trace from the 100% functionalized pNTA polymer (Figure 20, blue trace), the polymerization proceeded with a significantly better control. The shift towards higher molar masses confirmed the successful block copolymer formation. After purification and removal of unreacted macroinitiator, the final polymer displayed a narrow polydispersity (Figure 20, black trace). The stable particle dispersion was analyzed by DLS and exhibited an average hydrodynamic diameter of 99 nm and a narrow distribution (Figure 20B). Afterwards, the particles were deprotected and purified using the same procedure as above.

### 3. Amphiphilic Block Copolymer Nanoparticles by Nitroxide-Mediated Polymerization

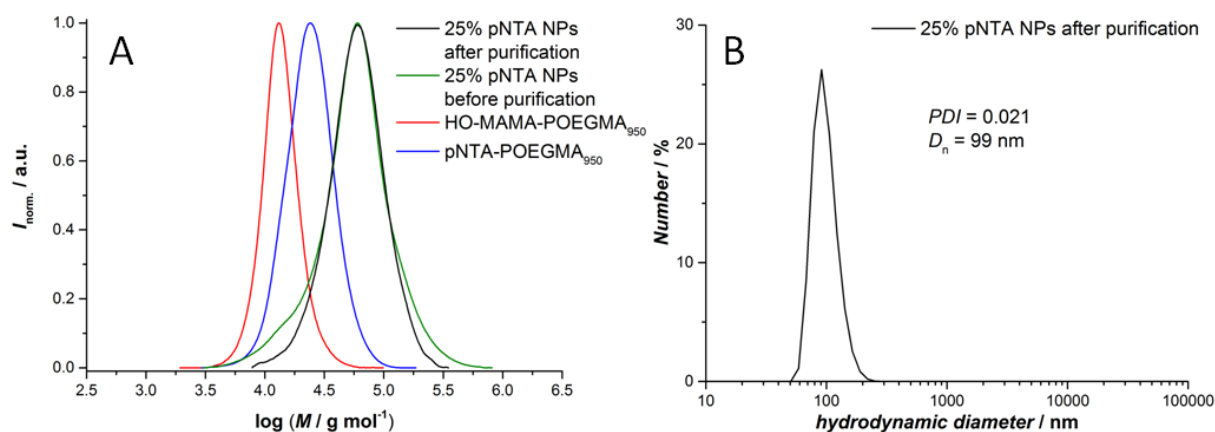


**Figure 20.** (A) SEC traces of deprotected and purified 25% functionalized poly(POEGMA<sub>950</sub>-*b*-BMA) PISA products obtained from simultaneous initiation with **macro2** and **macro4** (red and blue). (B) Corresponding DLS results.

### 3.6. Enzyme Immobilization and Biocatalytic Assay on Functionalized PISA Nanoparticles

In order to evidence the ability to complex His-tagged proteins, both deprotected nanoparticle dispersions (100% NTA and 25% NTA) were subjected to metal complexation. For enzyme purification using His-tagged proteins, resins with Ni<sup>2+</sup> as a chelator are commonly employed. Figure 21 displays the DLS data obtained after nickel complexation for both particle dispersions. The average hydrodynamic diameter did not change drastically for either nanoparticle solution but for both cases the particle size distribution slightly broadened. Inductively coupled plasma optical emission spectrometry (ICP-OES) measurements were performed to determine the amount of nickel complexed by the particles. In order to estimate the number of nickel ions per particle, the number of molar concentration of particles  $N_p$  was calculated by:

$$N_p = \frac{c_{\text{polymer}}}{m_{\text{particle}}} \quad (2)$$

with  $c_{\text{polymer}}$ , the gravimetrically measured concentration of polymer within the dispersion, and the mass of a single particle,  $m_{\text{particle}}$ . The mass of a single particle is

### 3.6. Enzyme Immobilization and Biocatalytic Assay on Functionalized PISA Nanoparticles

defined by its volume and density. However, the current particles consisted of a solid core (PBMA) and a solvated corona (POEGMA). First, the thickness of the solvated shell was roughly estimated with the general assumption that the ethylene glycol units of POEGMA induce a pronounced stretch of the C-C backbone.<sup>178</sup> Considering the degree of polymerization ( $DP_n = 21$ ) of POEGMA, the contribution of the hydrophilic corona to the particles  $D_{shell}$  was assumed to be 10.5 nm ( $21 \text{ units} \times 2.5 \text{ \AA} \times 2$ ). Since the number-average hydrodynamic diameter  $D$  of the particle dispersions was measured by DLS, the core diameter  $D_{core}$  was calculated by:

$$D_{core} = D_{DLS} - 10.5 \text{ nm} \quad (3)$$

The mass of the core  $m_{core}$  was then established by:

$$m_{core} = d_{PBMA} \times V_{core} = \frac{4}{3} \times \pi \times d_{PBMA} \times \left(\frac{D_{core}}{2}\right)^3 \quad (4)$$

$d_{PBMA} = \text{density of PBMA } (1.07 \text{ g cm}^{-3}).$

Based on the conversion during PISA, the mass of a single particle  $m_{particle}$  was obtained by  $m_{shell}/m_{core}$ . Lastly, the number of nickel ions per particle is given by:

$$N_{Ni \text{ per particle}} = \frac{c_{Ni}}{N_p} \quad (5)$$

An average of 7360 and 2919 nickel ions per particle were calculated for 100% and 25% functionalized nanoparticles (**NP2** and **NP3**, respectively). Furthermore, the average area occupied by a nickel atom at the surface  $A_{per Ni}$  was calculated by:

$$A_{per Ni} = \frac{A_{DLS}}{N_{Ni \text{ per particle}}} = \frac{4 \times \pi \times \left(\frac{D_{DLS}}{2}\right)^2}{N_{Ni \text{ per particle}}} \quad (6)$$

$A_{DLS} = \text{surface area of a nanoparticle based on number-average DLS results.}$

### 3. Amphiphilic Block Copolymer Nanoparticles by Nitroxide-Mediated Polymerization

The average distance between two nickel ions was calculated as follows:

$$d_{btwn Ni} = \left( \frac{A_{per Ni}}{\pi} \right)^{1/2} \quad (7)$$

Therefore, each nickel atom occupies an area of 3.9 and 10.5 nm<sup>2</sup>, which translates to a distance between neighboring nickel ions of 1.1 nm and 1.8 nm in average for **NP2** and **NP3**, respectively (see Experimental Section 7.2.2. for a detailed table). Considering the enzymes steric structure, the results suggest that only a fraction of NTA/Ni<sup>2+</sup> complexes will be able to partake in enzyme immobilization.

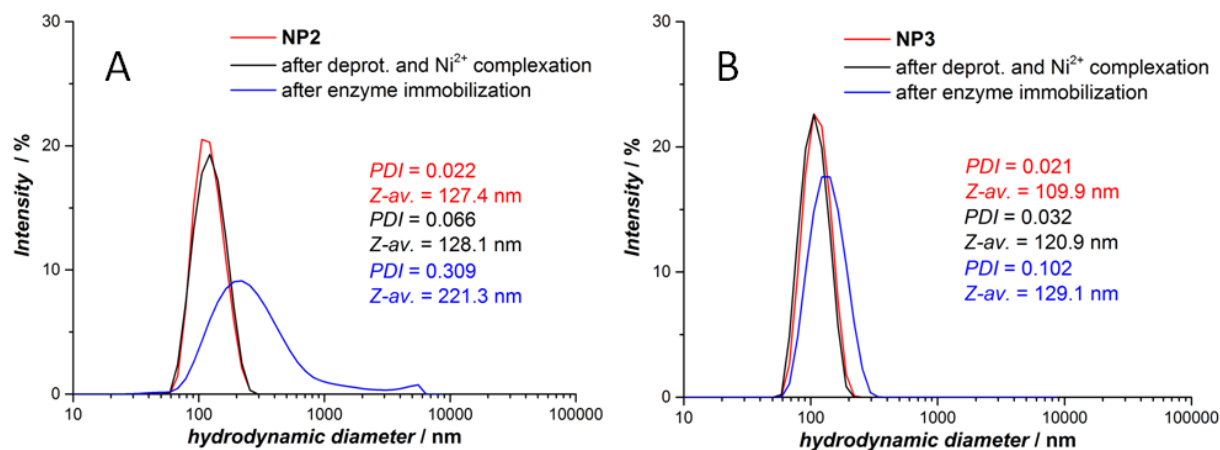


**Figure 21.** Intensity distribution of hydrodynamic diameters of the NTA-functionalized nanoparticles (A) 100% and (B) 25% during different experimental stages.

In order to investigate the particles immobilization capabilities, two His-tagged recombinant proteins, namely horseradish peroxidase (HRP-His) and ester hydrolase (Mes1 esterase-His), were employed. After nickel complexation, incubation with His-tagged enzymes, and purification of the latter, the enzymatic activity was investigated. The successful immobilization is demonstrated by the catalytic activity for both particle dispersions depicted in Figure 22. With increasing enzyme concentrations, faster substrate turnovers were observed. The introduction of HO-functionalized spacer groups in **NP3** (25% NTA functionality) did show less activity as compared to the 100% NTA nanoparticle sample (**NP2**). For both enzymes, similar results were achieved when the effect of the dilution of NTA groups over the kinetic parameter  $k_{cat}$  of the immobilized enzymes was compared, as values for **NP2** ( $2120 \pm 100 \text{ min}^{-1}$  for HRP-His

### 3.6. Enzyme Immobilization and Biocatalytic Assay on Functionalized PISA Nanoparticles

and  $13720 \pm 395 \text{ min}^{-1}$  for Mes1-His) dropped to  $750 \pm 10 \text{ min}^{-1}$  and  $6700 \pm 280 \text{ min}^{-1}$  (2.8 and 2.0-fold reduction, respectively) when NP3 was used as solid support. This indicates that even for lower NTA concentrations (NP3) not all NTA/ $\text{Ni}^{2+}$  complexes may take part in His-tag complexation.

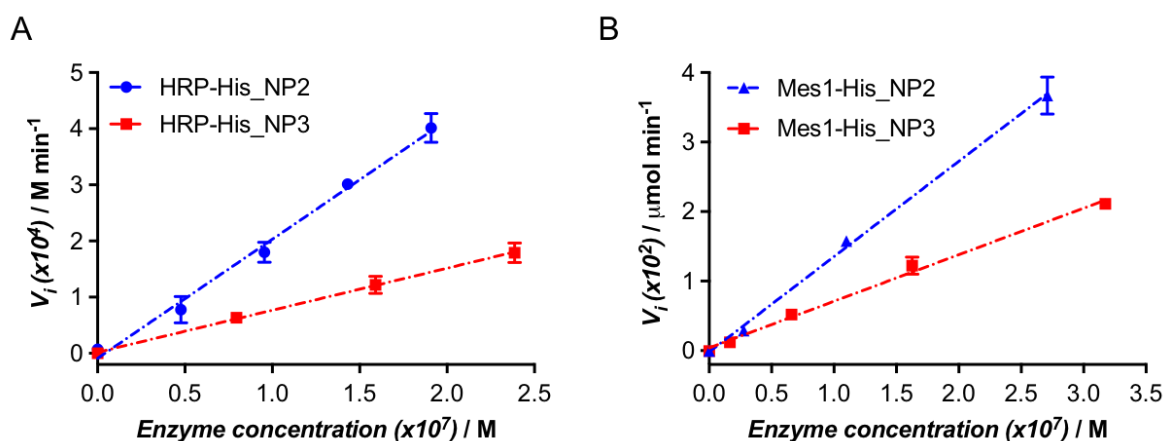


**Figure 22.** Initial velocity vs enzyme concentration plots for (A) HRP-His\_NP2 and HRP-His\_NP3 and (B) Mes1-His\_NP2 and Mes1-His\_NP3. The slope of the linear regression represents  $k_{\text{cat}}$ .

After enzyme immobilization, the nanoparticle dispersion were analyzed anew by DLS. The results are shown in Figure 21. For the 100% functionalized nanoparticles, a large increase in particle size distribution, as well as in hydrodynamic diameter was observed. However, the employed HRP did possess two His-tags at both the *N*- and *C*-termini, which could bridge multiple particles and form large polymer-protein clusters. While the raise in particle size distribution for the 100% functionalized particle dispersion is apparent, the actual intensity derived from these aggregates ( $> 400 \text{ nm}$ ) is very low and only a fraction of the particles aggregated. A similar effect was also observed for the 25% functionalized NPs while the gain in particle size distribution remained small compared to the aforementioned dispersion. Here, the spacer units introduced through the HO-functionalized macroinitiator seemed to have a positive influence on the stability of the nanoparticles.

### 3.7. Conclusion and Outlook

To summarize the investigation, a newly functionalized NMP initiator based on the well-known MAMA-SG1 was synthesized and its initiation potential and end-group attachment to poly(*tert*-butyl acrylate) was successfully demonstrated using mass spectrometry. Afterwards, two functionalized POEGMA-based hydrophilic macroinitiators were synthesized and used in two approaches to obtain nanoparticles. While the chain extension with styrene in bulk and subsequent nanoprecipitation (co-solvent method) of the block copolymer lead to functionalized nanoparticles, the morphologies of the resulting nano-objects could not be sufficiently controlled. Therefore, a second route using the PISA process was employed. In general, PISA is a versatile tool to obtain various morphologies depending on the degree of polymerization. In this investigation only spherical particles could be synthesized even though the DP of the hydrophobic monomer ranged from 170 monomer units (100% NTA functionalized nanoparticles) to 330 monomer units (25% functionalized NTA nanoparticles) of the final block copolymer. These nanoparticles were then utilized for enzyme immobilization experiments. The result of these experiments showed the successful immobilization of His-tagged horseradish peroxidase and esterase on both nanoparticle dispersions with different degrees of surface functionalization and further kinetic assays confirmed that the catalytic activity of the enzymes remained intact after immobilization. At any experimental stage, the particle dispersions demonstrated high stability as suggested by the DLS results.

In conclusion this study demonstrated the successful approach of using functionalized amphiphilic block copolymers by NMPISA and by chain extension as supports for enzyme immobilization. However, the results suggest that NMPISA may not be an adequate system because of its limited range of hydrophobic monomers and low conversion rates after polymerization. Switching the PISA process to a RAFT-based system, which in general are more widely explored than NMPISA, may lead to an improvement in both macromolecular and morphological controls.

Further investigations in various degrees of polymerization with butyl methacrylate may give access to further nano-objects, as mentioned above. Yet, Cryo-TEM would be needed to investigate the actual morphologies of these polymers. Since poly(butyl methacrylate) has a  $T_g$  of around 20 °C, it was not possible to see any morphologies in a non cryo-TEM because of polymer film formation upon drying the sample at ambient temperature.



# Amphiphilic Block Copolymer Nanoparticles by RAFT-Mediated Polymerization

The aim of the work presented in this chapter was the synthesis of amphiphilic block copolymer nanoparticles bearing multiple functional groups on their surface for potential protein immobilization. It is strongly related to Chapter 3, yet is dedicated to increasing the complexity of the final materials, as well as solving issues encountered in this first part of the doctoral work. Therefore, three new functional controlling agents possessing protein-anchoring groups were synthesized. To determine the final surface functionalization of the nanoparticles fluorescent monomers were copolymerized with oligo(ethylene glycol) methyl ether methacrylate (OEGMA<sub>500</sub>) and analyzed *via* fluorescence spectroscopy. RAFT polymerization was utilized in this work, since it has shown an increase in popularity and a steady growth in RAFT-mediated polymerization-induced self-assembly (PISA) formulations during the last decade.<sup>179</sup> While NMPPISA worked, as seen in the previous chapter, it generally suffers from a narrower range of experimental conditions and low conversions.<sup>81</sup> Benzyl methacrylate (BzMA) as a core-forming segment has been successfully employed in RAFT-mediated PISA formulations and has shown to yield a variety of high order morphologies. Even though spherical nanoparticles were here the primary aim, showcasing that other morphologies can be readily attained with a functionalized macromolecular chain transfer agent (macroCTA) may be beneficial for future applications such as biocatalytic hydrogels. Furthermore, a second route towards functionalized nanoparticles *via* chain extension with styrene and

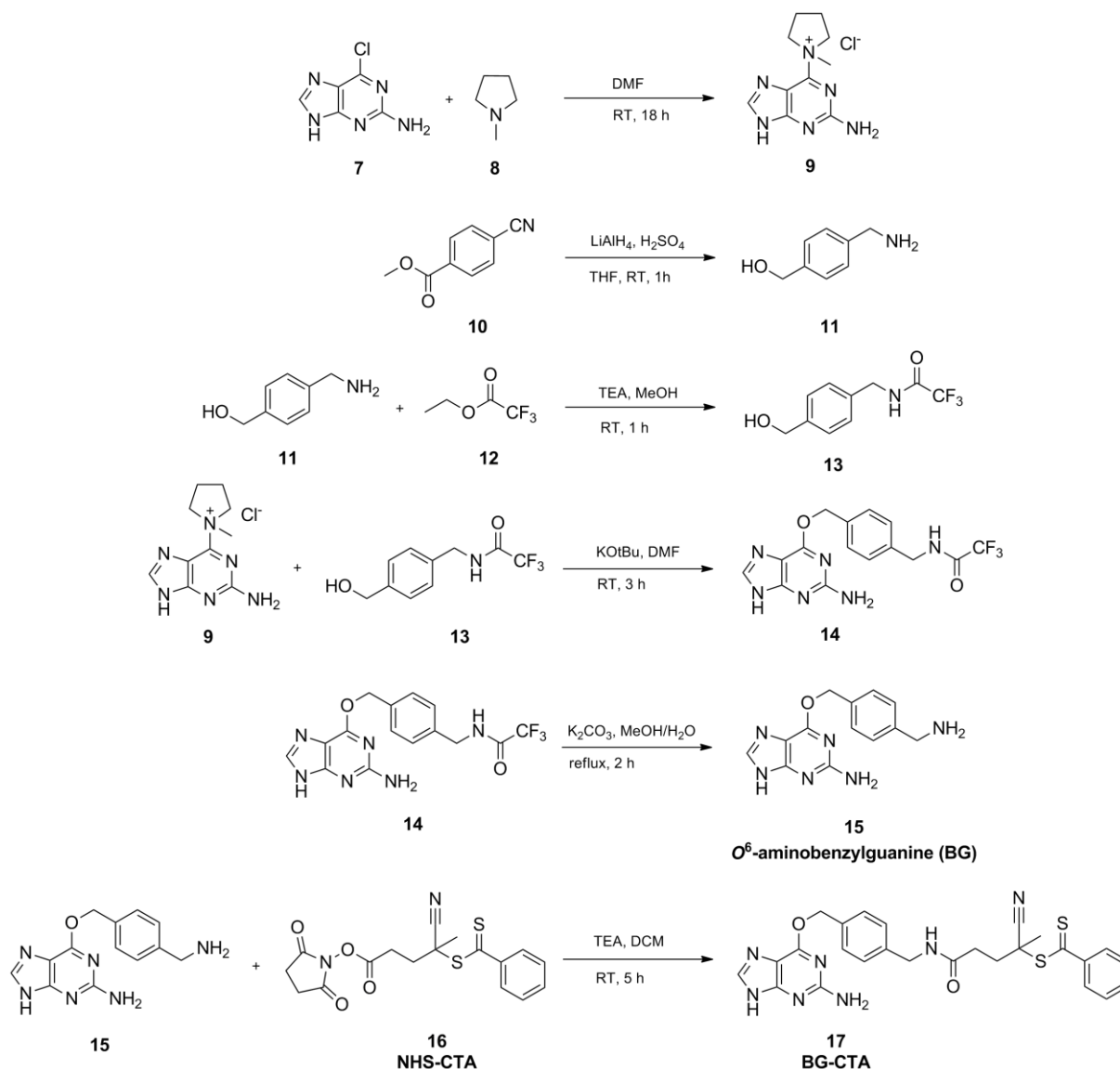
#### 4. Amphiphilic Block Copolymer Nanoparticles by RAFT-Mediated Polymerization

subsequent nanoprecipitation - in analogy to Chapter 3 - was investigated and compared to RAFT-mediated PISA results. Lastly, the concentrations of functional end-groups on the particles corona could be determined based on the particles fluorescence, thanks to an pre-established relationship between fluorescent macroCTA and functional end group.

##### 4.1. Synthesis of Functionalized RAFT CTAs

In order to obtain multifunctional nanoparticles, new chain transfer agents for RAFT polymerization were synthesized. As shown in the previous chapter, immobilization of His-tagged enzymes was accomplished thanks to a NTA-functionalized initiator. Even though the immobilization was successful, the chelat between NTA-Ni<sup>2+</sup> and the His-tagged enzyme is based on non-covalent metal complexation and is therefore relatively unstable, relying on ionic interactions, as compared to other protein tags that bind covalently to their respective substrates. Also, determining the nickel concentration within the particle dispersion to infer to the actual binding moiety concentration on the surface is not a trivial matter and is prone to errors arising from the low amounts obtained after polymerization. Therefore, two protein tags beyond polyhistidine were targeted. As described in Chapter 2.3., SNAP- and Halo-tags are suitable candidates for this purpose. For each protein tag, a suitable anchoring group/substrate needed to be synthesized. For binding to the SNAP-tag, a benzylguanine derivative (*O*<sup>6</sup>-aminobenzylguanine (BG)) was obtained following literature procedures.<sup>152</sup> The synthetic route in Scheme 18 leading to a BG-functionalized RAFT chain transfer agent is shown. The synthesis involved five steps under Schlenk conditions and flash column chromatography after most steps until *O*<sup>6</sup>-aminobenzylguanine was obtained. While the reactions gave yields comparable to those found in literature reports, the amount of final product was in the range of 200-400 mg. Indeed, BG has so far been reported mostly in chemical biology or surface functional-related contexts.<sup>180</sup> In these cases, only small amounts are required. Upscaling the reactions lead to a significant decrease in yields and hence would waste precious starting material. For this reason, the complete synthesis of BG was performed repeatedly until a sufficient amount could be obtained. In the sixth step, a coupling reaction between the primary amine of BG and the activated NHS ester

moiety of a commercially available RAFT agent, 4-cyano-4-(phenylcarbonothioylthio)pentanoic acid *N*-succinimidyl ester (NHS-CTA), was performed. The yields after purification ranged from 25-45% and required multiple synthetic repeats to isolate roughly 700 mg of BG-functionalized RAFT agent (BG-CTA **17**). The new RAFT agent retained the characteristic red color of the dithiobenzoate group and could be stored for indefinite time if kept in dark and cooled conditions.



**Scheme 18.** Complete synthetic pathway to obtain BG and BG-functionalized RAFT agent.

Proton NMR verified the successful synthesis with all significant peaks being assigned to the expected CTA structure (Figure 23). While the final coupling step was performed in

#### 4. Amphiphilic Block Copolymer Nanoparticles by RAFT-Mediated Polymerization

DMF, it was not possible to completely remove DMF from the final product (as shown in Figure 23), even after several purification steps ranging from extraction of DMF, co-evaporation with toluene, to lyophilisation. Nevertheless, ESI-MS analysis confirmed the successful synthesis of BG-CTA (**17**) ( $[M+Na]^+$   $m/z_{\text{calc}}$ : 554.1403  $m/z_{\text{found}}$ : 554.1411).

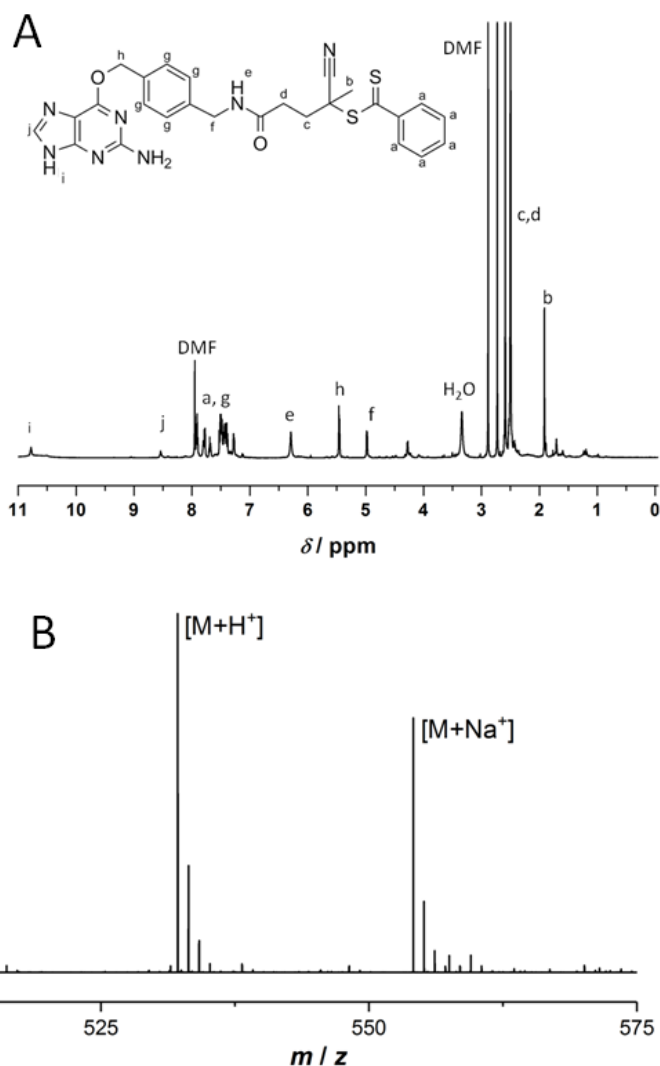
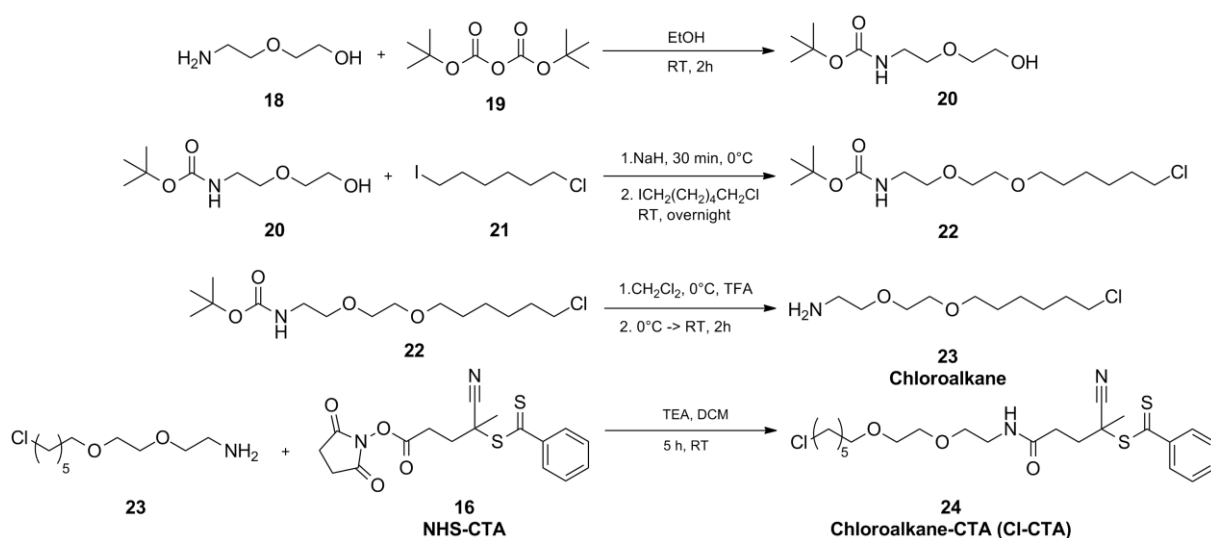


**Figure 23.** (A) <sup>1</sup>H NMR and (B) ESI-MS spectrum of BG-CTA.

The second functionalized RAFT agent (Cl-CTA) featured a 2-(2-((6-chlorohexyl)oxy)ethoxy)ethyl moiety able to covalently bind to Halo-tagged proteins. Following literature procedures, the synthesis involved four synthetic steps, the last one being an amidation reaction of the haloalkane with the NHS-activated RAFT agent (Scheme 19).<sup>181</sup> Similar to the aforementioned BG-CTA, all steps required Schlenk conditions with flash column chromatography as the purification method of choice. The

yields were in good agreement with literature for the synthesis of the chloroalkylamine derivative, while the final coupling step with the RAFT agent ranged from 20-40%. Considering that upscaling the reactions lead to no beneficial increase in yields, the synthetic steps had to be remade regularly in order to obtain 1 g of Cl-CTA.



**Scheme 19.** Complete synthetic pathway of 2-(2-((6-chlorohexyl)oxy)ethoxy)ethaneamine and Cl-functionalized RAFT agent.

Figure 24 displays the proton NMR and ESI-MS data acquired for the final Cl-CTA (**24**). The  $^1\text{H}$  NMR showed little to no impurities and the peaks could be assigned to the targeted chemical structure. Furthermore, ESI-MS analysis was in good agreement with the calculated  $m/z$  values for Cl-CTA ( $[[\text{M}+\text{Na}]^+ m/z_{\text{calc}}: 507.1513 m/z_{\text{found}}: 507.1524]$ ) displaying the chlorine isotops  $^{35}\text{Cl}$  and  $^{37}\text{Cl}$  and confirming the successful synthesis of the RAFT agent. Similarly to BG-CTA, the Cl-CTA exhibited a deep red color and could be stored for indefinite time if kept in dark and cooled conditions.

#### 4. Amphiphilic Block Copolymer Nanoparticles by RAFT-Mediated Polymerization

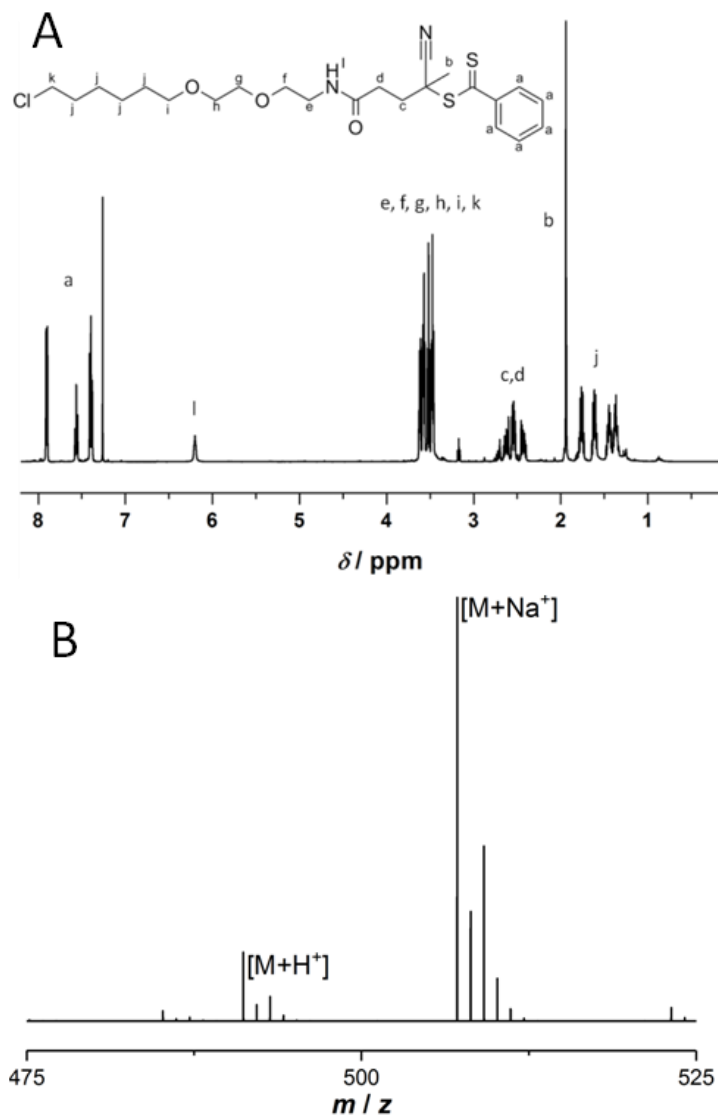
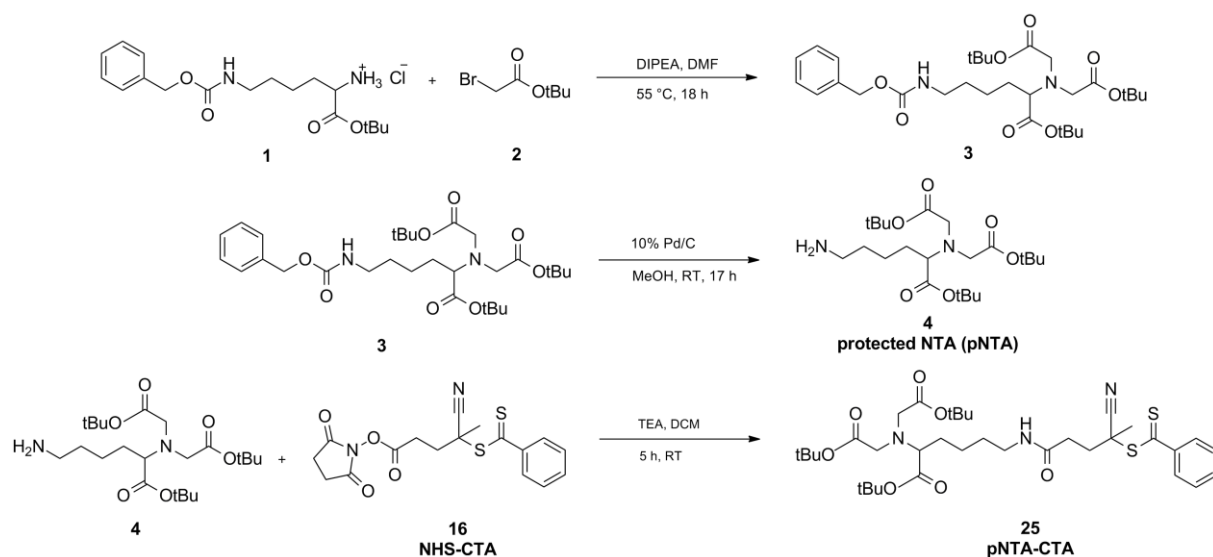


**Figure 24.** (A)  $^1\text{H}$  NMR and (B) ESI-MS spectrum of Cl-CTA.

Lastly, a pNTA-functionalized RAFT agent was synthesized with the previously obtained pNTA amine and RAFT group (Scheme 20). The coupling step between pNTA and NHS-CTA required Schlenk conditions with flash column chromatography as the purification method of choice. After purification, the reaction yielded 60% (550 mg) of pure pNTA-CTA (**25**).

## 4.1.

## Synthesis of Functionalized RAFT CTAs



**Scheme 20.** Complete synthetic pathway of pNTA and pNTA-functionalized RAFT agent.

Proton NMR verified the successful synthesis of pure pNTA-CTA with all significant peaks being assigned to the CTA structure (Figure 25). Subsequent ESI-MS measurements were in good agreement with calculated  $m/z$  values ( $[M+Na]^+$   $m/z_{\text{calc}}$ : 714.3217  $m/z_{\text{found}}$ : 714.3229). Similarly to the previous chain transfer agents, the pNTA-CTA exhibited a deep red color and could be stored for indefinite time if kept in dark and cooled conditions.

4. Amphiphilic Block Copolymer Nanoparticles by RAFT-Mediated Polymerization

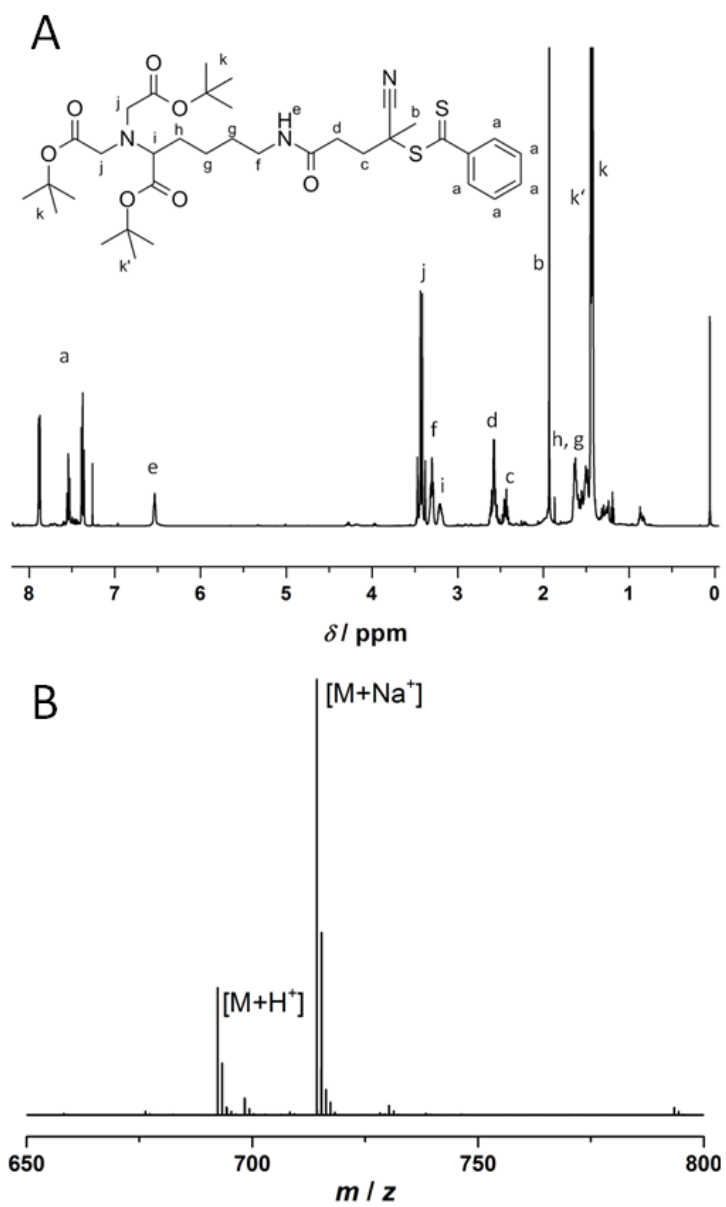


**Figure 25.** (A) <sup>1</sup>H NMR and (B) ESI-MS spectra of pNTA-CTA.

## 4.2. Synthesis of Fluorescent Hydrophilic Block Segments for PISA

Because of the beneficial properties mentioned in Chapter 3.3., oligo(ethylene glycol) methyl ether methacrylate (OEGMA) was again chosen as hydrophilic block forming monomer. OEGMA monomer with a number-average molar mass of 500 g mol<sup>-1</sup> was utilized in the RAFT polymerizations. Even though OEGMA<sub>950</sub> may stabilize nanoparticles better through its longer brush segments than the smaller OEGMAs and is not known to have neither UCST nor LCST behavior in water or any other polar solvent, the purification of an OEGMA<sub>950</sub>-based polymer is not trivial. Precipitation in cold diethylether/pentane results in co-precipitation of the oligomeric monomer making separation of polymer and residual monomer difficult. Also, dialysis in water is not suitable since the dithiobenzoate end-group of the polymer is prone to hydrolysis ( $k_{\text{hydrolysis}} = 2.5 \times 10^5 \text{ s}^{-1}$  at pH 7).<sup>182</sup> Chain extension of a macroCTA with a partly hydrolysed RAFT end-group would result in incomplete chain extension, broad molar mass distributions, and an overall poor control of the polymerization, leaving behind a non-negligible amount of water-soluble chains. OEGMA<sub>300</sub> was known to exhibit a thermo responsive behavior in aqueous and polar solvent, which initial PISA test reactions with a non-functionalized OEGMA<sub>300</sub>-based macroCTA confirmed. Hence it was not utilized further.<sup>183</sup>

In order to evaluate the concentration of functional groups on the particle surface, the hydrophilic macroCTA were independently fluorescently tagged. For this purpose, fluorescent monomers that could be added to a RAFT polymerization process were utilized. Their chemical structure is depicted in Figure 26.

#### 4. Amphiphilic Block Copolymer Nanoparticles by RAFT-Mediated Polymerization

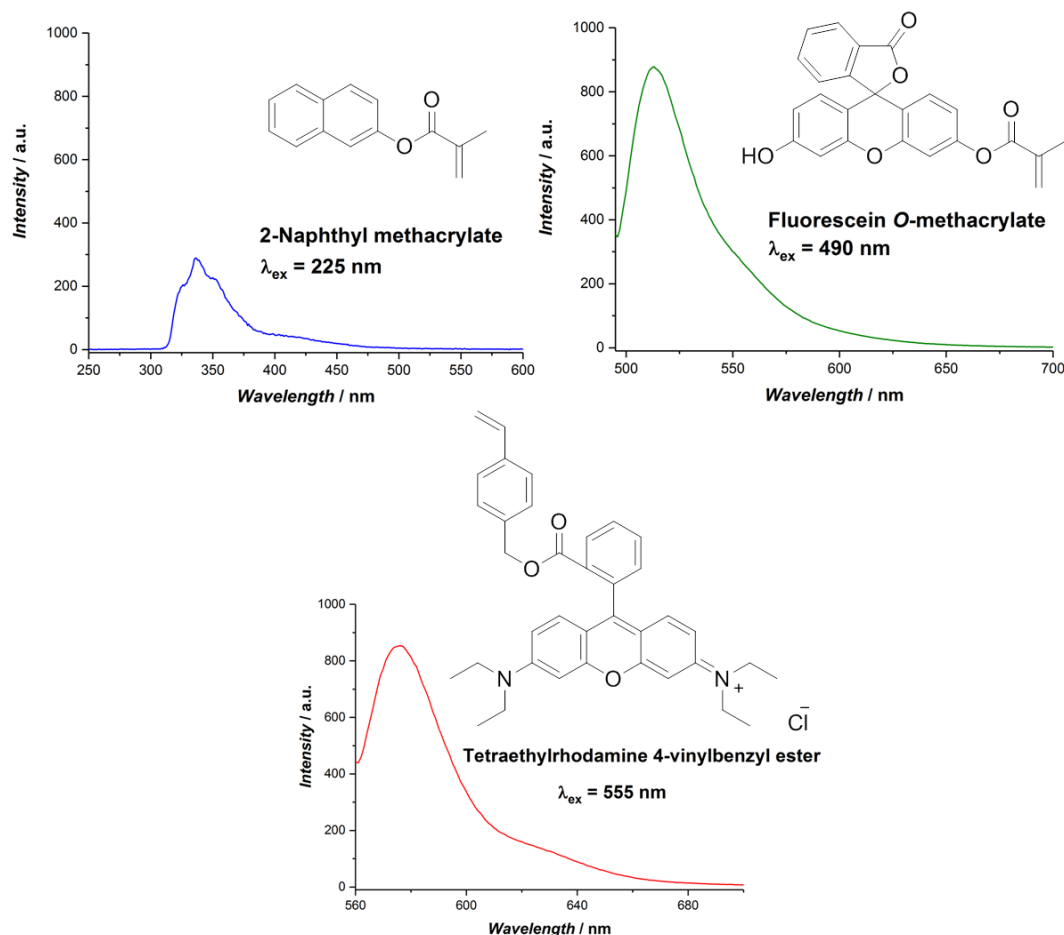


**Figure 26.** Emission spectra of naphthyl methacrylate (NMA), fluorescein *O*-methacrylate (FMA), and tetraethylrhodamine 4-vinylbenzyl ester (VBR) and their corresponding chemical structure.

The choice over commercial fluorescent monomers with suitable excitation wavelengths that would not overlap with each other was limited. Fluorescein methacrylate (FMA) and naphthyl methacrylate (NMA) were selected since their absorption maxima lay at 490 nm and 225 nm, respectively. Tetraethylrhodamine 4-vinylbenzyl ester (VBR) showed an absorption maximum at 555 nm similarly to rhodamine B (540-550 nm), yet with a slight red shift of about 10 nm.<sup>184</sup> VBR was synthesized following a literature procedure.<sup>185</sup>

In order to obtain nano-objects by PISA the molecular weight of macroCTAs was a crucial factor. Hence, two different molar masses between 5000-6000 g mol<sup>-1</sup> and 11000-12000 g mol<sup>-1</sup> were targeted. In a typical polymerization 5 mol% of fluorescent monomer was added to the polymerization. Furthermore, a non-functionalized

macroCTA was synthesized from 2-cyano-2-propyl dithiobenzoate (CPDB) as the chain transfer agent and was utilized in PISA as a spacer unit between functional groups on the particles surface. The characteristics of the synthesized macroCTAs are listed in Table 2.

**Table 2.** Main characteristics of the final macroCTAs utilized in bulk or emulsion polymerization.

	structure	target $M_n$ (g mol <sup>-1</sup> ) <sup>a</sup>	$X_{NMR}$ (%) <sup>b</sup>	$M_{n,NMR}$ (g mol <sup>-1</sup> ) <sup>c</sup>	$M_{n,SEC}$ (g mol <sup>-1</sup> ) <sup>d</sup>	$\mathcal{D}^c$
<b>macro CTA1</b>	Cl-P(OEGMA <sub>500</sub> -co-FMA)	5 500	-	5 800	5 500	1.12
<b>macro CTA2</b>	Cl-P(OEGMA <sub>500</sub> -co-FMA)	12 000	91	12 400	10 400	1.13
<b>macro CTA3</b>	BG-P(OEGMA <sub>500</sub> -co-NMA)	5 500	90	4 600	6 600	1.09
<b>macro CTA4</b>	BG-P(OEGMA <sub>500</sub> -co-NMA)	12 000	89	12 000	13 600	1.13
<b>macro CTA5</b>	P(OEGMA <sub>500</sub> -co-VBR)	12 000	-	11 100	8 200	1.32
<b>macro CTA6</b>	pNTA-P(OEGMA <sub>500</sub> -co-VBR)	12 000	-	9 200	7 000	1.18

<sup>a</sup>at full conversion. <sup>b</sup>OEGMA conversion determined by <sup>1</sup>H NMR spectroscopy. <sup>c</sup>Molar mass was determined by aromatic protons signals of the RAFT benzyl group. <sup>d</sup>Experimental  $M_n$  obtained by SEC in DMAc using PS calibration.

All functional chain transfer agents were able to successfully control the polymerization of OEGMA<sub>500</sub> which resulted in well-defined, functionalized, and fluorescent polymers. The molar masses of the hydrophilic polymers were determined by SEC and <sup>1</sup>H NMR spectroscopy. No adequate SEC calibration is available for brush-like POEGMA. Therefore, NMR calculations based on the aromatic proton signals of the RAFT end group represent the actual molar mass of the polymers more accurately. SEC analysis of the final polymers indicated narrow molar mass distributions and thus controlled RAFT polymerizations.

#### 4. Amphiphilic Block Copolymer Nanoparticles by RAFT-Mediated Polymerization

Successful incorporation of fluorescent monomer into the final polymer was confirmed by  $^1\text{H}$  NMR spectroscopy and fluorescence spectroscopy. Using the number-average molar mass, the intensity of emission of each macroCTA could directly be related to the concentration of functional end-groups by establishing calibration curves. For this, different dilutions of a fixed amount of macroCTA were prepared and their emission spectrum was recorded in a fluorometer. Figure 27 is a collection of the emission spectra of the three macroCTAs for several concentrations in water.

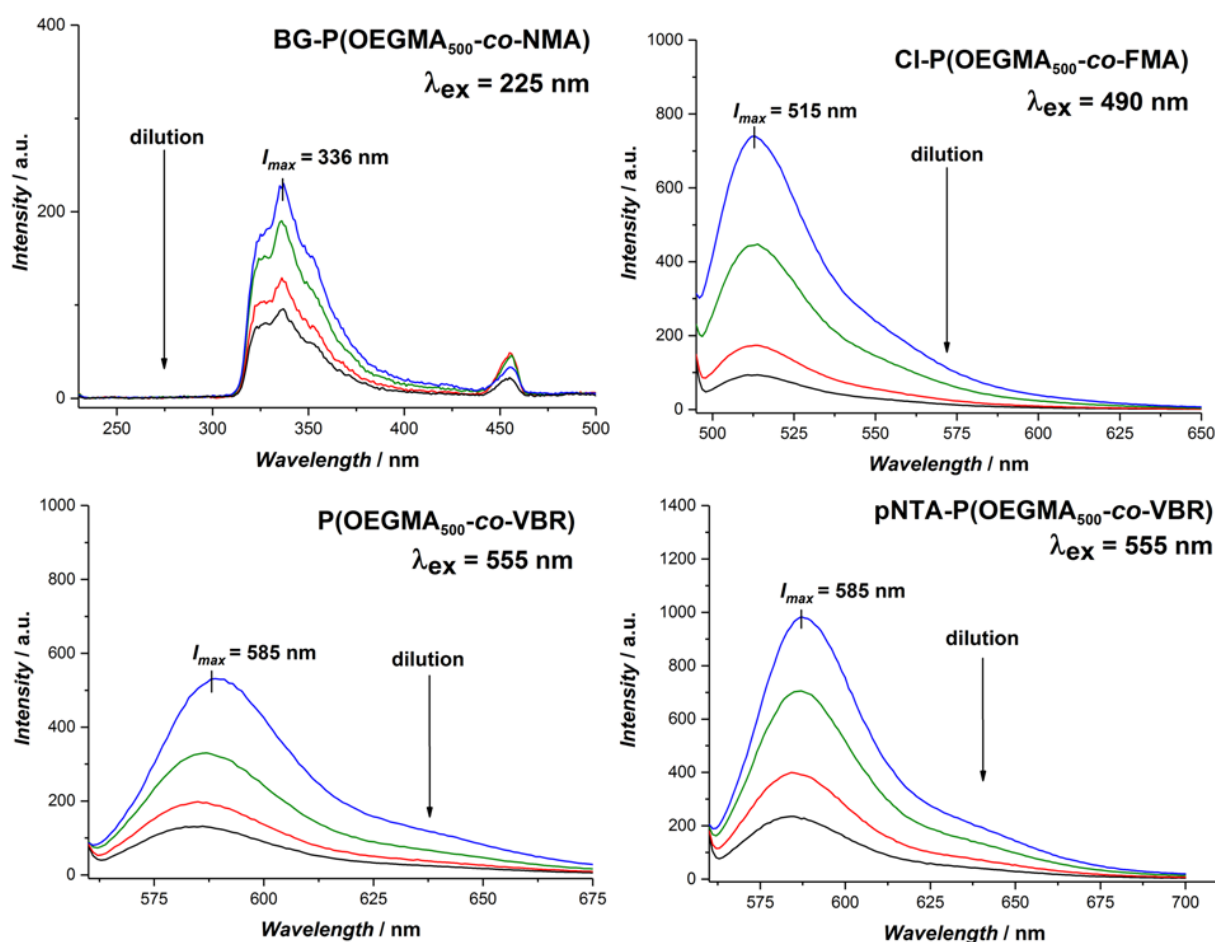


**Figure 27.** Emission spectra obtained by fluorescence spectroscopy for varying macroCTA dilutions.

Fluorescence intensity is typically proportional to concentration but certain factors may negatively affect the linear relationship. If the concentration of the sample is too high, light is not able to pass through to cause excitation of the fluorophore. Therefore at high concentrations the measured intensity will decrease. Another problem arises at intermediate concentrations in which the volume closest to the incident light absorbs so

much light that little remains for the rest of the sample, resulting in non linear readings. However, at intermediate concentrations it is possible to establish a calibration curve where the intensity of emitted light is proportional to the fluorophore concentration.<sup>186</sup>

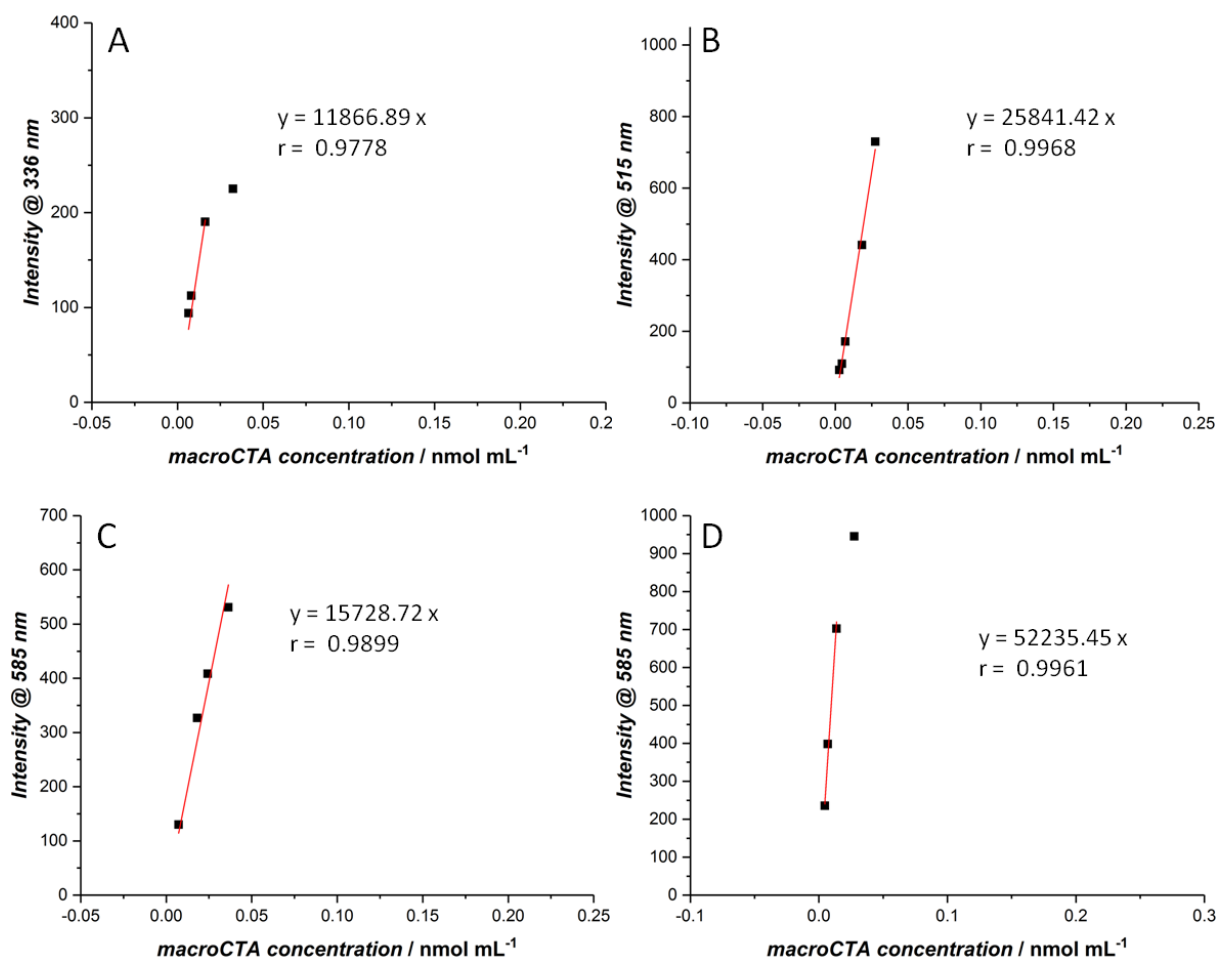


**Figure 28.** Calibration curves of (A) BG-P(OEGMA<sub>500</sub>-*co*-NMA) (**macroCTA4**), (B) Cl-P(OEGMA<sub>500</sub>-*co*-FMA) (**macroCTA2**), (C) P(OEGMA<sub>500</sub>-*co*-VBR) (**macroCTA5**), and (D) pNTA-P(OEGMA<sub>500</sub>-*co*-VBR) (**macroCTA6**).

Considering that the molar mass of macroCTAs was calculated by <sup>1</sup>H NMR through the benzoate end-group of the functionalized RAFT agent and assuming that > 99% chains have been initiated by the functional R group, the concentration of macroCTA was equivalent to the concentration of the functional group attached to it. Since the fluorescence intensity was directly proportional to the functional end-group of the polymer, the concentration of functional end-groups on the particle surfaces could be

#### 4. Amphiphilic Block Copolymer Nanoparticles by RAFT-Mediated Polymerization

calculated through the linear regression of the calibration curves of the respective macroCTAs (Figure 28). Solving the linear equation (8)

$$I_{max,fluorophore} = m * [macroCTA] + b \quad (8)$$

with a fixed interception  $b$  at 0 for the concentration of macroCTA, gave equation (9):

$$[macroCTA] = \frac{I_{max,fluorophore}}{m} = [functional\ end\ group] \quad (9)$$

$m = slope.$

### 4.3. Multifunctional Nanoparticles via Chain Extension and Nanoprecipitation

The classical approach towards multifunctional nanoparticles was chain extension of the macroCTAs with a hydrophobic block in a non-selective solvent, followed by nanoprecipitation. Similarly to Chapter 3.4., polystyrene was chosen as the solvophobic segment of the amphiphilic block copolymer. **MacroCTAs 2, 4 and 5** with a molar mass of about 12000 g mol<sup>-1</sup> were utilized in the bulk polymerization since larger quantities of those chain transfer agents were available. The polymerizations were conducted at 120 °C for 5 h, the crude polymer was purified by precipitation of in cold methanol. The purified block copolymers retained the red coloration of the dithiobenzoate group, with slight variations because of the incorporated fluorophores. The three resulting block copolymers are listed in Table 3.

**Table 3.** Characteristics of the amphiphilic block copolymers obtained by bulk RAFT polymerization of styrene.

structure	$X_{\text{NMR}}$ (%) <sup>a</sup>	actual <i>Sty</i> $DP_n$ <sup>a</sup>	$M_{n,\text{NMR}}$ (g mol <sup>-1</sup> ) <sup>b</sup>	$M_{n,\text{SEC}}$ (g mol <sup>-1</sup> ) <sup>c</sup>	$D^b$
Cl-P(OEGMA <sub>500-co</sub> -FMA)- <i>b</i> -PS	16	430	44 800	24 200	1.19
BG-P(OEGMA <sub>500-co</sub> -NMA)- <i>b</i> -PS	17	447	46 500	40 700	1.46
P(OEGMA <sub>500-co</sub> -VBR)- <i>b</i> -PS	27	414	43 000	18 500	1.17
pNTA-P(OEGMA <sub>500-co</sub> -VBR)- <i>b</i> -PS	22	318	36 300	33 200	1.25

<sup>a</sup>Degree of polymerization and conversion of styrene determined by <sup>1</sup>H NMR spectroscopy. <sup>b</sup>Molar mass was determined by proton signals of hydrophilic block segment. <sup>c</sup>Experimental  $M_n$  obtained by SEC in DMAc using PS calibration.

SEC traces of the block copolymers displayed a clear growth in molecular weight with reasonable dispersities (Figure 29). Yet, all polymers exhibited a shoulder at high molar mass which might be due to early termination events.<sup>187-188</sup> Macromolecular intermediate radical species can exhibit an increased stability which makes them prone to reactions with other propagating radical or with themselves which results in rate retardation and formation of “dead” higher molecular weight polymer.

#### 4. Amphiphilic Block Copolymer Nanoparticles by RAFT-Mediated Polymerization

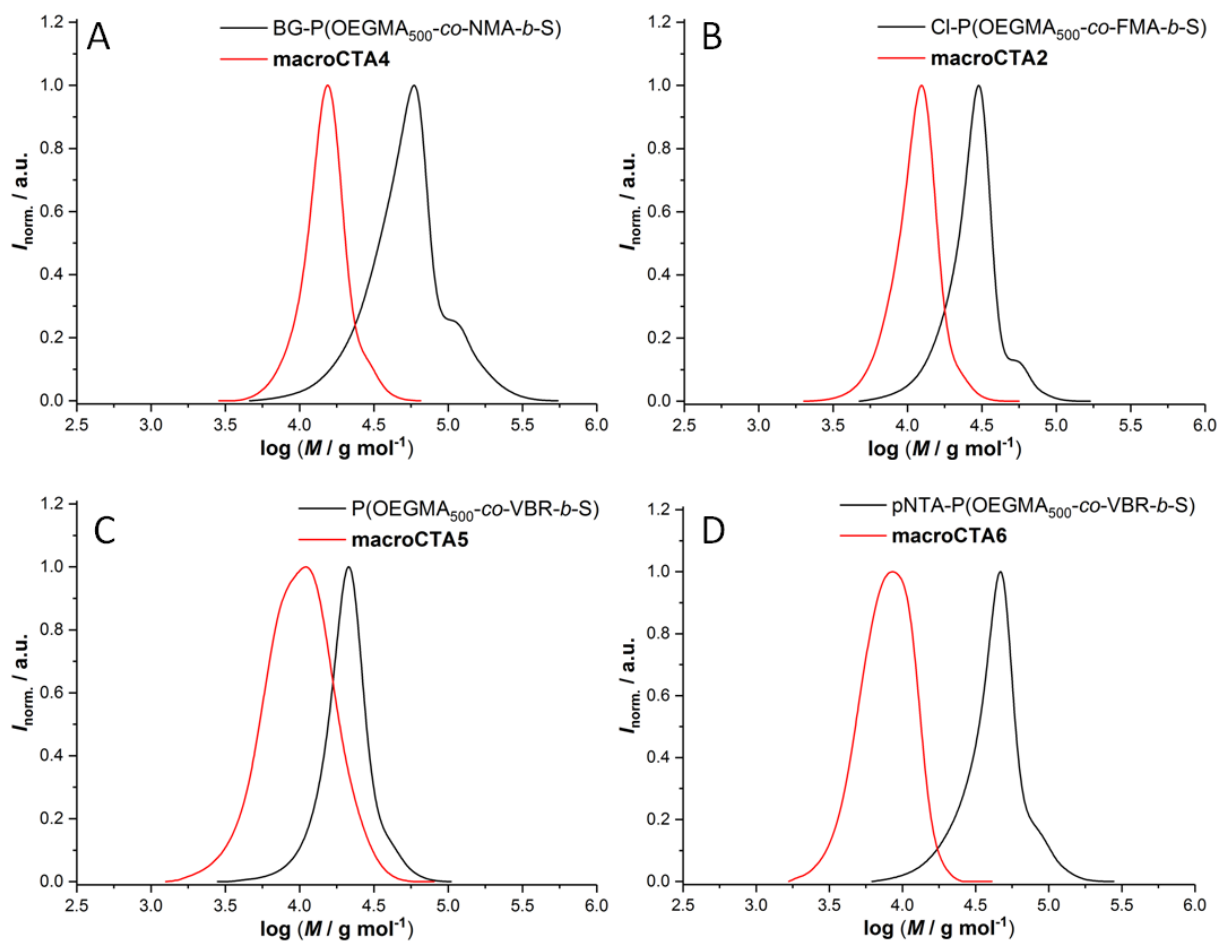


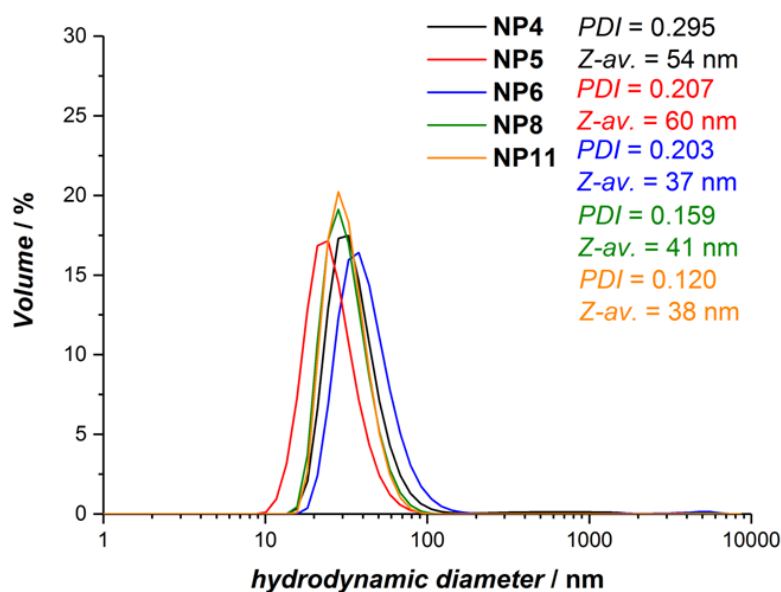
**Figure 29.** SEC traces of purified (A) BG-P(OEGMA<sub>500</sub>-*co*-NMA)-*b*-PS, (B) Cl-P(OEGMA<sub>500</sub>-*co*-FMA)-*b*-PS, (C) P(OEGMA<sub>500</sub>-*co*-VBR)-*b*-PS, and (D) pNTA-P(OEGMA<sub>500</sub>-*co*-VBR)-*b*-PS with their respective macroCTAs.

Different mixtures of amphiphilic block copolymers were used for nanoprecipitation to obtain (multi-)functionalized nanoparticles. For each block copolymer, one particle suspension with a 100% surface functionalization - that is from a single block copolymer - was prepared. Afterwards, nanoparticle suspensions with 50% : 50% Cl- and BG functionalization and 33% : 33% : 33% of Cl-, BG- and non-functional content were produced (Table 4).

**Table 4.** Nanoparticle suspensions obtained by nanoprecipitation and their respective DLS characteristics and functional surface content.

	<i>target surface functionalization</i>	<i>Z-av. (nm)<sup>a</sup></i>	<i>PDI<sup>a</sup></i>	<i>[functional end group] (<math>\mu\text{M}</math>)<sup>b</sup></i>
<b>NP4</b>	100 % blank	54	0.295	-
<b>NP5</b>	100% Cl	37	0.203	0.0079
<b>NP6</b>	100% BG	60	0.207	0.0156
<b>NP7</b>	100% NTA	136	0.241	0.0094
<b>NP8</b>	50% Cl	41	0.159	0.0087
	50% BG			0.0108
<b>NP9</b>	50% Cl	84	0.298	0.0012
	50% NTA			0.0084
<b>NP10</b>	50% BG	119	0.420	0.0049
	50% NTA			0.0089
<b>NP11</b>	33% Cl	38	0.120	0.0314
	33% BG			0.0721
	33% blank			-
<b>NP12</b>	33% Cl	55	0.171	0.0012
	33% BG			0.0047
	33% NTA			0.0123

<sup>a</sup>Volume-average hydrodynamic diameter and dispersity determined by DLS. <sup>b</sup>Concentration of functional end groups calculated from Eq. (9) (*vide supra*).

**Figure 30.** Hydrodynamic diameter volume distribution of the functional nanoparticles obtained *via* nanoprecipitation.

#### 4. Amphiphilic Block Copolymer Nanoparticles by RAFT-Mediated Polymerization

The resulting NP suspensions were directly analyzed by DLS without prior filtering. Figure 30 displays hydrodynamic diameter volume-average of these nanoparticles. All particle dispersions showed a monomodal distribution, punctually with minor aggregation or contamination above 1000 nm. The average hydrodynamic diameter for the dispersions was between 37-60 nm, while the dispersity did not exceed 0.295 indicating only moderate till narrow particle distributions. To confirm the actual size and morphology, the multifunctional particles were analyzed by TEM without prior staining. TEM images are shown in Figure 31 for **NP8** and **NP11**.

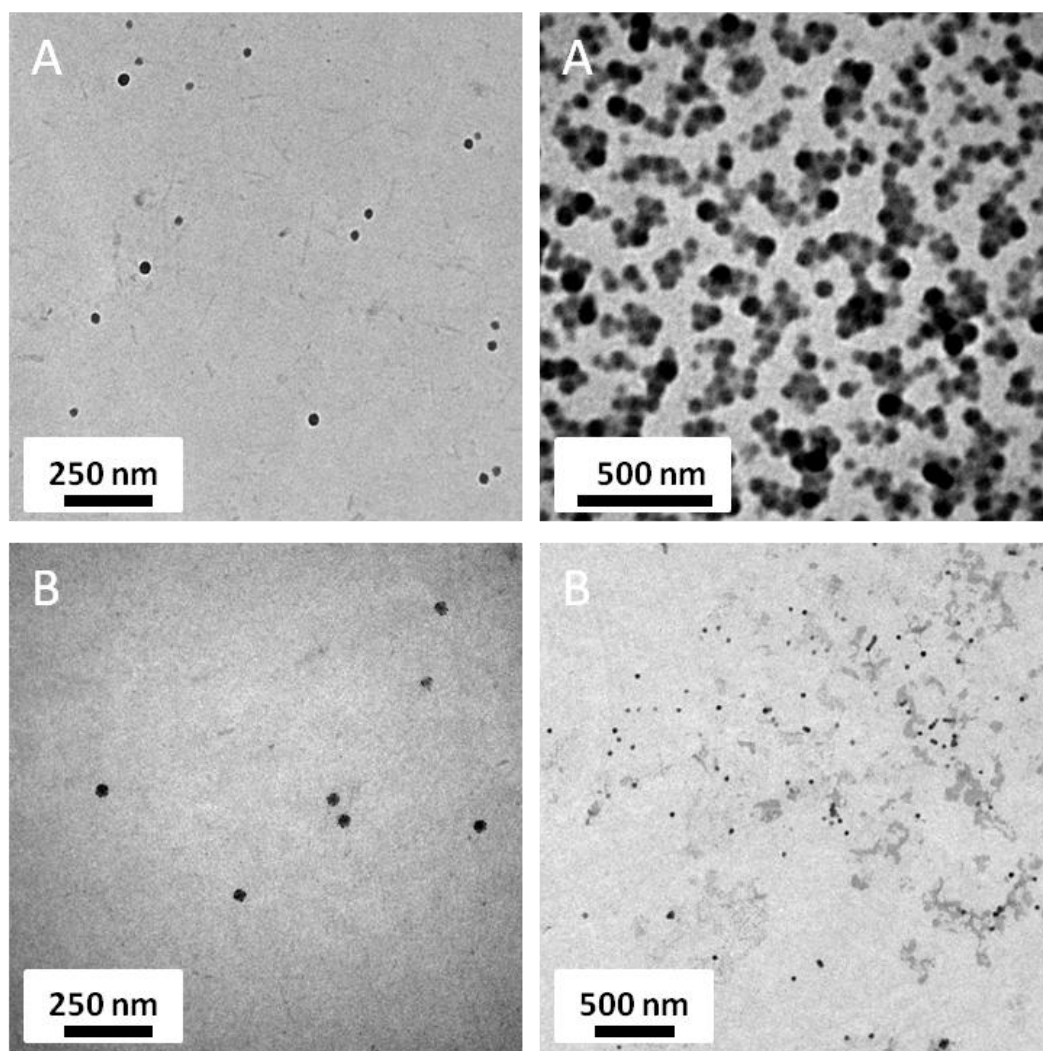


**Figure 31.** Representative TEM images of multifunctional nanoparticles (A) **NP8** and (B) **NP11** obtained *via* nanoprecipitation.

The multifunctional nanoparticle suspensions consisted of individual spherical particles with no visible aggregation. Other morphologies such as rods or donut-like structure were not observed. For both suspensions, TEM confirmed average particle sizes below 50 nm and uniform size distribution which was in very good agreement with the aforementioned DLS results.

In order to detect fluorescence derived from the nanoparticles, all suspensions were analyzed in a fluorometer. The recorded emission spectra from the particle suspensions showed the specific intensity maxima of each incorporated fluorophore. The functional end-group concentrations were then calculated using the previously established calibration curves (Figure 28) and equation 9. Concentrations were in the low micromolar range which was expected since the amount of copolymer used for nanoprecipitation was small to begin with (see Experimental Section 7.3.2.). For multifunctional NP solutions **NP8** and **NP11** the ratios of haloalkane- and benzylguanine end-groups were 1 : 1.2 and 1 : 2.3 respectively. While functional end-group ratios of **NP8** were close to the theoretical 1 : 1 ratio, calculations for **NP11** pointed at a larger BG ratio. The lower apparent concentration of haloalkane functionalization for **NP11** can be explained if the third fluorophore, VBR incorporated in the non-functional macroCTA, is taken into account. Figure 32 schematically displays the normalized emission spectrum of fluorescein at 490 nm and the absorbance spectrum of VBR in order to demonstrate the overlapping regions of the spectra.

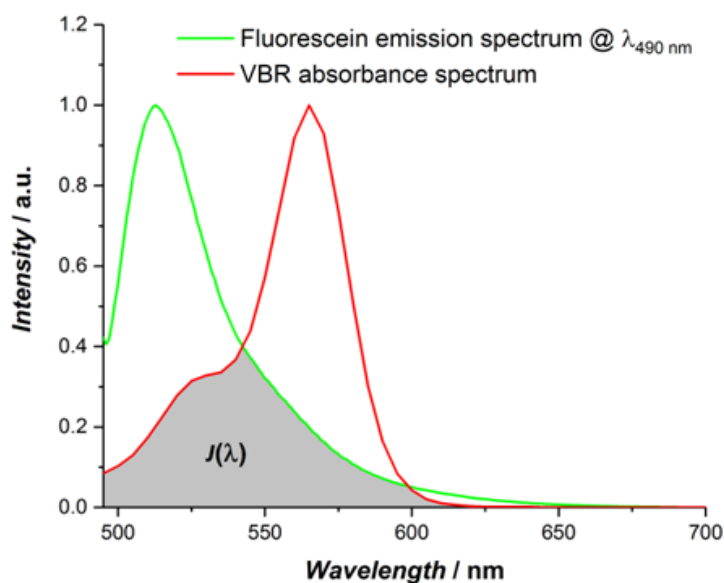


**Figure 32.** Schematic depiction of the normalized emission spectrum of fluorescein and absorbance spectrum of VBR with spectral overlap integral  $J(\lambda)$  (gray).

#### 4. Amphiphilic Block Copolymer Nanoparticles by RAFT-Mediated Polymerization

Parts of the fluorescein emission spectrum can overlap with the VBR absorbance spectrum, making an energy transfer from fluorescein to VBR feasible which in turn would diminish the apparent fluorescence of fluorescein. This phenomenon is known as Förster resonance energy transfer (FRET). In FRET, a donor fluorophore (here, fluorescein) in its electronic excited state, transfers energy to a parallel-oriented acceptor fluorophore (here, VBR) through non-radiative dipole-dipole coupling. Yet, the efficiency of FRET heavily relies on the distance  $r$  between donor and acceptor as indicated by equation (10):

$$k_{ET} = k_D \frac{R_0^6}{r^6} \quad (10)$$

*k<sub>ET</sub>* = rate of energy transfer, *k<sub>D</sub>* = radiative emission rate of donor, *R<sub>0</sub>* = Förster distance, *r* = donor-acceptor separation distance.

Therefore, FRET only occurs if the donor-acceptor distance is between 1-10 nm. This conversely suggests that the fluorophores, and thus the functional end-groups, are located on the same nanoparticles, which is obviously expected.<sup>189</sup>

In conclusion the analytical results for the nanoparticle suspensions obtained from chain extension with styrene and subsequent nanoprecipitation confirmed the successful synthesis of multifunctional amphiphilic nanoparticles.

#### 4.4. Multifunctional Nano-Objects by RAFT PISA

An alternative route towards nanoparticle formation was polymerization-induced self-assembly. Because of its reduced synthetic effort and mild reaction conditions PISA was the method of choice. Initial RAFT PISA experiments were carried out with a non-functional macroCTA ( $M_{n,SEC} = 8200 \text{ g mol}^{-1}$ ,  $\mathcal{D} = 1.13$ ) based on OEGMA<sub>500</sub> in ethanol at various temperatures and with different radical initiators. In contrast to the NMPISA experiments in Chapter 3.5., benzylmethacrylate (BzMA) was used as the hydrophobic monomer. The main advantage of BzMA over BMA is that the glass transition temperature of the PBzMA ( $T_g = 54 \text{ °C}$ ) is high enough to allow for TEM characterization, yet low enough to enable a dispersion polymerization process in alcohol. In general, a

total solids weight content of 10 wt% for the PISA experiments was used, which is supposed to yield different nano-morphologies with increasing degree of polymerization ( $DP_n$ ) for PBzMA.<sup>190-191</sup> First experiments with the non-functionalized CPDB macroCTA in ethanol were performed with V-70 at 30 °C for 24 h. V-70, an azo initiator, was chosen since its 10 h half-life decomposition temperature was 30 °C offering very mild reaction conditions. <sup>1</sup>H NMR and SEC indicated no polymer formation after 24 h. The reaction was continued until 48 h: even after extended reaction times no polymer was formed. Therefore, V-70 was replaced with AIBN and the polymerizations were performed at 70 °C. Figure 33 illustrates the SEC results obtained from kinetic experiments.

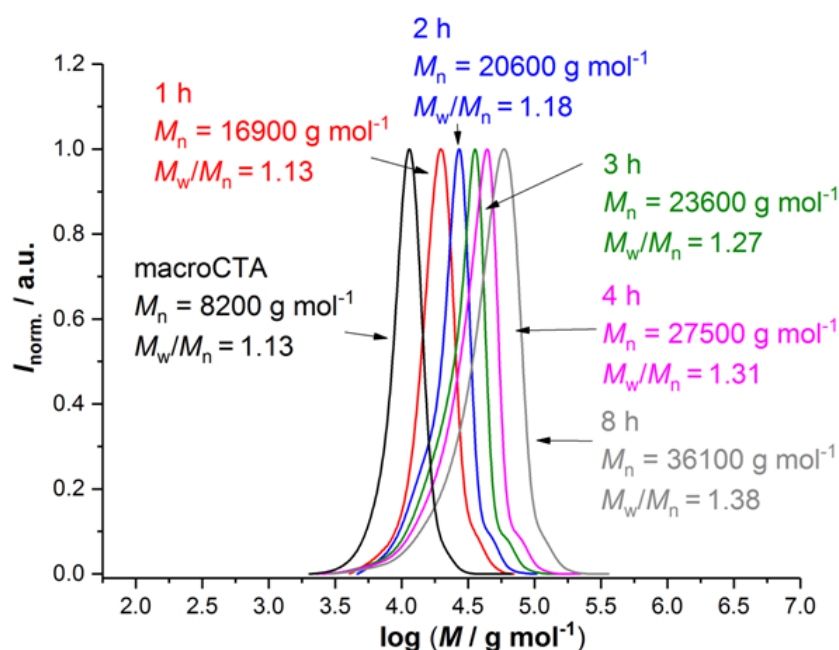


**Figure 33.** Evolution of the size-exclusion chromatograms during the RAFT PISA of benzyl methacrylate with AIBN at 70 °C in ethanol ( $[BzMA]/[macroCTA] = 500$ ).

SEC traces demonstrated a constant growth in molar mass and reasonable dispersities, suggesting a controlled polymerization. However, the traces displayed a slight shoulder at high molar mass due to the formation of coupled polymer chains as mentioned above. Interestingly, the medium did not show any turbidity during the reaction at 70 °C but nucleation appeared once the system was cooled down quickly. Afterwards, the dispersion seemed to be only stable at ambient temperature for about 5 h until a red polymer gel formed at the bottom. This heating and cooling cycle could be repeated several times with the exact same polymer behavior. UCST-like behavior for this

#### 4. Amphiphilic Block Copolymer Nanoparticles by RAFT-Mediated Polymerization

polymer system was reported in a recent publication by Yeow *et al.* in which they employed a light-mediated PISA in ethanol and demonstrated thermo responsive properties of the resulting polymers.<sup>192</sup> TEM investigations revealed worm morphologies in the gel state while spherical particles were observed once the dispersion was heated. Additionally, Armes and co-workers reported an UCST behavior of a poly(lauryl methacrylate-*b*-benzyl methacrylate) *via* PISA in *n*-dodecane leading to spheres, worms, and vesicles.<sup>193</sup> At concentrations above 10 wt% the polymer would form a worm gel at ambient temperature while spherical morphologies were obtained once the polymer dispersion was heated.

Clearly, PISA in ethanol resulted in amphiphilic polymers that indicated thermo responsive morphology changes. The system was not further investigated since stable spherical particles suspensions at room temperature were required. Therefore, the solvent was changed to water in which the polymer system is not known to show any thermo responsive behavior. The aforementioned non-functionalized CPDB macro RAFT agent and VA-044, a water-soluble azo initiator ( $T_{\text{decomp., 10 h}} = 44\text{ }^{\circ}\text{C}$ ), were utilized and the polymerization temperature were set to 50 °C. SEC traces of a PISA experiment in water are shown in Figure 34B. The SEC traces displayed a steady macromolecular growth until full conversion was reached (within 24 h), with reasonable dispersities. After 24 h, high molar mass shoulders indicated a loss of control due to termination reactions at very high conversions. DLS results exhibited narrow particle distributions after 8 h ( $DP_{\text{n BzMA}} \approx 115$ ) and two major particle distributions at 24 h due to the higher degree of polymerization of the hydrophobic block ( $DP_{\text{n BzMA}} \approx 500$ ) and the resulting partial phase transition from spherical to higher order morphologies (Figure 34C). Particle dispersions from 8 h remained stable over a long period of time at ambient temperature and showed no coagulation. However, dispersions obtained after 24 h displayed phase separation: an upper turbid nanoparticle phase and a coagulated phase of copolymer at the bottom.

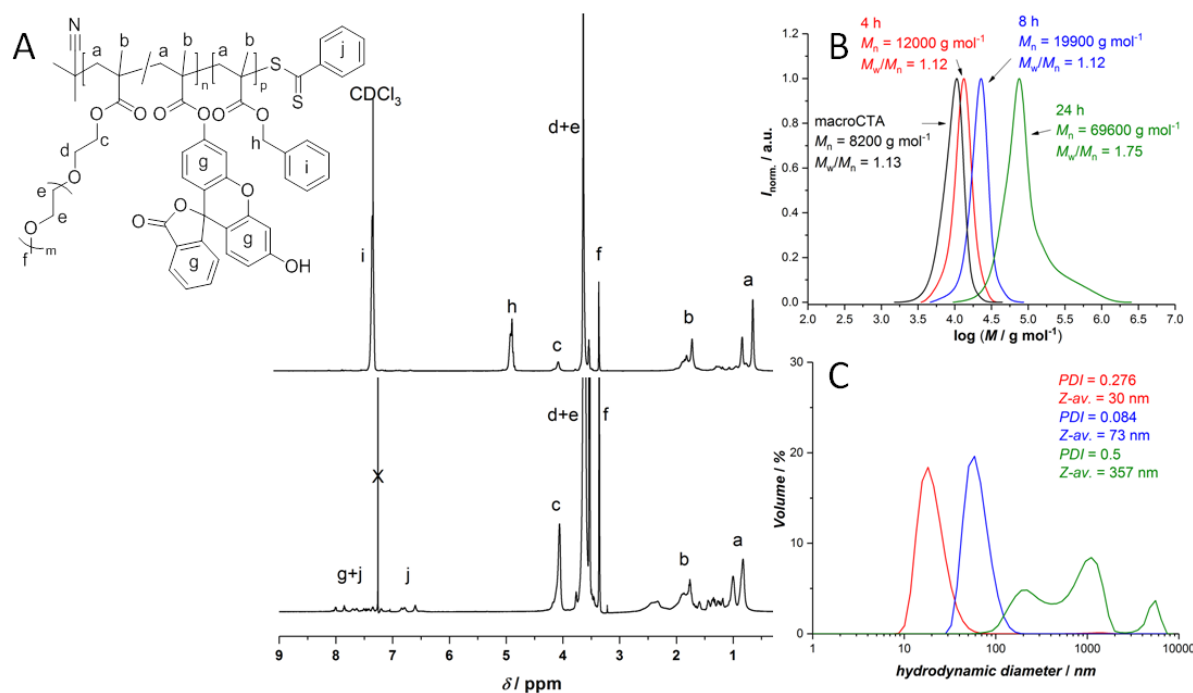


**Figure 34.** (A) <sup>1</sup>H NMR of a non-functionalized P(OEGMA<sub>500</sub>-co-FMA) (bottom) and P(OEGMA<sub>500</sub>-co-FMA)-b-BzMA (top). (B) SEC traces during RAFT PISA of benzyl methacrylate at 50 °C in H<sub>2</sub>O from non-functionalized macroCTA ([BzMA]/[macroCTA] = 500) and (C) corresponding hydrodynamic diameter volume distributions.

Since preliminary PISA experiments in water with a non-functionalized macroCTA showed promising results, following polymerizations were conducted using the Cl-functionalized **macroCTA2**. DLS results in Figure 34 confirmed that a  $DP_n$  of 500 for the core-forming BzMA gave two large nano-object distributions. To limit the amount of higher order morphologies, the degree of polymerization at full conversion was reduced to 75, 150, and 250 respectively. The resulting SEC traces of these polymerizations are shown in Figure 35. All SEC traces displayed a clear shift towards higher molecular weights with reasonable dispersities. Yet, for higher molecular weights SEC values differed significantly from theoretical molecular weights at full conversion because no adequate calibration for this branched polymer system was available and might therefore not represent the actual weight of the polymer. <sup>1</sup>H NMR analysis of the dried samples revealed higher  $DP_n$ s for BzMA than targeted (see Table 5). A possible explanation is a lowered end-group fidelity of the utilized macroCTA since conversions after RAFT polymerization were generally quite high (Table 2). It is known that in RAFT polymerizations the end-group fidelity continually decreases over time and that at very

#### 4. Amphiphilic Block Copolymer Nanoparticles by RAFT-Mediated Polymerization

high conversions radical initiator moieties can potentially replace the RAFT end-group rendering parts of the polymer inactive for further chain extensions.<sup>194-195</sup>

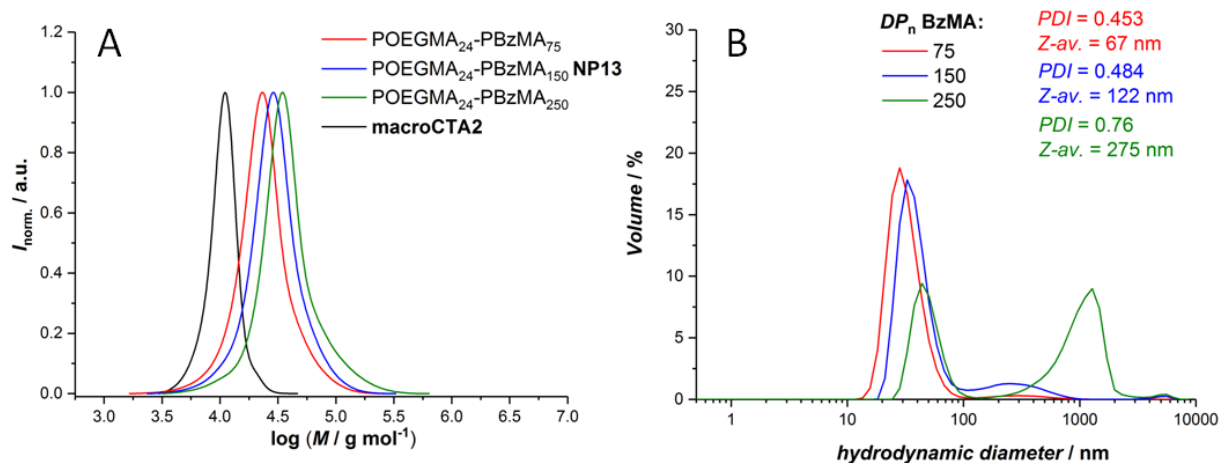


**Figure 35.** (A) SEC traces after RAFT PISA (24 h) with varying  $DP_n$  in H<sub>2</sub>O from Cl-functionalized **macroCTA2** ( $M_{n,\text{NMR}} = 12400 \text{ g mol}^{-1}$ ) and (B) corresponding hydrodynamic diameter volume distributions.

**Table 5.** Characteristics of functionalized amphiphilic block copolymers obtained by RAFT PISA.

<i>target structure</i>	<i>actual BzMA DP<sub>n</sub><sup>a,b</sup></i>	<i>M<sub>n,NMR</sub> (g mol<sup>-1</sup>)<sup>c</sup></i>	<i>M<sub>n,SEC</sub> (g mol<sup>-1</sup>)<sup>d</sup></i>	<i>Đ<sup>d</sup></i>	<i>Z-av. (nm)<sup>e</sup></i>	<i>PDI<sup>e</sup></i>	<i>[end group] (μM)<sup>f</sup></i>
Cl-POEGMA <sub>24</sub> -PBzMA <sub>75</sub>	114	20 100	22 300	1.29	67	0.45	-
Cl-POEGMA <sub>24</sub> -PBzMA <sub>150</sub>	183	32 300	24 500	1.33	122	0.48	0.694
<b>NP13</b>							
Cl-POEGMA <sub>24</sub> -PBzMA <sub>250</sub>	292	51 500	30 800	1.41	275	0.76	-
Cl-POEGMA <sub>12</sub> -PBzMA <sub>75</sub>	82	14 400	12 000	1.23	120	0.39	-
Cl-POEGMA <sub>12</sub> -PBzMA <sub>150</sub>	173	30 600	19 400	1.44	219	0.49	-
Cl-POEGMA <sub>12</sub> -PBzMA <sub>250</sub>	284	50 000	27 100	1.56	208	0.37	-
BG-POEGMA <sub>23</sub> -PBzMA <sub>150</sub>	156	27 500	35 200	1.33	69	0.40	1.676
<b>NP14</b>							
BG/Cl-POEGMA <sub>23</sub> -PBzMA <sub>150</sub>	178	31 400	25 000	1.25	50	0.13	1.976 1.119
<b>NP15</b>							
BG/Cl/nonfct-POEGMA <sub>23</sub> -PBzMA <sub>150</sub>	179	31 500	27 100	1.31	46	0.12	1.470 0.469
<b>NP16</b>							

<sup>a</sup>at full conversion. <sup>b</sup>BzMA conversion determined by <sup>1</sup>H NMR spectroscopy. <sup>c</sup>Molar mass was determined by proton signals of hydrophilic block segment. <sup>d</sup>Experimental *M<sub>n</sub>* obtained by SEC in DMAc using PS calibration. <sup>e</sup>Volume-average hydrodynamic diameter and polydispersity determined by DLS. <sup>f</sup>Concentration of functional end groups calculated from Eq. (9) (*vide supra*).

Hydrodynamic diameter volume distributions obtained by DLS displayed two major particle populations for each degree of polymerization. As expected with an increase in *DP<sub>n</sub>* the amount of small particles below 100 nm decreased while a second distribution between 500-1500 nm became more prominent because of the aforementioned phase transition during the polymerization. To further investigate the polymer morphologies, TEM images from the suspensions were recorded. Prior to imaging, the polymers were stained with uranyl acetate (20 wt% in EtOH) since non-stained samples were not visible under the microscope. Figure 36 illustrates representative TEM images for each suspension. The obtained images displayed an abundance of highly uniform, spherical particles with an average size below 50 nm. Even though DLS analysis suggested a second particle distribution for *DP<sub>n</sub>* 150, no other morphologies were visible. Polymers

#### 4. Amphiphilic Block Copolymer Nanoparticles by RAFT-Mediated Polymerization

with a  $DP_n$  250 on the other hand, showed vesicular nano-objects as well as spherical particles. Based on the diblock asymmetry more higher order morphologies for  $DP_n$  150 and 250 were expected but all samples exhibited largely kinetically-trapped spherical particles. Presumably, the long hydrophilic POEGMA-block effectively stabilized spherical particles such that only few micelle formation occurred. However, micelle fusion is the first essential step towards phase transition, which would lead to high order morphologies such as worm, formation of "jellyfish" structures, and finally vesicles.<sup>97</sup>

The most promising results for biological applications were polymerizations with  $DP_n$  150 of benzyl methacrylate. While the particle size did not differ greatly from  $DP_n$  75, the polymer suspensions of  $DP_n$  150 appeared to be more stable over long periods of time, showed greater turbidity and an easier separation of particles from the solvent after centrifugation.

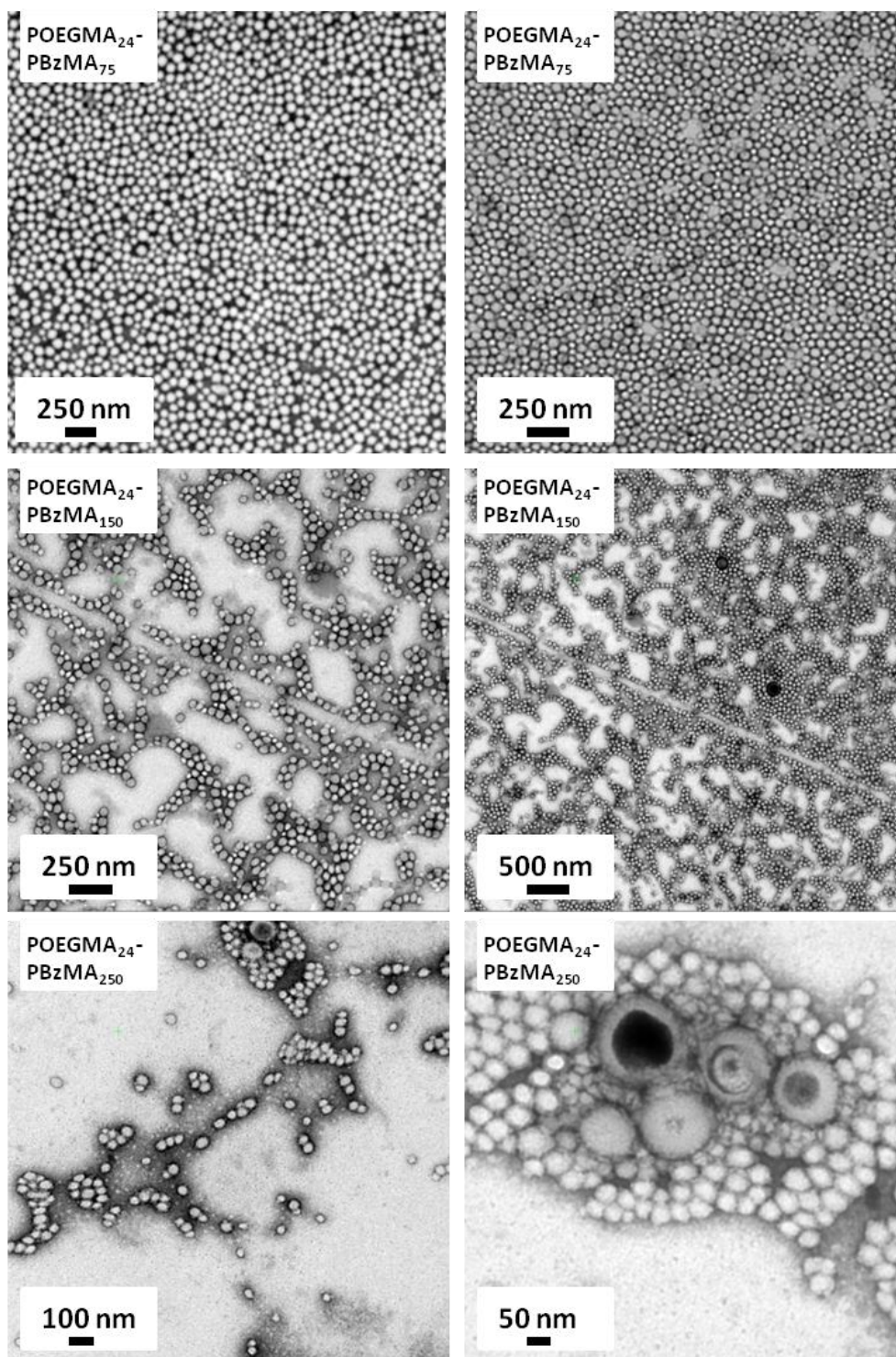


**Figure 36.** TEM images of RAFT PISA polymers with varying degrees of polymerization from Cl-functionalized **macroCTA2** ( $M_{n,NMR} = 12400 \text{ g mol}^{-1}$ ).

Apart from the degree of polymerization of the core-forming polymer, morphological changes in PISA are also highly dependent on the aforementioned size of the hydrophilic block segment. Therefore, a smaller Cl-functionalized **macroCTA1** ( $M_{n,NMR} = 5800 \text{ g}$

#### 4. Amphiphilic Block Copolymer Nanoparticles by RAFT-Mediated Polymerization

mol<sup>-1</sup>) was utilized and previous experiments with varying  $DP_n$  were repeated. The analytical characteristics are listed in Table 2. In Figure 37, the SEC traces after 24 h for each  $DP_n$  are shown. All SEC traces displayed a clear shift towards higher molar masses while maintaining reasonable polydispersities. After 24 h, reactions reached full conversion and the actual molar mass of the resulting polymers was determined by <sup>1</sup>H NMR. As seen in Table 5, the calculated molar mass by NMR were close to the theoretical molar mass at 100% conversion. DLS results suggested multimodal particle distributions for each polymerization. Comparing these DLS results with the previous ones (Figure 35), one can observe similar size distributions for polymerizations with  $DP_n$  75 but significant differences for  $DP_n$  of 150 and 250, indicating higher order morphologies (Figure 37B).

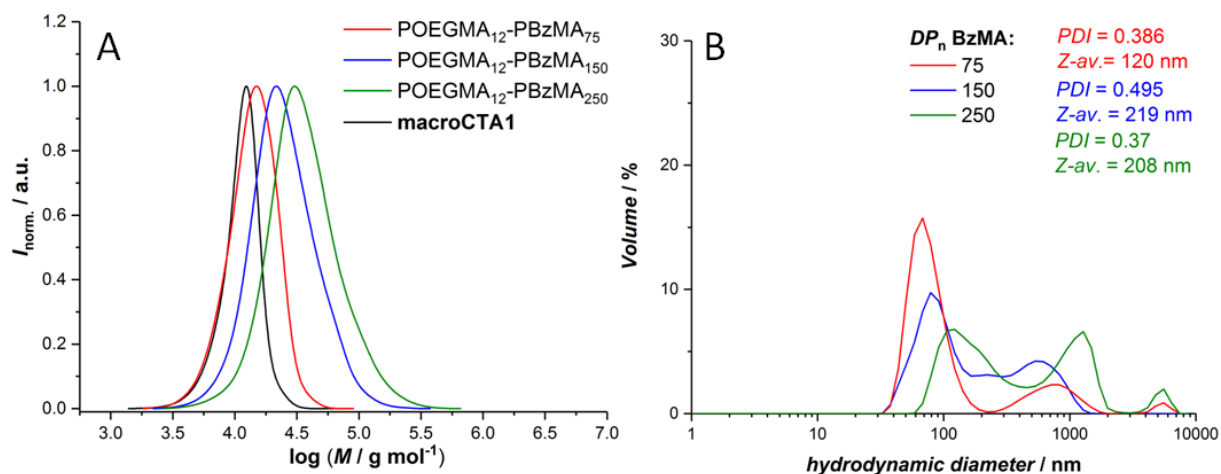


**Figure 37.** (A) SEC traces after RAFT PISA (24 h) with varying  $DP_n$  in H<sub>2</sub>O from Cl-functionalized **macroCTA1** ( $M_{n,NMR} = 5800 \text{ g mol}^{-1}$ ) and (B) corresponding hydrodynamic diameter volume distributions.

Particle suspensions were then stained and analyzed by TEM with the resulting images shown in Figure 38. As expected from the DLS results, amphiphilic block copolymers with a BzMA  $DP_n$  of 75 formed spherical particles exclusively with an average size of less than 100 nm and a narrow dispersity. Even though the average size of these particles was slightly larger than those obtained with the bigger **macroCTA2** ( $Z\text{-av.} < 50 \text{ nm}$ ) - certainly due to the lesser stabilizing nature of shorter hydrophilic segments -, their uniform shape and dispersity were comparable. A mixed phase system of worms and spherical particles with varying sizes was observed for a polymerization with  $DP_n$  150.

For  $DP_n$  250 the majority of morphologies were vesicles and smaller spheres. Vesicles showed no clear spherical shape but a gel-like behavior which might be due to the staining agent. Alternatively, reaction times of 24 h were not sufficient enough to reach a thermodynamically preferred equilibrium state in which small spheres would eventually transform into vesicles completely. In order to access pure vesicular and worm phases further polymerizations would have to be carried out with higher copolymer concentrations (e.g, 20-25 wt%) and varying  $DP_n$  to construct a full phase diagram. Nevertheless, the analytical results proved the successful synthesis of functional nano-objects.

4. Amphiphilic Block Copolymer Nanoparticles by RAFT-Mediated Polymerization

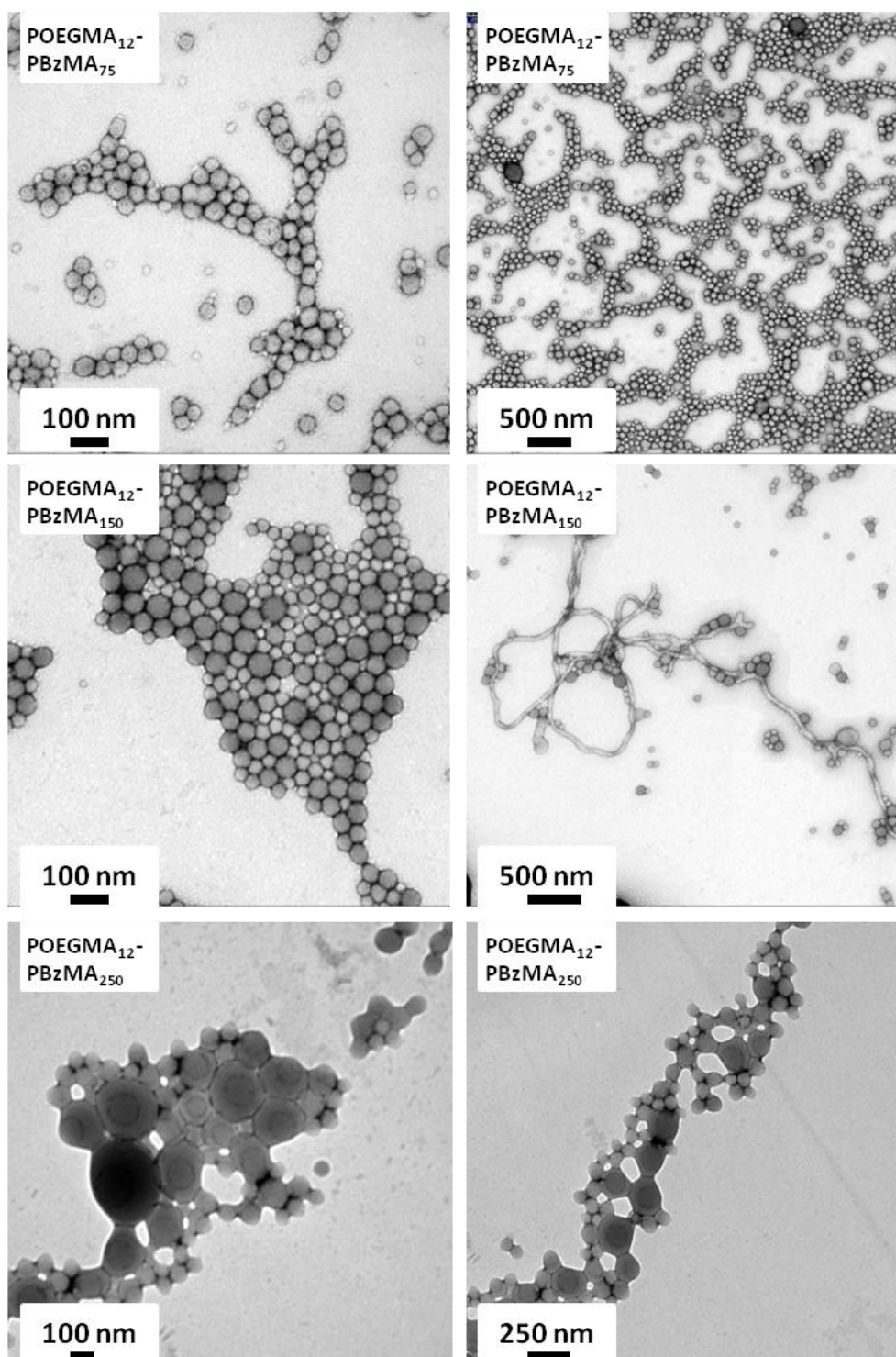


**Figure 38.** TEM images of RAFT PISA polymers with varying degrees of polymerization from Cl-functionalized **macroCTA1** ( $M_{n,NMR} = 5800 \text{ g mol}^{-1}$ ).

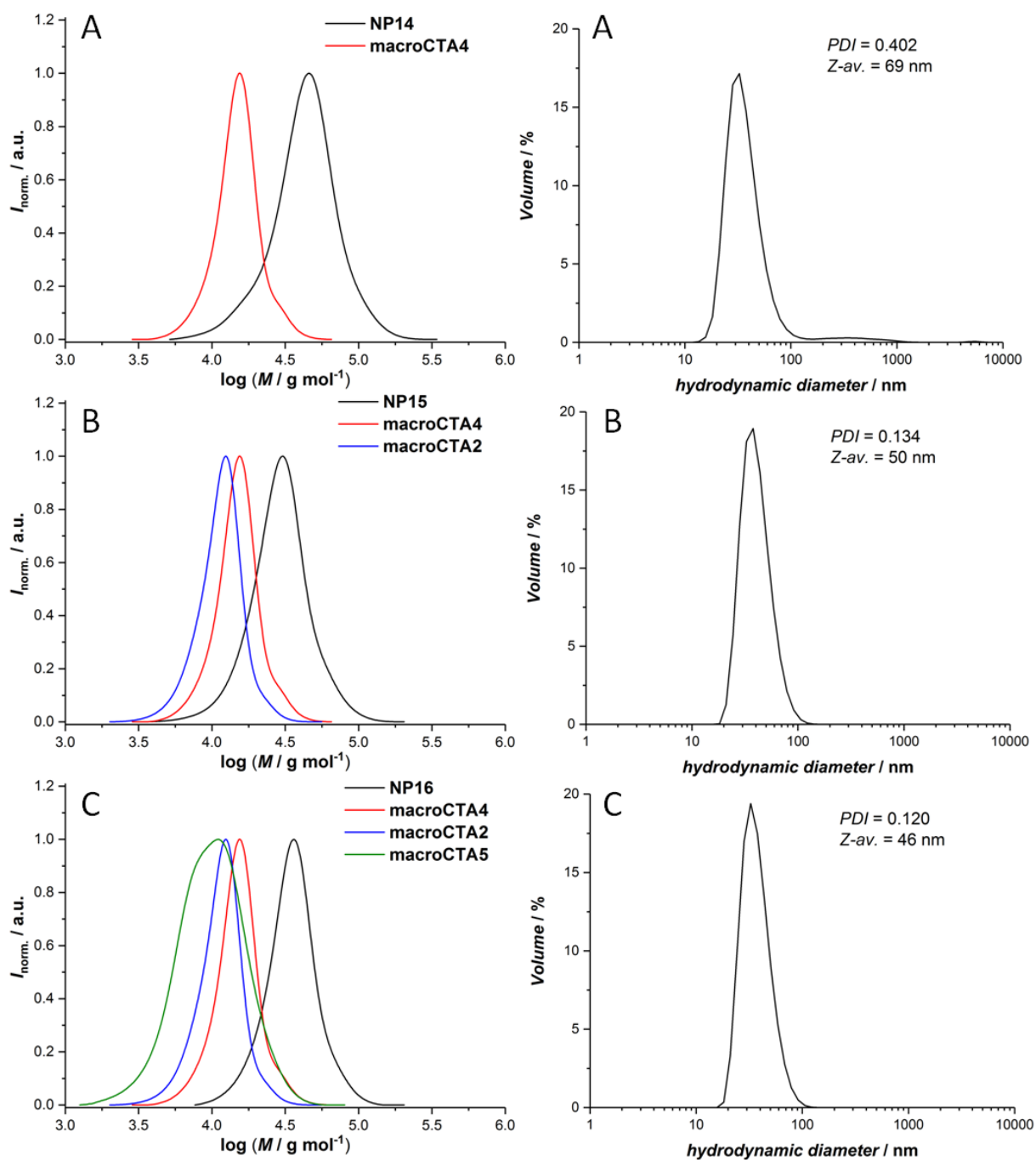


**Figure 39.** SEC traces and hydrodynamic diameter volume distributions by DLS after RAFT PISA for (A) BG-POEGMA<sub>23</sub>-PBzMA<sub>150</sub>, (B) BG/Cl-POEGMA<sub>23</sub>-PBzMA<sub>150</sub> and (C) BG/Cl/nonfct-POEGMA<sub>23</sub>-PBzMA<sub>150</sub>.

PISA experiments with BzMA ( $DP_n$  150) were repeated with the BG-functionalized **macroCTA4** ( $M_{n,NMR} = 12000 \text{ g mol}^{-1}$ ). Subsequently, BG- and Cl-functionalized **macroCTA2-4** (50% : 50%) and non-functionalized **macroCTA5** (33% : 33% : 33%) were utilized in PISA in order to obtain multifunctionalized nanoparticles with different

#### 4. Amphilic Block Copolymer Nanoparticles by RAFT-Mediated Polymerization

surface functionalization ratios. The resulting SEC traces displayed an increase in molar mass with narrow polydispersities for each reaction indicating good control over the polymerizations (Figure 39), while  $^1\text{H}$  NMR analysis suggested that full conversions for each polymerization were reached. Nanoparticle sizes below 100 nm and mostly monomodal distributions were observed by DLS (Figure 39) and were in good agreement with previous results. TEM studies of the polymers indicated the formation of spherical nanoparticles of around 30-50 nm with homogenous size distributions as well as worm morphologies (Figure 40).

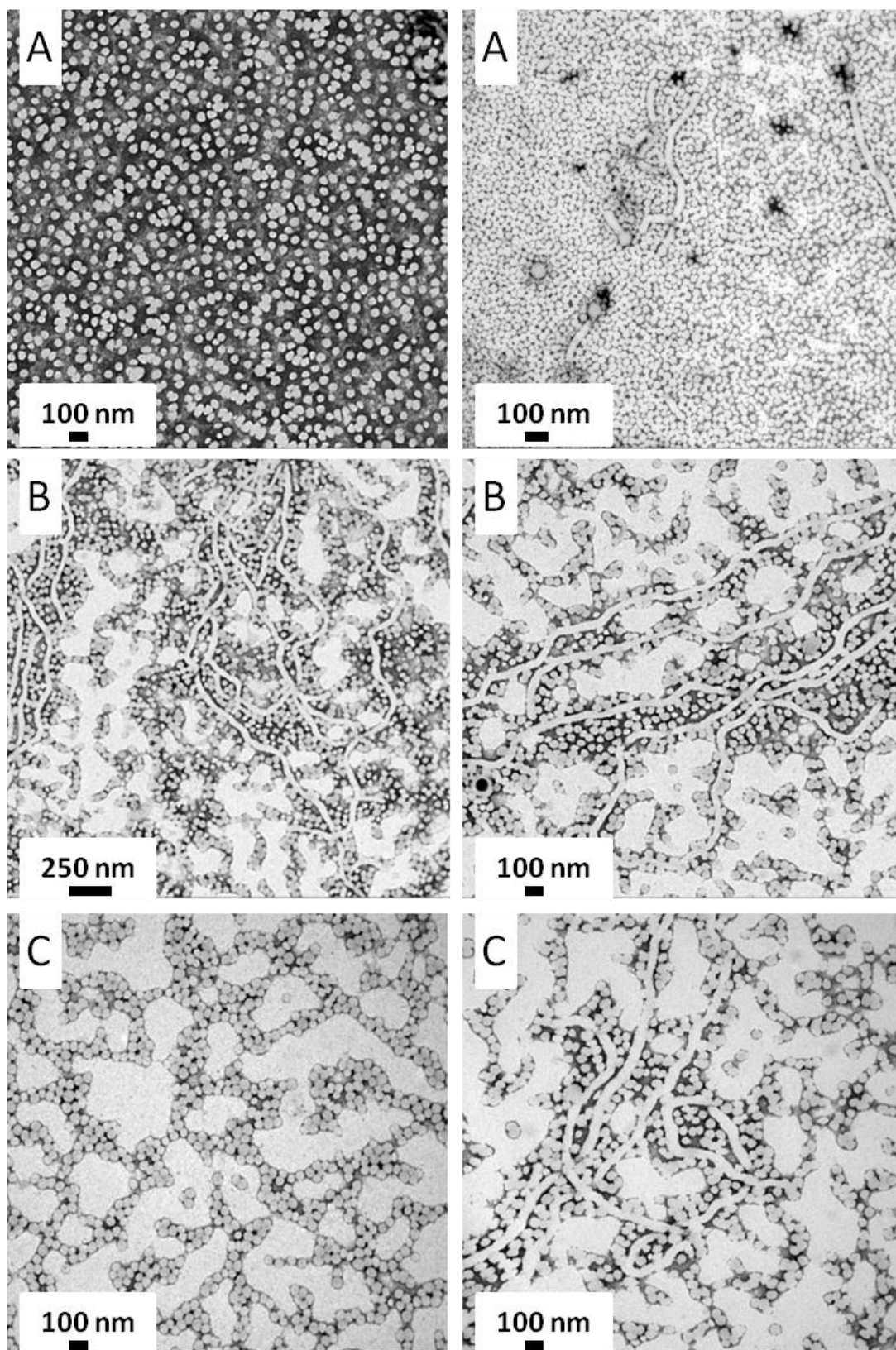


**Figure 40.** Representative TEM images of RAFT PISA polymers POEGMA<sub>24</sub>-PBzMA<sub>150</sub> with (A) 100% BG-functionalization **NP14**, (B) 50% : 50% BG- and Cl-functionalization **NP15** and (C) 33% : 33% : 33% BG- and Cl-functionalization **NP16** with spacer units (macroCTA5).

#### 4. Amphiphilic Block Copolymer Nanoparticles by RAFT-Mediated Polymerization

The amount of surface functionalization based on the incorporated fluorophores in the nanoparticles was analyzed and calculated according to Eq. (9) (Table 5). For multifunctional nanoparticle solutions **NP15** and **NP16** the ratios of haloalkane and benzylguanine end-groups were 1 : 1.7 and 1 : 3.1, respectively. Apparently BG-functionalization seemed to be higher, which might be due to a higher end-group fidelity in the BG-functionalized **macroCTA4** as compared to Cl-functionalized **macroCTA2** or to the fact that fluorescein is unstable under sun light and might therefore have partially degraded over time.<sup>196</sup> Alternatively or additionally, since the rhodamine-derivative VBR was present in **NP16** FRET has likely diminished the measured fluorescence of fluorescein as indicated by the second absorbance at 585 nm in the fluorescein spectrum (Figure 41, right). As a result, the calculated concentration of haloalkane on the particles was low. In conclusion RAFT-mediated PISA experiments in water lead to (multi-)functional nanoparticles, worms, and vesicles for protein immobilization.

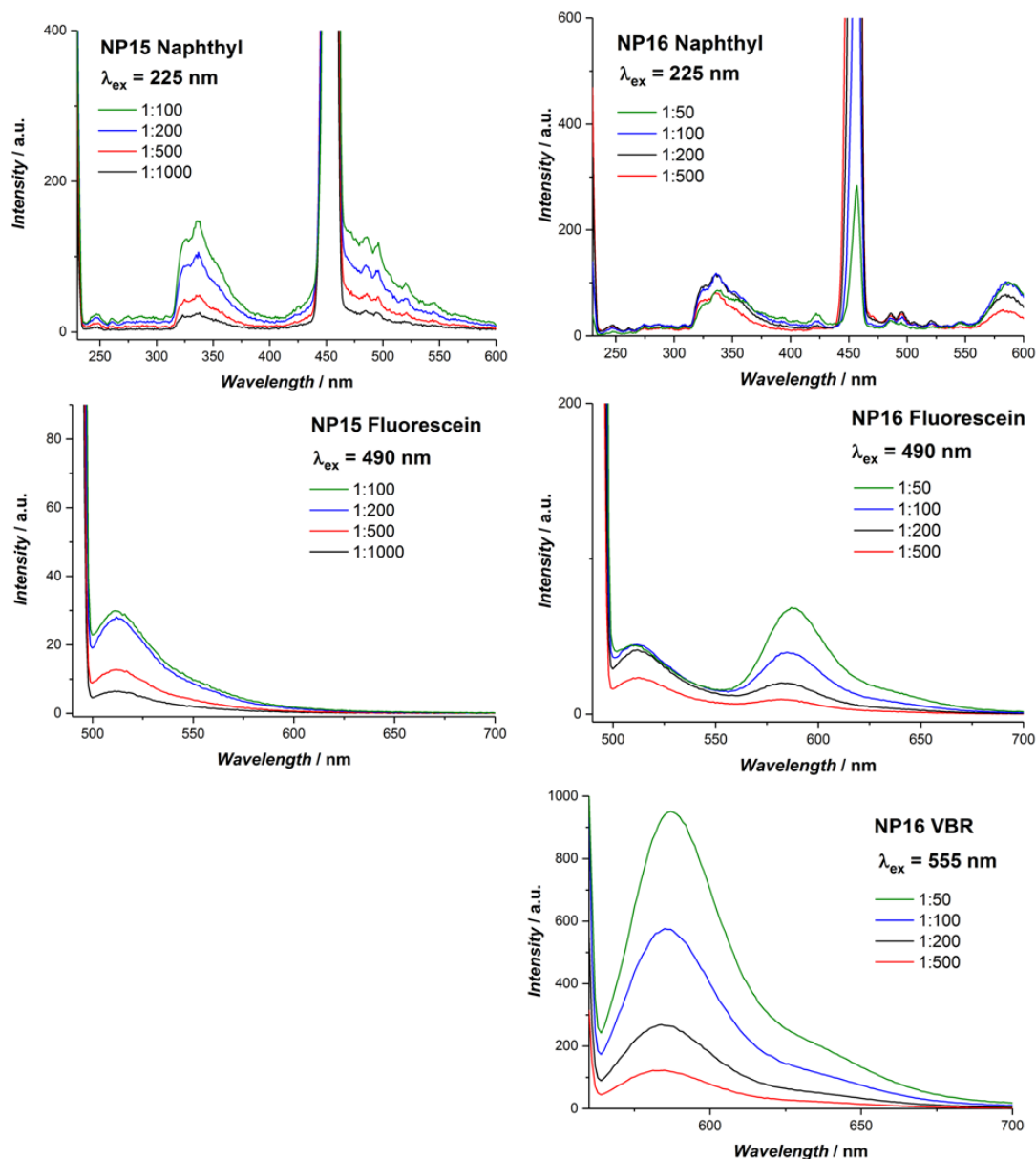


**Figure 41.** (Left) Emission spectra of **NP15** and (right) **NP16** for incorporated fluorophores at various dilutions (NP suspension:water).

## 4.5. Conclusion and Outlook

In summary, this chapter demonstrated the successful synthesis of two functionalized RAFT chain transfer agents. Based on these RAFT agents, POEGMA<sub>500</sub> macroCTAs containing different fluorophores were polymerized which were used in subsequent reactions. Nanoparticle formation was accomplished *via* two different approaches: chain extension of functionalized macroCTA with styrene and subsequent nanoprecipitation of

#### 4. Amphiphilic Block Copolymer Nanoparticles by RAFT-Mediated Polymerization

the amphiphilic copolymer and by RAFT PISA. While both methods worked equally well, the favored technique would be PISA because of the corresponding reduced synthetic effort, and the access to various nano-morphologies demonstrated in this work. These nano-objects were analyzed by different methods such as  $^1\text{H}$  NMR, SEC, DLS, TEM and fluorescence spectroscopy. All nanoparticle suspensions demonstrated good stability over long periods of time as well as fluorescent properties which were used to calculate the extent of surface functionalization.

Further investigations in various degrees of polymerization with benzyl methacrylate, a suitably small macroCTA and higher solid concentrations, will likely result in pure phases. Additionally, changing the hydrophobic core-forming monomer for the very promising 2-hydroxypropyl methacrylate (HPMA) may result in facile synthesis of hydrogels as current developments in our group suggest. Recently trithiocarbonate-based RAFT agents have been used more often for PISA as compared to the dithiobenzoate RAFT agent utilized in this work. A possible explanation is that the dithiobenzoate group is more susceptible to hydrolysis in aqueous systems than trithiocarbonate end-groups and might therefore be used less often in aqueous RAFT PISA experiments.<sup>197-198</sup> Irrespective of which chain transfer agent is used for further experiments the limiting factor will still be the costly synthesis of functional groups. Without sufficient amounts of functionalized chain transfer agents only small scale reaction formulations will be feasible making kinetic investigations and analytics in general more arduous. In retrospective, first promising results towards thermo-responsive PBzMA nanomaterials *via* PISA in ethanol could be obtained but were not further investigated. Therefore, utilizing functionalized macroCTAs for RAFT PISA in ethanol with BzMA may likely result in biocatalytic nanomaterials with thermo-switchable phase transition properties.

An alternative route towards immobilized enzymes on nano-object surfaces could be the direct immobilization of enzymes onto functionalized macroCTAs before chain extensions. Afterwards PISA experiments at room temperature could be performed. Biocatalytic assays before and after PISA would reveal if the polymerization process altered the enzymatic activity. Mild reaction conditions such as a light-mediated RAFT PISA at ambient temperature which was published recently may be ideal for this purpose.<sup>199-200</sup>



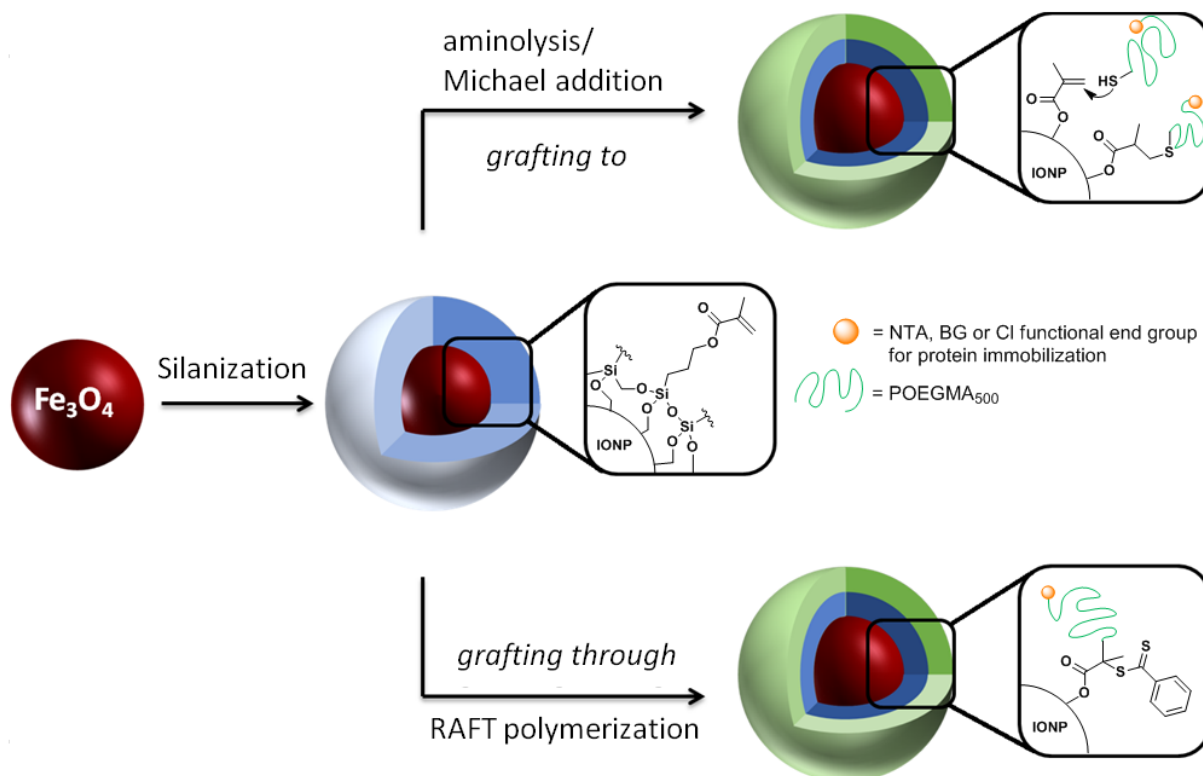


# Polymer-Coated Iron Oxide Nanoparticles for Enzyme Immobilization

Iron oxide nanoparticles (IONPs,  $\text{Fe}_3\text{O}_4$ ) have gained considerable attention in biomedical application. Their intrinsic biocompatibility and magnetic properties offer a range of applications such as contrast agents in magnetic resonance imaging (MRI), magnetically guided drug delivery, hyperthermia, and in magnetic separation processes for purification and cell separation.<sup>201-203</sup> However, a drawback of IONPs is the irreversible aggregation over time due to Van der Waals forces and magnetic forces. Therefore, the loss of superparamagnetic properties that is tied to their nanodimensions needs to be prevented. By coating the magnetite nanoparticles with small non-organic molecules or polymers, the magnetic features remain intact, making facile purification of surface-bound molecules by magnetic separation possible.

Based on the aforementioned benefits, polymer-coated IONPs are used as solid supports for protein immobilization. Recent publications demonstrated the use of polymer-coated magnetic nanoparticles to immobilize and purify enzymes such as lipase<sup>204-206</sup> and horseradish peroxidase.<sup>207</sup> However, enzymes were either immobilized by adsorption or non-specific covalent binding to the particles. While enzymatic activity was reported in all cases, the system could further be improved if site-specific immobilization of the enzymes to the surface would be employed. To this aim, functional RAFT agents described in Chapter 4.2. were utilized in RAFT-mediated polymerizations of OEGMA<sub>500</sub>. Coating with solvophilic POEGMA would increase the IONPs water dispersity, prevent aggregation of particles, and reduce non-specific adsorption between nanoparticles and

proteins. At the same time, the functional end-group would allow for specific protein immobilization. IONPs were first coated with a methacrylate-capped silane (TESPMA) and subsequently through distinct reactions at the methacrylate end-group *via* "grafting to" or "grafting through" approaches, macro RAFT agents could covalently bind to the IONPs resulting in magnetic nanocomposites for protein immobilization (Scheme 21).



**Scheme 21.** Overall strategy towards functionalized IONPs. 1. Silanization with 3-(Triethoxysilyl)propyl methacrylate (TESPMA). 2. "Grafting to" *via* aminolysis/Michael addition of CPDB-POEGMA<sub>500</sub> or "grafting through" *via* RAFT polymerization of surface-bound methacrylate units.

## 5.1. Synthesis of Functionalized Low Molar Mass RAFT CTAs

Oligo(ethylene glycol) methyl ether methacrylate (OEGMA) with a number-average molecular mass of  $500 \text{ g mol}^{-1}$  was employed as main monomer for the solvophilic segment to ensure steric stabilization of polymer-coated IONPs in water. Copolymerization of OEGMA with small amounts of fluorescent monomer (5 mol%) would allow to quantify the functional end-groups on the nanocomposites through fluorescence measurements (see 4.2.). To introduce functionality onto the particles surface, functionalized macro RAFT agents were employed. For this purpose, the functionalized chain transfer agents BG-CTA (**17**), Cl-CTA (**24**), and pNTA-CTA (**25**) were utilized to control the polymerization of OEGMA<sub>500</sub>. The characteristics of the resulting low molar mass macroCTAs are listed in Table 6. Figure 42 depicts the corresponding SEC traces. While BG- and Cl-functionalized macroCTAs exhibited monomodal distributions and a good control over the polymerization, pNTA showed the formation of a high molar mass shoulder. Since VBR was a styrene-derivative, terminations by combination may have led to an extent of coupled polymer chains, which is a known problem of styrenic monomers at high conversions.<sup>187-188</sup> While number-average molar masses determined by SEC were higher than the target molar mass, NMR calculations of  $M_n$  based on the aromatic proton signals of the RAFT end group represented the actual molar mass more accurately.

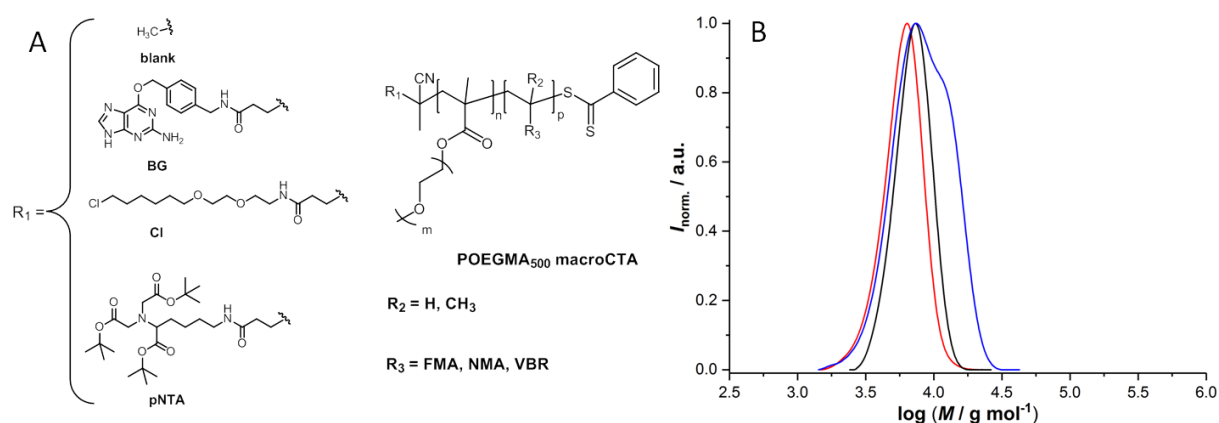


**Figure 42.** (A) Chemical structures and (B) SEC traces of POEGMA<sub>500</sub> macroCTAs with (black) BG, (red) Cl, and (blue) pNTA end-chain functionality.

**Table 6.** Main characteristics of the macroCTAs used in this chapter.

structure	target $M_n$ (g mol <sup>-1</sup> ) <sup>a</sup>	$X_{\text{NMR}}$ (%) <sup>b</sup>	$M_{n,\text{NMR}}$ (g mol <sup>-1</sup> ) <sup>c</sup>	$M_{n,\text{SEC}}$ (g mol <sup>-1</sup> ) <sup>d</sup>	$\mathcal{D}^d$
Cl-P(OEGMA <sub>500</sub> -co-FMA)	5 500	52	5 800	5 500	1.12
BG-P(OEGMA <sub>500</sub> -co-NMA)	5 500	90	4 600	6 600	1.09
pNTA-P(OEGMA <sub>500</sub> -co-VBR)	5 500	-	6 000	7 400	1.24
blank-P(OEGMA <sub>500</sub> -co-FMA)	11 000	76	8 700	8 700	1.13

<sup>a</sup>at full conversion. <sup>b</sup>OEGMA conversion determined by <sup>1</sup>H NMR spectroscopy. <sup>c</sup>Molar mass was determined by aromatic protons signals of the RAFT benzyl group. <sup>d</sup>Experimental  $M_n$  obtained by SEC in DMAc using PS calibration.

Since the functional macroCTAs were rather precious with regards to the multi-step synthesis of the corresponding CTAs, a non-functional 2-cyano-2-propyl dithiobenzoate-based macroCTA (**blank-macroCTA**,  $M_{n,\text{SEC}} = 8700 \text{ g mol}^{-1}$ ,  $\mathcal{D} = 1.13$ ) was utilized in test reactions to find suitable conditions for the IONP functionalization.

## 5.2. Functionalization of Iron Oxide Nanoparticles

Commercially available Fe<sub>3</sub>O<sub>4</sub> (MagPrep Silica) nanoparticles with a small layer of silicon oxide dispersed in water were utilized as the starting material in the following experiments. The mean particle size of 100 nm was stated by the manufacturer. However, DLS experiments revealed much larger particle sizes (> 1000 nm) with two main particle distributions (Figure 43A). This result might be explained by the strong magnetic behavior of the particles leading to agglomeration over time. Therefore, the particles were demagnetized by placing the suspension in a magnetic coil ( $f = 50 \text{ Hz}$ ) and were sonicated for 20 min afterwards. While DLS analysis of the demagnetized particles showed only one main particle distribution with a hydrodynamic diameter of 1170 nm, particle sizes of 100 nm could not be obtained after demagnetization/sonification. However, DLS is known to overemphasize larger particles and while DLS settings for the angle of scattered light for IONPs are generally 90°, only scattering light angles of 173° could be measured and might therefore not represent the actual particle sizes.<sup>208</sup> TEM measurements depicted large IONP aggregates and the cubic structure of the individual magnetite IONPs (Figure 43B). Whether the formation of particle aggregates was due to

the TEM sample preparation or particle aggregation within the suspension could not be determined with certainty.

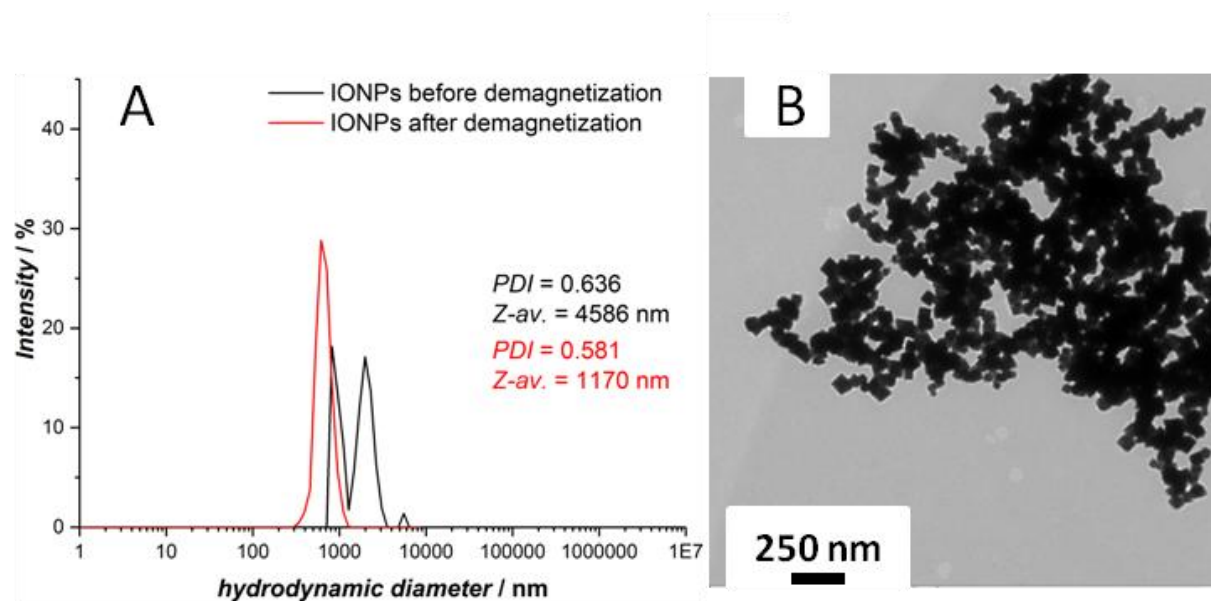
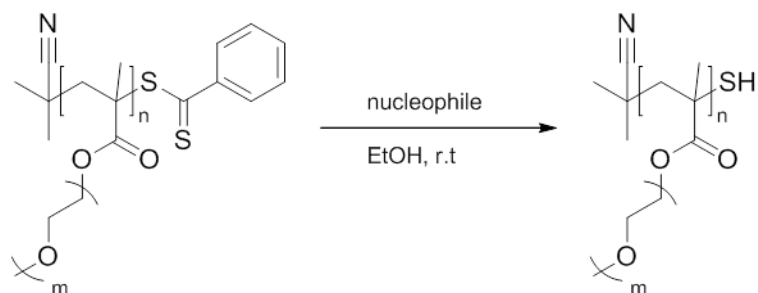


**Figure 43.** (A) Intensity-based hydrodynamic diameter distributions of commercial IONPs before and after demagnetization. (B) TEM of IONPs after demagnetization.

In order to functionalize IONP with the macromolecular chain transfer agents, a suitable silane with a reactive end-group was employed in order to introduce a reactive group at the surface of the IONPs. 3-(Triethoxysilyl)propyl methacrylate (TESPMA) was chosen since two possible reactions could be carried out utilizing the methacrylate moiety. Indeed, RAFT grafting-through polymerizations of the surface-anchored methacrylate group using the macroCTAs was the most obvious approach and could be realized by various initiating systems (*vide infra*). Alternatively, aminolysis of the macroCTA, generating a free thiol under cleavage of the thiocarbonylthio RAFT group, and subsequent Michael addition onto the methacrylate double bond was utilized (Scheme 22).

5. Polymer-Coated Iron Oxide Nanoparticles for Enzyme Immobilization



**Scheme 22.** Aminolysis of a dithiobenzoate-based POEGMA<sub>500</sub> macroCTA.

A small-scale test reaction of TESPMA and demagnetized IONPs in a water/ethanol (4/6 v/v) mixture was performed in the presence of hydroquinone in order to avoid thermal polymerization of the methacrylate moiety. Subsequent washing with DCM, ethanol, and water removed excess TESPMA and hydroquinone. Silane-coated IONPs were dried and analyzed by attenuated total reflection Fourier transform infrared spectroscopy (ATR-FTIR) and TEM as depicted in Figure 44.

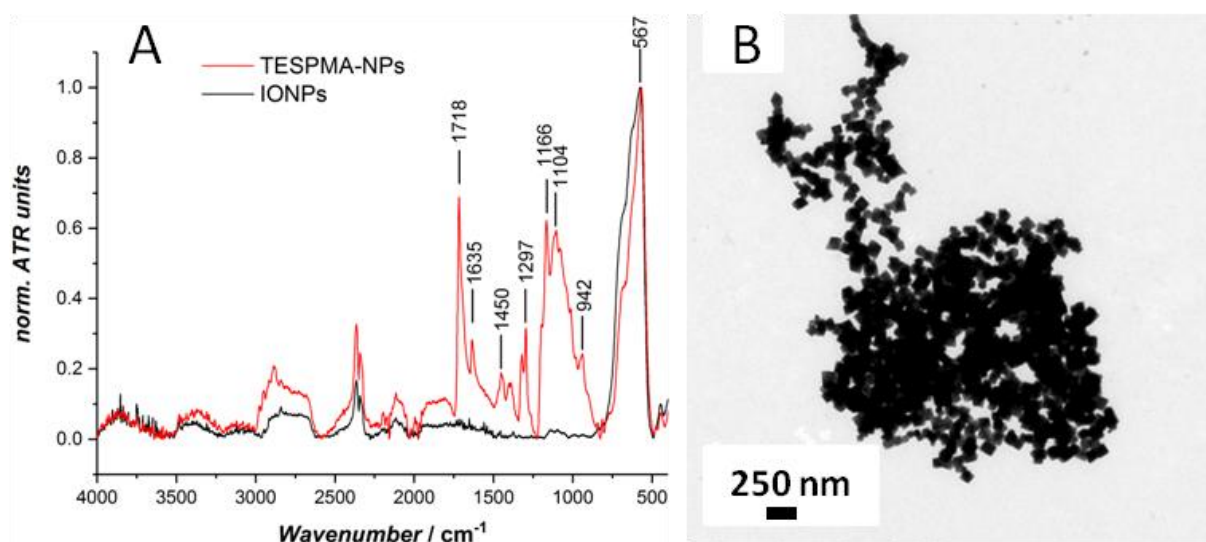


**Figure 44.** (A) ATR-FTIR spectrum and (B) TEM image of TESPMA-functionalized magnetite nanoparticles.

ATR-FTIR analysis confirmed the successful silanization as indicated by the appearance of the bands at 942-1104  $\text{cm}^{-1}$ , which can be ascribed to Si-O and Si-O-Si vibrations. Apart from the Fe-O stretching bands at 567  $\text{cm}^{-1}$ , the spectrum showed C-O-C and C=O bands at 1166  $\text{cm}^{-1}$  (1450  $\text{cm}^{-1}$ ) and 1718  $\text{cm}^{-1}$ , respectively, and C-H bands at 1297  $\text{cm}^{-1}$ . Furthermore, the double bond of the methacrylate was still present after the silylation as the C=C stretching band at 1635  $\text{cm}^{-1}$  indicates. TEM analysis did not show any changes regarding particle aggregation even though an increase in steric stabilization and hence less magnetic interactions of the coated particles could have been expected. The silanization with TESPMA was repeated and performed on a larger scale to afford a suitable amount for subsequent experiments. Surprisingly, ATR-FTIR analysis of the newly synthesized TESPMA-NPs did not show any of the aforementioned silane absorption bands (Figure 44A). This result could not be explained with certainty as no alterations to the reaction were made besides upscaling. Possibly incomplete silanization on the nanoparticle surface occurred because of larger aggregate clusters covering most of the inside particles based on inefficient mixing of the compounds. In order to avoid clustering of particle aggregates during the reactions, nanoparticle suspensions were placed in a ultrasonic bath during the reaction but no improvements in mixing could be achieved and intense magnetic stirring remained the option of choice even though the large majority of particles would stick to the magnetic stir bar. To verify whether parts of the aggregates surface was TESPMA-coated, the particle suspension was analyzed by energy-dispersive X-ray (EDX) spectroscopy (Figure 45).

5. Polymer-Coated Iron Oxide Nanoparticles for Enzyme Immobilization

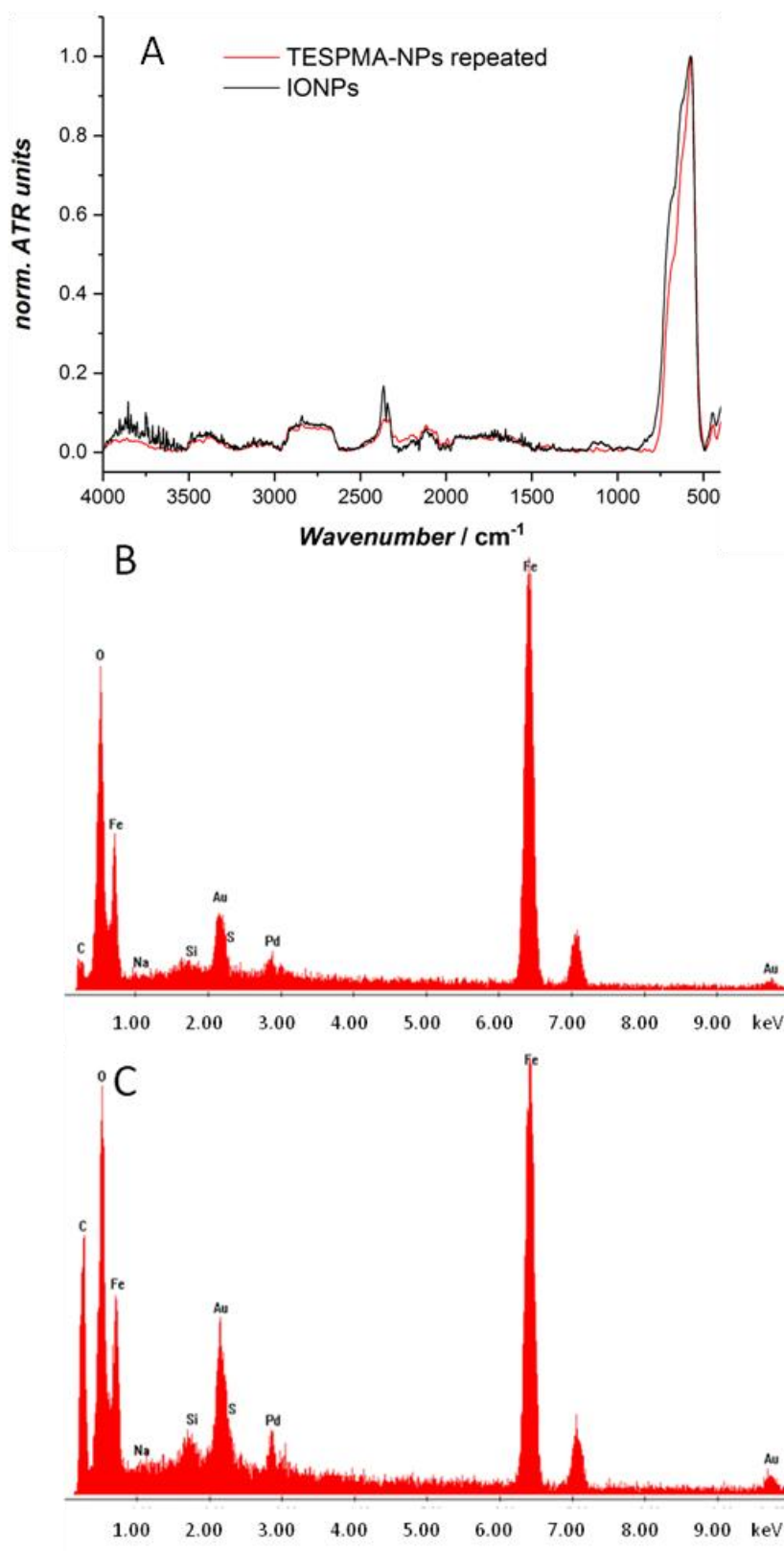


**Figure 45.** (A) ATR-FTIR and EDX spectra of (B) non-functional IONPs and (C) TESPMA-NPs.

As seen in Figure 45 (Band C), EDX measurements of non-coated IONPs and TESPMA-NPs differ mainly in the carbon content of the samples (IONP < 1 wt% vs 22.5 wt%, respectively) as the weight percentages of Si and Fe remained the same. The overall increase in carbon content indicated that at least parts of the TESPMA-NPs may have been functionalized.

### **5.3. TESPMA-IONP Surface Functionalization by Aminolysis and Michael Addition**

The first synthetic route to conjugate TESPMA-NPs and macro RAFT agents was through aminolysis and sequential Michael addition of the macro RAFT agent. Therefore, preliminary experiments with the aforementioned blank-macroCTA and dimethylphenylphosphonate (DMPP) with additional butylamine were performed. End-group removal appeared within 5 min after deoxygenation, which could be observed by the disappearance of characteristic red color of the dithiobenzoate end-group. After precipitation the polymer was analyzed by NMR and UV-Vis measurements. Figure 46A shows two  $^1\text{H}$  NMR spectra, before and after treatment of the macro RAFT agent. Successful end-group cleavage was confirmed by the loss of the aromatic proton signals of the thiobenzoate group at 7.35, 7.5, and 7.85 ppm. Furthermore, UV-Vis analysis showed no absorption band at 320 nm after the reaction, which derives from the thiobenzoate end-group while SEC traces retained its monomodal distribution without any formation of coupled polymers through possible occurring disulfide bonds.

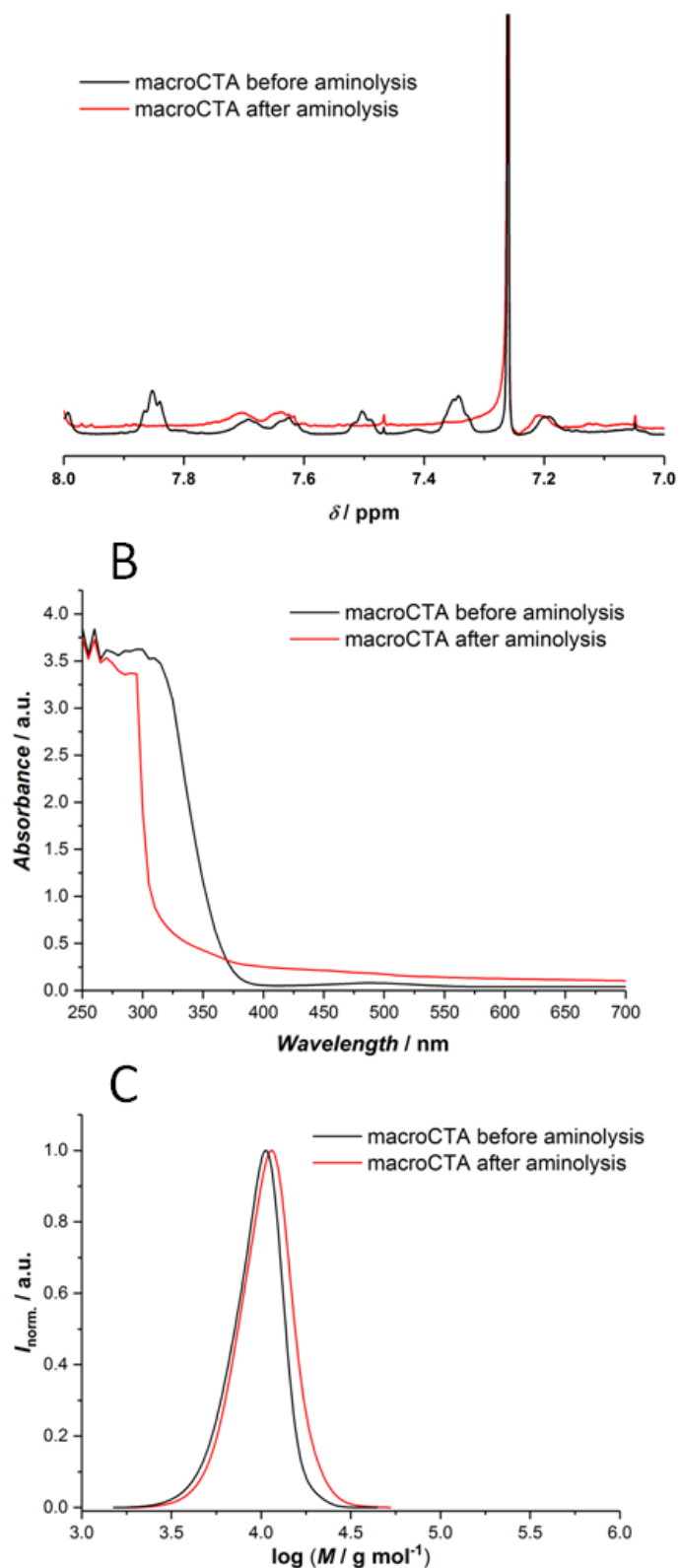


**Figure 46.** (A)  $^1\text{H}$  NMR spectra, (B) UV-Vis spectra, and (C) SEC traces before and after aminolysis of macroCTA.

#### 5.4. TESPMA-IONP Surface Functionalization by "Grafting Through"

Based on the previous results, thiol transformation was performed at a larger scale followed by sequential Michael addition onto the TESPMA-coated nanoparticles which were added to the reaction mixture after 2.5 h. After purification the nanoparticles were analyzed by ATR-FTIR and SEM, as depicted in Figure 47. No absorption bands (1100-1700  $\text{cm}^{-1}$ ) of the attached macro RAFT agent could be detected by the ATR-FTIR. SEM showed no change in particle aggregation as compared to the TESPMA-NPs and EDX analysis indicated a decrease in carbon content after the Michael addition (from 22.5 to 8.9 wt%). Therefore, the analytical results did not lead to the conclusion that Michael addition occurred. A different approach towards polymer-coated magnetite particles was investigated, namely "grafting through".

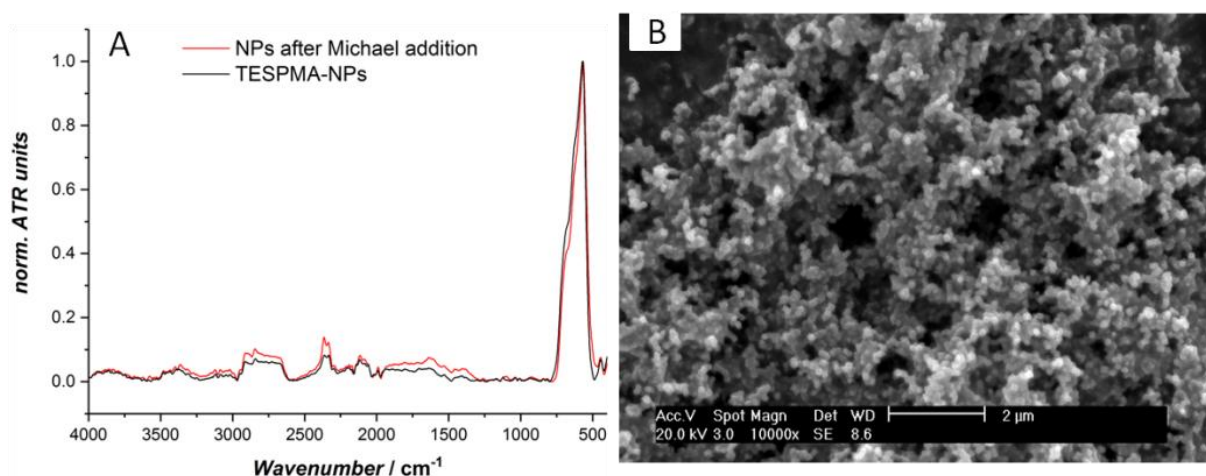


**Figure 47.** (A) ATR-FTIR and (B) SEM measurements after Michael addition of TESPMA-NPs.

#### 5.4. TESPMA-IONP Surface Functionalization by "Grafting Through"

An alternative route towards coated ferrofluids utilizing a RAFT-mediated "grafting through" mechanism was employed. Test experiments in water with an inorganic redox initiating system  $\text{K}_2\text{S}_2\text{O}_8/\text{Na}_2\text{S}_2\text{O}_3$  ( $[\text{macroCTA}]:[\text{K}_2\text{S}_2\text{O}_8]:[\text{Na}_2\text{S}_2\text{O}_3] = 1:0.25:0.2$ ) were performed. This initiating system has been previously used in aqueous RAFT polymerizations at room temperature and was chosen for its mild homolysis conditions, which might be beneficial for future RAFT experiments with protein-coupled macroCTAs.<sup>209</sup> Furthermore, in a second experiment, methyl methacrylate

5. Polymer-Coated Iron Oxide Nanoparticles for Enzyme Immobilization

([MMA]:[macroCTA] = 5) was added to the reaction in order to ensure proper propagation of oligomeric radical species and facilitate transfer to the macro RAFT agent. The reactions were degassed using 5 freeze-pump-thaw cycles and were then placed on a shaker (750 rpm) for 24 h at ambient temperature. After several washing steps with DCM, ethanol, and water, the particle suspensions were dried and analyzed by ATR-FTIR spectroscopy and SEM (Figure 48).

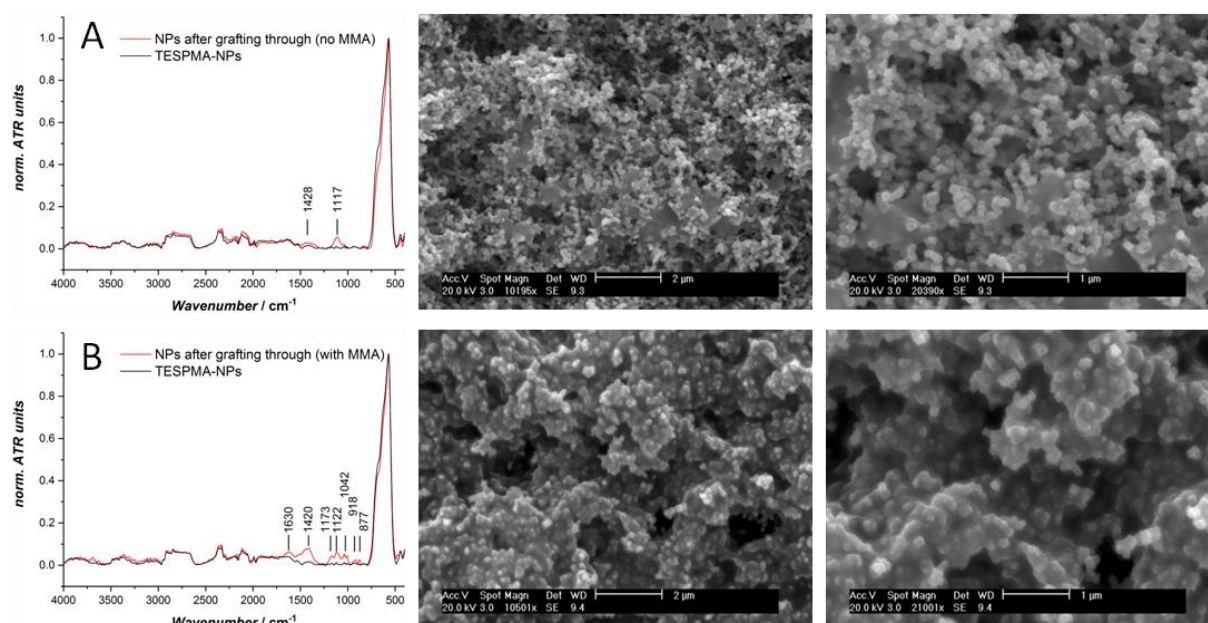


**Figure 48.** ATR-FTIR and SEM measurements of (A) grafted nanoparticles without additional MMA and (B) grafted nanoparticles with additional MMA ([macroCTA]:[MMA] = 5).

Comparing the absorption bands of TESPMA-NPs and polymer-grafted nanoparticles revealed new signals even though measured intensities were low, indicating only partial functionalization. Polymerization without additional MMA showed two absorption bands at 1428  $\text{cm}^{-1}$  and 1117  $\text{cm}^{-1}$ , which can be ascribed to C-O-C and Si-O-Si bands, respectively (Figure 48A, left). In the second experiment, with MMA, ATR-FTIR analysis revealed stretching bands at 1630  $\text{cm}^{-1}$  (C=O), 1173  $\text{cm}^{-1}$  (C-O), 1420  $\text{cm}^{-1}$ , and 1040  $\text{cm}^{-1}$  (C-O-C), which can be attributed to either TESPMA or polymer-coated nanoparticles. However, nitrile vibrations of the macroCTA at around 2250  $\text{cm}^{-1}$  were not observed. Unexpectedly, Si-O stretching and Si-O-H bending vibrations at 877-

918  $\text{cm}^{-1}$ , as well as Si-O-Si stretching bands at 1122  $\text{cm}^{-1}$  were observed, as opposed to the original TESPMA-NPs. Indeed, in both IR spectra the Si bands were clearly visible as compared to the TESPMA-functionalized nanoparticles, possibly due to lower amounts being measured for the latter. SEM images of the functionalized nanoparticles showed large polymer films between particles as well as areas with no polymer coating. Interestingly, a thick layer of polymer surrounding magnetite aggregates throughout the whole sample was observed if additional MMA was placed to the RAFT polymerization. However, in both samples the polymer layers seemed to have merged between neighboring particles, which resulted in interparticle polymer films (Figure 48A, right) and lumpy polymer-magnetite aggregates (Figure 48B, right). An explanation for this behavior might be the close proximity of radical species during the polymerization, which may result in polymer chain couplings between adjacent particles at high conversions. In the case of the polymerization with additional MMA, a process akin to emulsion polymerization may also have occurred, leading to the formation of composite polymer-iron oxide particles. Prior to the analysis the particle suspensions were purified with organic solvents and water assuring that any unreacted and non-covalently bound macro RAFT agent, monomer, or polymer was removed. Therefore, the SEM images represent iron oxide nanoparticle aggregates with incorporated polymer. Subsequent EDX analysis of the particle film exhibited changes in carbon content for both samples. While the weight percentage of carbon slightly decreased for grafted nanoparticles without MMA (19.8 wt%) as compared to the TESPMA-NPs (22.5 wt%), a large increase was observed for grafted nanoparticles with MMA (41.8 wt%). It remained unclear why the carbon content decreased for grafted nanoparticles upon reaction with the macroCTA alone. Polymerization under these conditions could not be optimized due to time constraints and reiterations of these experiments lead to no functionalization of the nanoparticles. Whether this was due to insufficient deoxygenation or problems with the freshly prepared stock solution of the redox initiator could not be determined.

In a second set of experiments the initiating agent was changed from the aforementioned redox system in water to an AIBN/EtOH system. In order to find suitable polymerization conditions four experiments with varying ratios of AIBN and MMA were performed (blank1-4 NPs, see Experimental Section 7.4.2.) utilizing the non-functional macro RAFT agent mentioned above. Furthermore, the same set of experiments were conducted in parallel with the functionalized macroCTAs. Even

though magnetic stirring was set to 750 rpm, a substantial amount of nanoparticles strongly assembled onto the stir bar. After washing steps with DCM, ethanol, and water, the particles were dried and analyzed by ATR-FTIR spectroscopy but no clear absorption bands for any functional group were visible (Figure 49). The measurements were repeated three times yet no changes could be observed. SEM analysis did not show any polymer films or aggregates within the samples.

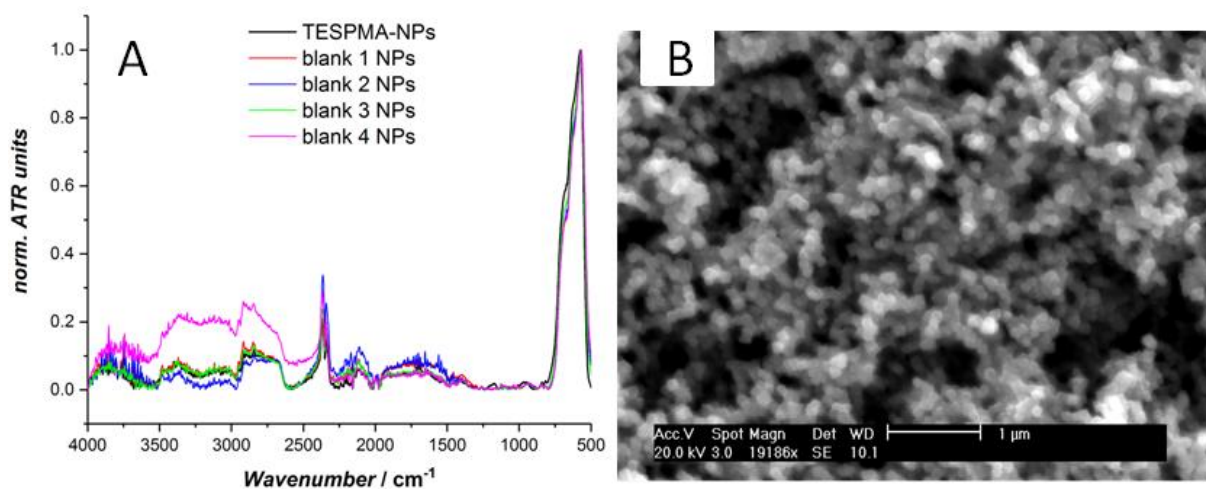


**Figure 49.** (A) ATR-FTIR spectra of TESPMA-NPs and polymer-functionalized nanoparticles blank1-4 via "grafting through" and (B) representative SEM picture of polymer-coated nanoparticles (blank4 NP).

For further analysis, samples synthesized with the Cl-functionalized macroCTA ( $M_{n,SEC} = 5500 \text{ g mol}^{-1}$ ,  $D = 1.12$ ) were examined by time-of-flight secondary ion mass spectrometry (ToF-SIMS) and X-ray photoelectron spectroscopy (XPS). Figure 50 demonstrates detected fragments of the samples surface based on their  $m/z$  values. While  $\text{SiO}_2$  fragments were visible, iron oxide fragments ( $\text{FeO}_2$ ) were observed on all samples, leading to the conclusion that silicon oxide did not form a dense and homogenous layer on the particles and that the silanization step may not have been optimal (Figure 50A-B). Sulfur signal arising from the RAFT end-group were detected within the samples, yet the intensities were very low (Figure 50B). CN fragments of cyano groups within the RAFT polymer was also observable, however non-functional IONPs and TESPMA-NPs depicted these fragment as well possibly due to contaminations within the respective samples. Similarly, Cl fragments were visible in all samples and were especially prominent in Cl-functionalized particles (Figure 50E). Lastly, ethylene

5.4. TESPMA-IONP Surface Functionalization by "Grafting Through"

glycol repeating units originating from the polymers side chain were detected. While one polymer-coated NP sample showed the highest intensity of PEG fragments, a large quantity of ethylene glycol was also observed in TESPMA-NPs, which may be ascribed to an incomplete hydrolysis of triethoxysilane (Figure 50F).

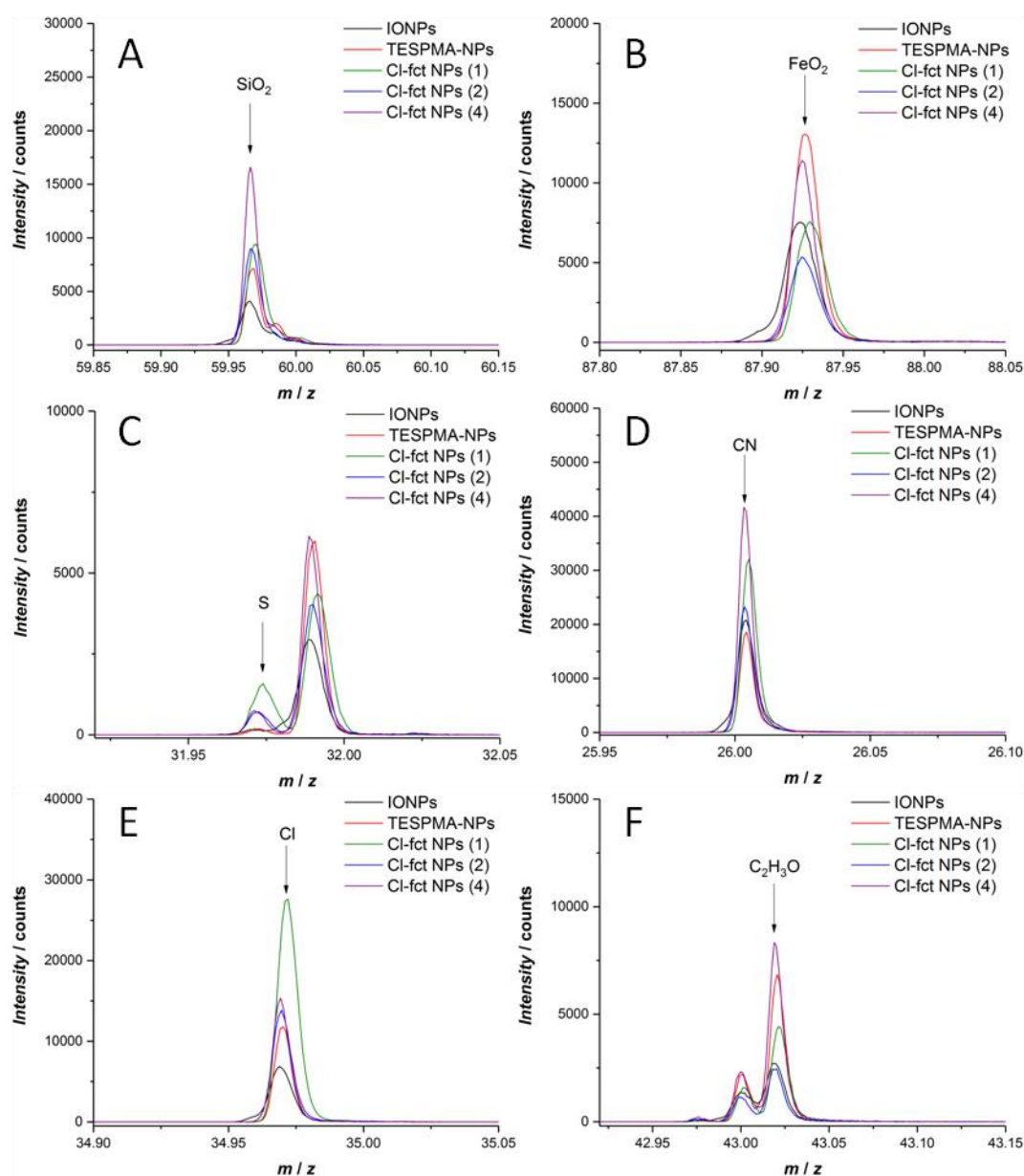


**Figure 50.** ToF-SIMS spectra for non-functionalized IONPs (black), TESPMA-NPs (red), and Cl-functionalized nanoparticles 1 (green, [macroCTA]:[MMA]:[initiator] = 1:0:0.25), 2 (blue [macroCTA]:[MMA]:[initiator] = 1:0:1) and 4 (gray, [macroCTA]:[MMA]:[initiator] = 1:25:1).

XPS analysis revealed that the overall iron content during the functionalization steps remained the same ( $\sim 17$  at%). Furthermore, C-C and C-H contents remained the same during all steps and carbon-based signals even observable for non-functionalized IONP samples (Figure 51). However, a strong increase of C-O content (Figure 51, green trace) compared to C-C was measured in all grafted samples almost as abundant as in a reference measurement of the macro RAFT agent. This could be ascribed to PEG repeating units of the macro RAFT agent attached to the magnetite particles, which may conversely confirm a grafting process. Binding energies of O=C-O ester groups could also be determined in all samples but no change was detectable even for experiments with additional MMA to improve the grafting. With the rise in C-O content due to incorporated macro RAFT agent and the aforementioned analytical results it may be suggested that at least partial polymer-coating of the iron oxide nanoparticles occurred.

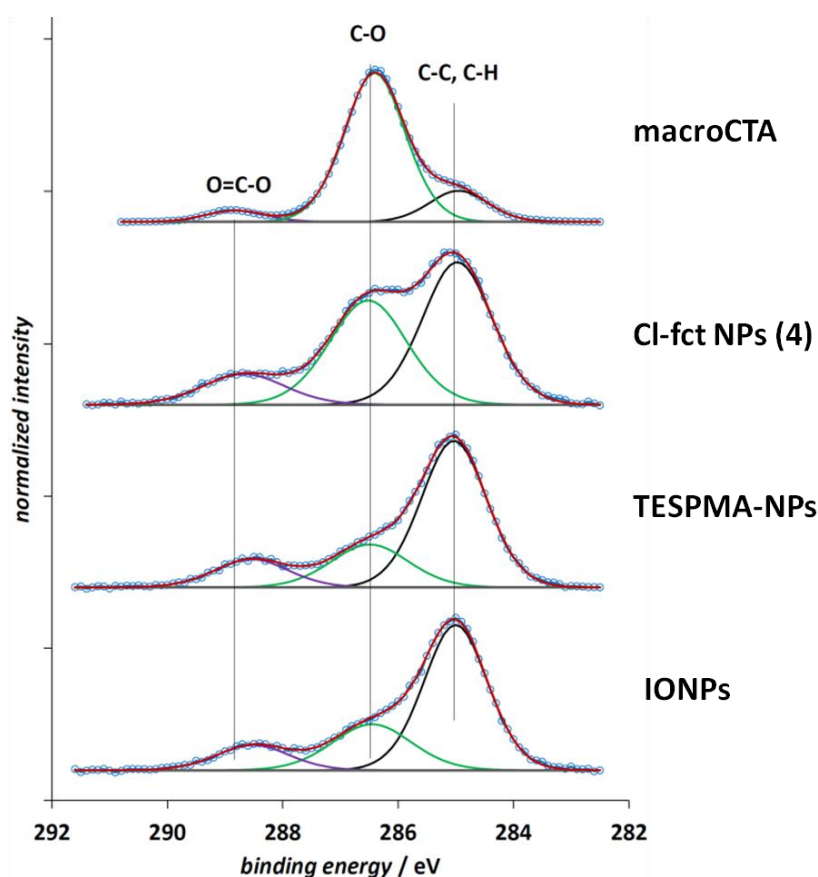


**Figure 51.** Stacked XPS spectra of macro RAFT agent, grafted nanoparticles ([macroCTA]:[MMA]:[initiator] = 1:25:1), TESPMA-NPs and non-functionalized IONPs (top to bottom). Green trace represent binding energies of C-O at 286.5 eV.

## 5.5. Conclusion and Outlook

Combining the analytical results demonstrated in this chapter, it can be stated that the formation of polymer-coated magnetite particles could not be performed satisfyingly. While end-group removal of macro RAFT agents was successful, sequential Michael addition between the thiols of the macroCTAs and methacrylate double bonds did not lead to the desired product. In the "grafting through" route, inconclusive results were obtained as some reactions with the water-based redox system demonstrated entrapped polymers within magnetite aggregates. However, large polymer film and aggregate formation between iron oxide particles was unexpected and could not be explained entirely since polymer shells surrounding the particles were thought to form thin coatings. Changing the radical initiator from a redox system to AIBN did not lead to any improvements as ATR-FTIR, ToF-SIMS, and XPS analysis confirmed. "Grafting through" experiments with functional macroCTAs, which were performed in parallel most likely did not work either since the reaction conditions remained the same. Even though sulfur, chloride, and PEG fragments could be detected by ToF-SIMS in Cl-functionalized nanoparticles, the results were not entirely convincing since the same fragments were observed in non-functional IONP and TESPMA-NP samples, possibly due to contaminations prior to the measurements. However, due to time constraints no deeper investigations and optimizations of reaction conditions could be carried out. Still, the work described in this chapter provides a suitable starting point for future research since functionalization parameters for iron oxide particles have been explored.

In order to resolve the two major problems described in this chapter, i.e., formation of large IONP aggregates and incomplete functionalization with TESPMA, commercial magnetite nanoparticles should not be utilized further. Therefore, the onset for continuative experiments should be the synthesis of small magnetite particles *via* various methods such as co-precipitation, sol-gel or sonochemical synthesis, offering a good control over size and polydispersity.<sup>210-212</sup> However, particle size below ~30 nm should be avoided since protein immobilization on such small sizes may become irrelevant for further applications. Another crucial step is the synthesis of TESPMA-functionalized nanoparticles that needs to be optimized. High temperature and short reaction times were employed to functionalize magnetite particles and reactions under these conditions should be repeated with newly synthesized magnetite nanoparticles to

confirm silanization. If however the functionalization with silane was insufficient, longer reaction times have to be employed at either lower temperatures or with addition of radical inhibitors such as hydroquinone to prevent thermal initiation of the methacrylate group. Furthermore, magnetic stirring should be avoided in future experiments since magnetite particles strongly self-assemble to the stir bars preventing a full functionalization of the IONPs. If synthesized iron oxide nanoparticles demonstrate no aggregation due to their intrinsic superparamagnetism, reactions may be conducted under sonification. Lastly, to improve the "grafting through" process, the polymerization should be carried out in a non-polar solvent such as acetonitrile or DCM to ensure that polymer-coated nanoparticles with incorporated PMMA will not flocculate during the reaction (i.e., emulsion polymerization mechanism).





# 6

## Conclusion

The use of enzymes as biocatalysts is a sustainable alternative to conventional chemical synthesis. Enzymes offer numerous advantages such as mild reaction conditions, accelerated reactions and a high catalytic activity resulting in excellent product yields. However, utilizing enzymes in solution has an intrinsic drawback since separation of from the product becomes a necessity, potentially inactivating the enzyme in the process. However, enzymes can be immobilized onto solid carriers to enable a facile separation from the reaction mixture as well as stabilization of the tertiary structure of the enzyme. Ideally, immobilization onto solid substrates should be site-specific as adsorption or other non-specific immobilizations can negatively affect their catalytic activity. The use of polymers has the advantage to offer control over size, morphology and biocompatibility over immobilization substrates. Therefore, the main goal of the current thesis was the synthesis of multifunctional amphiphilic block copolymer nanoparticles as solid supports for site-specific protein immobilization.

In Chapter 3 a novel NTA-containing NMP initiator based on the well-known MAMA-SG1 structure was synthesized and utilized to prepare functionalized POEGMA-based hydrophilic macroinitiators. Subsequent chain extension with styrene in bulk and nanoprecipitation of the block copolymer lead to NTA-functionalized nanoparticles whose morphologies could not be controlled. In a second route, a PISA process was employed in order to obtain various morphologies. However, in this investigation only spherical particles could be synthesized most likely due to the high molar mass of the macroinitiators. Enzyme immobilization experiments were conducted by metal ion chelation between His-tagged enzymes and NTA-functionalized nanoparticle dispersions. While DLS analysis confirmed the structural stability of the particles, UV-Vis measurements showed catalytic activity of the His-tagged HRP and esterase with their

respective substrates, thereby confirming the successful immobilization of enzymes. The formation of multifunctional nano-objects was achieved and investigated in Chapter 4. The polymerization technique was changed to a RAFT process and three novel chain transfer agents, with functional moieties at their  $\alpha$ -end to bind His-, SNAP-, and Halo-tagged enzymes, were synthesized. These RAFT agents were used in the controlled polymerization of fluorescent POEGMA-based macro chain transfer agents. By varying the amount of employed macro RAFT agent, the bulk polymerization of styrene and nanoprecipitation resulted in multifunctional nanoparticles, as SEC, DLS, and TEM measurements indicated. Similarly to the aforementioned method, fluorescent nanoparticles could be obtained by aqueous emulsion polymerization with hydrophobic benzyl methacrylate. Variations in the degree of polymerization of PBzMA and molar mass of macro RAFT agents during the PISA process led to the range of various end group functionalized particle morphologies such as spheres, worms, and vesicles, which were characterized by DLS and TEM.

In the last chapter, low molar mass macro RAFT agents were used for the synthesis of coated iron oxide nanoparticles. Through silanization, the nanoparticle surface was functionalized with methacrylate moieties for the direct attachment of the polymers. In the first route, a "grafting to" approach *via* aminolysis of the macro chain transfer agent and subsequent Michael addition to the methacrylates was investigated, which did not lead to a successful polymer coating of the nanoparticles. Hence, RAFT polymerization in alcoholic media was employed in a "grafting through" approach. A range of experimental parameters such as initiator and additional monomer concentration were investigated, leading to partially coated iron oxide particles, which were characterized by ATR-FTIR, ToF-SIMS, and XPS measurements.

In conclusion, novel functionalized amphiphilic block copolymer nanoparticles were developed by RDRP techniques, such as NMP and RAFT polymerization and fully characterized. Synthetic routes towards nanoparticle formation were demonstrated with a strong focus on the PISA process. Enzymes were successfully immobilized on the particles surfaces and by changing formulation parameters such as  $DP_n$  of solvophobic segment and  $M_n$  of the macroCTA, high order morphologies were obtained. The present thesis is thus a contribution to the development of novel strategies for the synthesis of polymeric nanocarriers with tunable properties for site-specific protein immobilization.





# Experimental Section

## 7.1. Characterization Methods

*Nuclear magnetic resonance spectrometry (NMR).*  $^1\text{H}$  measurements were performed on a Bruker AM 500 spectrometer at 500 MHz. The analytes were dissolved in  $\text{CDCl}_3$  and the residual solvent peaks were employed for shift correction.

*Size exclusion chromatography (SEC)* with *N,N*-dimethylacetamide (DMAc) as eluent was accomplished with a sample concentration of  $2 \text{ g L}^{-1}$  on a Polymer Laboratories PL-GPC 50 Plus Integrated system comprising an autosampler, a PLgel 2,5  $\mu\text{m}$  bead-size guard column ( $50 \times 7.5 \text{ mm}$ ) followed by three PLgel 5  $\mu\text{m}$  MixedC columns ( $300 \times 7.5 \text{ mm}$ ), and a flow rate of  $1 \text{ mL min}^{-1}$ . The SEC system was calibrated against linear poly(methyl methacrylate) standards with molar masses ranging from 700 to  $2 \times 10^6 \text{ Da}$ . The samples were filtered through polytetrafluorethylene (PTFE) membranes with a pore size of  $0.2 \mu\text{m}$  prior to injection.

*Electrospray ionization mass spectrometry (ESI-MS).* Spectra were recorded on an LXQ mass spectrometer (Thermo Fisher Scientific, San Jose, CA) equipped with an atmospheric pressure ionization source operating in the nebulizer assisted electrospray mode. The instrument was calibrated in the  $m/z$  range 195–1822 using a standard containing caffeine, Met-Arg-Phe-Ala acetate (MRFA), and a mixture of fluorinated phosphazenes (Ultramark 1621) (all from Aldrich). A constant spray voltage of 4.5 kV was used. Nitrogen at a dimensionless sweep gas flow rate of 2 (approximately  $3 \text{ L}$

min<sup>-1</sup>) and a dimensionless sheath gas flow rate of 5 (approximately 0.5 L min<sup>-1</sup>) was applied. The capillary voltage, the tube lens offset voltage, and the capillary temperatures were set to 34 V, 90 V, and 275 °C, respectively. The samples were dissolved at a concentration of 0.1 mg mL<sup>-1</sup> in a mixture of THF and MeOH (3:2) containing sodium trifluoroacetic acid (0.14 µg L<sup>-1</sup>).

*Dynamic light scattering (DLS).* DLS measurements were performed on a Malvern Zetasizer Nano ZS. Nanoparticles obtained from PISA and nanoprecipitation were not filtered prior to the measurements. Experiments were performed at 25 °C and 10 readouts were taken in 10 independent measurements for each sample with the attenuator set at 10. The particle polydispersity index (PDI) was calculated by the instrument through equation (11) with the second cumulant  $\mu$  and the average decay rate  $\Gamma$ . PDI ranges from 0 to 1 with values < 0.1 suggesting a nearly monodisperse sample.

$$PDI = \frac{\mu_2}{\bar{I}^2} \quad (11)$$

*Scanning electron microscopy (SEM).* Before SEM measurements, all samples were coated with an approximately 5 nm thick gold-platinum film (Bal-Tec/MED020 Coating System, Macclesfield, United Kingdom). Prepared samples were imaged by scanning electron microscope (FEI Philips XL30 FEG-ESEM, Philips, Amsterdam, Netherlands) equipped with an SE detector under high vacuum conditions in SEM mode using an acceleration voltage of 10-20 keV.

*Inductively coupled plasma optical emission spectrometry/mass spectrometry (ICP-OES/MS).* Ni was determined by optical emission spectrometry (ICP-OES, OPTIMA 4300 DV from PerkinElmer) and mass spectroscopy (ICP-MS, 7500ce from Agilent) 400 µL of the samples (accuracy better than ± 0.8%) was dissolved in 2 mL hydrochloric acid and 8 mL nitric acid at 499 K for 5 min in a microwave (Speedwave Xpert from Berghof). The analysis of Ni content was accomplished with four different calibration solutions and an internal standard (Sc). The range of the calibration solutions did not exceed a decade. Three wavelengths (ICP-OES) and three masses (ICP-MS, 58, 60, 62) of the element were used for calculation.

*UV/Vis spectroscopy.* UV-Vis measurements were carried out on a Biotek Epoch 2 spectrophotometer using 96-well plates (F-Bottom, Cellstar®). Spectra were recorded in water or acetone at 25 °C. Spectra were collected between 200 and 700 nm.

*Fluorescence spectroscopy.* Fluorescence emission spectra were recorded on a Varian Cary Eclipse spectrometer employing an excitation slit width of 5 nm, a resolution of 0.5 nm, and a scan rate of 30 nm min<sup>-1</sup>. All spectra were recorded in water at 25 °C. The dilution series of water-to-polymers were ranging from 1:1 (highest polymer concentration) to 1:1000 (lowest polymer concentration). Depending on the employed fluorescent monomer the excitation wavelengths were  $\lambda = 225$  nm (NMA), 490 nm (FMA), and 555 nm (VBR).

*Transmission electron microscopy (TEM).* Prior to TEM measurements, aqueous particles dispersions (10  $\mu$ L) were mixed and stained with a 20 wt% uranyl acetate solution (2  $\mu$ L) for 45 seconds and were spotted on 75-mesh Formvar 1 coated copper grids (Sigma Aldrich), dried at room temperature, and observed with a Zeiss EM 109T transmission electron microscope (Oberkochen, Germany).

*Attenuated total reflection Fourier transform infrared spectroscopy (ATR-FTIR).* ATR-FTIR spectra were measured using a Bruker Tensor27 spectrometer (Bruker Optics, Ettlingen, GER) equipped with a Bruker Platinum® ATR accessory (diamond crystal, single reflection, 1 mm<sup>2</sup> sampling area) and a deuterated tri-glycine sulfate detector (DTGS) against an air background. For each sample 32 scans were collected with a spectral resolution of four wavenumbers and a bandwidth from 370 – 4000 cm<sup>-1</sup>.

*Time-of-flight secondary ion mass spectrometry (ToF-SIMS).* ToF-SIMS was performed on a TOF.SIMS5 instrument (ION-TOF GmbH, Münster, Germany). Samples were drop cast onto silicon wafers and air dried. The spectrometer is equipped with a bismuth cluster primary ion source and a reflectron type time-of-flight analyzer. UHV base pressure was  $< 2 \times 10^{-8}$  mbar. For high mass resolution the Bi source was operated in the “high current bunched” mode providing short Bi<sub>3</sub><sup>+</sup> primary ion pulses at 25 keV energy and a lateral resolution of approx. 4  $\mu$ m. The short pulse length of 1.0 ns allowed for high mass

resolution. For all experiments 128×128 pixel on a 500×500 μm<sup>2</sup> field of view are analyzed and primary ion doses were fixed at 10<sup>11</sup> ions/cm<sup>2</sup> (static SIMS limit). To compensate for sample charging under primary ion bombardment an electron flood gun, emitting electrons at 21 eV energy, was applied and the reflectron tuned accordingly. Spectra were calibrated on the omnipresent C<sup>-</sup>, CH<sup>-</sup>, CH<sub>2</sub><sup>-</sup>, C<sub>2</sub><sup>-</sup>, and SiO<sub>2</sub><sup>-</sup>; or on the C<sup>+</sup>, CH<sup>+</sup>, CH<sub>2</sub><sup>+</sup>, CH<sub>3</sub><sup>+</sup>, and Fe<sup>+</sup> peaks. Based on these datasets the chemical assignments for characteristic fragments were determined.

*Energy dispersive X-ray spectroscopy (EDX).* Energy-dispersive X-ray spectroscopy (EDX) measurements were conducted on a Genesis 2000 microanalysis system with a Si(Li) detector (EDAX, Wiesbaden, Germany).

*X-ray photoelectron spectroscopy (XPS).* XPS measurements were performed using a K-Alpha+ XPS spectrometer (ThermoFisher Scientific, East Grinstead, UK). Data acquisition and processing using the Thermo Avantage software is described elsewhere.<sup>213</sup> All samples were analyzed using a microfocused, monochromated Al Kα X-ray source (400 μm spot size). The K-Alpha charge compensation system was employed during analysis, using electrons of 8 eV energy, and low-energy argon ions to prevent any localized charge build-up. The kinetic energy of the electrons was measured by a 180° hemispherical energy analyzer operated in the constant analyzer energy mode (CAE) at 50 eV pass energy for elemental spectra. The spectra were fitted with one or more Voigt profiles (BE uncertainty: ±0.2eV) and Scofield sensitivity factors were applied for quantification. All spectra were referenced to the C 1s peak (C-C, C-H) at 285.0 eV binding energy controlled by means of the well known photoelectron peaks of metallic Cu, Ag, and Au, respectively.

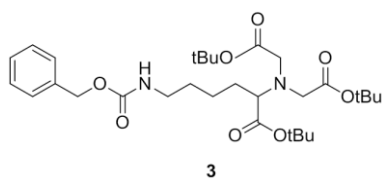
## 7.2. Amphiphilic Block Copolymer Nanoparticles by NMP-Mediated Polymerization

### 7.2.1. Materials

*n*-Butyl methacrylate (BMA; Merck), *tert*-butyl acrylate (tBA; 98%, Sigma-Aldrich), styrene (S; 99.5%, Acros), and oligo(ethylene glycol) methacrylate  $M_n = 300$  (OEGMA<sub>300</sub>; Sigma-Aldrich) were eluted through a basic alumina column (Roth) to remove the inhibitor. Acrylonitrile (AN; 99+%, Acros), H-lysine (Z)-OtBu HCl (BACHEM), *tert*-butyl bromoacetate (98%, Sigma-Aldrich), *N*-hydroxysuccinimide (NHS; 98+%, Acros), oligo(ethylene glycol) methacrylate  $M_n = 950$  (OEGMA<sub>950</sub>; Sigma-Aldrich), nickel(II)sulfate hexahydrate (99%, Acros), ethanol (Fisher), and xylene (Roth) were used as received. 2-methyl-2-[*N*-*tert*-butyl-*N*-(1-diethoxyphosphoryl)-2,2-dimethylpropyl]aminoxy]-*N*-propionyloxysuccinimide (NHS-MAMA-SG1) was obtained following a literature procedure.<sup>214</sup>

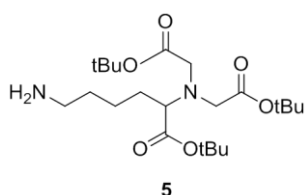
### 7.2.2. Synthetic Procedures

*Synthesis of di-tert-butyl 2,2'-((6-(((benzyloxy)carbonyl)amino)-1-(tert-butoxy)-1-oxohexan-2-yl)azanediyl)diacetate 3*



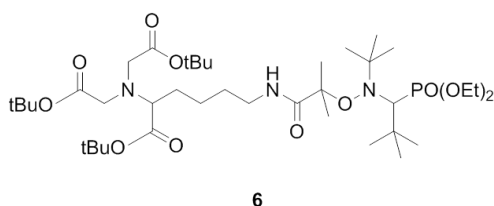
In a dried Schlenk, flask H-lysine (Z)-OtBu HCl (1.0 g, 2.52 mmol, **1**) was dissolved in dry DMF (25 mL). *tert*-Butyl bromoacetate (3.9 mL, 25.2 mmol, **2**) and *N,N*-diisopropylethylamine (DIPEA) (2.3 mL, 13.2 mmol) were added under nitrogen. The reaction mixture was stirred overnight (16 h) at 55°C. DMF was evaporated in vacuo at 65 °C. Subsequently, the organic phase was washed three times with H<sub>2</sub>O (15 mL), dried over Na<sub>2</sub>SO<sub>4</sub>, and concentrated under reduced pressure at room temperature. The crude product was purified by silica gel column chromatography using cyclohexane/ethyl acetate (4:1 v/v) to yield *di-tert-butyl 2,2'-((6-(((benzyloxy)carbonyl)amino)-1-(tert-butoxy)-1-oxohexan-2-yl)azanediyl)diacetate* (1.3 g, 96%) as a colorless oil. <sup>1</sup>H NMR (500 MHz, CDCl<sub>3</sub>, δ): 7.35-7.31 (m, 5H), 5.08 (s, 2H), 3.46 (q, 4H), 3.29 (t, 1H), 3.19 (bs, 2H), 1.63 (m, 2H), 1.55 (m, 4H), 1.45 (s, 9H), 1.42 (s, 18H).

*Synthesis of di-tert-butyl 2,2'-((6-amino-1-(tert-butoxy)-1-oxohexan-2-yl)azanediyl)diacetate 5*



In a dried Schlenk flask, protected amine (1.28 g, 2.26 mmol, **3**) was dissolved in dry methanol (40 mL) under nitrogen and 10% Pd/C (120 mg) was added. The reaction mixture was vigorously stirred for 9 h under hydrogen atmosphere at room temperature. Pd/C was filtered off over celite, and the filtrate was evaporated under reduced pressure to yield pNTA amine **5** (0.33 g, 32%) as a colorless oil. <sup>1</sup>H NMR (500 MHz, CDCl<sub>3</sub>, δ): 3.48 (q, 5H), 3.30 (t, 1H), 2.68 (t, 2H), 1.63 (m, 6H), 1.45 (s, 9H), 1.44 (s, 18H).

*Synthesis of pNTA-MAMA-SG1 6*



In a dried Schlenk flask, pNTA amine (357.2 mg, 0.80 mmol, **5**) was dissolved in dry DCM (5 mL) and deoxygenated by nitrogen bubbling for 20 min at 0 °C. In a second flask NHS-MAMA-SG1 (384.2 mg, 0.80 mmol, **4**) was dissolved in dry DCM (10 mL) and deoxygenated by nitrogen bubbling for 20 min at 0 °C. The latter solution was then introduced to the pNTA amine solution and the resulting mixture was stirred for 2 h at 0 °C. Subsequently, the organic phase was washed three times with H<sub>2</sub>O (15 mL), dried over Na<sub>2</sub>SO<sub>4</sub>, and concentrated under reduced pressure at room temperature. The crude product was purified by silica gel column chromatography using cyclohexane/ethyl acetate (1:1 v/v) to yield pNTA-MAMA-SG1 **6** (356.9 mg, 56%) as a colorless oil. <sup>1</sup>H NMR (500 MHz, CDCl<sub>3</sub>, δ): 7.99 (s, 1H), 4.21–4.06 (m, 4H), 3.46 (q, 4H), 3.33 (s, 1H), 3.24 (m, 1H), 3.01 (brs, 1H), 1.65 (s, 5H), 1.54 (s, 5H), 1.43 (s, 9H), 1.42 (s, 18H), 1.33–1.29 (m, 8H), 1.18 (s, 9H), 1.08 (s, 9H) ppm. MS (ESI, m/z): [M+Na<sup>+</sup>] calc.: 816.5110, found: 816.5115.

*Synthesis of pNTA-functionalized poly(*t*-butyl acrylate) (pNTA-PtBA)*

pNTA-MAMA-SG1 (40.9 mg, 0.05 mmol, **6**) and SG1 (1.4 mg, 0.005 mmol) were dissolved in tBA (2.4 mL, 2.27 mmol). This mixture was deoxygenated by five freeze-pump-thaw cycles and subsequently heated to 115 °C for 20 min. After cooling to room temperature, the crude product (22%, 1300 g mol<sup>-1</sup>) was precipitated in methanol, filtered, and dried under vacuum. This product was further analyzed by direct injection in ESI-MS (see main text). The polymerization was performed anew on a larger scale for 1 h with the same monomer-to-initiator ratio of 45 to analyze the resulting polymer by SEC.

*Synthesis of pNTA-functionalized POEGMA<sub>300</sub> (macro1)*

In a typical OEGMA<sub>300</sub> nitroxide-mediated polymerization, OEGMA<sub>300</sub> (1.65 mL, 5.67 mmol), styrene (0.04 mL, 0.55), functionalized alkoxyamine initiator **2** (79.1 mg, 0.1 mmol), and SG1 (2.9 mg, 0.08 mmol) were dissolved in xylene (6 mL). The mixture was deoxygenated by six free-pump-thaw cycles and then heated to 95 °C. Samples were periodically withdrawn to determine monomer conversion using <sup>1</sup>H NMR spectroscopy. The polymerization was later performed on a larger scale to produce a sufficient amount of macroinitiator for further experiments. According to the preliminary kinetic study, the reaction was carried out for 18 h and the final product was precipitated in cold pentane, filtered, and dried under vacuum.

*Synthesis of pNTA-functionalized POEGMA<sub>950</sub> (macro2)*

In a typical OEGMA<sub>950</sub> polymerization, OEGMA<sub>950</sub> (2.4 g, 2.52 mmol), styrene (0.03 mL, 0.252 mmol), functionalized alkoxyamine initiator **2** (100 mg, 0.12 mmol), and SG1 (0.37 mL, 0.012 mmol) stock solution (10 mg/mL in EtOH) were dissolved in ethanol (9.2 mL) and deoxygenated by nitrogen bubbling for 35 min at room temperature. The mixture was then heated to 79 °C. Samples were periodically withdrawn to follow monomer conversion using <sup>1</sup>H NMR spectroscopy. The polymerization was later performed on a larger scale to produce sufficient amounts of macroinitiator for further experiments. According to the preliminary kinetic study, the reaction was carried out for

6 h and the final product was precipitated in diethyl ether, filtered, and dried under vacuum.

#### *Synthesis of HO-functionalized POEGMA macroinitiator (**macro3-4**)*

The same recipes as for the pNTA-functionalized macroinitiators above was applied, at the exception that pNTA-MAMA-SG1 was replaced by HO-MAMA-SG1.

#### *Synthesis of pNTA- and HO-functionalized POEGMA<sub>300</sub>-b-PS amphiphilic block copolymers*

In a typical chain extension in homogeneous medium, styrene (0.2 mL, 1.58 mmol) was polymerized in bulk at 120 °C for 1 h, using either **macro1** or **macro3** (49.6 mg, 0.0027 mmol) as macroinitiator. In each case, the crude product was precipitated in cold methanol, filtered, and dried under vacuum to yield either pNTA-(POEGMA<sub>300</sub>-co-S)-b-PS **pNTA-BCP** ( $M_n = 98400 \text{ g mol}^{-1}$ ,  $D = 1.70$ ) and non-functionalized amphiphilic block copolymer HO-(POEGMA<sub>300</sub>-co-S)-b-PS **HO-BCP** ( $M_n = 76600 \text{ g mol}^{-1}$ ,  $D = 1.40$ ).

#### *Formation of NTA-functionalized nanoparticles by nanoprecipitation (**NP1**)*

2.0 mg of the functionalized amphiphilic block copolymer NTA-POEGMA<sub>300</sub>-b-PS ( $M_n = 98400 \text{ g mol}^{-1}$ ,  $D = 1.70$ ) and 13.8 mg the hydroxyl-functionalized amphiphilic block copolymer HO-POEGMA<sub>300</sub>-b-PS ( $M_n = 76600 \text{ g mol}^{-1}$ ,  $D = 1.4$ ) were dissolved in filtered THF (2 mL). Through a syringe pump water (18 mL) was added to the organic phase within one hour under constant stirring. The solution was then dialyzed (MWCO 1 kDa) against water for 24 h to completely remove the THF. (DLS)  $Z_{av} = 397 \text{ nm}$ ;  $PDI = 0.149$ .

#### *Butyl methacrylate polymerization-induced self-assembly (PISA)*

In a typical PISA polymerization given amounts of (p)NTA-functionalized macroalkoxyamine **macro2** (20.0 mg, 0.001 mmol) and HO-functionalized macroalkoxyamine **macro4** (40.0 mg, 0.003 mmol) were first dissolved in water

## 7.2. Amphiphilic Block Copolymer Nanoparticles by NMP-Mediated Polymerization

(1.125 mL). The monomers, BMA (336.7 mL, 2.1 mmol) and styrene (22.0 mL, 0.19 mmol), were added to this solution and the resulting mixture was deoxygenated by nitrogen bubbling for 35 min. The mixture was then heated to 85 °C for 6 h. After PISA experiments the particle solution was dialyzed (MWCO 1 kDa) for 72 h changing the surrounding water 10 times, in order to remove non-polymerized monomers. Dead/unreacted macroinitiator was removed via three washing cycles. Each cycle consisted of three steps: centrifugation (4000 rpm) at 4 °C for 40 min, removing the supernatant containing excess dead macroinitiator, and redispersing the pellet in MilliQ water.

### *Deprotection of pNTA-functionalized nanoparticles*

To a nanoparticle dispersion obtained by either PISA or the co-solvent method (0.4 mL), H<sub>3</sub>PO<sub>4</sub> (85 wt% in H<sub>2</sub>O, 0.15 mL) was added. The mixture was stirred overnight at room temperature and then dialyzed (MWCO 1 kDa) for 24 h, changing the water 4 times in the process.

### *Nickel complexation with NTA-functionalized nanoparticles*

A 1 M NiSO<sub>4</sub> solution was prepared in MilliQ water. 200 µL of the nickel solution was added to a small Eppendorf vial containing 1 mL of deprotected NTA-functionalized NP solution. The particle solution was placed on a shaker at ambient temperature for 2 h. Excess Ni<sup>2+</sup> was removed by three washing cycles. Each cycle consisted of three steps: centrifugation (4000 rpm) at 4 °C for 40 min, removing the supernatant containing excess Ni<sup>2+</sup>, and redispersing the pellet in MilliQ water.

### *Production and purification of His-tagged horseradish peroxidase (HRP-His) and His-esterase (Mes1-His)*

These tasks were carried out by Dr Ana Beloqui (Delaittre group, KIT) and Monic Martinez-Martinez (CSIC, Madrid, Spain). Horseradish peroxidase gene (GeneBank code CAA00083.1, from *Armoracia rusticana*) was purchased from Invitrogen and cloned into pET32b+ vector. pET32b+\_hrp plasmid was transformed into *E coli* BL21 strain and

expressed under  $\beta$ -D-1-thiogalactopyranoside (IPTG) induction. The protein was expressed as inclusion bodies, which were separated, purified, and refolded in order to yield pure (> 95%) and active protein. Mes1 ester hydrolase enzyme was retrieved from a fosmid clone library created from sediment samples of Messina harbour (Sicily, Italy) (GeneBank code KR107252). The gene encoding Mes1 was cloned into Ek/LIC 46 (Novagen) expression vector using a PCR-based approach, appropriate fosmid DNA sample as template, and *Escherichia coli* BL22 as host.

### *Enzyme Immobilization*

These tasks were carried out by Dr Ana Beloqui (Delaittre group, KIT). Nanoparticle solutions (50  $\mu$ L) were mixed with enzyme solutions (200  $\mu$ L, 1 mg mL<sup>-1</sup>) in binding buffer (30 mM, 150 mM NaCl, pH 7.4) and stirred for 2 h at RT. Non-bound protein was removed from the polymeric material through 3 centrifugation cycles (14000 x *g*, 10 min) using washing buffer (binding buffer with 50 mM of imidazole). Washed biocatalytic particles were suspended in 75  $\mu$ L of sodium phosphate buffer (30 mM, pH 7.0) and kept ready for activity assays.

### *Biocatalytic Assays*

These tasks were carried out by Dr Ana Beloqui (Delaittre group, KIT). Activity measurements were performed using a Biotek Epoch 2 spectrophotometer at 25 °C in 96-well plates. Biocatalytic activity was assayed in triplicate by mixing the enzyme modified nanoparticle suspensions (10  $\mu$ L) with the adequate substrate (190  $\mu$ L). Peroxidase activity was evaluated in sodium citrate buffer (50 mM, pH 5.1) with H<sub>2</sub>O<sub>2</sub> (2.9 mM) and ABTS (0.27 mM) and ester hydrolase activity in Tris-HCl buffer (50 mM, pH 7.0) with *p*-nitrophenylbutyrate (pNPC4, 0.8 mM). The absorptions arising from oxidized ABTS and the release of *p*-nitrophenol were recorded at 416 and 405 nm, respectively. Initial transformation rates and extinction coefficient values of 36000 M<sup>-1</sup> cm<sup>-1</sup> for ABTS and 13400 M<sup>-1</sup> cm<sup>-1</sup> for *p*-nitrophenol were used for the calculation of the specific activity.

*Calculated Data for Nickel after Metal Complexation on Particles*

	unit	NP2	NP3
$\%NTA_{theo}$		100	25
$D_{DLS}$	nm	96	99
$C_{polymer}$	wt%	0.73	1.11
	g L <sup>-1</sup>	7.33	11.07
$C_{Ni}$	wt%	0.00082	0.000617
	g L <sup>-1</sup>	8.20E-03	6.17E-03
	mol L <sup>-1</sup>	1.40E-04	1.05E-04
$D_{core}$	nm	85.5	88.5
$V_{core}$	cm <sup>3</sup>	3.27E-16	3.63E-16
$m_{core}$	g	3.50E-16	3.88E-16
$m_{shell}/m_{core}$		0.83	0.31
$m_{particle}$	g	6.41E-16	5.10E-16
$N_p$	L <sup>-1</sup>	1.14E+16	2.17E+16
	mol L <sup>-1</sup>	1.90E-08	3.60E-08
<b><math>N_{Ni}</math> per particle</b>		<b>7360</b>	<b>2919</b>
$A_{DLS}$	nm <sup>2</sup>	28953	30791
$A_{per Ni}$	nm <sup>2</sup>	3.93	10.55
<b><math>d_{btwn Ni}</math></b>	<b>nm</b>	<b>1.1</b>	<b>1.8</b>

Measured values are in green.  $\%NTA_{theo}$  corresponds to the percentage of NTA-functionalized macroinitiators employed during PISA.

### 7.3. Amphiphilic Block Copolymer Nanoparticles by RAFT-Mediated Polymerization

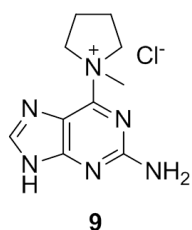
#### 7.3.1. Materials

2,2'-Azobis(2-methylpropionitrile) (AIBN; 98 %, Sigma-Aldrich), 2,2'-azobis(2-(2-imidazolin-2-yl)propane)dihydrochloride (VA-044; >97%, Wako), 2,2'-azobis(4-methoxy-2,4-dimethylvaleronitrile) (V-70; Wako), 2-cyano-2-propyl benzodithioate (CPDB; >97%, Sigma-Aldrich), 4-cyano-4-(phenylcarbonothioylthio)pentanoic acid N-succinimidyl ester (NHS-CTA; Sigma-Aldrich), fluorescein *O*-methacrylate (FMA; 97%

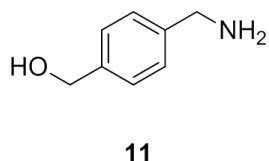
Sigma-Aldrich), 2-naphthyl methacrylate (NMA; 95%, Alfa), rhodamine (98+%, Acros), 2-(2-aminoethoxy)ethanol (98%, Sigma-Aldrich), Boc<sub>2</sub>O (≥99%, Sigma-Aldrich), 6-iodo-1-chlorohexane (96%, Sigma-Aldrich), TFA (99%, Sigma-Aldrich), 4-cyano-4-(phenylcarbonothioylthio)pentanoic acid *N*-succinimidyl ester (Sigma-Aldrich), 1-methylpyrrolidine (98%, Sigma-Aldrich), 2-amino-6-chloropurine (≥99%, Sigma-Aldrich), lithium aluminium hydride (≥97%, Sigma-Aldrich), 4-cyanobenzoate (99%, Sigma-Aldrich), trifluoroacetic acid ethyl ester (99%, Sigma-Aldrich), potassium *tert*-butoxide (≥98%, Sigma-Aldrich), ethanol (Sigma-Aldrich), dichloromethane (Fisher), triethylamine (>99%, Fisher), and acetonitrile (Fisher) were used as received. Benzyl methacrylate (BzMA; 96%, Sigma-Aldrich), styrene (S; 99.5%, Acros), 4-vinylbenzyl chloride (90%, Sigma-Aldrich), and oligo(ethylene glycol) methacrylate  $M_n = 500$  (OEGMA<sub>500</sub>; Sigma-Aldrich) were eluted through a basic alumina column (Roth) to remove the inhibitor.

### 7.3.2. Synthetic Procedures

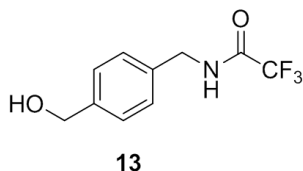
#### *Synthesis of 1-(2-amino-7H-purin-6-yl)-1-methyl pyrrolidinium chloride 9*



In a dried Schlenk flask, 2-amino-6-chloropurine (3.0 g, 17.7 mmol, **7**) was dissolved in DMF (100 mL) at 40 °C. The solution was allowed to cool to room temperature and 1-methylpyrrolidine (3.31 g, 38.9 mmol, **8**) was added. The reaction mixture was stirred overnight at room temperature. Acetone (6 mL) was added to quench the reaction and the mixture was stored for 1.5 h at 4 °C. The white solid was filtered off, washed twice with cold Et<sub>2</sub>O (50 mL), and dried under reduced pressure to yield 1-(2-amino-7H-purin-6-yl)-1-methyl pyrrolidinium chloride (1.92 g, 41%) as a colorless oil. <sup>1</sup>H NMR (500 MHz, DMSO-d<sub>6</sub>, δ): 13.32 (s, 1H), 8.35 (s, 1H), 7.12 (s, 2H), 4.58 (m, 2H), 3.95 (m, 2H), 3.64 (s, 3H), 2.24 (s, 2H), 2.05 (s, 2H).

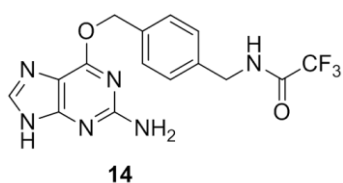
*Synthesis of 4-(aminomethyl)-benzyl alcohol 11*

In a dried Schlenk flask, lithium aluminium hydride (2.83 g, 74.5 mmol) was dissolved in dry THF (150 mL). Sulfuric acid (99.99%, 1.9 mL, 37.2 mmol) was added dropwise under cooling and stirred for 1 h under room temperature. In a second flask, 4-cyanobenzoate (2.0 g, 12.4 mmol, **10**) was dissolved in dry THF (12 mL) and added dropwise to the previous solution. The reaction mixture was refluxed for 2 h and quenched with H<sub>2</sub>O (20 mL). NaOH (7.4 g) dissolved in H<sub>2</sub>O (60 mL) was added and the organic layer of the mixture was decanted. The water phase was washed with Et<sub>2</sub>O and EtOAc twice (60 mL each). The combined organic phases were dried over Na<sub>2</sub>SO<sub>4</sub>, and concentrated under reduced pressure at room temperature to yield 4-(aminomethyl)-benzyl alcohol (1.43 g, 84%) as a colorless solid. <sup>1</sup>H NMR (500 MHz, CDCl<sub>3</sub>, δ): 7.31-7.28 (dd, 4H), 4.65 (s, 2H), 3.83 (s, 2H), 1.87 (s, 3H).

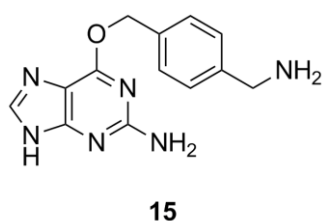
*Synthesis of 2,2,2-trifluoro-N-(4-hydroxymethyl-benzyl)-acetamide 13*

In a dried Schlenk flask, 4-(aminomethyl)-benzyl alcohol (85.0 mg, 6.2 mmol, **11**) and triethylamine (0.87 mL, 6.2 mmol) were dissolved in MeOH (10 mL). Trifluoroacetic acid ethyl ester (0.96 mL, 8.06 mmol, **12**) was added dropwise and stirred for 45 min at room temperature. The reaction mixture was diluted with EtOAc (10 mL) and H<sub>2</sub>O (10 mL). Subsequently, the aqueous phase was washed three times with EtOAc (20 mL). The combined organic phases were washed with brine, dried over Na<sub>2</sub>SO<sub>4</sub>, and concentrated under reduced pressure at room temperature. The crude product was purified by silica gel column chromatography using cyclohexane/ethyl acetate (2:1 v/v) to yield 2,2,2-trifluoro-N-(4-hydroxymethyl-benzyl)-acetamide (1.12 g, 77%) as a colorless solid. <sup>1</sup>H NMR (500 MHz, CDCl<sub>3</sub>, δ): 7.38-7.31 (m, 4H), 6.50 (s, 1H), 4.72 (d, 2H), 4.53 (d, 2H), 1.67 (s, 1H).

*Synthesis of N-[4-(2-amino-9H-purin-6-ylloxymethyl)-benzyl]-2,2,2-trifluoroacetamide 14*



In a dried Schlenk flask, trifluoro-*N*-(4-hydroxymethyl-benzyl)-acetamide (118.0 mg, 0.51 mmol, **13**) and potassium *tert*-butoxide (199.9 mg, 1.75 mmol) were dissolved in DCM (10 mL). In a second Schlenk flash 1-(2-amino-7H-purin-6-yl)-1-methyl pyrrolidinium chloride (100.8 mg, 0.40 mmol, **9**) was dissolved in DCM (5 mL). The latter solution was added to the former and the resulting red reaction mixture was stirred over night under room temperature. The organic phase was concentrated under reduced pressure at room temperature and the crude product was purified by silica gel column chromatography using DCM/MeOH (10:1 v/v) to yield *N*-

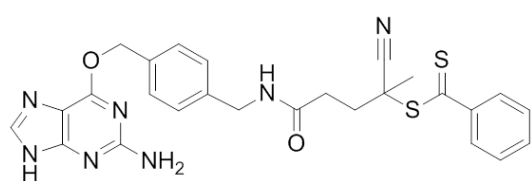


[4-(2-amino-9H-purin-6-yloxymethyl)-benzyl]-2,2,2-trifluoroacetamide (55.0 mg, 37%) as a colorless solid. <sup>1</sup>H NMR (500 MHz, DMSO-*d*<sub>6</sub>, δ): 12.41 (s, 1H), 10.01 (s, 1H), 7.81 (s, 1H), 7.50 (d, 2H), 7.31 (d, 2H), 6.30 (s, 2H), 5.47 (s, 2H), 4.41 (s, 2H).

#### Synthesis of *O*<sup>6</sup>-(4-amino-methyl-benzyl)guanine **15**

In a dried Schlenk flask, *N*-[4-(2-amino-9H-purin-6-yloxymethyl)-benzyl]-2,2,2-trifluoroacetamide (301.0 mg, 0.82 mmol, **14**) and K<sub>2</sub>CO<sub>3</sub> were dissolved in a mixture of MeOH (34 mL) and H<sub>2</sub>O (2 mL). The reaction mixture was refluxed at 85 °C for 2 h and cooled to room temperature. The solvents were removed under reduced pressure at room temperature and the crude product was purified by silica gel column chromatography using DCM/MeOH/TEA (5:1:0.01 v/v/v) to yield *O*<sup>6</sup>-(4-amino-methyl-benzyl)guanine (175.0 mg, 79%) as a pale yellow solid. <sup>1</sup>H NMR (500 MHz, DMSO-*d*<sub>6</sub>, δ): 7.82 (s, 1H), 7.43 (d, 2H), 7.36 (d, 2H), 7.50 (d, 2H), 6.28 (s, 2H), 5.45 (s, 2H), 3.47 (s, 2H).

#### Synthesis of 5-((4-(((2-amino-9H-purin-6-yl)oxy)methyl)benzyl)amino)-2-cyano-5-oxopentan-2-yl benzodithioate (BG-CTA **17**)

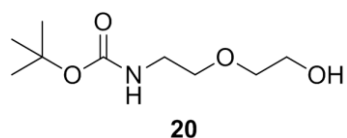


In a dried Schlenk flask, *O*<sup>6</sup>-(4-amino-methyl-benzyl)guanine (717.9 mg, 2.66 mmol, **15**) and triethylamine (537.6 mg, 5.31 mmol) were

### 7.3. Amphiphilic Block Copolymer Nanoparticles by RAFT-Mediated Polymerization

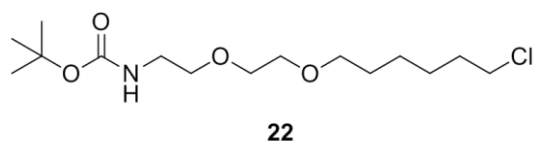
dissolved in dry DCM (15 mL) and deoxygenated by nitrogen bubbling for 25 min at 0 °C. In a second Schlenk flask, 4-cyano-4-(phenylcarbonothioylthio)pentanoic acid *N*-succinimidyl ester (1.00 g, 2.66 mmol) was dissolved in dry DCM (10 mL) and deoxygenated by nitrogen bubbling for 25 min at 0 °C. The solution containing the red RAFT agent was introduced to the benzylguanine solution and the reaction mixture was stirred for 5 h at ambient temperature. Subsequently, the organic phase was washed three times with H<sub>2</sub>O (25 mL), dried over Na<sub>2</sub>SO<sub>4</sub>, and concentrated under reduced pressure at room temperature. The crude product was purified by silica gel column chromatography using dichloromethane/methanol (5:1 v/v) to yield BG-CTA **17** (643.0 mg, 46%) as a deep red oil. <sup>1</sup>H NMR (500 MHz, DMSO-d<sub>6</sub>, δ): 10.79 (bs, 1 H, **k**), 8.54 (s, 1 H, **j**), 7.91-7.28 (m, 9 H, **a, g**), 6.29 (s, 1 H, **e**), 5.46 (s, 1 H, **h**), 4.97 (s, 1 H, **f**), 2.59 (s, 4 H, **c, d**), 1.91 (s, 3 H, **b**). <sup>13</sup>C NMR (500 MHz, CDCl<sub>3</sub>, δ): 175.04, 172.78, 144.63, 133.14, 128.68, 126.78, 118.63, 53.56, 45.84, 36.98, 33.39, 31.86, 25.48, 24.09. MS (ESI, m/z): [M+Na<sup>+</sup>] calc.: 554.1403, found: 554.1411.

#### Synthesis of *tert*-butyl (2-(2-((6-chlorohexyl)oxy)ethoxy)ethyl)carbamate **20**



In a dried Schlenk flask, 2-(2-aminoethoxy)ethanol (1.9 mL, 19.22 mmol, **18**) was dissolved in EtOH (40 mL) and cooled to 0 °C. Boc<sub>2</sub>O (4.80 mL, 20.9 mmol, **19**) was added and the solution was stirred for 2 h at room temperature. After evaporation of EtOH the crude product was dissolved in DCM and extracted three times with H<sub>2</sub>O (20 mL), dried over Na<sub>2</sub>SO<sub>4</sub>, and concentrated under reduced pressure at room temperature to yield *tert*-butyl (2-(2-((6-chlorohexyl)oxy)ethoxy)ethyl)carbamate (2.70 g, 67%) as a brown liquid. <sup>1</sup>H NMR (500 MHz, CDCl<sub>3</sub>, δ): 5.09 (bs, 1H), 3.71 (m, 2H), 3.57 (m, 4H), 3.32 (s, 2H), 1.43 (s, 9 H).

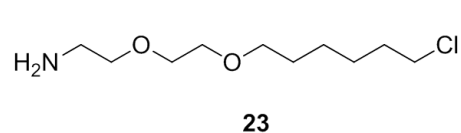
#### Synthesis of 2-(2-((6-chlorohexyl)oxy)ethoxy)ethanamine **22**



In a dried Schlenk flask, *tert*-butyl (2-(2-((6-chlorohexyl)oxy)ethoxy)ethyl)carbamate (2.0 g, 9.75 mmol, **20**) was dissolved in a mixture of THF (14 mL) and DMF (7 mL) at 0 °C. Sodium hydride (0.354 g, 11.7 mmol) was added to the reaction. After stirring the mixture for 30 min at 0 °C, 6-iodo-1-

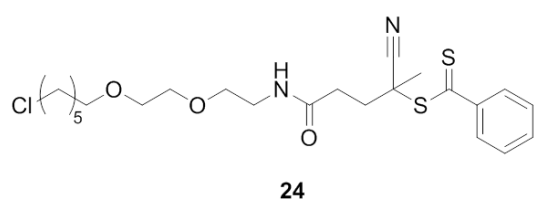
chlorohexane (2.0 mL, 16.65 mmol, **21**) was added and the solution was stirred at room temperature over night. The reaction was quenched with saturated  $\text{NH}_4\text{Cl}$  and extracted with EtOAc. The organic phase was washed with  $\text{H}_2\text{O}$  and brine, dried over  $\text{Na}_2\text{SO}_4$ , and concentrated under reduced pressure at room temperature. The crude product was purified by silica gel column chromatography using cyclohexane/ethyl acetate (4:1 v/v) to yield 2-(2-((6-chlorohexyl)oxy)ethoxy)ethanamine (1.5 g, 48%) as a brown liquid.  $^1\text{H}$  NMR (500 MHz,  $\text{CDCl}_3$ ,  $\delta$ ): 5.01 (bs, 1H), 3.55-3.43 (m, 10H), 1.75 (m, 2H), 1.59 (m, 2H), 1.42-1.33 (m, 13 H).

### Synthesis of 2-(2-((6-chlorohexyl)oxy)ethoxy)ethanamine **23**



In a dried Schlenk flask, 2-(2-((6-chlorohexyl)oxy)ethoxy)ethanamine (1.44 g, 4.44 mmol, **22**) was dissolved in DCM (12 mL) at  $0^\circ\text{C}$ . TFA (4.8 mL, 62.2 mmol) was slowly added and the mixture was allowed to warm up to room temperature and stirred for 2 h. The solvent was evaporated under reduced pressure and the residue was treated with  $\text{K}_2\text{CO}_3$  in MeOH (10 mL). The mixture was filtered under the filtrate was concentrated under reduced pressure at room temperature. The crude product was purified by silica gel column chromatography using cyclohexane/ethyl acetate (1:2 v/v) to yield 2-(2-((6-chlorohexyl)oxy)ethoxy)ethanamine (604 mg, 61%) as a colorless liquid.  $^1\text{H}$  NMR (500 MHz,  $\text{CDCl}_3$ ,  $\delta$ ): 5.61 (bs, 2H), 3.61-3.45 (m, 10H), 3.03 (t, 2H), 1.76 (m, 2H), 1.58 (m, 2H), 1.44 (m, 2H), 1.34 (m, 2 H).

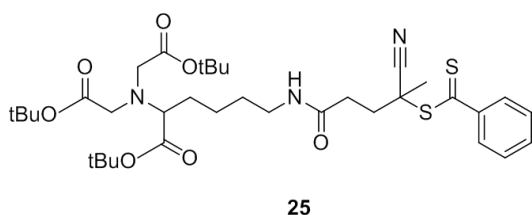
### Synthesis of 5-((2-(2-((6-chlorohexyl)oxy)ethyl)amino)-2-cyano-5-oxopentan-2-yl)benzodithioate (Cl-CTA **24**)



In a dried Schlenk flask, 2-(2-((6-chlorohexyl)oxy)ethoxy)ethanamine (493.3 mg, 2.20 mmol, **23**) and triethylamine (446.2 mg, 4.41 mmol) were dissolved in dry DCM (15 mL) and deoxygenated by nitrogen bubbling for 25 min at  $0^\circ\text{C}$ . In a second Schlenk flask, 4-cyano-4-(phenylcarbonothioylthio)pentanoic acid *N*-succinimidyl ester (830.0 mg, 2.20 mmol) was dissolved in DCM (10 mL) and deoxygenated by nitrogen

bubbling for 25 min at 0 °C. The solution containing the red RAFT agent was introduced to the haloalkane solution and the reaction mixture was stirred for 5 h at ambient temperature. Subsequently, the organic phase was washed three times with H<sub>2</sub>O (25 mL), dried over Na<sub>2</sub>SO<sub>4</sub>, and concentrated under reduced pressure at room temperature. The crude product was purified by silica gel column chromatography using cyclohexane/ethyl acetate (1:1 v/v) to yield the haloalkane RAFT agent, Cl-CTA **24** (290.0 mg, 27%) as a deep red oil. <sup>1</sup>H NMR (500 MHz, CDCl<sub>3</sub>, δ): 7.89-7.55 (m, 5H, **a**), 6.28 (s, 1 H, **l**), 3.61-3.46 (m, 12 H, **e, f, g, h, i, k**), 2.54-2.42 (m, 4 H, **c, d**), 1.94 (s, 3 H, **b**), 1.74-1.25 (m, 8 H, **j**). <sup>13</sup>C NMR (500 MHz, CDCl<sub>3</sub>, δ): 170.38, 144.70, 133.13, 128.70, 126.80, 118.84, 71.44, 70.46, 70.15, 69.73, 46.20, 45.18, 39.54, 34.25, 32.63, 31.94, 29.57, 26.78, 25.52, 24.33. MS (ESI, m/z): [M+Na<sup>+</sup>] calc.: 507.1513, found: 507.1524.

*Synthesis of di-tert-butyl 2,2'-((1-(tert-butoxy)-6-(4-cyano-4-((phenylcarbonothioyl)thio)pentanamido)-1-oxohexan-2-yl)azanediyl)diacetate (pNTA-CTA **25**)*



In a dried Schlenk flask, pNTA amine (590.5 mg, 1.33 mmol, **5**) and triethylamine (268.3 mg, 2.66 mmol) were dissolved in dry DCM (30 mL) and deoxygenated by nitrogen bubbling for 25 min at 0 °C. In a second Schlenk flask, 4-cyano-4-(phenylcarbonothioylthio)pentanoic acid *N*-succinimidyl ester (500.0 mg, 1.33 mmol) was dissolved in dry DCM (30 mL) and deoxygenated by nitrogen bubbling for 25 min at 0 °C. The solution containing the red RAFT agent was introduced to the pNTA amine solution and the reaction mixture was stirred for 5 h at ambient temperature. Subsequently, the organic phase was washed three times with H<sub>2</sub>O (60 mL), dried over Na<sub>2</sub>SO<sub>4</sub>, and concentrated under reduced pressure at room temperature. The crude product was purified by silica gel column chromatography using cyclohexane/ethyl acetate (1:1 v/v) to yield pNTA-CTA **25** (557.8 mg, 60%) as a deep red oil. <sup>1</sup>H NMR (500 MHz, CDCl<sub>3</sub>, δ): 7.87-7.39 (m, 5 H, **a**), 6.54 (s, 1 H, **e**), 3.41 (q, 4 H, **j**), 3.30 (t, 2 H, **f**), 3.21 (s, 1 H, **i**), 2.57-2.44 (m, 4 H, **c, d**), 1.93 (s, 3 H, **b**), 1.63-1.51 (m, 6 H, **h, g**), 1.45 (s, 9 H, **k'**), 1.42 (s, 18 H, **k**). <sup>13</sup>C NMR (500 MHz, CDCl<sub>3</sub>, δ): 172.46, 170.78, 144.75, 132.97, 128.92, 128.60, 127.35, 126.74, 118.74, 81.42, 81.12, 64.65, 54.09, 46.23,

39.39, 34.35, 31.48, 29.42, 28.30, 28.21, 27.80, 24.14, 22.59. MS (ESI, m/z): [M+Na<sup>+</sup>] calc.: 714.3217, found: 714.3229.

*Synthesis of tetraethylrhodamine 4-vinylbenzyl ester (VBR)*

In a dried Schlenk flask, rhodamine B (4.02 g, 8.4 mmol) and potassium carbonate (0.38 g, 2.7 mmol) were dissolved in DMF (75 mL). 4-Vinylbenzyl chloride (1.8 mL, 12.6 mmol) was added to the former solution. The reaction mixture was stirred for 48 h at 55 °C under nitrogen atmosphere. Subsequently, the solvent was removed under reduced pressure at 65 °C, the residual slur was dissolved with chloroform und washed three times with H<sub>2</sub>O (100 mL). The combined organic phases were dried over Na<sub>2</sub>SO<sub>4</sub>, and concentrated under reduced pressure at room temperature. The crude product was purified by silica gel column chromatography using dichloromethane/methanol (9:1 v/v) to yield tetraethylrhodamine 4-vinylbenzyl ester (2.55 g, 50%) as a deep red liquid. <sup>1</sup>H NMR (500 MHz, CDCl<sub>3</sub>, δ): 8.33-8.27 (m, 1H), 7.86 (m, 1H), 7.48-7.27 (m, 3H), 6.97-6.84 (m, 4H), 6.72 (m, 1H), 5.83 (m, 1H), 5.30 (m, 1H), 4.95 (s, 2H), 3.62 (q, 8H), 1.21 (12H).

*Exemplary synthesis of fluorescent functionalized macroCTA with high molar mass (macroCTA2, 4, 5)*

In a typical OEGMA<sub>500</sub> RAFT-mediated polymerization, OEGMA<sub>500</sub> (572.6 μL, 1.23 mmol), fluorescein *O*-methacrylate (26.4 mg, 0.066 mmol), Cl-CTA (40.0 mg, 0.082 mmol), and AIBN (2.7 mg, 0.016 mmol) were dissolved in acetonitrile (1.73 mL). The mixture was deoxygenated by nitrogen bubbling for 30 min and was then placed into a preheated oil bath at 70 °C for 6 h under constant stirring. After 6 h the mixture was placed into an ice bath, precipitated in cold diethyl ether/pentane (1:1 v/v), and dried under vacuum.

*Exemplary synthesis of fluorescent functionalized macroCTA with low molar mass (macroCTA1, 3)*

In a typical OEGMA<sub>500</sub> RAFT-mediated polymerization, OEGMA<sub>500</sub> (299.6  $\mu$ L, 0.66 mmol), fluorescein *O*-methacrylate (16.5 mg, 0.041 mmol), Cl-CTA (80.0 mg, 0.16 mmol), and AIBN (5.4 mg, 0.033 mmol) were dissolved in acetonitrile (1.05 mL). The mixture was deoxygenated by nitrogen bubbling for 30 min and was then placed into a preheated oil bath at 70 °C for 6 h under constant stirring. After 6 h the mixture was placed into an ice bath, precipitated in cold diethyl ether/pentane (1:1 v/v) and dried under vacuum.

*Synthesis of functionalized POEGMA<sub>500</sub>-b-PS amphiphilic block copolymers*

In a typical chain extension in homogeneous medium, styrene (1.85 mL, 16.1 mmol) was polymerized in bulk at 120 °C for 5 h, using **macroCTA2** (80.0 mg, 6.4  $\mu$ mol) and AIBN (0.26 mg, 1.6  $\mu$ mol). In each case, the crude product was precipitated in cold methanol, filtered, and dried under vacuum to yield Cl-P(OEGMA<sub>500</sub>-*co*-FMA)-*b*-PS ( $M_n = 24200$  g mol<sup>-1</sup>,  $\bar{D} = 1.19$ ). Experiments were repeated for macroCTA **4-5** resulting in BG-P(OEGMA<sub>500</sub>-*co*-NMA)-*b*-PS ( $M_n = 40700$  g mol<sup>-1</sup>,  $\bar{D} = 1.46$ ) and non-functionalized amphiphilic block copolymer P(OEGMA<sub>500</sub>-*co*-VBR)-*b*-PS ( $M_n = 18500$  g mol<sup>-1</sup>,  $\bar{D} = 1.17$ ).

*Formation of single-functionalized nanoparticles by nanoprecipitation (NP4-6)*

20.0 mg of the functionalized amphiphilic block copolymer Cl-P(OEGMA<sub>500</sub>-*co*-FMA)-*b*-PS ( $M_{n,NMR} = 44800$  g mol<sup>-1</sup>) was dissolved in filtered THF (2 mL). Through a syringe pump the organic solvent was added to water (18 mL) within one hour under constant stirring. The solution was then dialyzed (MWCO 1 kDa) against water for 24 h to completely remove the THF.

*Formation of multi-functionalized nanoparticles by the nanoprecipitation (NP8 and 11)*

10.0 mg (0.21 nmol) of the functionalized amphiphilic block copolymer BG-P(OEGMA<sub>500</sub>-*co*-NMA)-*b*-PS ( $M_{n,NMR} = 46500$  g mol<sup>-1</sup>) and 9.6 mg (0.21 nmol) Cl-P(OEGMA<sub>500</sub>-*co*-FMA)-*b*-PS ( $M_{n,NMR} = 44800$  g mol<sup>-1</sup>) were dissolved in filtered THF (2 mL). Through a syringe pump the organic solvent was added to water (18 mL) within one hour under

constant stirring. The solution was then dialyzed (MWCO 1 kDa) against water for 24 h to completely remove the THF.

#### *RAFT-mediated PISA formulation for single-functionalized nanoparticles (NP13-14)*

In a typical PISA polymerization given amounts of functionalized **macroCTA2/4** (30.0 mg, 2.4 nmol) was first dissolved in 845.5  $\mu$ L water. BzMA (61.5  $\mu$ L, 0.36 mmol) and VA-044 (0.15 mg, 0.48 nmol) were added to this solution and the resulting mixture was deoxygenated by nitrogen bubbling for 30 min. The mixture was then heated to 50 °C for 24 h. After PISA experiments the particle solution was dialyzed (MWCO 1 kDa) for 48 h changing the surrounding water 10 times, in order to remove non-polymerized monomers.

#### *RAFT-mediated PISA formulation for multi-functionalized nanoparticles (NP15-16)*

In a typical PISA polymerization given amounts of functionalized **macroCTA2** (40.0 mg, 3.2 nmol) and **macroCTA4/5** (38.7 mg, 3.2 nmol) were first dissolved in 2.24 mL water. BzMA (164  $\mu$ L, 0.97 mmol) and VA-044 (0.52 mg, 1.61 nmol) were added to this solution and the resulting mixture was deoxygenated by nitrogen bubbling for 30 min. The mixture was then heated to 50 °C for 24 h. After PISA experiments the particle solution was dialyzed (MWCO 1 kDa) for 48 h changing the surrounding water 10 times, in order to remove non-polymerized monomers.

## **7.4. Polymer-Coated Iron Oxide Nanoparticles for Enzyme Immobilization**

### **7.4.1. Materials**

2,2'-Azobis(2-methylpropionitrile) (AIBN; 98 %, Sigma-Aldrich), 2-cyano-2-propyl benzodithioate (CPDB; >97%, Sigma-Aldrich), dimethylphenylphosphine (DMPP;  $\geq$ 97%, VWR), butylamine (99.5%, Sigma-Aldrich), 3-(Triethoxysilyl)propyl methacrylate (TESPMA; >98%, TCI), potassium peroxosulfate (98%, VWR), sodium thiosulfate (Sigma-Aldrich), ethanol (Sigma-Aldrich), dichloromethane (Fisher), tetrahydrofuran (THF; Sigma-Aldrich) were used as received. Methyl methacrylate (MMA; Merck) was eluted

through a basic alumina column (Roth) to remove the inhibitor. MagPrep® Silica Particles (100 nm, Merck) were provided by Prof. M. Franzreb (IFG, KIT).

#### 7.4.2. Synthetic Procedures

##### *Synthesis of 3-(triethoxysilyl)propyl methacrylate functionalized magnetite $Fe_3O_4$ nanoparticles (TESPMA-MNPs)*

MagPrep silica magnetic nanoparticles (5 mL, 150 mg), 3-(triethoxysilyl)propyl methacrylate (5 ml, 5.2 g, 17.9 mmol) and hydroquinone (100 mg, 0.9 mmol) were refluxed at 120 °C for 3 h in water/ethanol (40 mL, 4:6 v/v) under intense magnetic stirring. Afterwards the particles were washed 5 times with water and 5 times with ethanol. Purified particles suspensions were stored in ethanol.

##### *General procedure of polymer-coated IONPs via aminolysis and sequential Michael addition ("grafting to")*

In a dried Schlenk flask, **blank-macroCTA** (20 mg, 2.3  $\mu$ mol), DMPP (4.9  $\mu$ L, 0.03 mmol) and butylamine (0.46  $\mu$ L, 4.6 mmol) were combined in DMF (1 mL). The mixture was deoxygenated by nitrogen bubbling for 25 min and stirred at room temperature for 2.5 h. 0.5 mL TESPMA-MNPs was added through a syringe to the decolorized solution and the reaction proceeded for 6 h. The particles were washed three times with DCM, three times with ethanol and three times with water.

##### *General procedure of polymer-coated IONPs via "grafting through" process*

In a dried Schlenk flask, TESPMA-MNPs (0.5 mL), **blank-macroCTA** (25 mg, 2.9  $\mu$ mol) and AIBN (0.1 mg, 0.73  $\mu$ mol) were combined in 0.5 mL ethanol. The mixture was deoxygenated by nitrogen bubbling for 25 min and placed into a preheated oil bath at 70 °C for 24 h. The particles were washed three times with DCM, three times with ethanol, and three times with water. The reaction was repeated with small molar mass functional macro RAFT agents (BG/Cl/pNTA functionality) and various ratios of initiator and MMA (Table 7).

**Table 7.** Experiment names based on utilized macroCTA and initiator/MMA ratios for "grafting through" reactions.

general name	[macroCTA]:[AIBN]	[macroCTA]:[MMA]
blank 1 / BG 1 / Cl 1 /pNTA 1	1 : 0.25	-
blank 2 / BG 2 / Cl 2 /pNTA 2	1 : 1.25	-
blank 3 / BG 3 / Cl 3 /pNTA 3	1 : 0.25	1 : 5
blank 4 / BG 4 / Cl 4 /pNTA 4	1 : 1.25	1 : 25

# Bibliography

1. Huisman, G. W.; Gray, D., Towards novel processes for the fine-chemical and pharmaceutical industries. *Current opinion in biotechnology* **2002**, *13* (4), 352-358.
2. Straathof, A. J. J.; Panke, S.; Schmid, A., The production of fine chemicals by biotransformations. *Current Opinion in Biotechnology* **2002**, *13* (6), 548-556.
3. Fjerbaek, L.; Christensen, K. V.; Norddahl, B., A review of the current state of biodiesel production using enzymatic transesterification. *Biotechnology and bioengineering* **2009**, *102* (5), 1298-1315.
4. Apetrei, I. M.; Rodriguez-Mendez, M. L.; Apetrei, C.; de Saja, J. A., Enzyme sensor based on carbon nanotubes/cobalt(II) phthalocyanine and tyrosinase used in pharmaceutical analysis. *Sensors and Actuators B: Chemical* **2013**, *177*, 138-144.
5. Ferri, S.; Kojima, K.; Sode, K., Review of Glucose Oxidases and Glucose Dehydrogenases: A Bird's Eye View of Glucose Sensing Enzymes. *Journal of Diabetes Science and Technology* **2011**, *5* (5), 1068-1076.
6. Petri, A.; Marconcini, P.; Salvadori, P., Efficient immobilization of epoxide hydrolase onto silica gel and use in the enantioselective hydrolysis of racemic para-nitrostyrene oxide. *Journal of Molecular Catalysis B: Enzymatic* **2005**, *32* (5), 219-224.
7. Diaz, J. F.; Balkus, K. J., Enzyme immobilization in MCM-41 molecular sieve. *Journal of Molecular Catalysis B: Enzymatic* **1996**, *2* (2-3), 115-126.
8. Liang, H.; Jiang, S.; Yuan, Q.; Li, G.; Wang, F.; Zhang, Z.; Liu, J., Co-immobilization of multiple enzymes by metal coordinated nucleotide hydrogel nanofibers: improved stability and an enzyme cascade for glucose detection. *Nanoscale* **2016**, *8* (11), 6071-6078.
9. Ren, Y.; Rivera, J. G.; He, L.; Kulkarni, H.; Lee, D.-K.; Messersmith, P. B., Facile, high efficiency immobilization of lipase enzyme on magnetic iron oxide nanoparticles via a biomimetic coating. *BMC biotechnology* **2011**, *11* (1), 63.
10. Poitry, S.; Poitry-Yamat, C.; Innocent, C.; Cosnier, S.; Tsacopoulos, M., Detection of glutamate released by neurons with an enzyme-based microelectrode: applications and limitations. *Electrochimica Acta* **1997**, *42* (20), 3217-3223.
11. Cosnier, S.; Innocent, C.; Allien, L.; Poitry, S.; Tsacopoulos, M., An electrochemical method for making enzyme microsensors. Application to the detection of dopamine and glutamate. *Analytical chemistry* **1997**, *69* (5), 968-971.
12. Hans, M. L.; Lowman, A. M., Biodegradable nanoparticles for drug delivery and targeting. *Current Opinion in Solid State and Materials Science* **2002**, *6* (4), 319-327.
13. Charleux, B.; Delaittre, G.; Rieger, J.; D'Agosto, F., Polymerization-induced self-assembly: from soluble macromolecules to block copolymer nano-objects in one step. *Macromolecules* **2012**, *45* (17), 6753-6765.
14. Moad, G.; Solomon, D. H., *The chemistry of radical polymerization*. Elsevier: 2006.
15. Jenkins Aubrey, D.; Jones Richard, G.; Moad, G., Terminology for reversible-deactivation radical polymerization previously called "controlled" radical or "living" radical polymerization (IUPAC Recommendations 2010). In *Pure and Applied Chemistry*, 2009; Vol. 82, p 483.
16. Braunecker, W. A.; Matyjaszewski, K., Controlled/living radical polymerization: Features, developments, and perspectives. *Progress in Polymer Science* **2007**, *32* (1), 93-146.
17. Roy, D.; Semsarilar, M.; Guthrie, J. T.; Perrier, S., Cellulose modification by polymer grafting: a review. *Chemical Society Reviews* **2009**, *38* (7), 2046-2064.
18. Buback, M.; Gilbert, R. G.; Hutchinson, R. A.; Klumperman, B.; Kuchta, F. D.; Manders, B. G.; O'Driscoll, K. F.; Russell, G. T.; Schweer, J., Critically evaluated rate coefficients for free-radical

- polymerization, 1. Propagation rate coefficient for styrene. *Macromolecular Chemistry and Physics* **1995**, *196* (10), 3267-3280.
19. Asua, J. M.; Beuermann, S.; Buback, M.; Castignolles, P.; Charleux, B.; Gilbert, R. G.; Hutchinson, R. A.; Leiza, J. R.; Nikitin, A. N.; Vairon, J. P., Critically evaluated rate coefficients for free-radical polymerization, 5. *Macromolecular Chemistry and Physics* **2004**, *205* (16), 2151-2160.
20. Ayrey, G.; Humphrey, M.; Poller, R., Radiochemical studies of free-radical vinyl polymerizations: 7. Polymerization of methyl acrylate. *Polymer* **1977**, *18* (8), 840-844.
21. Barth, J.; Buback, M.; Russell, G. T.; Smolne, S., Chain-Length-Dependent Termination in Radical Polymerization of Acrylates. *Macromolecular Chemistry and Physics* **2011**, *212* (13), 1366-1378.
22. Solomon, D. H.; Rizzardo, E.; Cacioli, P., Free radical polymerization and the produced polymers. *European Patent Application* **1985**, *1985*, 63.
23. Hawker, C. J.; Bosman, A. W.; Harth, E., New polymer synthesis by nitroxide mediated living radical polymerizations. *Chemical Reviews* **2001**, *101* (12), 3661-3688.
24. Fukuda, T.; Terauchi, T.; Goto, A.; Ohno, K.; Tsujii, Y.; Miyamoto, T.; Kobatake, S.; Yamada, B., Mechanisms and kinetics of nitroxide-controlled free radical polymerization. *Macromolecules* **1996**, *29* (20), 6393-6398.
25. Fischer, H., The persistent radical effect in "living" radical polymerization. *Macromolecules* **1997**, *30* (19), 5666-5672.
26. Greszta, D.; Mardare, D.; Matyjaszewski, K., "Living" radical polymerization. 1. Possibilities and limitations. *Macromolecules* **1994**, *27* (3), 638-644.
27. Johnson, C. H.; Moad, G.; Solomon, D. H.; Spurling, T. H.; Vearing, D., The Application of Supercomputers in Modeling Chemical Reaction Kinetics: Kinetic Simulation of 'Quasi-Living' Radical Polymerization. *Australian Journal of Chemistry* **1990**, *43* (7), 1215-1230.
28. Nilsen, A.; Braslau, R., Nitroxide decomposition: Implications toward nitroxide design for applications in living free-radical polymerization. *Journal of Polymer Science Part A: Polymer Chemistry* **2006**, *44* (2), 697-717.
29. Bagryanskaya, E. G.; Marque, S. R., Scavenging of organic C-centered radicals by nitroxides. *Chemical reviews* **2014**, *114* (9), 5011-5056.
30. Blinco, J. P.; Hodgson, J. L.; Morrow, B. J.; Walker, J. R.; Will, G. D.; Coote, M. L.; Bottle, S. E., Experimental and theoretical studies of the redox potentials of cyclic nitroxides. *The Journal of organic chemistry* **2008**, *73* (17), 6763-6771.
31. Sato, H.; Kathirvelu, V.; Fielding, A.; Blinco, J. P.; Micallef, A.; Bottle, S. E.; Eaton, S. S.; Eaton, G. R., Impact of molecular size on electron spin relaxation rates of nitroxyl radicals in glassy solvents between 100 and 300 K. *Molecular Physics* **2007**, *105* (15-16), 2137-2151.
32. Matyjaszewski, K.; Woodworth, B. E.; Zhang, X.; Gaynor, S. G.; Metzner, Z., Simple and efficient synthesis of various alkoxyamines for stable free radical polymerization. *Macromolecules* **1998**, *31* (17), 5955-5957.
33. Georges, M. K.; Veregin, R. P.; Kazmaier, P. M.; Hamer, G. K., Narrow molecular weight resins by a free-radical polymerization process. *Macromolecules* **1993**, *26* (11), 2987-2988.
34. Veregin, R. P.; Georges, M. K.; Kazmaier, P. M.; Hamer, G. K., Free radical polymerizations for narrow polydispersity resins: electron spin resonance studies of the kinetics and mechanism. *Macromolecules* **1993**, *26* (20), 5316-5320.
35. Benoit, D.; Harth, E.; Fox, P.; Waymouth, R. M.; Hawker, C. J., Accurate structural control and block formation in the living polymerization of 1, 3-dienes by nitroxide-mediated procedures. *Macromolecules* **2000**, *33* (2), 363-370.
36. Bertin, D.; Gimes, D.; Marque, S. R.; Tordo, P., Polar, steric, and stabilization effects in alkoxyamines C–ON bond homolysis: a multiparameter analysis. *Macromolecules* **2005**, *38* (7), 2638-2650.
37. Nicolas, J.; Dire, C.; Mueller, L.; Belleney, J.; Charleux, B.; Marque, S. R.; Bertin, D.; Magnet, S.; Couvreur, L., Living character of polymer chains prepared via nitroxide-mediated controlled free-radical polymerization of methyl methacrylate in the presence of a small amount of styrene at low temperature. *Macromolecules* **2006**, *39* (24), 8274-8282.

## Bibliography

38. Nicolas, J.; Brusseau, S.; Charleux, B., A minimal amount of acrylonitrile turns the nitroxide-mediated polymerization of methyl methacrylate into an almost ideal controlled/living system. *Journal of Polymer Science Part A: Polymer Chemistry* **2010**, *48* (1), 34-47.
39. Greene, A. C.; Grubbs, R. B., Synthesis and evaluation of N-phenylalkoxyamines for nitroxide-mediated polymerization. *Macromolecules* **2009**, *42* (13), 4388-4390.
40. Greene, A. C.; Grubbs, R. B., Nitroxide-mediated polymerization of methyl methacrylate and styrene with new alkoxyamines from 4-nitrophenyl 2-methylpropionat-2-yl radicals. *Macromolecules* **2010**, *43* (24), 10320-10325.
41. Detrembleur, C.; Jérôme, C.; De Winter, J.; Gerbaux, P.; Clément, J.-L.; Guillaeneuf, Y.; Gimes, D., Nitroxide mediated polymerization of methacrylates at moderate temperature. *Polymer Chemistry* **2014**, *5* (2), 335-340.
42. Simula, A.; Aguirre, M.; Ballard, N.; Veloso, A.; Leiza, J. R.; van Es, S.; Asua, J. M., Novel alkoxyamines for the successful controlled polymerization of styrene and methacrylates. *Polymer Chemistry* **2017**, *8* (10), 1728-1736.
43. Ballard, N.; Aguirre, M.; Simula, A.; Leiza, J. R.; van Es, S.; Asua, J. M., High solids content nitroxide mediated miniemulsion polymerization of n-butyl methacrylate. *Polymer Chemistry* **2017**, *8* (10), 1628-1635.
44. Gimes, D., *Nitroxide Mediated Polymerization: From Fundamentals to Applications in Materials Science*. Royal Society of Chemistry: 2015.
45. Versace, D.-L.; Guillaeneuf, Y.; Bertin, D.; Fouassier, J. P.; Lalevée, J.; Gimes, D., Structural effects on the photodissociation of alkoxyamines. *Organic & biomolecular chemistry* **2011**, *9* (8), 2892-2898.
46. Guillaeneuf, Y.; Versace, D. L.; Bertin, D.; Lalevée, J.; Gimes, D.; Fouassier, J. P., Importance of the position of the chromophore group on the dissociation process of light sensitive alkoxyamines. *Macromolecular rapid communications* **2010**, *31* (21), 1909-1913.
47. Telitel, S.; Telitel, S.; Bosson, J.; Spangenberg, A.; Lalevée, J.; Morlet-Savary, F.; Clément, J. L.; Guillaeneuf, Y.; Gimes, D.; Soppera, O., Nitroxide Mediated Photopolymerization: A Versatile Tool for the Fabrication of Complex Multilayer Polyfunctional Copolymer Nanostructures. *Advanced Materials Interfaces* **2014**, *1* (5).
48. Telitel, S.; Amamoto, Y.; Poly, J.; Morlet-Savary, F.; Soppera, O.; Lalevée, J.; Matyjaszewski, K., Introduction of self-healing properties into covalent polymer networks via the photodissociation of alkoxyamine junctions. *Polymer Chemistry* **2014**, *5* (3), 921-930.
49. Veronese, F. M., Peptide and protein PEGylation: a review of problems and solutions. *Biomaterials* **2001**, *22* (5), 405-417.
50. Veronese, F. M.; Harris, J. M., Introduction and overview of peptide and protein pegylation. *Advanced drug delivery reviews* **2002**, *54* (4), 453-6.
51. Chenal, M.; Boursier, C.; Guillaeneuf, Y.; Taverna, M.; Couvreur, P.; Nicolas, J., First peptide/protein PEGylation with functional polymers designed by nitroxide-mediated polymerization. *Polymer Chemistry* **2011**, *2* (7), 1523-1530.
52. Molawi, K.; Studer, A., Reversible switching of substrate activity of poly-N-isopropylacrylamide peptide conjugates. *Chemical Communications* **2007**, (48), 5173-5175.
53. Luo, R.; Sen, A., Electron-transfer-induced iron-based atom transfer radical polymerization of styrene derivatives and copolymerization of styrene and methyl methacrylate. *Macromolecules* **2008**, *41* (12), 4514-4518.
54. Wang, G.; Zhu, X.; Zhu, J.; Cheng, Z., Iron-mediated atom transfer radical polymerization of styrene with tris (3, 6-dioxaheptyl) amine as a ligand. *Journal of Polymer Science Part A: Polymer Chemistry* **2006**, *44* (1), 483-489.
55. Kato, M.; Kamigaito, M.; Sawamoto, M.; Higashimura, T., Polymerization of methyl methacrylate with the carbon tetrachloride/dichlorotris-(triphenylphosphine) ruthenium (II)/methylaluminum bis (2, 6-di-tert-butylphenoxide) initiating system: possibility of living radical polymerization. *Macromolecules* **1995**, *28* (5), 1721-1723.

## Bibliography

56. Ando, T.; Kato, M.; Kamigaito, M.; Sawamoto, M., Living Radical Polymerization of Methyl Methacrylate with Ruthenium Complex: Formation of Polymers with Controlled Molecular Weights and Very Narrow Distributions 1. *Macromolecules* **1996**, *29* (3), 1070-1072.
57. di Lena, F.; Matyjaszewski, K., Transition metal catalysts for controlled radical polymerization. *Progress in Polymer Science* **2010**, *35* (8), 959-1021.
58. Inoue, Y.; Matyjaszewski, K., New amine-based tripodal copper catalysts for atom transfer radical polymerization. *Macromolecules* **2004**, *37* (11), 4014-4021.
59. Wang, G.; Schmitt, M.; Wang, Z.; Lee, B.; Pan, X.; Fu, L.; Yan, J.; Li, S.; Xie, G.; Bockstaller, M. R., Polymerization-Induced Self-Assembly (PISA) Using ICAR ATRP at Low Catalyst Concentration. *Macromolecules* **2016**, *49* (22), 8605-8615.
60. Chiefari, J.; Chong, Y.; Ercole, F.; Krstina, J.; Jeffery, J.; Le, T. P.; Mayadunne, R. T.; Meijs, G. F.; Moad, C. L.; Moad, G., Living free-radical polymerization by reversible addition– fragmentation chain transfer: the RAFT process. *Macromolecules* **1998**, *31* (16), 5559-5562.
61. Quinn, J. F.; Barner, L.; Barner-Kowollik, C.; Rizzardo, E.; Davis, T. P., Reversible addition– fragmentation chain transfer polymerization initiated with ultraviolet radiation. *Macromolecules* **2002**, *35* (20), 7620-7627.
62. Moad, G.; Rizzardo, E.; Thang, S. H., Living Radical Polymerization by the RAFT Process – A Third Update. *Australian Journal of Chemistry* **2012**, *65* (8), 985-1076.
63. Barner-Kowollik, C.; Buback, M.; Charleux, B.; Coote, M. L.; Drache, M.; Fukuda, T.; Goto, A.; Klumperman, B.; Lowe, A. B.; Mccleary, J. B., Mechanism and kinetics of dithiobenzoate-mediated RAFT polymerization. I. The current situation. *Journal of Polymer Science Part A: Polymer Chemistry* **2006**, *44* (20), 5809-5831.
64. Aoyagi, N.; Endo, T., Functional RAFT agents for radical-controlled polymerization: Quantitative synthesis of trithiocarbonates containing functional groups as RAFT agents using equivalent amount of CS<sub>2</sub>. *Journal of Polymer Science Part A: Polymer Chemistry* **2009**, *47* (14), 3702-3709.
65. Keddie, D. J.; Moad, G.; Rizzardo, E.; Thang, S. H., RAFT Agent Design and Synthesis. *Macromolecules* **2012**, *45* (13), 5321-5342.
66. Chong, Y.; Krstina, J.; Le, T. P.; Moad, G.; Postma, A.; Rizzardo, E.; Thang, S. H., Thiocarbonylthio compounds [SC (Ph) S– R] in free radical polymerization with reversible addition– fragmentation chain transfer (RAFT Polymerization). Role of the free-radical leaving group (R). *Macromolecules* **2003**, *36* (7), 2256-2272.
67. Lai, J. T.; Filla, D.; Shea, R., Functional polymers from novel carboxyl-terminated trithiocarbonates as highly efficient RAFT agents. *Macromolecules* **2002**, *35* (18), 6754-6756.
68. Moad, G.; Chong, Y. K.; Postma, A.; Rizzardo, E.; Thang, S. H., Advances in RAFT polymerization: the synthesis of polymers with defined end-groups. *Polymer* **2005**, *46* (19), 8458-8468.
69. Aqil, A.; Qiu, H.; Greisch, J.-F.; Jérôme, R.; De Pauw, E.; Jérôme, C., Coating of gold nanoparticles by thermosensitive poly(N-isopropylacrylamide) end-capped by biotin. *Polymer* **2008**, *49* (5), 1145-1153.
70. Aamer, K. A.; Tew, G. N., RAFT polymerization of a novel activated ester monomer and conversion to a terpyridine-containing homopolymer. *Journal of Polymer Science Part A: Polymer Chemistry* **2007**, *45* (23), 5618-5625.
71. Liu, J.; Liu, H.; Boyer, C.; Bulmus, V.; Davis, T. P., Approach to peptide decorated micelles via RAFT polymerization. *Journal of Polymer Science Part A: Polymer Chemistry* **2009**, *47* (3), 899-912.
72. Liu, J.; Bulmus, V.; Herlambang, D. L.; Barner-Kowollik, C.; Stenzel, M. H.; Davis, T. P., In situ formation of protein–polymer conjugates through reversible addition fragmentation chain transfer polymerization. *Angewandte Chemie International Edition* **2007**, *46* (17), 3099-3103.
73. Li, M.; De, P.; Gondi, S. R.; Sumerlin, B. S., Responsive polymer-protein bioconjugates prepared by RAFT polymerization and copper-catalyzed azide-alkyne click chemistry. *Macromolecular Rapid Communications* **2008**, *29* (12-13), 1172-1176.

## Bibliography

74. De, P.; Li, M.; Gondi, S. R.; Sumerlin, B. S., Temperature-regulated activity of responsive polymer– protein conjugates prepared by grafting-from via RAFT polymerization. *Journal of the American Chemical Society* **2008**, *130* (34), 11288-11289.
75. Gao, Z.; Varshney, S. K.; Wong, S.; Eisenberg, A., Block copolymer" crew-cut" micelles in water. *Macromolecules* **1994**, *27* (26), 7923-7927.
76. Lepeltier, E.; Bourgaux, C.; Couvreur, P., Nanoprecipitation and the "Ouzo effect": Application to drug delivery devices. *Advanced drug delivery reviews* **2014**, *71*, 86-97.
77. Maeda, H.; Wu, J.; Sawa, T.; Matsumura, Y.; Hori, K., Tumor vascular permeability and the EPR effect in macromolecular therapeutics: a review. *Journal of controlled release* **2000**, *65* (1), 271-284.
78. Maeda, H., Macromolecular therapeutics in cancer treatment: the EPR effect and beyond. *Journal of Controlled Release* **2012**, *164* (2), 138-144.
79. Gaucher, G.; Marchessault, R. H.; Leroux, J.-C., Polyester-based micelles and nanoparticles for the parenteral delivery of taxanes. *Journal of controlled release* **2010**, *143* (1), 2-12.
80. Bilati, U.; Allémann, E.; Doelker, E., Development of a nanoprecipitation method intended for the entrapment of hydrophilic drugs into nanoparticles. *European Journal of Pharmaceutical Sciences* **2005**, *24* (1), 67-75.
81. Canning, S. L.; Smith, G. N.; Armes, S. P., A critical appraisal of RAFT-mediated polymerization-induced self-assembly. *Macromolecules* **2016**, *49* (6), 1985-2001.
82. Rieger, J., Guidelines for the synthesis of block copolymer particles of various morphologies by RAFT dispersion polymerization. *Macromolecular rapid communications* **2015**, *36* (16), 1458-1471.
83. Sun, J.-T.; Hong, C.-Y.; Pan, C.-Y., Formation of the block copolymer aggregates via polymerization-induced self-assembly and reorganization. *Soft Matter* **2012**, *8* (30), 7753-7767.
84. Derry, M. J.; Fielding, L. A.; Armes, S. P., Polymerization-induced self-assembly of block copolymer nanoparticles via RAFT non-aqueous dispersion polymerization. *Progress in Polymer Science* **2016**, *52*, 1-18.
85. Zehm, D.; Ratcliffe, L. P.; Armes, S. P., Synthesis of diblock copolymer nanoparticles via raft alcoholic dispersion polymerization: effect of block copolymer composition, molecular weight, copolymer concentration, and solvent type on the final particle morphology. *Macromolecules* **2012**, *46* (1), 128-139.
86. Delaittre, G.; Nicolas, J.; Lefay, C.; Save, M.; Charleux, B., Surfactant-free synthesis of amphiphilic diblock copolymer nanoparticles via nitroxide-mediated emulsion polymerization. *Chemical communications* **2005**, (5), 614-616.
87. Groison, E.; Brusseau, S. g. n.; D'Agosto, F.; Magnet, S. p.; Inoubli, R.; Couvreur, L.; Charleux, B., Well-defined amphiphilic block copolymer nanoobjects via nitroxide-mediated emulsion polymerization. *ACS Macro Letters* **2011**, *1* (1), 47-51.
88. Sugihara, S.; Sugihara, K.; Armes, S. P.; Ahmad, H.; Lewis, A. L., Synthesis of biomimetic poly (2-(methacryloyloxy) ethyl phosphorylcholine) nanolatexes via atom transfer radical dispersion polymerization in alcohol/water mixtures. *Macromolecules* **2010**, *43* (15), 6321-6329.
89. Sugihara, S.; Armes, S. P.; Lewis, A. L., One-Pot Synthesis of Biomimetic Shell Cross-Linked Micelles and Nanocages by ATRP in Alcohol/Water Mixtures. *Angewandte Chemie International Edition* **2010**, *49* (20), 3500-3503.
90. He, W.-D.; Sun, X.-L.; Wan, W.-M.; Pan, C.-Y., Multiple morphologies of PAA-b-PSt assemblies throughout RAFT dispersion polymerization of styrene with PAA Macro-CTA. *Macromolecules* **2011**, *44* (9), 3358-3365.
91. Sugihara, S.; Blanazs, A.; Armes, S. P.; Ryan, A. J.; Lewis, A. L., Aqueous Dispersion Polymerization: A New Paradigm for in Situ Block Copolymer Self-Assembly in Concentrated Solution. *Journal of the American Chemical Society* **2011**, *133* (39), 15707-15713.
92. Yang, P.; Ratcliffe, L. P. D.; Armes, S. P., Efficient Synthesis of Poly(methacrylic acid)-block-Poly(styrene-alt-N-phenylmaleimide) Diblock Copolymer Lamellae Using RAFT Dispersion Polymerization. *Macromolecules* **2013**, *46* (21), 8545-8556.

## Bibliography

93. Chambon, P.; Blanazs, A.; Battaglia, G.; Armes, S., Facile synthesis of methacrylic ABC triblock copolymer vesicles by RAFT aqueous dispersion polymerization. *Macromolecules* **2012**, *45* (12), 5081-5090.
94. Wan, W.-M.; Pan, C.-Y., Formation of polymeric yolk/shell nanomaterial by polymerization-induced self-assembly and reorganization. *Macromolecules* **2010**, *43* (6), 2672-2675.
95. Su, Y.; Xiao, X.; Li, S.; Dan, M.; Wang, X.; Zhang, W., Precise evaluation of the block copolymer nanoparticle growth in polymerization-induced self-assembly under dispersion conditions. *Polymer Chemistry* **2014**, *5* (2), 578-587.
96. Warren, N. J.; Armes, S. P., Polymerization-Induced Self-Assembly of Block Copolymer Nano-objects via RAFT Aqueous Dispersion Polymerization. *Journal of the American Chemical Society* **2014**, *136* (29), 10174-10185.
97. Blanazs, A.; Madsen, J.; Battaglia, G.; Ryan, A. J.; Armes, S. P., Mechanistic insights for block copolymer morphologies: how do worms form vesicles? *Journal of the American Chemical Society* **2011**, *133* (41), 16581-16587.
98. Verber, R.; Blanazs, A.; Armes, S., Rheological studies of thermo-responsive diblock copolymer worm gels. *Soft Matter* **2012**, *8* (38), 9915-9922.
99. Karagoz, B.; Esser, L.; Duong, H. T.; Basuki, J. S.; Boyer, C.; Davis, T. P., Polymerization-Induced Self-Assembly (PISA)—control over the morphology of nanoparticles for drug delivery applications. *Polymer Chemistry* **2014**, *5* (2), 350-355.
100. Napoli, A.; Boerakker, M. J.; Tirelli, N.; Nolte, R. J.; Sommerdijk, N. A.; Hubbell, J. A., Glucose-oxidase based self-destructing polymeric vesicles. *Langmuir* **2004**, *20* (9), 3487-3491.
101. Ahmed, F.; Discher, D. E., Self-porating polymersomes of PEG-PLA and PEG-PCL: hydrolysis-triggered controlled release vesicles. *Journal of controlled release* **2004**, *96* (1), 37-53.
102. Geng, Y.; Dalhaimer, P.; Cai, S.; Tsai, R.; Tewari, M.; Minko, T.; Discher, D. E., Shape effects of filaments versus spherical particles in flow and drug delivery. *Nature nanotechnology* **2007**, *2* (4), 249-255.
103. Lee, L.-C.; Lu, J.; Weck, M.; Jones, C. W., Acid-base bifunctional shell cross-linked micelle nanoreactor for one-pot tandem reaction. *ACS Catalysis* **2016**, *6* (2), 784-787.
104. Broz, P.; Driamov, S.; Ziegler, J.; Ben-Haim, N.; Marsch, S.; Meier, W.; Hunziker, P., Toward intelligent nanosize bioreactors: a pH-switchable, channel-equipped, functional polymer nanocontainer. *Nano letters* **2006**, *6* (10), 2349-2353.
105. Zhou, W.; Qu, Q.; Yu, W.; An, Z., Single Monomer for Multiple Tasks: Polymerization Induced Self-Assembly, Functionalization and Cross-Linking, and Nanoparticle Loading. *ACS Macro Letters* **2014**, *3* (12), 1220-1224.
106. Huang, J.; Zhu, H.; Liang, H.; Lu, J., Salicylaldehyde-functionalized block copolymer nano-objects: one-pot synthesis via polymerization-induced self-assembly and their simultaneous cross-linking and fluorescence modification. *Polymer Chemistry* **2016**, *7* (29), 4761-4770.
107. Zhang, X.; Cardozo, A. F.; Chen, S.; Zhang, W.; Julcour, C.; Lansalot, M.; Blanco, J. F.; Gayet, F.; Delmas, H.; Charleux, B., Core-Shell Nanoreactors for Efficient Aqueous Biphasic Catalysis. *Chemistry—A European Journal* **2014**, *20* (47), 15505-15517.
108. Delaittre, G.; Save, M.; Charleux, B., Nitroxide-Mediated Aqueous Dispersion Polymerization: From Water-Soluble Macroalkoxyamine to Thermosensitive Nanogels. *Macromolecular rapid communications* **2007**, *28* (15), 1528-1533.
109. Karagoz, B.; Yeow, J.; Esser, L.; Prakash, S. M.; Kuchel, R. P.; Davis, T. P.; Boyer, C., An Efficient and Highly Versatile Synthetic Route to Prepare Iron Oxide Nanoparticles/Nanocomposites with Tunable Morphologies. *Langmuir* **2014**, *30* (34), 10493-10502.
110. Tan, J.; Rao, X.; Yang, J.; Zeng, Z., Synthesis of Highly Monodisperse Surface-Functional Microspheres by Photoinitiated RAFT Dispersion Polymerization Using Macro-RAFT Agents. *Macromolecules* **2013**, *46* (21), 8441-8448.
111. Hanisch, A.; Yang, P.; Kulak, A. N.; Fielding, L. A.; Meldrum, F. C.; Armes, S. P., Phosphonic Acid-Functionalized Diblock Copolymer Nano-Objects via Polymerization-Induced Self-Assembly: Synthesis, Characterization, and Occlusion into Calcite Crystals. *Macromolecules* **2016**, *49* (1), 192-204.

## Bibliography

112. Warren, N. J.; Rosselgong, J.; Madsen, J.; Armes, S. P., Disulfide-Functionalized Diblock Copolymer Worm Gels. *Biomacromolecules* **2015**, *16* (8), 2514-2521.
113. Penfold, N.; Lovett, J.; Warren, N.; Verstraete, P.; Smets, J.; Armes, S., pH-Responsive non-ionic diblock copolymers: protonation of a morpholine end-group induces an order–order transition. *Polymer Chemistry* **2016**, *7* (1), 79-88.
114. Admiral, V.; Semsarilar, M.; Canton, I.; Armes, S. P., Polymerization-Induced Self-Assembly of Galactose-Functionalized Biocompatible Diblock Copolymers for Intracellular Delivery. *Journal of the American Chemical Society* **2013**, *135* (36), 13574-13581.
115. Kapishon, V.; Whitney, R. A.; Champagne, P.; Cunningham, M. F.; Neufeld, R. J., Polymerization induced self-assembly of alginate based amphiphilic graft copolymers synthesized by single electron transfer living radical polymerization. *Biomacromolecules* **2015**, *16* (7), 2040-2048.
116. Liu, X.; Gao, W., In Situ Growth of Self-Assembled Protein-Polymer Nanovesicles for Enhanced Intracellular Protein Delivery. *ACS Applied Materials & Interfaces* **2017**.
117. An, Z.; Tang, W.; Wu, M.; Jiao, Z.; Stucky, G. D., Heterofunctional polymers and core–shell nanoparticles via cascade aminolysis/Michael addition and alkyne–azide click reaction of RAFT polymers. *Chemical Communications* **2008**, (48), 6501-6503.
118. Rosselgong, J.; Blanz, A.; Chambon, P.; Williams, M.; Semsarilar, M.; Madsen, J.; Battaglia, G.; Armes, S. P., Thiol-Functionalized Block Copolymer Vesicles. *ACS Macro Letters* **2012**, *1* (8), 1041-1045.
119. Maiti, B.; Bauri, K.; Nandi, M.; De, P., Surface functionalized nano-objects from oleic acid-derived stabilizer via non-polar RAFT dispersion polymerization. *Journal of Polymer Science Part A: Polymer Chemistry* **2017**, *55* (2), 263-273.
120. Teo, G. H.; Kuchel, R. P.; Zetterlund, P. B.; Thickett, S. C., Polymer-inorganic hybrid nanoparticles of various morphologies via polymerization-induced self assembly and sol–gel chemistry. *Polymer Chemistry* **2016**, *7* (43), 6575-6585.
121. St Thomas, C.; Guerrero-Santos, R.; D'Agosto, F., Alkoxyamine-functionalized latex nanoparticles through RAFT polymerization-induced self-assembly in water. *Polymer Chemistry* **2015**, *6* (30), 5405-5413.
122. St Thomas, C.; Cabello-Romero, J. N.; Garcia-Valdez, O.; Jiménez-Regalado, E. J.; Maldonado-Textle, H.; Guerrero-Santos, R., Surface-initiated nitroxide-mediated polymerization of sodium 4-styrene sulfonate from latex particles. *Journal of Polymer Science Part A: Polymer Chemistry* **2017**, *55* (3), 437-444.
123. Pei, Y.; Noy, J. M.; Roth, P. J.; Lowe, A. B., Soft Matter Nanoparticles with Reactive Coronal Pentafluorophenyl Methacrylate Residues via Non-Polar RAFT Dispersion Polymerization and Polymerization-Induced Self-Assembly. *Journal of Polymer Science Part A: Polymer Chemistry* **2015**, *53* (20), 2326-2335.
124. Pei, Y.; Noy, J.-M.; Roth, P. J.; Lowe, A. B., Thiol-reactive Passerini-methacrylates and polymorphic surface functional soft matter nanoparticles via ethanolic RAFT dispersion polymerization and post-synthesis modification. *Polymer Chemistry* **2015**, *6* (11), 1928-1931.
125. Jia, Z.; Bobrin, V. A.; Truong, N. P.; Gillard, M.; Monteiro, M. J., Multifunctional Nanoworms and Nanorods through a One-Step Aqueous Dispersion Polymerization. *Journal of the American Chemical Society* **2014**, *136* (16), 5824-5827.
126. Delaittre, G.; Dire, C.; Rieger, J.; Putaux, J.-L.; Charleux, B., Formation of polymer vesicles by simultaneous chain growth and self-assembly of amphiphilic block copolymers. *Chemical Communications* **2009**, (20), 2887-2889.
127. Delaittre, G.; Save, M.; Gaborieau, M.; Castignolles, P.; Rieger, J.; Charleux, B., Synthesis by nitroxide-mediated aqueous dispersion polymerization, characterization, and physical core-crosslinking of pH-and thermoresponsive dynamic diblock copolymer micelles. *Polymer Chemistry* **2012**, *3* (6), 1526-1538.
128. Kang, Y.; Pitto-Barry, A.; Willcock, H.; Quan, W.-D.; Kirby, N.; Sanchez, A. M.; O'Reilly, R. K., Exploiting nucleobase-containing materials—from monomers to complex morphologies using RAFT dispersion polymerization. *Polymer Chemistry* **2015**, *6* (1), 106-117.

## Bibliography

129. van Iersel, M. F. M.; van Dieren, B.; Rombouts, F. M.; Abee, T., Flavor formation and cell physiology during the production of alcohol-free beer with immobilized *Saccharomyces cerevisiae*. *Enzyme and Microbial Technology* **1999**, *24* (7), 407-411.
130. Hakala, T. K.; Liitiä, T.; Suurnäkki, A., Enzyme-aided alkaline extraction of oligosaccharides and polymeric xylan from hardwood kraft pulp. *Carbohydrate Polymers* **2013**, *93* (1), 102-108.
131. Robles-Medina, A.; González-Moreno, P. A.; Esteban-Cerdán, L.; Molina-Grima, E., Biocatalysis: Towards ever greener biodiesel production. *Biotechnology Advances* **2009**, *27* (4), 398-408.
132. Hanefeld, U.; Gardossi, L.; Magner, E., Understanding enzyme immobilisation. *Chemical Society Reviews* **2009**, *38* (2), 453-468.
133. Homaei, A. A.; Sariri, R.; Vianello, F.; Stevanato, R., Enzyme immobilization: an update. *Journal of chemical biology* **2013**, *6* (4), 185-205.
134. Mateo, C.; Palomo, J. M.; Fernandez-Lorente, G.; Guisan, J. M.; Fernandez-Lafuente, R., Improvement of enzyme activity, stability and selectivity via immobilization techniques. *Enzyme and Microbial Technology* **2007**, *40* (6), 1451-1463.
135. Brena, B. M.; Batista-Viera, F., Immobilization of Enzymes. In *Immobilization of Enzymes and Cells*, Guisan, J. M., Ed. Humana Press: Totowa, NJ, 2006; pp 15-30.
136. Mattiasson, B.; Kaul, R., Determination of coupling yields and handling of labile proteins in immobilization technology. *Bioprocess technology* **1991**, *14*, 161.
137. Young, C. L.; Britton, Z. T.; Robinson, A. S., Recombinant protein expression and purification: a comprehensive review of affinity tags and microbial applications. *Biotechnology journal* **2012**, *7* (5), 620-634.
138. Quijoch, F. A.; Richards, F. M., The enzymic behavior of carboxypeptidase-A in the solid state. *Biochemistry* **1966**, *5* (12), 4062-4076.
139. Jegan Roy, J.; Emilia Abraham, T., Strategies in making cross-linked enzyme crystals. *Chemical Reviews* **2004**, *104* (9), 3705-3722.
140. Schoevaart, R.; Wolbers, M.; Golubovic, M.; Ottens, M.; Kieboom, A.; Van Rantwijk, F.; Van der Wielen, L.; Sheldon, R., Preparation, optimization, and structures of cross-linked enzyme aggregates (CLEAs). *Biotechnology and Bioengineering* **2004**, *87* (6), 754-762.
141. Terpe, K., Overview of tag protein fusions: from molecular and biochemical fundamentals to commercial systems. *Applied microbiology and biotechnology* **2003**, *60* (5), 523-533.
142. Halliwell, C. M.; Morgan, G.; Ou, C.-P.; Cass, A. E. G., Introduction of a (Poly)histidine Tag in L-Lactate Dehydrogenase Produces a Mixture of Active and Inactive Molecules. *Analytical Biochemistry* **2001**, *295* (2), 257-261.
143. Hochuli, E.; Döbeli, H.; Schacher, A., New metal chelate adsorbent selective for proteins and peptides containing neighbouring histidine residues. *Journal of Chromatography A* **1987**, *411*, 177-184.
144. Lauer, S. A.; Nolan, J. P., Development and characterization of Ni-NTA-bearing microspheres. *Cytometry Part A* **2002**, *48* (3), 136-145.
145. Nieba, L.; Nieba-Axmann, S. E.; Persson, A.; Hämäläinen, M.; Edebratt, F.; Hansson, A.; Lidholm, J.; Magnusson, K.; Karlsson, Å. F.; Plückthun, A., BIACORE Analysis of Histidine-Tagged Proteins Using a Chelating NTA Sensor Chip. *Analytical Biochemistry* **1997**, *252* (2), 217-228.
146. Ganesana, M.; Istarnboulie, G.; Marty, J.-L.; Noguier, T.; Andreescu, S., Site-specific immobilization of a (His)<sub>6</sub>-tagged acetylcholinesterase on nickel nanoparticles for highly sensitive toxicity biosensors. *Biosensors and Bioelectronics* **2011**, *30* (1), 43-48.
147. Miyazaki, M.; Maeda, H., Microchannel enzyme reactors and their applications for processing. *Trends in Biotechnology* **2006**, *24* (10), 463-470.
148. Keppler, A.; Gendreizig, S.; Gronemeyer, T.; Pick, H.; Vogel, H.; Johnsson, K., A general method for the covalent labeling of fusion proteins with small molecules in vivo. *Nature biotechnology* **2003**, *21* (1), 86-89.
149. Pegg, A. E., Repair of O<sup>6</sup>-alkylguanine by alkyltransferases. *Mutation Research/Reviews in Mutation Research* **2000**, *462* (2-3), 83-100.

## Bibliography

150. Damoiseaux, R.; Keppler, A.; Johnsson, K., Synthesis and Applications of Chemical Probes for Human O6-Alkylguanine-DNA Alkyltransferase. *ChemBioChem* **2001**, *2* (4), 285-287.
151. Keppler, A.; Pick, H.; Arrivoli, C.; Vogel, H.; Johnsson, K., Labeling of fusion proteins with synthetic fluorophores in live cells. *Proceedings of the National Academy of Sciences of the United States of America* **2004**, *101* (27), 9955-9959.
152. Keppler, A.; Kindermann, M.; Gendreizig, S.; Pick, H.; Vogel, H.; Johnsson, K., Labeling of fusion proteins of O 6-alkylguanine-DNA alkyltransferase with small molecules in vivo and in vitro. *Methods* **2004**, *32* (4), 437-444.
153. Regoes, A.; Hehl, A. B., SNAP-tag™ mediated live cell labeling as an alternative to GFP in anaerobic organisms. *Biotechniques* **2005**, *39* (6), 809.
154. Kampmeier, F.; Ribbert, M.; Nachreiner, T.; Dembski, S.; Beaufile, F.; Brecht, A.; Barth, S., Site-specific, covalent labeling of recombinant antibody fragments via fusion to an engineered version of 6-O-alkylguanine DNA alkyltransferase. *Bioconjugate chemistry* **2009**, *20* (5), 1010-1015.
155. Petershans, A.; Wedlich, D.; Fruk, L., Bioconjugation of CdSe/ZnS nanoparticles with SNAP tagged proteins. *Chemical Communications* **2011**, *47* (38), 10671-10673.
156. Newman, J.; Peat, T. S.; Richard, R.; Kan, L.; Swanson, P. E.; Affholter, J. A.; Holmes, I. H.; Schindler, J. F.; Unkefer, C. J.; Terwilliger, T. C., Haloalkane Dehalogenases: Structure of a Rhodococcus Enzyme†. *Biochemistry* **1999**, *38* (49), 16105-16114.
157. Urh, M.; Rosenberg, M., HaloTag, a platform technology for protein analysis. *Current chemical genomics* **2012**, *6* (1).
158. de Gennes, P., Conformations of polymers attached to an interface. *Macromolecules* **1980**, *13* (5), 1069-1075.
159. Prucker, O.; Rühle, J., Polymer layers through self-assembled monolayers of initiators. *Langmuir* **1998**, *14* (24), 6893-6898.
160. Kadir, M. A.; Park, J. H.; Lee, J.; Lee, C.; Lee, S. H.; Lee, S. G.; Paik, H. j., Multivalent (Nitrilotriacetic Acid)-End-Functionalized Polystyrenes by ATRP and Their Self-Assembly. *Macromolecular Chemistry and Physics* **2013**, *214* (18), 2027-2035.
161. Guégain, E.; Delplace, V.; Trimaille, T.; Gignes, D.; Siri, D.; Marque, S. R.; Guillaneuf, Y.; Nicolas, J., On the structure–control relationship of amide-functionalized SG1-based alkoxyamines for nitroxide-mediated polymerization and conjugation. *Polymer Chemistry* **2015**, *6* (31), 5693-5704.
162. Muñoz-Bonilla, A.; van Herk, A. M.; Heuts, J. P., Preparation of hairy particles and antifouling films using brush-type amphiphilic block copolymer surfactants in emulsion polymerization. *Macromolecules* **2010**, *43* (6), 2721-2731.
163. Jon, S.; Seong, J.; Khademhosseini, A.; Tran, T.-N. T.; Laibinis, P. E.; Langer, R., Construction of nonbiofouling surfaces by polymeric self-assembled monolayers. *Langmuir* **2003**, *19* (24), 9989-9993.
164. Han, D. K.; Park, K.; Park, K. D.; Ahn, K. D.; Kim, Y. H., In Vivo Biocompatibility of Sulfonated PEO-grafted Polyurethanes for Polymer Heart Valve and Vascular Graft. *Artificial organs* **2006**, *30* (12), 955-959.
165. Sheibat-Othman, N.; Bourgeat-Lami, E., Use of Silica Particles for the Formation of Organic–Inorganic Particles by Surfactant-Free Emulsion Polymerization. *Langmuir* **2009**, *25* (17), 10121-10133.
166. Bourgeat-Lami, E.; Guimaraes, T. R.; Pereira, A. M. C.; Alves, G. M.; Moreira, J. C.; Putaux, J. L.; dos Santos, A. M., High Solids Content, Soap-Free, Film-Forming Latexes Stabilized by Laponite Clay Platelets. *Macromolecular rapid communications* **2010**, *31* (21), 1874-1880.
167. Guégain, E.; Guillaneuf, Y.; Nicolas, J., Nitroxide-Mediated Polymerization of Methacrylic Esters: Insights and Solutions to a Long-Standing Problem. *Macromolecular rapid communications* **2015**, *36* (13), 1227-1247.
168. Zhang, C.; Lessard, B.; Maric, M., Synthesis and characterization of benzyl methacrylate/styrene random copolymers prepared by NMP. *Macromolecular Reaction Engineering* **2010**, *4* (6-7), 415-423.
169. Xu, F. J.; Li, H. Z.; Li, J.; Teo, Y. H. E.; Zhu, C. X.; Kang, E. T.; Neoh, K. G., Spatially well-defined binary brushes of poly(ethylene glycol)s for micropatterning of active proteins on anti-fouling surfaces. *Biosensors and Bioelectronics* **2008**, *24* (4), 773-780.

## Bibliography

170. Lutz, J. F., Polymerization of oligo (ethylene glycol)(meth) acrylates: toward new generations of smart biocompatible materials. *Journal of Polymer Science Part A: Polymer Chemistry* **2008**, *46* (11), 3459-3470.
171. Trimaille, T.; Mabrouk, K.; Monnier, V. r.; Charles, L.; Bertin, D.; Gignes, D., SG1-Functionalized Peptides as Precursors for Polymer– Peptide Conjugates: A Straightforward Approach. *Macromolecules* **2010**, *43* (11), 4864-4870.
172. Barrère, C.; Chendo, C.; NT Phan, T.; Monnier, V.; Trimaille, T.; Humbel, S.; Viel, S.; Gignes, D.; Charles, L., Successful MALDI-MS Analysis of Synthetic Polymers with Labile End-Groups: The Case of Nitroxide-Mediated Polymerization Using the MAMA-SG1 Alkoxyamine. *Chemistry–A European Journal* **2012**, *18* (25), 7916-7924.
173. Li, B.; Berliner, M.; Buzon, R.; Chiu, C. K.-F.; Colgan, S. T.; Kaneko, T.; Keene, N.; Kissel, W.; Le, T.; Leeman, K. R., Aqueous phosphoric acid as a mild reagent for deprotection of tert-butyl carbamates, esters, and ethers. *The Journal of organic chemistry* **2006**, *71* (24), 9045-9050.
174. Schubert, S.; Delaney Jr, J. T.; Schubert, U. S., Nanoprecipitation and nanoformulation of polymers: from history to powerful possibilities beyond poly (lactic acid). *Soft Matter* **2011**, *7* (5), 1581-1588.
175. Zhang, X.; Rieger, J.; Charleux, B., Effect of the solvent composition on the morphology of nano-objects synthesized via RAFT polymerization of benzyl methacrylate in dispersed systems. *Polymer Chemistry* **2012**, *3* (6), 1502-1509.
176. Qiao, X. G.; Lansalot, M.; Bourgeat-Lami, E.; Charleux, B., Nitroxide-Mediated Polymerization-Induced Self-Assembly of Poly(poly(ethylene oxide) methyl ether methacrylate-co-styrene)-b-poly(n-butyl methacrylate-co-styrene) Amphiphilic Block Copolymers. *Macromolecules* **2013**, *46* (11), 4285-4295.
177. Lessard, B.; Marić, M., Incorporating glycidyl methacrylate into block copolymers using poly (methacrylate-ran-styrene) macroinitiators synthesized by nitroxide-mediated polymerization. *Journal of Polymer Science Part A: Polymer Chemistry* **2009**, *47* (10), 2574-2588.
178. Delaittre, G.; Nicolas, J.; Lefay, C.; Save, M.; Charleux, B., Aqueous suspension of amphiphilic diblock copolymer nanoparticles prepared in situ from a water-soluble poly (sodium acrylate) alkoxyamine macroinitiator. *Soft Matter* **2006**, *2* (3), 223-231.
179. Figg, C. A.; Simula, A.; Gebre, K. A.; Tucker, B. S.; Haddleton, D. M.; Sumerlin, B. S., Polymerization-induced thermal self-assembly (PITSA). *Chemical Science* **2015**, *6* (2), 1230-1236.
180. Tugulu, S.; Arnold, A.; Sielaff, I.; Johnsson, K.; Klok, H.-A., Protein-functionalized polymer brushes. *Biomacromolecules* **2005**, *6* (3), 1602-1607.
181. Singh, V.; Wang, S.; Kool, E. T., Genetically encoded multispectral labeling of proteins with polyfluorophores on a DNA backbone. *Journal of the American Chemical Society* **2013**, *135* (16), 6184-6191.
182. Thomas, D. B.; Convertine, A. J.; Hester, R. D.; Lowe, A. B.; McCormick, C. L., Hydrolytic susceptibility of dithioester chain transfer agents and implications in aqueous RAFT polymerizations. *Macromolecules* **2004**, *37* (5), 1735-1741.
183. Lutz, J. F., Thermo-Switchable Materials Prepared Using the OEGMA-Platform. *Advanced Materials* **2011**, *23* (19), 2237-2243.
184. DelaCruz, J.; Blanchard, G., Understanding the balance between ionic and dispersion interactions in aqueous micellar media. *The Journal of Physical Chemistry B* **2003**, *107* (29), 7102-7108.
185. Lutz, J.-F.; Pfeifer, S.; Chanana, M.; Thünemann, A. F.; Bienert, R., H-Bonding-directed self-assembly of synthetic copolymers containing nucleobases: organization and colloidal fusion in a noncompetitive solvent. *Langmuir* **2006**, *22* (17), 7411-7415.
186. Guilbault, G. G., *Practical fluorescence*. CRC Press: 1990; Vol. 3.
187. Goldmann, A. S.; Quémener, D.; Millard, P.-E.; Davis, T. P.; Stenzel, M. H.; Barner-Kowollik, C.; Müller, A. H., Access to cyclic polystyrenes via a combination of reversible addition fragmentation chain transfer (RAFT) polymerization and click chemistry. *Polymer* **2008**, *49* (9), 2274-2281.
188. Barner-Kowollik, C.; Quinn, J. F.; Morsley, D. R.; Davis, T. P., Modeling the reversible addition–fragmentation chain transfer process in cumyl dithiobenzoate-mediated styrene

## Bibliography

- homopolymerizations: Assessing rate coefficients for the addition–fragmentation equilibrium. *Journal of Polymer Science Part A: Polymer Chemistry* **2001**, *39* (9), 1353-1365.
189. Piston, D. W.; Kremers, G.-J., Fluorescent protein FRET: the good, the bad and the ugly. *Trends in Biochemical Sciences* **32** (9), 407-414.
190. Jones, E. R.; Semsarilar, M.; Blanazs, A.; Armes, S. P., Efficient synthesis of amine-functional diblock copolymer nanoparticles via RAFT dispersion polymerization of benzyl methacrylate in alcoholic media. *Macromolecules* **2012**, *45* (12), 5091-5098.
191. Jones, E.; Mykhaylyk, O.; Semsarilar, M.; Boerakker, M.; Wyman, P.; Armes, S., How Do Spherical Diblock Copolymer Nanoparticles Grow during RAFT Alcoholic Dispersion Polymerization? *Macromolecules* **2015**, *49* (1), 172-181.
192. Yeow, J.; Xu, J.; Boyer, C., Polymerization-Induced Self-Assembly Using Visible Light Mediated Photoinduced Electron Transfer–Reversible Addition–Fragmentation Chain Transfer Polymerization. *ACS Macro Letters* **2015**, *4* (9), 984-990.
193. Fielding, L. A.; Lane, J. A.; Derry, M. J.; Mykhaylyk, O. O.; Armes, S. P., Thermo-responsive diblock copolymer worm gels in non-polar solvents. *Journal of the American Chemical Society* **2014**, *136* (15), 5790-5798.
194. Perrier, S.; Takolpuckdee, P.; Mars, C. A., Reversible addition– fragmentation chain transfer polymerization: end group modification for functionalized polymers and chain transfer agent recovery. *Macromolecules* **2005**, *38* (6), 2033-2036.
195. Boyer, C.; Liu, J.; Bulmus, V.; Davis, T. P.; Barner-Kowollik, C.; Stenzel, M. H., Direct synthesis of well-defined heterotelechelic polymers for bioconjugations. *Macromolecules* **2008**, *41* (15), 5641-5650.
196. Feuerstein, D. L.; Selleck, R. E., Fluorescent Tracers for Dispersion Measurement. *Journal of the Sanitary Engineering Division* **1963**, *89* (4), 1-22.
197. Herfurth, C.; de Molina, P. M.; Wieland, C.; Rogers, S.; Gradzielski, M.; Laschewsky, A., One-step RAFT synthesis of well-defined amphiphilic star polymers and their self-assembly in aqueous solution. *Polymer Chemistry* **2012**, *3* (6), 1606-1617.
198. Semsarilar, M.; Ladmiral, V.; Blanazs, A.; Armes, S., Anionic polyelectrolyte-stabilized nanoparticles via RAFT aqueous dispersion polymerization. *Langmuir* **2011**, *28* (1), 914-922.
199. Ng, G.; Yeow, J.; Xu, J.; Boyer, C., Application of oxygen tolerant PET-RAFT to polymerization-induced self-assembly. *Polymer Chemistry* **2017**, *8* (18), 2841-2851.
200. Blackman, L. D.; Doncom, K. E.; Gibson, M. I.; O'Reilly, R. K., Comparison of photo- and thermally initiated polymerization-induced self-assembly: a lack of end group fidelity drives the formation of higher order morphologies. *Polymer Chemistry* **2017**, *8* (18), 2860-2871.
201. Theppaleak, T.; Tumcharern, G.; Wichai, U.; Rutnakornpituk, M., Synthesis of water dispersible magnetite nanoparticles in the presence of hydrophilic polymers. *Polymer bulletin* **2009**, *63* (1), 79-90.
202. Majewski, P.; Thierry, B., Functionalized magnetite nanoparticles—synthesis, properties, and bio-applications. *Critical Reviews in Solid State and Materials Sciences* **2007**, *32* (3-4), 203-215.
203. Ito, A.; Kuga, Y.; Honda, H.; Kikkawa, H.; Horiuchi, A.; Watanabe, Y.; Kobayashi, T., Magnetite nanoparticle-loaded anti-HER2 immunoliposomes for combination of antibody therapy with hyperthermia. *Cancer Letters* **212** (2), 167-175.
204. Liu, X.; Guan, Y.; Shen, R.; Liu, H., Immobilization of lipase onto micron-size magnetic beads. *Journal of Chromatography B* **2005**, *822* (1), 91-97.
205. Kumar, V.; Jahan, F.; Raghuwanshi, S.; Mahajan, R. V.; Saxena, R. K., Immobilization of *Rhizopus oryzae* lipase on magnetic Fe<sub>3</sub>O<sub>4</sub>-chitosan beads and its potential in phenolic acids ester synthesis. *Biotechnology and bioprocess engineering* **2013**, *18* (4), 787-795.
206. Yong, Y.; Bai, Y.; Li, Y.; Lin, L.; Cui, Y.; Xia, C., Preparation and application of polymer-grafted magnetic nanoparticles for lipase immobilization. *Journal of Magnetism and Magnetic Materials* **2008**, *320* (19), 2350-2355.
207. Bayramoğlu, G.; Arica, M. Y., Enzymatic removal of phenol and p-chlorophenol in enzyme reactor: Horseradish peroxidase immobilized on magnetic beads. *Journal of Hazardous Materials* **2008**, *156* (1), 148-155.

## Bibliography

208. Thode, K.; Müller, R. H.; Kresse, M., Two-time window and multiangle photon correlation spectroscopy size and zeta potential analysis—Highly sensitive rapid assay for dispersion stability. *Journal of pharmaceutical sciences* **2000**, *89* (10), 1317-1324.
209. Bai, W.; Zhang, L.; Bai, R.; Zhang, G., A Very Useful Redox Initiator for Aqueous RAFT Polymerization of N-Isopropylacrylamide and Acrylamide at Room Temperature. *Macromolecular Rapid Communications* **2008**, *29* (7), 562-566.
210. Wu, J.-H.; Ko, S. P.; Liu, H.-L.; Kim, S.; Ju, J.-S.; Kim, Y. K., Sub 5 nm magnetite nanoparticles: Synthesis, microstructure, and magnetic properties. *Materials Letters* **2007**, *61* (14), 3124-3129.
211. Itoh, H.; Sugimoto, T., Systematic control of size, shape, structure, and magnetic properties of uniform magnetite and maghemite particles. *Journal of Colloid and Interface Science* **2003**, *265* (2), 283-295.
212. Dang, F.; Enomoto, N.; Hojo, J.; Enpuku, K., Sonochemical synthesis of monodispersed magnetite nanoparticles by using an ethanol–water mixed solvent. *Ultrasonics Sonochemistry* **2009**, *16* (5), 649-654.
213. Parry, K. L.; Shard, A.; Short, R.; White, R.; Whittle, J.; Wright, A., ARXPS characterisation of plasma polymerised surface chemical gradients. *Surface and interface analysis* **2006**, *38* (11), 1497-1504.
214. Vinas, J.; Chagneux, N.; Gimes, D.; Trimaille, T.; Favier, A.; Bertin, D., SG1-based alkoxyamine bearing a N-succinimidyl ester: A versatile tool for advanced polymer synthesis. *Polymer* **2008**, *49* (17), 3639-3647.

## A

## Appendix

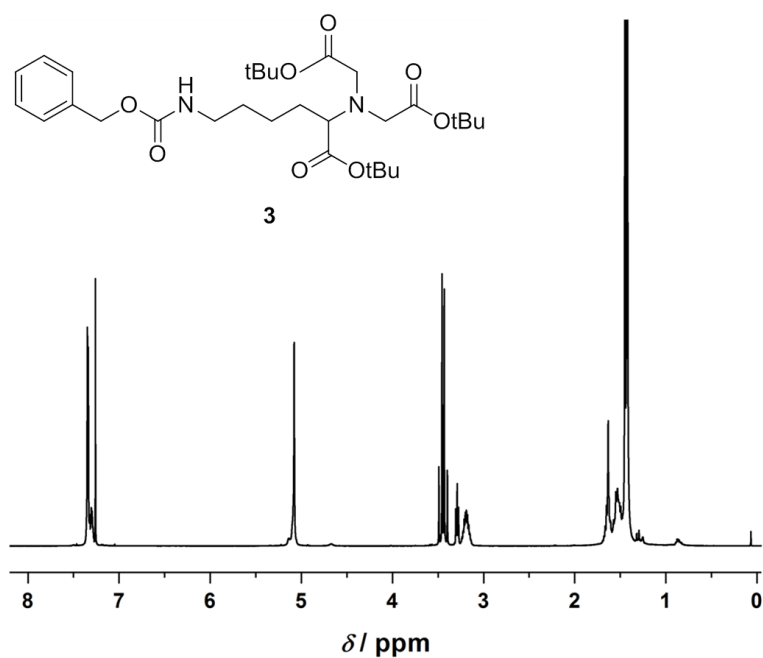


**Figure A.1.** <sup>1</sup>H NMR spectrum of *di-tert-butyl 2,2'-((6-(((benzyloxy)carbonyl)amino)-1-(tert-butoxy)-1-oxohexan-2-yl)azanediyl)diacetate 3*.

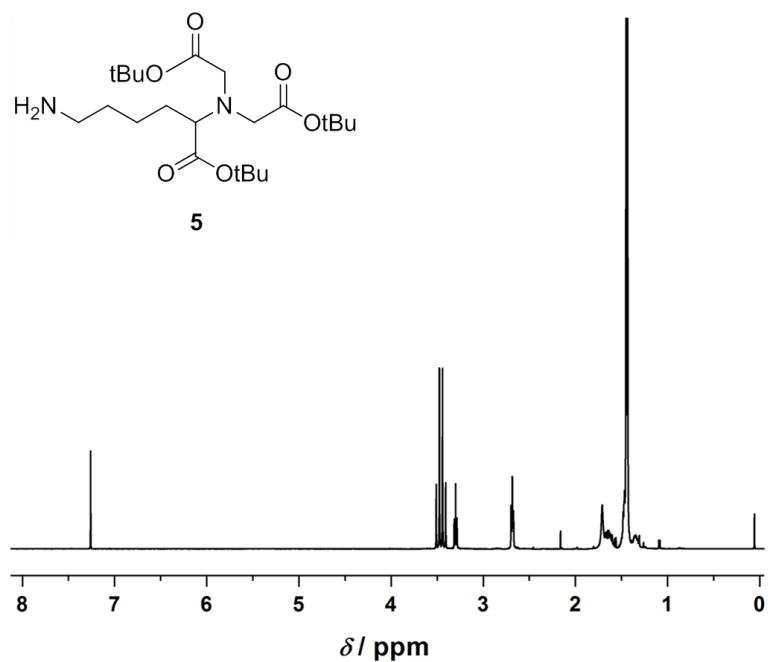


**Figure A.2.** <sup>1</sup>H NMR spectrum of *di-tert-butyl 2,2'-((6-amino-1-(tert-butoxy)-1-oxohexan-2-yl)azanediyl)di-acetate 5*.

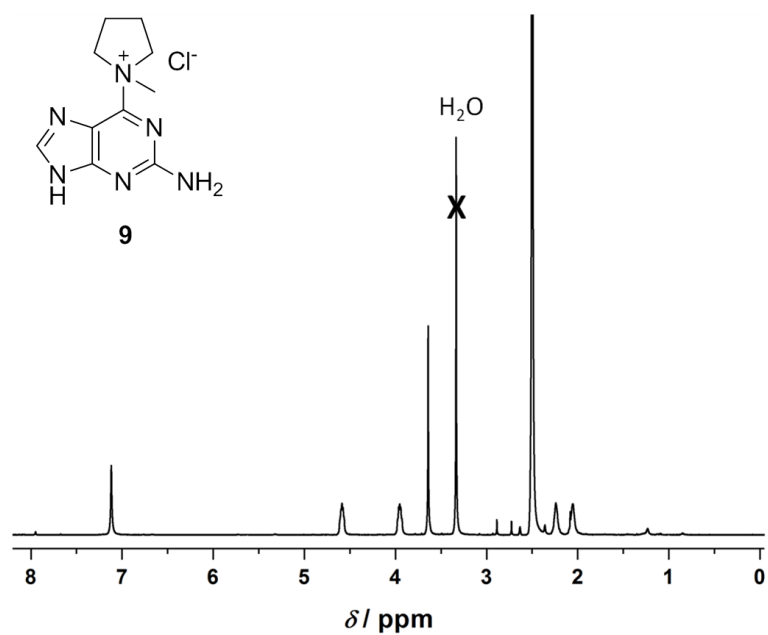


**Figure A.3.** <sup>1</sup>H NMR spectrum of *1-(2-amino-7H-purin-6-yl)-1-methyl pyrrolidinium chloride 9*.

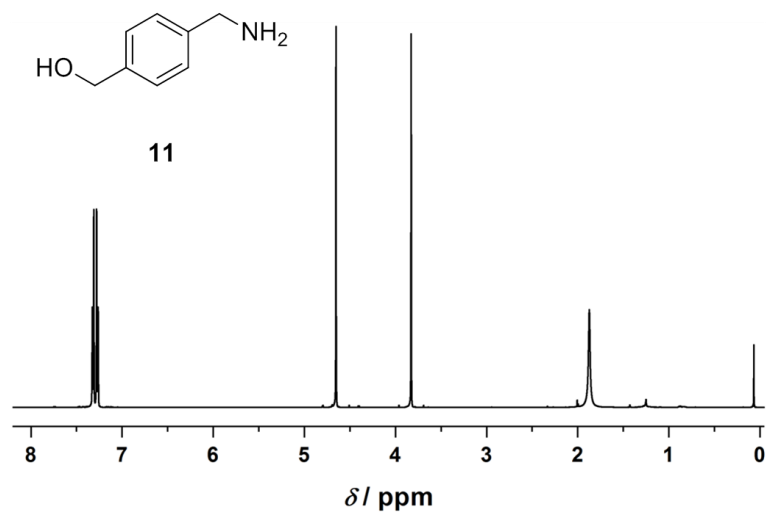


**Figure A.4.**  $^1\text{H}$  NMR spectrum of 4-(aminomethyl)-benzyl alcohol **11**.

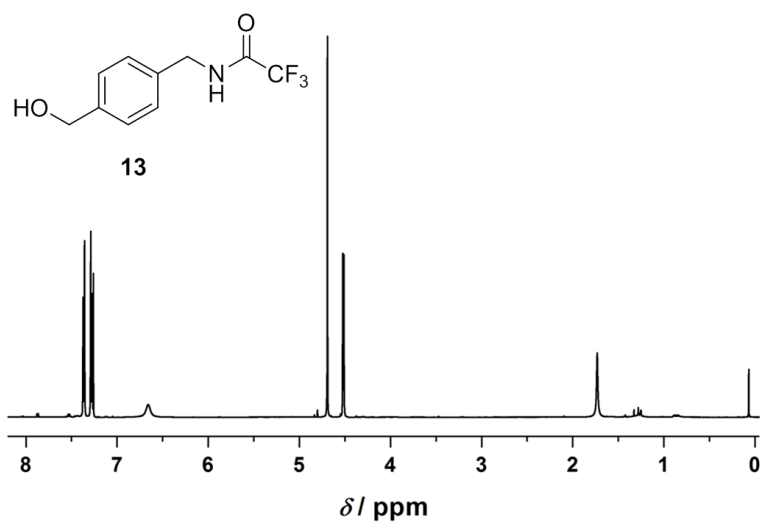


**Figure A.5.**  $^1\text{H}$  NMR spectrum of 2,2,2-trifluoro-N-(4-hydroxymethyl-benzyl)-acetamide **13**.

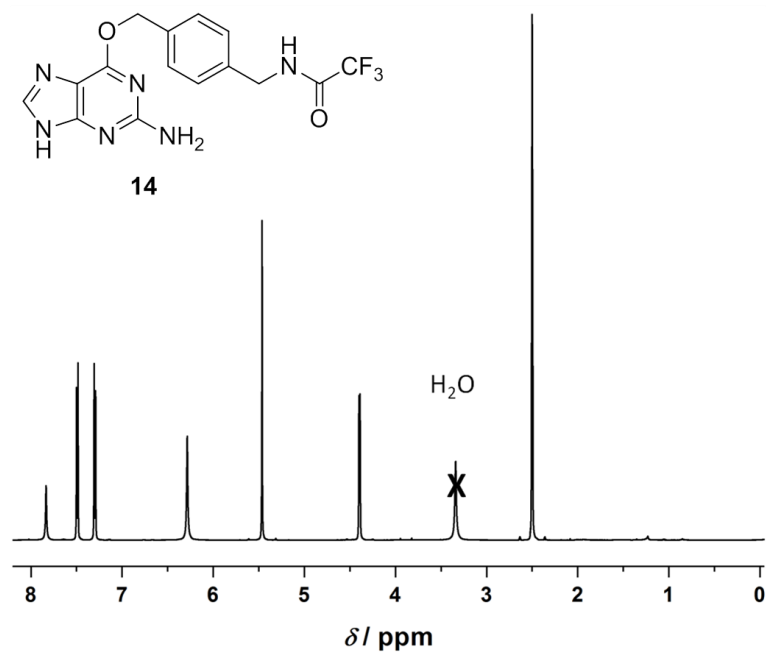


**Figure A.6.** <sup>1</sup>H NMR spectrum of *N*-[4-(2-amino-9H-purin-6-yloxymethyl)-benzyl]-2,2,2-trifluoroacetamide **14**.

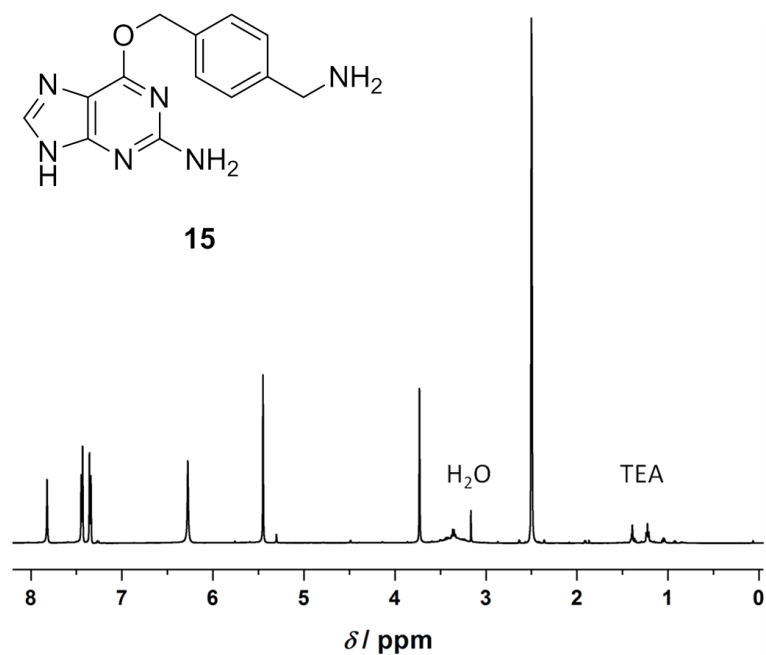


**Figure A.7.** <sup>1</sup>H NMR spectrum of *O*<sup>6</sup>-(4-amino-methyl-benzyl)guanine **15**.

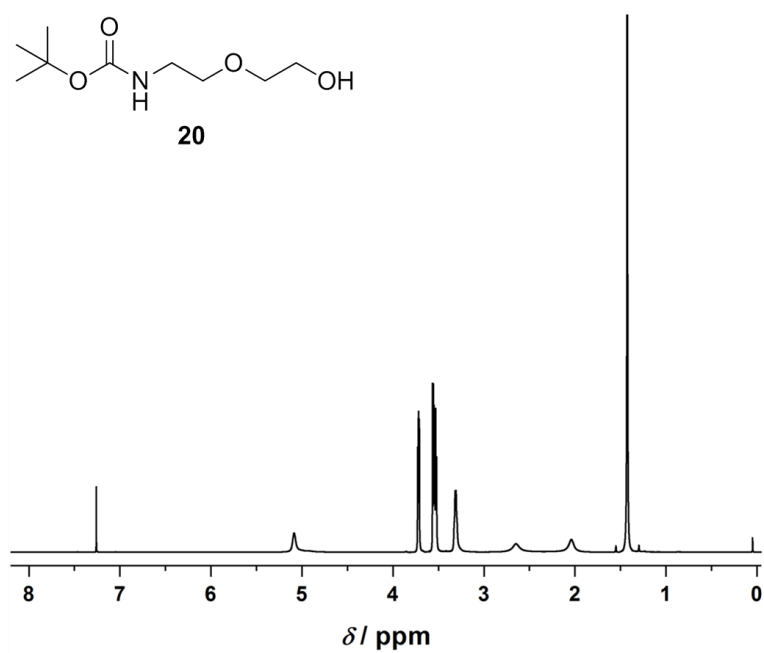


**Figure A.8.** <sup>1</sup>H NMR spectrum of *tert*-butyl (2-(2-((6-chlorohexyl)oxy)ethoxy)ethyl)carbamate **20**.

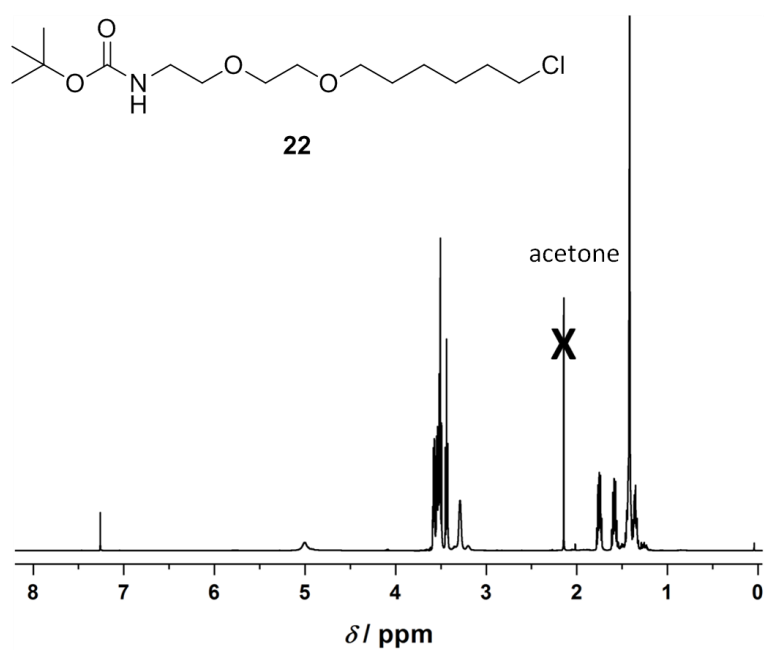


**Figure A.9.** <sup>1</sup>H NMR spectrum of 2-(2-((6-chlorohexyl)oxy)ethoxy)ethanamine **22**.

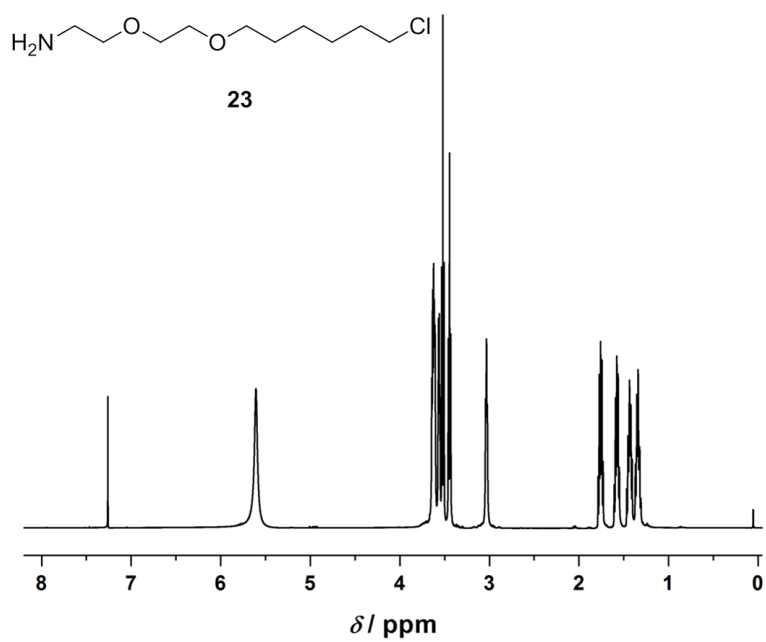


**Figure A.10.**  $^1\text{H}$  NMR spectrum of 2-(2-((6-chlorohexyl)oxy)ethoxy)ethanamine **23**.

# Abbreviations

a.u.	arbitrary units
AIBN	2,2'-azobis(2-methylpropionitrile)
AN	acrylonitrile
ATR-FTIR	attenuated total reflection Fourier transform infrared spectroscopy
ATRP	atom-transfer radical polymerization
<i>b</i>	block
BCP	block copolymer
BG	benzylguanine
BMA	<i>n</i> -butyl methacrylate
BzMA	benzyl methacrylate
C	Celsius
Cl	chloro
CPDB	2-cyano-2-propyl benzodithioate
CTA	chain transfer agent
$\delta$	chemical shift
$\bar{D}$	dispersity
Da	Dalton
DCM	dichloromethane
DIPEA	<i>N,N</i> -diisopropylethylamine
DLS	dynamic light scattering
DMAc	dimethylacetamide
DMF	dimethylformamide
DMPP	dimethylphenylphosphine
DMSO	dimethylsulfoxide
$DP_n$	degree of polymerization
EDX	energy dispersive X-ray spectroscopy
ESI-MS	electrospray ionization mass spectrometry
Et <sub>2</sub> O	diethyl ether

## Abbreviations

EtOAc	ethyl acetate
EtOH	ethanol
FMA	fluorescein <i>O</i> -methacrylate
FRP	free radical polymerization
h	hours
His	histidine
HRP	horseradish peroxidase CDCl <sub>3</sub> deuterated chloroform
ICP-OES	inductively coupled plasma optical emission spectrometry
IONP	iron oxide nanoparticle
k	kilo
$\lambda$	wavelength
L	liters
M	molar
MA	methyl acrylate
MeOH	methanol
MHz	Megahertz
min.	minutes
MMA	methyl methacrylate
$M_n$	number-average molar mass
$M_w$	weight-average molar mass
MWCO	molecular weight cut-off
NHS	<i>N</i> -hydroxysuccinimide
Ni	nickel
nm	nanometers
NMA	2-naphthyl methacrylate
NMP	nitroxide-mediated polymerization
NMR	nuclear magnetic resonance spectrometry
NP	nanoparticle
OEGMA	oligo(ethylene glycol) methacrylate
P	poly

## Abbreviations

Pd	palladium
PISA	polymerization-induced self-assembly
(p)NTA	(protected) nitrilotriacetic acid
ppm	part per million
RAFT	reversible addition-fragmentation chain transfer
RDRP	reversible-deactivation radical polymerization
ref.	reference
r.t.	room temperature
s	seconds
S	styrene
SEC	size exclusion chromatography
SEM	scanning electron microscopy
t	time
T	temperature
tBA	<i>tert</i> -butyl acrylate
TEA	triethylamine
TEM	transmission electron microscopy
TESPMA	3-(triethoxysilyl)propyl methacrylate
TFA	trifluoroacetic acid
$T_g$	glass transition temperature
THF	tetrahydrofuran
ToF-SIMS	time-of-flight secondary ion mass spectrometry
UV	ultraviolet (light)
v	volume
V-70	2,2'-azobis(4-methoxy-2,4-dimethylvaleronitrile)
VA-044	2,2'-azobis(2-(2-imidazolin-2-yl)propane)dihydrochloride
VBR	tetraethylrhodamine 4-vinylbenzyl ester
Vis	visible (light)
wt%	weight%
XPS	X-ray photoelectron spectroscopy

# Declaration

## Erklärung

Hiermit erkläre ich wahrheitsgemäß, dass ich die vorliegende Arbeit im Rahmen der Betreuung durch Dr. Guillaume Delaittre und Prof. Dr. Christopher Barner-Kowollik selbstständig verfasst und keine anderen Quellen und Hilfsmittel als die angegebenen verwendet habe. Wörtlich oder inhaltlich übernommene Stellen sind als solche kenntlich gemacht und die Satzung des Karlsruher Instituts für Technologie (KIT) zur Sicherung guter wissenschaftlicher Praxis wurde beachtet. Die elektronische Version der Arbeit stimmt mit der schriftlichen überein und die Abgabe und Archivierung der Primärdaten sind gemäß Abs. A (6) der Regeln zur Sicherung guter wissenschaftlicher Praxis des KIT beim Institut gesichert. Des Weiteren erkläre ich, dass ich mich derzeit in keinem weiteren laufenden Promotionsverfahren befinde und keine vorausgegangenen Promotionsversuche unternommen habe.

Karlsruhe, den 26.07.2017

\_\_\_\_\_

Dominic Keller

# Curriculum Vitae

Date of Birth: 23.06.1986

Place of Birth: Königstein / Ts., Germany

Nationality: German

## Education & Work Experience

03/2014 - 07/2017

**PhD at Karlsruhe Institute of Technology (Institute for Technical Chemistry and Polymer Chemistry)**

2013 - 2014

**Pro bono work at Bad Homburger Tafel - Tafel im Hochtaunuskreis**

2012 - 2013

**Research Scientist at Tufts University, Medford (USA)**

2007 - 2012

**Chemistry Studies at Philipps-University Marburg, Germany**

- Master of Science 2012
- Bachelor of Science 2010

## **School**

- Gymnasium Oberursel: Abitur 2006

# List of Publications

- Keller D., Beloqui A., Martínez-Martínez M., Ferrer M., Delaittre G., Nitrilotriacetic Amine-Functionalized Polymeric Core-Shell Nanoparticles as Enzyme Immobilization Supports, *Biomacromolecules* **2017**, DOI:10.1021/acs.biomac.7b00677.
- Keller D., Döbber J., Pohl M., Delaittre G., Core-Shell Polymeric Nano-Objects for the Immobilization of Protein Fusions (working title), *manuscript in preparation*.
- Keller D., Le D., Delaittre G., Surface-Functional Nano-Objects by PISA, *manuscript in preparation*.

# Acknowledgements

First and foremost, I want to thank my supervisor Guillaume Delaittre for being a great boss and a source of scientific inspiration. Your dedication and support lets the group thrive and I am very thankful to have been a part of your team. The many meetings and professional discussions we had helped me to become the scientist I am today. Ich danke dir dafür von ganzem Herzen.

I would like to acknowledge Prof. Christopher Barner-Kowollik for letting me be a part of the macroarc group.

Many thanks to Alexander Welle, Vanessa Trouillet, Stefan Heissler, Tawheed Mohamed, and Silvia Andraschko for helping me with the analytical measurements of my countless samples.

Furthermore, I would like to thank the whole macroarc group for providing such a great working atmosphere and all the barbecues during the last years. In particular, I want to thank Guillaume's group at Campus North for being an amazing team. In an alphabetical order, I would like to thank: Ana for doing the enzymatic experiments, Dao for continuing and expanding PISA experiments with my leftover materials, Divya for her constant supply of food, Gabi for the great talks we had during lunch times and in between, and all the past and present members, including master students and interns. I would also like to thank my (master) students, Rémi and Tobias, for their dedication and hard work.

Vielen Dank auch an das gesamte ComPlat-Team, das mir mit seinem Wissen und Chemikalien ausgeholfen haben. Ganz besonderen Dank an dieser Stelle gebührt meinem guten Freund Steven mit dem ich sowohl während der Laborarbeit, als auch beim Sport immer eine gute Zeit hatte.

Schließlich möchte ich meinen Freunden und meiner gesamten Familie danken. Besonders meinen Eltern und meiner Schwester gebührt hier großer Dank, da sie mich in jeder erdenklichen Weise unterstützt haben und immer für mich da waren!

## Acknowledgements

Die letzten Zeilen dieser Dissertation widme ich der wichtigsten Person in meinem Leben, Jannicke. Dank deiner Geduld, deiner Zuversicht und deinem ungebrochenen Glauben an mich bin ich endlich an diesem Punkt angekommen. Für die vergangenen wunderbaren Jahre und unsere weitere Zukunft danke ich dir, Liebste!

*But the sun is eclipsed by the moon.*

Pink Floyd (1973). *Eclipse*.